Vol. 282, No. 1, October 5, 1993

ANALYTICA CHIMICA ACTA

An international journal devoted to all branches of analytical chemistry

ELSEVIER

ANALYTICA CHIMICA ACTA

Scope. *Analytica Chimica Acta* publishes original papers, preliminary communications and reviews dealing with every aspect of modern analytical chemistry. Reviews are normally written by invitation of the editors, who welcome suggestions for subjects. Preliminary communications of important urgent work can be printed within four months of submission, if the authors are prepared to forego proofs.

Submission of Papers

Americas

Prof. Harry L. Pardue
Department of Chemistry
1393 BRWN Bldg, Purdue University
West Lafayette, IN 47907-1393
USA

Tel:(+1-317) 494 5320
Fax:(+1-317) 496 1200

Computer Techniques

Prof. J.T. Clerc
Universität Bern
Pharmazeutisches Institut
Baltzerstrasse 5, CH-3012 Bern
Switzerland

Tel:(+41-31) 654171
Fax:(+41-31) 654198

Prof. Sarah C. Rutan
Department of Chemistry
Virginia Commonwealth University
P.O. Box 2006
Richmond, VA 23284-2006
USA
Tel:(+1-804) 367 1298
Fax:(+1-804) 367 8599

Other Papers

Prof. Alan Townshend
Department of Chemistry
The University
Hull HU6 7RX
Great Britain

Tel:(+44-482) 465027
Fax:(+44-482) 466410

Prof. Willem E. van der Linden
Laboratory for Chemical Analysis
Department of Chemical Technology
Twente University of Technology
P.O. Box 217, 7500 AE Enschede
The Netherlands
Tel:(+31-53) 892629
Fax:(+31-53) 356024

Prof. Paul Worsfold
Dept. of Environmental Sciences
University of Plymouth
Plymouth PL4 8AA
Great Britain

Tel:(+44-752) 233006
Fax:(+44-752) 233009

Submission of an article is understood to imply that the article is original and unpublished and is not being considered for publication elsewhere. *Anal. Chim. Acta* accepts papers in English only. There are no page charges. Manuscripts should conform in layout and style to the papers published in this issue. See inside back cover for "Information for Authors".

Publication. *Analytica Chimica Acta* appears in 16 volumes in 1994 (Vols. 281-296). *Vibrational Spectroscopy* appears in 2 volumes in 1994 (Vols. 6 and 7). Subscriptions are accepted on a prepaid basis only, unless different terms have been previously agreed upon. It is possible to order a combined subscription (*Anal. Chim. Acta* **and** *Vib. Spectrosc.*).
Our p.p.h. (postage, packing and handling) charge includes surface delivery of all issues, except to subscribers in the U.S.A., Canada, Australia, New Zealand, China, India, Israel, South Africa, Malaysia, Thailand, Singapore, South Korea, Taiwan, Pakistan, Hong Kong, Brazil, Argentina and Mexico, who receive all issues by air delivery (S.A.L.-Surface Air Lifted) at no extra cost. For Japan, air delivery requires 25% additional charge of the normal postage and handling charge; for all other countries airmail and S.A.L. charges are available upon request.

Subscription orders. Subscription prices are available upon request from the publisher. Subscription orders can be entered only by calendar year and should be sent to: Elsevier Science Publishers B.V., Journals Department, P.O. Box 211, 1000 AE Amsterdam, The Netherlands. Tel: (+31-20) 5803 642, Telex: 18582, Telefax: (+31-20) 5803598, to which requests for sample copies can also be sent. Claims for issues not received should be made within six months of publication of the issues. If not they cannot be honoured free of charge. Readers in the U.S.A. and Canada can contact the following address: Elsevier Science Publishing Co. Inc., Journal Information Center, 655 Avenue of the Americas, New York, NY 10010, U.S.A. Tel: (+1-212) 6333750, Telefax: (+1-212) 6333990, for further information, or a free sample copy of this or any other Elsevier Science Publishers journal.
Advertisements. Advertisement rates are available from the publisher on request.

US mailing notice - Analytica Chimica Acta (ISSN 0003-2670) is published biweekly by Elsevier Science Publishers (Molenwerf 1, Postbus 211, 1000 AE Amsterdam). Annual subscription price in the USA US$ 3035.75 (subject to change), including air speed delivery. Second class postage paid at Jamaica, NY 11431. *USA Postmasters*: Send address changes to Anal. Chim. Acta, Publications Expediting, Inc., 200 Meacham Av., Elmont NY 11003. Airfreight and mailing in the USA by Publication Expediting.

ANALYTICA CHIMICA ACTA

An international journal devoted to all branches of analytical chemistry

(Full texts are incorporated in CJELSEVIER, a file in the Chemical Journals Online database available on STN International; Abstracted, indexed in: Aluminum Abstracts; Anal. Abstr.; Biol. Abstr.; BIOSIS; Chem. Abstr.; Curr. Contents Phys. Chem. Earth Sci.; Engineered Materials Abstracts; Excerpta Medica; Index Med.; Life Sci.; Mass Spectrom. Bull.; Material Business Alerts; Metals Abstracts; Sci. Citation Index)

VOL. 282 NO. 1 CONTENTS OCTOBER 5, 1993

(Continued overleaf)

ANALYTICA CHIMICA ACTA
VOL. 282 (1993)

ANALYTICA CHIMICA ACTA

An international journal devoted to all branches of analytical chemistry
Revue internationale consacrée à tous les domaines de la chimie analytique
Internationale Zeitschrift für alle Gebiete der analytischen Chemie

Anal. Chim. Acta, Vol. 282 (1993)

ELSEVIER, Amsterdam–London–New York–Tokyo

0003-2670/93/$06.00

Analytica Chimica Acta, 282 (1993) vii
Elsevier Science Publishers B.V., Amsterdam

Publisher's note

Rapid Publication Letters Section

The editors and publisher of *Analytica Chimica Acta* are pleased to announce the introduction of a *Letters* section in the journal. The *Letters* section will allow the analytical chemist to communicate rapidly short papers that describe innovative research. The new section will be included in regular issues of the journal, which will appear approximately weekly from 1994 onwards. Submissions to the new section will be subjected to a strict quality control. The criteria for accepting letters are novelty, quality, significance, urgency and brevity.

The editors invite analytical scientists to submit research results meeting the criteria mentioned above. The following publication procedure will apply for letters:

- A letter should occupy no more than *two printed pages*, i.e., an equivalent of 7200 characters including space for figures, tables, abstract and references.
- An abstract is *essential*, but should be short (e.g., 3 lines). Only the most significant experimental details, if any, should be given. Only key references should be added.
- To reduce publication time, proofs will not be sent to authors. Accordingly, it is critical for authors to check manuscripts carefully before submission.
- A letter should be submitted – preferably by FAX – to one of the editors. A disk with the text, and original figures should be sent to the same editor by separate mail. Submission on disk will facilitate the rapid publication process.
- The editor will have the letter reviewed: reviewers will be invited to recommend acceptance or rejection of the letter. No revision will be possible.
- After acceptance the letter will be published in the first available issue of the journal.
- If the guidelines are adhered to, the total publication time of a letter, from submission to publication, will not exceed 4 months.

It is hoped that the analytical community will benefit from *Analytica Chimica Acta*'s new service for the rapid communication of important research.

Analytica Chimica Acta, 282 (1993) ix
Elsevier Science Publishers B.V., Amsterdam

Editorial

Fast Publication Section

From time to time scientists make important discoveries that they wish to report rapidly to the scientific community. With this issue we announce a new *Letters* section of *Analytica Chimica Acta* designed to speed the publication process relative to that for manuscripts handled in the usual way. Specifically, the goal is to reduce publication time to a maximum of four months. The purpose of the section is to provide scientists space in a leading analytical journal where they can report brief descriptions of new discoveries that will be developed and reported in greater detail at a later date. The maximum length of papers will be two printed pages, equivalent to about 7200 character spaces, including space for tables, figures and critical references. The primary criteria for papers in the *Letters* section are novelty, significance, quality, urgency and brevity. Reviewers selected for manuscripts submitted for the *Letters* section will be asked to respond quickly, advising editors primarily if and why manuscripts should or should not be published. To speed the publication process, manuscripts will be processed from floppy disks, there will be no revisions after the manuscript is submitted, proofs will not be sent to authors, and each paper will be published in the first available issue, which will appear approximately weekly from the beginning of 1994 onward. More complete details are included in the publisher's note elsewhere in this issue. The editors and publisher encourage scientists doing research in any aspects of analytical chemistry to submit manuscripts that meet the criteria for this new section. We look forward to serving the analytical community with this new medium for fast publication of important new discoveries.

Harry L. Pardue

Analytica Chimica Acta, 282 (1993) 1–17
Elsevier Science Publishers B.V., Amsterdam

Interpretation of the influence of temperature on the solvation properties of gas chromatographic stationary phases using Abraham's solvation parameter model

Colin F. Poole and Theophilus O. Kollie

Department of Chemistry, Wayne State University, Detroit, MI 48202 (USA)

(Received 24th February 1993; revised manuscript received 27th April 1993)

Abstract

Abraham's solvation parameter model is used to interpret the influence of temperature on the contribution of cavity formation and solute–solvent intermolecular interactions to the solvation of a varied group of 62 solutes on ten representative stationary phases used in gas chromatography. It was observed that the magnitude of polar interactions increased at lower temperatures and that the change in the characteristic phase constants deduced from Abraham's model as a function of temperature could be described by a second-order polynomial function. Since the susceptibility of a solvent for a particular intermolecular interaction changes in a phase-specific manner as a function of temperature the observed ranking of phases for a particular intermolecular interaction at one temperature cannot be used to predict phase rankings at another temperature for the same interaction. A comparison of Abraham's model with an alternative cavity model proposed by Poole for the sum of the cavity and dispersion contributions to solvation shows similar trends as a function of temperature but differences in the magnitude of the contribution of the cavity–dispersion term to the overall free energy change for the solvation process. Agreement for the contribution of polar interactions to the solvation process is only qualitative for the two models unless a correction is made for the difference in magnitude for the cavity–dispersion contribution. A correction can be made by dividing the c term in Abraham's model into two contributions; a constant term independent of temperature which is assigned to the cavity–dispersion contribution to solvation and a temperature dependent term which is assigned to the polar interaction contribution to solvation. With this construct the two solvation models agree within experimental error for the relative contribution made by the cavity–dispersion term and solute–solvent polar interaction forces to the solvation process.

Keywords: Gas chromatography; Cavity formation; Dispersion; Polar interaction; Solvation process; Stationary phases

Numerous methods have been proposed to characterize the solvent properties of stationary liquid phases used in gas chromatography. These methods encompass a wide range of sophistication and have been reviewed elsewhere [1–8]. The most recent (and generally useful) approaches are the solvation parameter models developed by Abraham and co-workers [9–13] and Carr and co-workers [14–17] and the free energy solvation model developed by Poole and co-workers [8,18–21]. These models are derived from the cavity model of solvation [22,23], in which the process of solute transfer from the gas phase to solution in the stationary phase is considered to occur in three stages: (1) the creation of a cavity in the solvent of a suitable size to accommodate the solute; (2) reorganization of the solvent molecules around the cavity; and (3) introduction of the solute into the cavity where it is able to

Correspondence to: C.F. Poole, Department of Chemistry, Wayne State University, Detroit, MI 48202 (USA).

interact with the surrounding solvent molecules. The Gibbs free energy change for the transfer process is simply the sum of the free energy changes for each step. The creation of a cavity in the solvent is an endoergic process that requires the disruption of solvent–solvent interactions. The free energy change associated with reorganization of the solvent molecules around the cavity (although not necessarily the enthalpy and entropy change) is assumed to be negligible compared to the free energy changes associated with steps (1) and (3). The free energy change associated with the solute–solvent interactions formed in step (3) are exoergic and must exceed the free energy change associated with step (1) for solvation to occur.

There is no exact method to calculate the individual contributions to the total free energy change for the solvation process, as defined above, and it is necessary to resort to empirical approaches to estimate the changes involved using experimentally accessible parameters. It is at this point that the different models vary. Poole and co-workers derived the following general expression for the solvation process [19]:

$$\Delta G_S^{Soln}(X) = \Delta G_S^{Soln}(HC)^V + \Delta G_{SQ}^P(X) + \Delta G_S^{Int}(X) \quad (1)$$

where $\Delta G_S^{Soln}(X)$ is the partial Gibbs free energy of solution for the transfer of solute X from the gas phase to the stationary phase S, $\Delta G_S^{Soln}(HC)^V$ is the partial Gibbs free energy of solution for an *n*-alkane with an identical Van der Waals volume to solute X in the stationary phase S, $\Delta G_{SQ}^P(X)$ is the partial Gibbs free energy of interaction for the polar contribution of solute X in a non-polar reference solvent squalane, SQ, and $\Delta G_S^{Int}(X)$ is the partial Gibbs free energy of interaction for the polar contributions of solute X to solvation in solvent S. Experimentally, the Van der Waals volume of solute X is calculated along with the coefficients describing the linear fit for log(gas–liquid partition coefficient) against the Van der Waals volume of a homologous series of *n*-alkanes on the reference non-polar solvent, squalane, and the solvent of interest, S, together with the partition coefficient for solute X on the reference solvent squalane and solvent S. All the terms in Eqn. 1 can then be evaluated. The contribution from cavity formation and dispersion interactions to the solvation process is then represented by the sum of the first two terms on the right-hand side of Eqn. 1. The $\Delta G_S^{Int}(X)$ parameter represents the sum of the polar interactions, such as hydrogen bond formation and orientation, which must be further deconvoluted if individual contributions to specific intermolecular interactions are to be identified. Principal component analysis has been used to identify the contributions from individual intermolecular interactions to $\Delta G_S^{Int}(X)$ but this approach is still in the process of refinement [6,19]. This makes $\Delta G_S^{Int}(X)$ a less useful parameter for studying the effect of temperature on the variation of individual intermolecular interactions but an ideal parameter for studying the variation of temperature on the total contribution of polar interactions to solvation and for predicting retention of solutes of known structure (for simple molecules $\Delta G_S^{Int}(X)$ depends on the type of functional groups present in the solute and can be treated as an incremental constant for prediction purposes [21]).

The approach taken by Abraham and co-workers is based on multiple linear regression analysis and is described by Eqn. (2) [9,10]:

$$\log K_L = c + rR_2 + s\pi_2^H + a\alpha_2^H + b\beta_2^H + l \log L^{16} \quad (2)$$

where K_L is the solute gas–liquid partition coefficient, c is a constant, R_2 the solute excess molar refraction, π_2^H the effective solute dipolarity/polarizability parameter, α_2^H the effective hydrogen-bond acidity, β_2^H the effective hydrogen-bond basicity, and L^{16} the gas–liquid partition coefficient on *n*-hexadecane at 25°C. This model is similar to the solvatochromic theory of solutions [24,25] except that the explanatory variables R_2, π_2^H, α_2^H, β_2^H and log L^{16} are solvation parameters derived from equilibrium measurements and further refined (and augmented) by multiple linear regression analysis on chromatographic solvents of assumed characteristic properties. The solvent parameters r, s, a, b and l are unambiguously defined: the r constant refers to the ability of the phase to interact with solute π- and n-electron pairs; the s constant to the ability of the phase to

take part in dipole–dipole and dipole–induced dipole interactions; the a constant is a measure of the hydrogen-bond basicity of the phase; the b constant is a measure of the hydrogen-bond acidity of the phase; and the l constant incorporates contributions from solvent cavity formation and dispersion interactions, and more specifically indicates how well the phase will separate members in a homologous series. Experimentally the phase-specific constants are determined from a number of measurements of log K_L for solutes with known explanatory variables using multiple linear regression. A sufficient number of solutes is required to statistically define each parameter and the reliability of the phase-specific constants is governed by the accuracy of the explanatory variables in characterizing the specific interaction they represent.

In spirit, the approach taken by Carr and co-workers is the same as that used by Abraham with slight modification [15]

$$\log K_L = c + d\delta_2 + s\pi_2^{*c} + a\alpha_2^c + b\beta_2^c + l \log L^{16} \quad (3)$$

where the empirical polarizability correction factor δ_2 (used in solvatochromic models) has been retained in place of R_2 used by Abraham and a new set of explanatory variables have been used and given the superscript c to indicate that they were obtained from chromatographic data. Since the explanatory variables are numerically different from those used by Abraham so are the characteristic phase constants derived from them in some cases. However, the qualitative, if not always the quantitative agreement between the two approaches is very good and the general conclusions reached by using either model are not at variance [8].

The significance of temperature in the classification of solvent properties using the above models has not been established. The data available to validate the models has been obtained at one or two temperatures only. It is well established that polar intermolecular forces are temperature dependent and are expected to decrease in magnitude with increasing temperature. The capacity of a solvent for specific intermolecular interactions determined at a single reference temperature may be quite misleading since it provides no perspective on how a solvent's susceptibility for a defined interaction changes with temperature, and thus ranking of solvents for a particular interaction may be quite different at different temperatures. By generating a data matrix over a reasonable temperature range the general relationship between the specific phase constants in Abraham's model (or Carr's model) can be revealed. Similar observations can be made for Poole's model but extensive application of Eqn. 1 to temperature dependent intermolecular interactions, other than the cavity–dispersion contribution and the polar contribution must await refinement of the methods used to deconvolute the contribution of individual intermolecular interactions to $\Delta G_S^{Int}(X)$.

In a study of the solvent properties *N*-formylmorpholine and *N*-methylpyrrolidinone in the temperature range 40–100°C and 50–70°C, respectively, Abraham et al. [26] found a linear relationship for a plot of the characteristic phase constants vs. $1/T$. It is noteworthy that the original data used in this study was not corrected for interfacial adsorption as a retention mechanism and because of the significant vapor pressure of these solvents the weight of liquid phase in the column was not well determined [27]. Thus, the above results may not be entirely reliable, but apart from this study the influence of temperature on the magnitude of the specific phase constant is not defined. It is also necessary to have an understanding of the change in the specific phase constants over a wider temperature range than in the above study since those phases of most use in gas chromatography have a wide temperature operating range and some indication of how their selectivity changes over a wide temperature range is required to define their use for different applications.

EXPERIMENTAL

The name, abbreviation and composition of the stationary phases used in this study are summarized in Table 1. Squalane, QF-1, CW-20M,

DEGS, TCEP and Chromosorb W AW (60–80 mesh) were obtained from Anspec (Ann Arbor, MI); OV-105, OV-17 and OV-225 from Ohio Valley Specialty Chemicals (Marietta, OH); and THPED and QPTS from Aldrich (Milwaukee, WI).

Column packings containing 8–18% (w/w) of liquid phase were prepared using the rotary evaporator technique [7]. After coating, the damp packings were dried in a fluidized-bed dryer and packed into glass columns of 2 m × 2 mm i.d. with the aid of suction and gentle vibration. Gas chromatographic measurements were made using a Varian 3700 gas chromatograph (Walnut Creek, CA) fitted with a flame ionization detector.

The experimental protocol used to determine gas–liquid partition coefficients is described in detail elsewhere [28,29]. A minimum of four phase loadings was used in the extrapolation method to define the gas–liquid partition coefficients. Phase loadings were determined by exhaustive Soxhlet extraction. A modified Lipkin bicapillary pycnometer was used to determine solvent densities as a function of temperature [30]. A mercury manometer was used to measure the column inlet pressures and a NIST-certified thermometer (±0.2°C) to measure ambient and column temperatures. Solute retention times were determined under infinite dilution/zero surface coverage conditions and are fully corrected for contributions from interfacial adsorption. The uncertainty in K_L is typically 3–5% R.S.D. for K_L values from 10 to 100 and 2–3% R.S.D. for K_L values from 100 to 1000.

TABLE 1

Stationary phases and their description

Abbreviation	Chemical description
SQ	Squalane
OV-105	Poly(cyanopropylmethyldimethylsiloxane)
OV-17	Poly(methylphenylsiloxane)
QF-1	Poly(trifluoropropylmethylsiloxane)
OV-225	Poly(cyanopropylmethylphenylmethylsiloxane)
CW-20M	Poly(ethylene glycol)
THPED	*N,N,N',N'*-Tetrakis(2-hydroxypropyl)-ethylenediamine
TCEP	1,2,3-Tris(2-cyanoethoxypropane)
DEGS	Poly(diethylene glycol succinate)
QPTS	Tetra-*n*-butylammonium 4-toluenesulfonate

The Van der Waals volume for test solutes was calculated with the molecular modeling program MacroModel 2.0 (Department of Chemistry, Columbia University, New York, NY) executed on a VAX 11/750 computer (Digital Equipment, Merrimack, NH). Multiple linear regression analysis was performed on an Epson Apex 200 computer using the program SPSS/PC + V3.1 (SPSS, Chicago, IL). The explanatory variables used for multiple linear regression analysis were taken from references [11–13] and are summarized in Table 2. Approximately 62 solutes were used for each temperature (60, 80, 100, 120 and 140°C) with about 10% of the solutes eliminated for measurements on some phases at 60 and 140°C due to excessive retention or inadequate retention, respectively. The high vapor pressure of squalane excluded measurements at 140°C and gas–liquid partition coefficients for this phase at 140°C were estimated by extrapolation of the values obtained between 60 and 120°C.

RESULTS AND DISCUSSION

The ten stationary phases used in this study were selected to represent the full range of solvent properties characteristic of contemporary stationary phases used in gas chromatography based on data obtained for a larger number of phases at 121.2°C [8]. The characteristic phase constants were then determined by multiple linear regression analysis at 20°C intervals for the temperature range from 60 to 140°C (120°C in the case of squalane) based on Eqn. 2 for the solutes identified in Table 2. It was intended that the full range of solute interactions would be probed in this study and we believe that this has been achieved in the data collected. The results from the multiple linear regression analysis are summarized in Table 3. The quality of the data must be judged by the statistics for the fit and whether the characteristic phase constants make chemical sense. The correlation constant and standard deviation are universally good and compare favorably with literature values obtained in similar

TABLE 2

Explanatory variables used in Eqn. 2

Solute	Explanatory variables				
	R_2	π_2^H	α_2^H	β_2^H	log L^{16}
Decane	0.000	0.00	0.00	0.00	4.686
Undecane	0.000	0.00	0.00	0.00	5.191
Dodecane	0.000	0.00	0.00	0.00	5.696
Tridecane	0.000	0.00	0.00	0.00	6.200
Tetradecane	0.000	0.00	0.00	0.00	6.705
Pentadecane	0.000	0.00	0.00	0.00	7.209
Hexadecane	0.000	0.00	0.00	0.00	7.714
Butan-2-one	0.166	0.68	0.00	0.51	2.282
Pentan-2-one	0.143	0.68	0.00	0.51	2.755
Hexan-2-one	0.136	0.68	0.00	0.51	3.262
Heptan-2-one	0.123	0.68	0.00	0.51	3.760
Octan-2-one	0.108	0.68	0.00	0.51	4.257
Nonan-2-one	0.119	0.68	0.00	0.51	4.735
Methyl hexanoate	0.080	0.60	0.00	0.45	3.874
Methyl heptanoate	0.079	0.60	0.00	0.45	4.356
Methyl octanoate	0.065	0.60	0.00	0.45	4.838
Methyl nonanoate	0.056	0.60	0.00	0.45	5.321
Methyl decanoate	0.053	0.60	0.00	0.45	5.803
Methyl undecanoate	0.050	0.60	0.00	0.45	6.285
Butan-1-ol	0.224	0.42	0.37	0.48	2.601
Pentan-1-ol	0.219	0.42	0.37	0.48	3.106
Hexan-1-ol	0.210	0.42	0.37	0.48	3.610
Heptan-1-ol	0.211	0.42	0.37	0.48	4.115
Octan-1-ol	0.199	0.42	0.37	0.48	4.619
Nonan-1-ol	0.193	0.42	0.37	0.48	5.124
2-Methyl-2-pentanol	0.169	0.30	0.31	0.60	3.081
cis-Hydrindane	0.439	0.25	0.00	0.00	4.635
Oct-2-yne	0.225	0.30	0.00	0.10	3.850
Dodec-1-yne	0.133	0.23	0.13	0.10	5.657
Benzene	0.610	0.52	0.00	0.14	2.803
Toluene	0.601	0.52	0.00	0.14	3.344
Ethylbenzene	0.613	0.52	0.00	0.15	3.789
Butylbenzene	0.600	0.51	0.00	0.15	4.730
Chlorobenzene	0.718	0.65	0.00	0.07	3.657
Bromobenzene	0.882	0.73	0.00	0.09	4.041
Iodobenzene	1.188	0.82	0.00	0.12	4.502
Benzaldehyde	0.820	1.00	0.00	0.39	4.008
Acetophenone	0.818	1.01	0.00	0.48	4.501
Benzonitrile	0.742	1.11	0.00	0.33	4.039
1,2-Dichlorobenzene	0.872	0.78	0.00	0.04	4.518
Aniline	0.955	0.96	0.16	0.53	3.993
N-Methylaniline	0.948	0.90	0.17	0.45	4.478
N,*N*-Dimethylaniline	0.957	0.84	0.00	0.42	4.708
2,6-Dimethylaniline	0.972	0.89	0.20	0.60	5.028
Phenol	0.805	0.89	0.60	0.31	3.766
1-Nitropropane	0.242	0.95	0.00	0.31	2.894
1-Nitropentane	0.212	0.95	0.00	0.29	3.938
1-Nitrohexane	0.203	0.95	0.00	0.29	4.416
Nitrocyclohexane	0.441	0.97	0.00	0.31	4.826
Nitrobenzene	0.871	1.10	0.00	0.27	4.511
1,1,2,2-Tetrachloroethane	0.595	0.76	0.16	0.12	3.803
2,4,6-Trimethylpyridine	0.634	0.72	0.00	0.50	4.200

TABLE 2 (continued)

Solute	Explanatory variables				
	R_2	π_2^H	α_2^H	β_2^H	log L^{16}
Methylphenyl ether	0.708	0.73	0.00	0.33	3.859
Di-*n*-hexyl ether	0.000	0.25	0.00	0.45	5.938
Nonanal	0.150	0.65	0.00	0.45	4.856
Dioxane	0.329	0.75	0.00	0.64	2.892
Benzodioxan	0.874	1.01	0.00	0.80	4.985
Pyridine	0.631	0.84	0.00	0.52	3.022
N,*N*-Dibutylformamide	0.255	1.11	0.00	0.75	5.927
Dimethyl sulfoxide	0.522	1.74	0.00	0.89	3.459
N,*N*-Dimethylacetamide	0.363	1.33	0.00	0.78	3.717
N,*N*-Dimethylformamide	0.367	1.31	0.00	0.74	3.173

studies. The best statistical fit may not always correspond to the fit that makes chemical sense. For example, the characteristic phase constants cannot have negative values (except for r on QF-1 and c for any phase). The negative r constant for QF-1 is not anomalous since solvents containing fluorocarbon groups have less ability to interact with solute π- and n-electron pairs than those with alkane groups [10,11,21]. In some cases the best statistical fit of the data results in coefficients with small negative values for a, b and r. These values are insignificant (t-test) and are replaced by the next best statistical fit that makes chemical sense (indicated by 2 in the note column of Table 3). These are the data used for interpretation in this report.

Of the ten phases studied only TCEP and DEGS show weak hydrogen-bond acid properties. This is consistent with previous studies by Abraham and co-workers [11,12], Carr and co-workers [16,17] and Poole and co-workers [19,20]. Those phases anticipated as having a potential for significant hydrogen-bond acid character among common stationary phases seem to prefer to associate as solvent hydrogen-bond complexes in preference to forming solute–solvent hydrogen-bond interactions. It has been shown recently that solvents such as bis(3-allyl-4-hydroxyphenyl)sulfone [26,31] and 4-dodecyl-α, α-bis(trifluoromethyl)benzyl alcohol [17,31] are significant hydrogen-bond acids but otherwise this interaction is insignificant for the most common stationary phases employed in gas chromatography. This area of stationary phase synthesis is worthy of further attention.

The influence of temperature on the capacity of an individual phase for a defined intermolecular interaction can be visualized by plotting the specific phase constant against $1/T$ (or T, Figs. 1–3). The general shape of the plots for the s, a and l constant against $1/T$ is similar, exhibiting an upward curvature going from high to lower temperatures. The curvature is most pronounced for those phases with a greater capacity for the particular interaction plotted. At any single temperature the relative contribution of a particular interaction to the solvation properties of the phases investigated can be read from the vertical axis. It is obvious that crossovers occur for individual phases at different temperatures demonstrating a change in relative ranking as a function of temperature. A more obvious trend, however, is the fanning out of the plots at lower temperatures. Selectivity differences between individual stationary phases are enhanced at lower temperatures, in general, although because of crossovers the maximum selectivity difference between any two phases will occur at a characteristic temperature, that is not necessarily the lowest temperature studied. It is clear, however, that the selectivity ranking of the stationary phases is temperature dependent, and the ranking obtained at one temperature cannot be used to predict the ranking at another temperature.

For all phases the plots of the characteristic phase constant against $1/T$ can be described by a

TABLE 3

Summary of results from multiple linear regression analysis

Solvent	Temperature (K)	Note [a]	Phase constants						Statistics	
			c	*r*	*s*	*a*	*b*	*l*	*r*	S.D.
SQ	394.4	1	−0.214	0.143		−0.050		0.583	0.9998	0.015
		2	−0.222	0.129	0.011			0.583	0.9998	0.017
	374.4	1	−0.207	0.112		−0.062	0.027	0.637	1.0000	0.005
		2	−0.210	0.089	0.022			0.637	0.9999	0.011
	354.4	1	−0.199	0.085		−0.094	0.047	0.719	1.0000	0.006
		2	−0.202	0.050	0.037			0.719	0.9999	0.016
	334.4	1	−0.207	0.033	0.021	−0.171	0.040	0.856	1.0000	0.009
		2	−0.220		0.050			0.858	0.9997	0.030
OV-105	414.4	1	−0.213	−0.030	0.396	0.439	−0.065	0.459	0.9992	0.025
		2	−0.221		0.354	0.420		0.460	0.9991	0.026
	394.4	1	−0.190	−0.062	0.417	0.442	−0.051	0.494	0.9996	0.020
		2	−0.203		0.364	0.407		0.496	0.9994	0.024
	374.4	1	−0.153	−0.110	0.446	0.446	−0.032	0.543	0.9998	0.015
		2	−0.173		0.377	0.388		0.547	0.9992	0.030
	354.4	1	−0.097	−0.180	0.489	0.451		0.616	0.9999	0.014
		2	−0.128		0.397	0.360		0.622	0.9983	0.050
	334.4	1	−0.010	−0.310	0.591	0.475		0.737	0.9996	0.031
		2	−0.063		0.433	0.317		0.748	0.9963	0.088
OV-17	414.4	1	−0.436	0.069	0.629	0.228		0.485	0.9980	0.042
	394.4	1	−0.372	0.070	0.653	0.263		0.518	0.9994	0.025
	374.4	1	−0.351	0.034	0.723	0.310		0.563	0.9994	0.026
	354.4	1	−0.289		0.798	0.393		0.632	0.9998	0.016
	334.4	1	−0.182	−0.049	0.930	0.513		0.746	0.9996	0.031
		2	−0.190		0.905	0.488		0.747	0.9995	0.033
QF-1	414.4	1	−0.287	−0.392	1.087	0.128		0.386	0.9942	0.064
	394.4	1	−0.269	−0.449	1.157	0.187		0.419	0.9964	0.054
	374.4	1	−0.246	−0.520	1.253	0.265		0.465	0.9983	0.041
	354.4	1	−0.211	−0.629	1.396	0.383		0.534	0.9993	0.031
	334.4	1	−0.151	−0.822	1.638	0.585		0.648	0.9985	0.053
OV-225	414.4	1	−0.570		1.231	1.014	−0.081	0.434	0.9992	0.028
		2	−0.574		1.198	1.010		0.434	0.9989	0.031
	394.4	1	−0.532	−0.036	1.274	1.088	−0.071	0.465	0.9995	0.023
		2	−0.541		1.226	1.065		0.466	0.9994	0.025
	374.4	1	−0.480	−0.090	1.325	1.191	−0.044	0.508	0.9997	0.020
		2	−0.498		1.261	1.142		0.511	0.9993	0.028
	354.4	1	−0.405	−0.173	1.401	1.342	−0.001	0.573	0.9997	0.022
		2	−0.434		1.312	1.253		0.579	0.9982	0.051
	334.1	1	−0.271	−0.323	1.565	1.607		0.679	0.9992	0.040
		2	−0.326		1.400	1.441		0.691	0.9954	0.095
CW-20M	414.4	1	−0.542	0.258	1.272	1.590	−0.107	0.412	0.9998	0.015
		2	−0.554	0.298	1.208	1.564		0.412	0.9996	0.021
	394.4	1	−0.539	0.244	1.374	1.932	−0.196	0.446	0.9998	0.015
		2	−0.560	0.317	1.256	1.883		0.447	0.9992	0.032
	374.4	1	−0.479	0.248	1.440	2.063	−0.178	0.482	0.9999	0.013
		2	−0.498	0.314	1.333	2.019		0.482	0.9994	0.028
	354.4	1	−0.481	0.251	1.578	2.269	−0.152	0.538	0.9999	0.015
		2	−0.497	0.309	1.486	2.231		0.538	0.9996	0.027
	334.4	1	−0.416	0.246	1.806	2.793	−0.189	0.634	0.9996	0.032
		2	−0.437	0.318	1.692	2.746		0.635	0.9992	0.042

TABLE 3 (continued)

Solvent	Temperature (K)	Note [a]	Phase constants						Statistics	
			c	*r*	*s*	*a*	*b*	*l*	*r*	S.D.
THPED	414.4	1	−0.454	−0.043	1.134	1.886		0.446	0.9987	0.037
		2	−0.461		1.112	1.864		0.447	0.9986	0.039
	394.4	1	−0.422	−0.136	1.198	2.139		0.472	0.9985	0.043
		2	−0.445		1.128	2.069		0.477	0.9973	0.056
	374.4	1	−0.379	−0.246	1.278	2.470		0.510	0.9995	0.025
		2	−0.421		1.152	2.345		0.519	0.9964	0.070
	354.4	1	−0.351	−0.432	1.429	2.974		0.572	0.9993	0.035
		2	−0.424		1.209	2.753		0.587	0.9918	0.120
	334.4	1	−0.225	−0.736	1.632	3.835		0.660	0.9994	0.038
		2	−0.350		1.257	3.459		0.687	0.9838	0.199
TCEP	414.4	1	−0.647	0.235	1.706	1.646	0.224	0.302	0.9983	0.047
	394.4	1	−0.670	0.202	1.816	1.792	0.244	0.332	0.9989	0.041
	374.4	1	−0.691	0.119	1.999	2.028	0.238	0.371	0.9995	0.030
	354.4	1	−0.723		2.263	2.356	0.261	0.427	0.9998	0.023
	334.4	1	−0.794	−0.148	2.673	2.911	0.273	0.529	0.9990	0.054
		2	−0.826		2.544	2.828	0.403	0.533	0.9986	0.063
DEGS	414.4	1	−0.764	0.358	1.492	1.495	0.104	0.343	1.0000	0.005
	394.4	1	−0.710	0.359	1.502	1.742	0.186	0.370	0.9999	0.012
	374.4	1	−0.652	0.233	1.559	2.099	0.192	0.408	0.9999	0.015
	354.4	1	−0.561		1.668	2.543	0.368	0.443	1.0000	0.004
	334.4	1	−0.406	−0.260	1.778	3.377	0.562	0.523	0.9997	0.028
		2	−0.460		1.552	3.226	0.790	0.531	0.9982	0.063
QPTS	414.4	1	−0.450		1.625	3.086	−0.328	0.394	0.9977	0.058
		2	−0.465	0.043	1.490	3.067		0.391	0.9955	0.081
	394.4	1	−0.515		1.714	3.350	−0.285	0.433	0.9981	0.057
		2	−0.528	0.040	1.597	3.333		0.430	0.9967	0.076
	374.4	1	−0.594		1.833	3.702	−0.221	0.487	0.9984	0.058
		2	−0.621	0.102	1.691	3.637		0.489	0.9981	0.064
	354.4	1	−0.765	0.109	1.916	4.202		0.569	0.9988	0.058
	334.4	1	−0.994	0.172	2.185	5.069	0.163	0.704	0.9992	0.057

[a] (1) Regression providing best statistical fit; (2) regression providing best statistical fit that makes chemical sense when different from (1).

second-order polynomial. The second choice would be log(characteristic phase constant) against $1/T$ which generally has a correlation coefficient $r^2 > 0.97$ for a linear fit. However, close inspection of the plots shows genuine curvature, and again a better fit to a second-order polynomial function.

The r and c phase constants are not as well behaved as the other characteristic constants. The contribution of the rR_2 term to the gas–liquid partition coefficient is generally small (in many cases negligible; see later) but its inclusion in Eqn. 2 improves the statistical fit to the regression model. In those cases where the r constant has a significant value and makes chemical sense (e.g., SQ, CW-20M, QPTS, and QF-1) there is no observable direct relationship with temperature, except for QF-1 which can be fitted to a second order polynomial. The c term shows a wide range of behavior as a function of temperature, see Fig. 4. The c term has no defined physical status. Its consistent sign would indicate that it is related in part to the cavity formation contribution to solvation. The complete description of the cavity term undoubtedly contains elements included in the l term which makes an unambiguous discussion of the c term mute.

An alternative approach to interpreting the

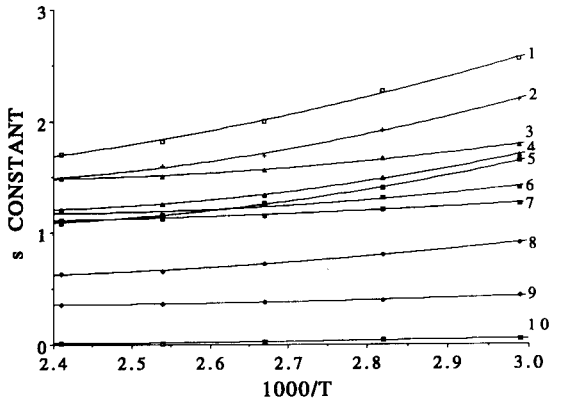

Fig. 1. Plot of the s constant as a function of temperature for 10 stationary phases of varied polarity. Phase identification: 1 = SQ; 2 = OV-105; 3 = OV-17; 4 = OV-225; 5 = THPED; 6 = QF-1; 7 = CW-20M; 8 = DEGS; 9 = QPTS; and 10 = TCEP.

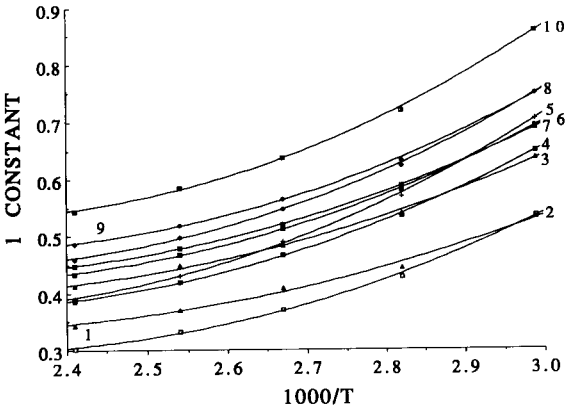

Fig. 3. Plot of the l constant as a function of temperature for 10 stationary phases of varied polarity. Phase identification: 1 = TCEP; 2 = DEGS; 3 = CW-20M; 4 = THPED; 5 = QPTS; 6 = OV-225; 7 = QF-1; 8 = OV-105; 9 = OV-17; and 10 = SQ.

influence of temperature on the selectivity of individual phases is to consider the relative contribution of specific intermolecular interactions to retention for a few selected solutes. Since 62 solutes were used to generate the retention data only a few representative examples can be discussed here. Figure 5 shows a plot of the contributions of the defined intermolecular interactions to the solvation of dioxane on TCEP as a function of temperature. TCEP is a polar phase with a capacity for all types of intermolecular interactions; dioxane has a significant capacity for orientation and hydrogen-bond base interactions but is not a hydrogen-bond acid. The interactions represented by the product terms rR_2 and $b\beta_2^H$ contribute little to the solvation properties of dioxane on TCEP. The major contributions to the retention of dioxane on TCEP result from dipole interactions and the cavity–dispersion term. Although dioxane has frequently been employed as a test solute to characterize stationary phase hydrogen-bond acid properties, its characteristic

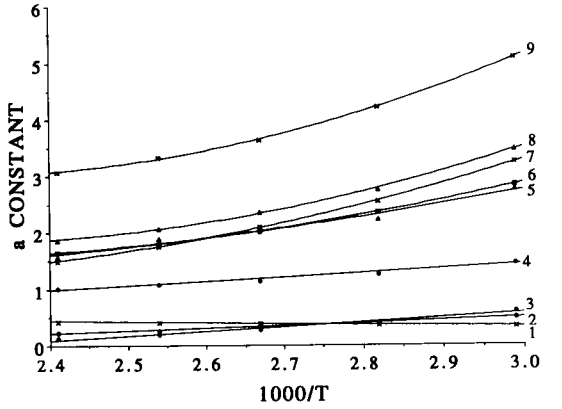

Fig. 2. Plot of the a constant as a function of temperature for 9 stationary phases of varied polarity. Phase identification: 1 = OV-105; 2 = OV-17; 3 = QF-1; 4 = OV-225; 5 = CW-20M; 6 = TCEP; 7 = DEGS; 8 = THPED; 9 = QPTS.

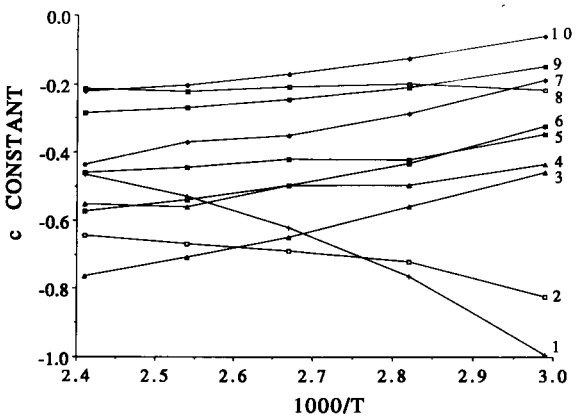

Fig. 4. Plot of the c constant as a function of temperature for 10 stationary phases of varied polarity. Phase identification: 1 = QPTS; 2 = TCEP; 3 = DEGS; 4 = CW-20M; 5 = THPED; 6 = OV-225; 7 = OV-17; 8 = SQ; 9 = QF-1; and 10 = OV-105.

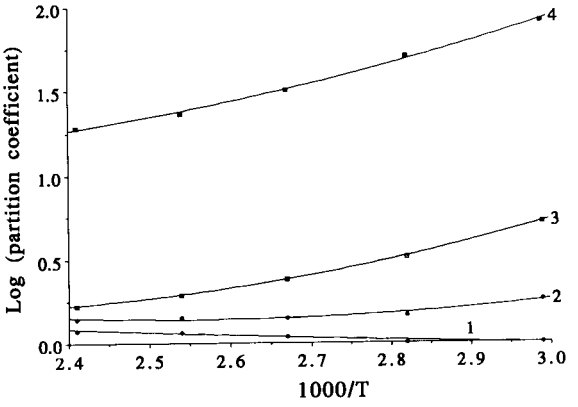

Fig. 5. Plot of the relative contribution of different intermolecular interactions and the cavity term to the solvation of dioxane in TCEP as a function of temperature. Identification: $1 = rR_2$; $2 = b\beta_2^H$; $3 = c + l \log L^{16}$; and $4 = s\pi_2^H$.

properties on most phases are, in fact, better considered as a probe of orientation interactions, as shown for TCEP. The trend observed for the cavity–dispersion term as a function of temperature in Fig. 5 is quite general and worthy of additional comment. Since we cannot separate the contributions attributable to dispersion interactions and cavity formation from each other the influence of temperature on these terms can only be considered in terms of their combined effect. In all cases studied in this work the cavity–dispersion term increases (more favorable for solute transfer to the stationary phase) as the temperature is decreased. Solvent–solvent interactions, which must be disrupted to form a cavity of a suitable size to hold the solute, should be greater at lower temperature and thus less favorable for solvation. Dispersion forces are not temperature dependent but are strongly dependent on the average intermolecular distance between interacting centers. Lowering the solvent temperature increases the solvent density and thus reduces the average intermolecular distance between solvent molecules (and also solute–solvent molecules at infinite dilution). The anticipated influence of temperature on the cavity–dispersion term is then to increase the work required to form a cavity in the solvent as the temperature is lowered due to stronger solvent–solvent interactions, which does not favor solute transfer from the gas phase to the stationary phase, and to increase the contribution to solvation from dispersion forces resulting from solute–solvent interactions arising from the reduction in average intermolecular distances, which favors the transfer of the solute from the gas phase to the stationary phase. In all cases the sum of the cavity and dispersion term favors transfer of the solute to the stationary phase as the temperature is reduced, even for highly cohesive solvents like TCEP, which possess strong polar solvent–solvent interactions. These results emphasize the general importance of dispersion forces which are never insignificant even for solutes dissolved in the most polar stationary phases since the cavity–dispersion term is always favorable for solute transfer to the stationary phase. This also implies that the dispersion forces characteristic of solute–solvent interactions must exceed the dispersion forces involved in solvent–solvent interactions that are overcome in forming the solvent cavity. This is difficult to accept unless formation of solute–solvent interactions causes reorganization of solvent molecules around the cavity with a net increase in the number of interactions between solute and solvent than existed in the solvent originally. This is not unreasonable in some cases studied here but it is hard to accept that this would occur in all cases, without additional supporting evidence. It seems possible that a contribution from the cavity–dispersion term may be mixed in with the other characteristic phase constants and has not been identified as yet.

We have explored some further characteristics of the cavity–dispersion term which are general in nature. Figure 6 shows a plot of the relative contribution of cavity formation and solute–solvent interactions to solvation on QPTS for a homologous series of *n*-alcohols (butanol to octanol) at 414.4 K. The alcohols show strong dipole and hydrogen-bond acid properties on this phase which are virtually constant reflecting the fact that the explanatory variables are constant as a function of molecular weight for the alcohols studied. The cavity–dispersion term increases linearly with increasing Van der Waals volume indicating that increasing the size of the solute favors

TABLE 4

Relationship between the cavity–dispersion term calculated according to the solvation models of Poole and Abraham for 1-nitropentane

Stationary phase	Temperature (°C)	Log K_L (cavity–dispersion) term			Regression equation [a]		
		Poole	Abraham	Difference	Slope (m)	Intercept (z)	r^2
OV-105	141.2	1.7470	1.5905	0.157	1.004	0.156	1.000
	121.2	1.9069	1.7502	0.157			
	101.2	2.1538	1.9811	0.173			
	81.2	2.4982	2.3214	0.177			
	61.2	3.0417	2.8826	0.159			
OV-17	141.2	1.5989	1.4739	0.125	1.004	0.124	1.000
	121.2	1.7897	1.6679	0.122			
	101.2	2.0160	1.8661	0.150			
	81.2	2.3320	2.1998	0.132			
	61.2	2.8832	2.7517	0.132			
QF-1	141.2	1.4661	1.2331	0.233	1.080	0.136	1.000
	121.2	1.6210	1.3810	0.240			
	101.2	1.8560	1.5852	0.271			
	81.2	2.1836	1.8919	0.292			
	61.2	2.7250	2.4008	0.324			
OV-225	141.2	1.2708	1.1351	0.136	1.104	0.020	1.000
	121.2	1.4405	1.2941	0.146			
	101.2	1.7048	1.5143	0.191			
	81.2	2.0624	1.8461	0.216			
	61.2	2.6601	2.3952	0.265			
CW-20M	141.2	1.2332	1.0685	0.165	1.176	−0.026	0.999
	121.2	1.3662	1.2003	0.166			
	101.2	1.6422	1.4001	0.242			
	81.2	1.8849	1.6216	0.263			
	61.2	2.3958	2.0636	0.332			
THPED	141.2	1.4872	1.2993	0.188	1.078	0.088	0.996
	121.2	1.6603	1.4334	0.227			
	101.2	1.8373	1.6228	0.215			
	81.2	2.0744	1.8876	0.187			
	61.2	2.6512	2.3554	0.296			
TCEP	141.2	0.8416	0.5423	0.299	1.155	0.209	0.999
	121.2	0.9280	0.6374	0.291			
	101.2	1.1078	0.7700	0.338			
	81.2	1.3222	0.9585	0.364			
	61.2	1.6756	1.2730	0.403			
DEGS	141.2	0.8543	0.5867	0.268	1.172	0.150	0.999
	121.2	1.0116	0.7471	0.265			
	101.2	1.2556	0.9547	0.301			
	81.2	1.5437	1.1835	0.360			
	61.2	2.0635	1.6311	0.432			
QPTS	141.2	1.3572	1.0748	0.282	0.973	0.308	1.000
	121.2	1.4371	1.1653	0.272			
	101.2	1.5793	1.3047	0.275			
	81.2	1.7473	1.4757	0.272			
	61.2	2.0381	1.7784	0.260			

[a] Eqn. 5.

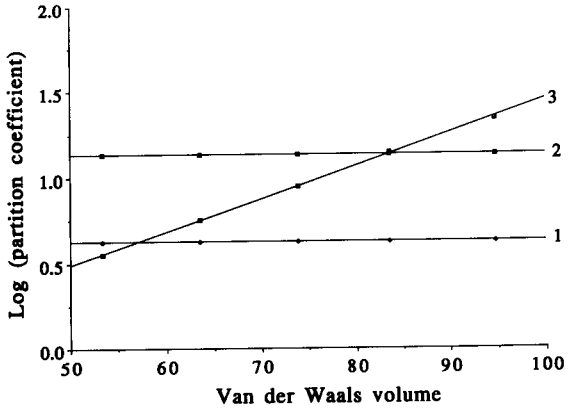

Fig. 6. Plot of the relative contribution of different intermolecular interactions and the cavity term to the solvation of a homologous series of *n*-alcohols at 414.4 K in QPTS as a function of the solute's Van der Waals volume. Identification: $1 = s\pi_2^H$; $2 = a\alpha_2^H$; and $3 = c + l \log L^{16}$.

transfer from the gas phase to the stationary phase since the contribution from dispersion interactions between solute and solvent increases faster than the work required to form a cavity of suitable size in the solvent. This is true for any temperature in the range studied in this report. It is possible to make a comparison between the models proposed by Abraham and by Poole, at least in terms of their calculation of the cavity–dispersion contribution and the sum of the polar solute–solvent interactions to the solvation process as a function of temperature which, until now, has not been possible. A comparison will be made in terms of the contribution of the overall gas–liquid partition coefficient characteristic of the cavity–dispersion term and the polar solute–solvent interaction term to the solvation process for both models. In principle for the cavity–dispersion contribution to the solvation process the following expression can be written to define the equivalence between the two models

$$\Delta G_S^{Soln}(HC)^V + \Delta G_{SQ}^P(X) = -2.303RT(c + l \log L^{16}). \quad (4)$$

There are several features characteristic of the agreement between the two models that we will illustrate by some typical examples. Consider the plot of log K_L (cavity–dispersion) as a function of the reciprocal of temperature for ethylbenzene

TABLE 5

Coefficients for the fit of the gas–liquid partition coefficient, Eqn. 5, to Abraham's and Poole's model of the cavity–dispersion term for the solvation process

Stationary phase	Solute	Slope (m)	Intercept (z)	Correlation coefficient (r^2)
OV-105	Hexan-1-ol	0.925	0.240	1.000
	Dioxane	0.954	0.219	0.995
OV-17	Hexan-l-ol	0.917	0.222	1.000
	Dioxane	0.926	0.219	0.997
QF-1	Hexan-l-ol	0.983	0.184	1.000
	Dioxane	1.052	0.171	0.996
OV-225	Hexan-l-ol	1.013	0.085	1.000
	Dioxane	1.095	o.061	0.997
CW-20M	Hexan-l-ol	1.041	0.075	0.999
	Dioxane	1.168	0.037	0.996
THPED	Hexan-l-ol	0.960	0.197	0.994
	Dioxane	1.035	0.166	0.994
TCEP	Hexan-l-ol	0.981	0.188	0.999
	Dioxane	1.010	0.235	0.993
DEGS	Hexan-l-ol	1.027	0.152	0.999
	Dioxane	1.099	0.213	0.993
QPTS	Hexan-l-ol	0.833	0.372	1.000
	Dioxane	0.825	0.384	0.964

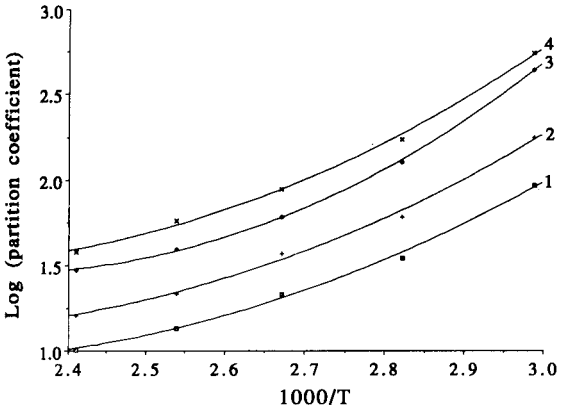

Fig. 7. Plot of the gas–liquid partition coefficient for the cavity–dispersion term contribution to solvation of ethylbenzene in OV-17 and CW-20M as a function of temperature. Identification: 1 = Abraham's model CW-20M; 2 = Poole's model CW-20M; 3 = Abraham's model OV-17; and 4 = Poole's model OV-17.

on OV-17 and CW-20M, Fig. 7. Both models predict the same trend in log K_L for the cavity–dispersion term as a function of temperature. The numerical value calculated by Poole's model is always slightly larger and in most cases the numerical difference between the two sets of calculated values is reasonably constant and independent of temperature. Representative data for 1-nitropentane on all phases are summarized in Table 4. The difference in numerical values, which varies from about 0.0 to 0.5 log units, increases in magnitude as the polarity of the stationary phase increases. The cavity–dispersion term contribution to solvation as calculated in both models is well correlated by the expression

$$\log K_L(\text{cavity–dispersion})^{\text{Poole}} = m \log (c + l \log L^{16}) + z \quad (5)$$

as demonstrated by the data in Table 4 and additional data for hexan-1-ol and dioxane summarized in Table 5. The slopes are generally close to 1.00 indicative of the simple proportionality between the two models. In a few cases, for example, 1-nitropentane on OV-225, CW-20M, TCEP and DEGS, the slopes exceed 1.10 indicating that there is a slight temperature dependence in the cavity–dispersion term as calculated for the two models; in this case Poole's model predicts a larger contribution for the cavity–dispersion term at lower temperatures compared to Abraham's model. It can be concluded then that the models proposed by Abraham and by Poole demonstrate the same general trend as a function of temperature for the contribution of the cavity–dispersion term to solvation but the two models differ in the numerical value for the contribution of the cavity–dispersion term to solvation in a manner which seems largely independent of temperature but dependent on the identity of the stationary phase.

The equivalence of the total contribution of the polar solute–solvent interactions to the solvation process for both models can be expressed as follows

$$\Delta G_S^{\text{Int}}(X) = -2.303RT\left(rR_2 + s\pi_2^H + a\alpha_2^H + b\beta_2^H\right) \quad (6)$$

In this case both models predict the same general trend in the gas–liquid partition coefficient for polar interactions as a function of temperature but the numerical differences between the calculated values for the two models are not independent of temperature. The general trends are illustrated in Fig. 8 for the plot of the gas–liquid partition coefficients as a function of temperature

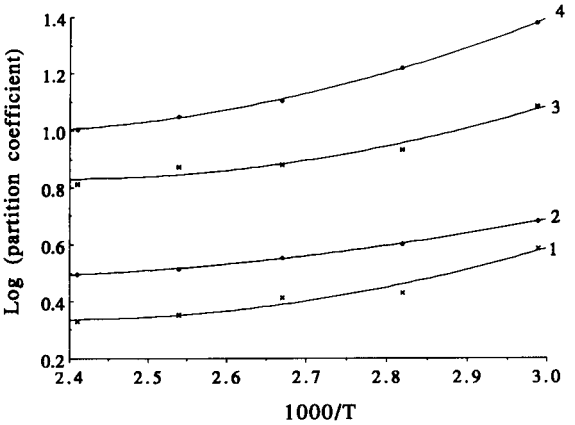

Fig. 8. Plot of the gas–liquid partition coefficient for the contribution of polar solute–solvent interactions to the solvation of dioxane in OV-17 and CW-20M as a function of temperature. Identification: 1 = Poole's model OV-17; 2 = Abraham's model OV-17; 3 = Poole's model CW-20M; and 4 = Abraham's model CW-20M.

TABLE 6

Relationship between the polar solute–solvent interaction term calculated according to Poole's model and Abraham's model for 1-nitropentane

Stationary phase	Temperature (°C)	Log K_L (polar interactions)			Regression equation [a]		
		Poole	Abraham	Difference	Slope (m)	Intercept (z)	r^2
OV-105	141.2	0.1765	0.3358	−0.159	2.068	−0.521	0.986
	121.4	0.2011	0.3459	−0.145			
	101.2	0.2126	0.3583	−0.146			
	81.2	0.2505	0.3770	−0.127			
	61.2	0.3350	0.4111	−0.076			
OV-17	141.2	0.4422	0.6125	−0.170	1.345	−0.387	0.990
	121.2	0.4803	0.6351	−0.155			
	101.2	0.5262	0.6944	−0.168			
	81.2	0.6275	0.7585	−0.131			
	61.2	0.7790	0.8597	−0.081			
QF-1	141.2	0.6472	0.9494	−0.302	1.019	−0.320	0.999
	121.2	0.7086	1.0042	−0.296			
	101.2	0.7750	1.0801	−0.305			
	81.2	0.8953	1.1926	−0.297			
	61.2	1.0892	1.3816	−0.292			
OV-225	141.2	1.0195	1.1380	−0.119	0.535	0.406	0.968
	121.2	1.0343	1.1647	−0.130			
	101.2	1.0348	1.1979	−0.163			
	81.2	1.0705	1.2465	−0.176			
	61.2	1.1219	1.3302	−0.208			
CW-20M	141.2	1.1020	1.2107	−0.109	0.614	0.367	0.977
	121.2	1.1684	1.2609	−0.093			
	101.2	1.1639	1.3326	−0.169			
	81.2	1.2735	1.4770	−0.204			
	61.2	1.3981	1.6745	−0.276			
THPED	141.2	0.8195	1.0559	−0.236	2.380	−1.697	0.876
	121.2	0.7906	1.0718	−0.281			
	101.2	0.9572	1.0946	−0.137			
	81.2	1.0847	1.1481	−0.063			
	61.2	1.1042	1.1938	−0.090			
TCEP	141.2	1.4487	1.7356	−0.287	0.913	−0.139	0.994
	121.2	1.5634	1.8392	−0.276			
	101.2	1.6644	1.9929	−0.329			
	81.2	1.8652	2.2255	−0.360			
	61.2	2.1947	2.5334	−0.339			
DEGS	141.2	1.2574	1.5228	−0.265	0.757	0.099	0.938
	121.2	1.2869	1.5567	−0.270			
	101.2	1.2889	1.5861	−0.297			
	81.2	1.3346	1.6555	−0.321			
	61.2	1.4046	1.7030	−0.298			
QPTS	141.2	1.1699	1.4246	−0.255	0.936	−0.161	0.999
	121.2	1.2637	1.5260	−0.262			
	101.2	1.3724	1.6276	−0.255			
	81.2	1.5555	1.8431	−0.288			
	61.2	1.8611	2.1593	−0.298			

[a] Eqn. 7.

for dioxane on OV-17 and CW-20M and by the representative data for 1-nitropentane on all stationary phases summarized in Table 6. The numerical value of the gas–liquid partition coefficient is always larger for Abraham's model. The correlation between the gas–liquid partition coefficients derived for the contribution of polar solute–solvent interactions to solvation for both models can be expressed by Eqn. 7

$$\log K_L(\text{polar interactions})^{\text{Poole}} = m\left(rR_2 + s\pi_2^H + a\alpha_2^H + b\beta_2^H\right) + z \quad (7)$$

and are generally good but the slopes frequently deviate from 1.00, in most cases the slopes being

TABLE 7

Calculation of the differences in the polar interaction term contribution to solvation in OV-17 and TCEP for the various representations of Poole's and Abraham's solvation models

Solute	Temperature (°C)	Difference in log K_L(X) for polar interactions			
		OV-17		TCEP	
		Eqn. 6	Eqn. 9	Eqn. 6	Eqn. 9
Ethylbenzene	141.2	0.187	0.041	0.380	0.059
	121.2	0.182	0.036	0.302	−0.019
	101.2	0.147	0.001	0.277	−0.044
	81.2	0.147	0.001	0.346	−0.025
	61.2	0.140	−0.006	0.338	0.017
Hexan-2-one	141.2	0.113	−0.033	0.133	−0.188
	121.2	0.120	−0.026	0.128	−0.193
	101.2	0.113	−0.033	0.154	−0.167
	81.2	0.089	−0.057	0.179	−0.142
	61.2	0.059	−0.087	0.194	−0.127
1-Nitropentane	141.2	0.170	0.024	0.282	−0.039
	121.2	0.155	0.009	0.276	−0.045
	101.2	0.168	0.022	0.329	0.008
	81.2	0.131	−0.015	0.360	0.039
	61.2	0.081	−0.065	0.339	0.018
Benzonitrile	141.2	0.227	0.081	0.525	0.204
	121.2	0.230	0.084	0.502	0.181
	101.2	0.244	0.098	0.542	0.221
	81.2	0.221	0.075	0.591	0.270
	61.2	0.228	0.082	0.643	0.322
Dioxane	141.2	0.166	0.020	0.237	−0.084
	121.2	0.161	0.015	0.229	−0.092
	101.2	0.141	−0.005	0.248	−0.073
	81.2	0.172	0.026	0.294	−0.027
	61.2	0.093	−0.053	0.286	−0.035
N-Methylaniline	141.2	0.254	0.108	0.569	0.248
	121.2	0.277	0.131	0.449	0.128
	101.2	0.253	0.107	0.579	0.258
	81.2	0.235	0.089	0.622	0.301
	61.2	0.259	0.113	0.758	0.437
Hexan-1-ol	141.2	0.084	−0.062	0.185	−0.136
	121.2	0.075	−0.071	0.163	−0.158
	101.2	0.072	−0.074	0.161	−0.160
	81.2	0.053	−0.093	0.157	−0.164
	61.2	0.000	−0.146	0.123	−0.198

greater than 1.00 for the weakly polar phases and less than 1.00 for the polar phases as indicated in Table 6. This corresponds to the trends illustrated in Fig. 8 with the weakly polar phase OV-17 showing a smaller numerical difference in the calculated results at lower temperatures and the more polar phase CW-20M the opposite trend. It is obvious that the observed trends are a direct result of the numerical difference in the cavity–dispersion term for the two models which is impressed on the polar interaction term since both models are able to predict solute gas–liquid partition coefficients adequately well. At this time the origin of the disagreement between the two models cannot be finalized until methods of deconvoluting the individual polar interactions contained in the $\Delta G_S^{Int}(X)$ term are finalized.

The numerical difference in the cavity–dispersion term for the two models was shown earlier to be dependent on the identity of the solvent but reasonably independent of the identity of the solute and temperature. Of the terms in Eqn. 5 only the c term possesses these properties and agreement between the two models could be achieved by separating the c term into a cavity–dispersion component and a polar interaction component. To evaluate this hypothesis some representative data for seven varied solutes on the moderately polar phase OV-17 and the polar phase TCEP at all temperatures are summarized in Table 7. If it is assumed that the c term can be separated into two parts c_1 and c_2, with c_1 being independent of temperature and defined by Eqn. 8

$$c_1 = \log K_L(HC)_S^V + \log K_L(X)_{SQ}^P - (c + l \log L^{16}) \quad (8)$$

This provides average values for c_1 of 0.146 for OV-17 and 0.321 for TCEP. The equivalence between the two models for the contribution of polar solute–solvent interactions to solvation can then be redefined as

$$\Delta G_S^{Int}(X) = -2.303RT(c_2 + rR_2 + s\pi_2^H + a\alpha_2^H + b\beta_2^H) \quad (9)$$

and compared to Eqn. 6. The residual contribution, the difference between the values predicted by the two models, is much smaller based on Eqn. 9 as demonstrated by the data in Table 7 and is no greater than the experimental error associated with the original data. The above construct between the two models can be easily justified since the c term has no clearly defined molecular basis. As well as a contribution to the cavity term it may contain a contribution from the fitting of the mathematical model to the data generated by the uncertainty in the absolute values of the explanatory variables. There is also uncertainty associated with the use of $\Delta G_{SQ}^P(X)$ as an absolute parameter to represent the sum of the polar interactions in a non-polar solvent. Numerically small changes could be expected by adopting a different reference phase. For aromatic solutes, for example, a difference in $\Delta G^P(X)$ of 0.030–0.200 kcal mol^{-1}, corresponding to log K_L = 0.017–0.111 at 121°C was observed when Apolane-87 was substituted for squalane as the reference non-polar solvent [8]. Constructively, it can be said that the two models differ by an approximately constant amount in the relative proportion of the solvation energy accredited to the cavity–dispersion term and polar solute–solvent interaction term. This difference could result from properties of either or both models. Trends in the cavity–dispersion term are not affected by this difference, only the numerical value of the contribution, but trends in the contribution of polar solute–solvent interactions to the solvation process can be significantly different between the two models attributable to the numerical difference in the values for the cavity–dispersion term.

REFERENCES

1 R.V. Golovnya and T.A. Misharina, J. High Resolut. Chromatogr., 3 (1980) 4 and 51.
2 R.V. Golovnya and B.M. Polanuer, J. Chromatogr., 517 (1990) 51.
3 J.A. Yancey, J. Chromatogr. Sci., 23 (1985) 161 and 370.
4 K.K. Unger, Packings and Stationary Phases in Chromatographic Techniques, Marcel Dekker, New York, NY, 1990.
5 H. Rotzsche, Stationary Phases in Gas Chromatography, Elsevier, Amsterdam, 1991.

6 C.F. Poole and S.K. Poole, Chem. Rev., 89 (1989) 377.
7 C.F. Poole and S.K. Poole, Chromatography Today, Elsevier, Amsterdam, 1991.
8 C.F. Poole, T.O. Kollie and S.K. Poole, Chromatographia, 34 (1992) 281.
9 M.H. Abraham, G.S. Whiting, R.M. Doherty and W.J. Shuely, J. Chem. Soc. Perkin Trans. 2, (1990) 1451.
10 M.H. Abraham, G.S. Whiting, R.M. Doherty and W.J. Shuely, J. Chromatogr., 518 (1990) 329.
11 M.H. Abraham, G.S. Whiting, R.M. Doherty and W.J. Shuely, J. Chromatogr., 587 (1991) 213 and 229.
12 M.H. Abraham and G.S. Whiting, J. Chromatogr., 594 (1992) 229.
13 M.H. Abraham, G.S. Whiting, R.M. Doherty, W.J. Shuely and P. Sakellariou, Polymer, 33 (1992) 2162.
14 J. Li, A.J. Dallas and P.W. Carr, J. Chromatogr., 517 (1990) 103.
15 J. Li, Y. Zahng, A.J. Dallas and P.W. Carr, J. Chromatogr., 550 (1991) 101.
16 J. Li, Y. Zhang and P.W. Carr, Anal. Chem., 64 (1992) 210.
17 J. Li, Y. Zhang, H. Ouyang and P.W. Carr, Am. Chem. Soc. J., 114 (1992) 9813.
18 T.O. Kollie and C.F. Poole, J. Chromatogr., 550 (1991) 213.
19 T.O. Kollie and C.F. Poole, J. Chromatogr., 556 (1991) 457.
20 T.O. Kollie, C.F. Poole, M.H. Abraham and G.S. Whiting, Anal. Chim. Acta, 259 (1992) 1.
21 T.O. Kollie and C.F. Poole, Chromatographia, 33 (1992) 551.
22 R.A. Pierotti, Chem. Rev., 76 (1976) 717.
23 M.H. Abraham, P.L. Grellier, I. Hamerton, R.A. McGill, D.V. Prior and G.S. Whiting, Faraday Disc. Chem. Soc., 85 (1988) 107.
24 R.W. Taft, J.-L.M. Abboud, M.J. Kamlet and M.H. Abraham, J. Solution Chem., 14 (1985) 153.
25 M.J. Kamlet, J.-L.M. Abboud and R.W. Taft, Prog. Phys. Org. Chem., 13 (1981) 485.
26 M.H. Abraham, G.S. Whiting, R.M. Doherty and W.J. Shuely, J. Chem. Soc. Perkin Trans. 2, (1990) 1851.
27 U. Weidlich, H.-J. Röhm and J. Gmehling, J. Chem. Eng. Data, 32 (1987) 450.
28 B.R. Kersten, S.K. Poole and C.F. Poole, J. Chromatogr., 468 (1989) 235.
29 S.K. Poole and C.F. Poole, J. Chromatogr., 500 (1990) 329.
30 K.G. Furton and C.F. Poole, J. Chromatogr., 399 (1987) 47.
31 M.H. Abraham, J. Andonian-Haftvan, I. Hamerton, C.F. Poole and T.O. Kollie, J. Chromatogr., in press.

Analytica Chimica Acta, 282 (1993) 19–31
Elsevier Science Publishers B.V., Amsterdam

Qualitative and quantitative response characteristics of a capillary gas chromatograph/ion mobility spectrometer to halogenated compounds

Zeev Karpas [1], Yuan-Feng Wang and Gary A. Eiceman
Chemistry Department, New Mexico State University, Las Cruces, NM 88003 (USA)

(Received 26th January 1993; revised manuscript received 26th April 1993)

Abstract

The response of a capillary column gas chromatograph/ion mobility spectrometer (GC/IMS) system to chlorinated and brominated alkanes and alkenes in nitrogen, air and nitrogen/CO_2 mixtures was studied. Product ions were formed through dissociative electron capture processes or charge transfer reactions, yielding chloride or bromide ions. The quantitative response was shown to depend on the composition of the carrier gas in which atmospheric pressure ionization processes occurred as well as on the IMS cell temperature. Large variations in the quantitative response of the GC/IMS to different halogenated compounds were observed. The results were compared to those reported for the doped electron capture detector (ECD). Practical implications of the GC/IMS system as a monitor and detector for halogenated aliphatic compounds are discussed.

Keywords: Gas chromatography; Capillary GC; Ion mobility spectrometer; Halogenated compounds

Since inception in 1970, ion mobility spectrometry (IMS) has been regarded as a potentially unique detector for gas chromatography [1]. In particular, IMS was considered attractive due to its parallel response with the electron capture detector (ECD); i.e. both are sensitive to compounds containing electronegative moieties [2]. However, IMS has two major advantages over the ECD detector: (a) qualitative information can be obtained on the types of negative ions formed, in addition to quantitative data supplied also by the ECD; and (b) the ion mobility spectrometer operates with a variety of carrier and drift gases, particularly with air, while the performance of the ECD is seriously degraded by air.

Studies on the response of ECD detectors to various halogenated compounds have indicated that large differences existed in its sensitivity toward compounds of this chemical class [3,4]. For example, the ECD response to carbontetrachloride was about four orders of magnitude greater than that to methylchloride [3]. Such differences were attributed to a combination of thermodynamic and kinetic factors as detailed in recent reviews and summaries of ECD theory [5,6; and references cited therein]. Thermodynamics control the energetics of the reaction, such as activation barriers and reaction enthalpies, and kinetic considerations include reaction rates which in turn are determined by parameters such as Franck-Condon factors [5,6].

A particularly interesting modification of ECD parameters was to change the supporting atmosphere in the ECD from nitrogen or argon with 5–10% methane through the intentional addition of a dopant reagent gas, such as oxygen, nitrous oxide, trimethylamine and others [3,6–10]. The dopant altered the ionization mechanism, from

Correspondence to: Z. Karpas, Analytical Chemistry Department, Nuclear Research Center, Negev, P.O. Box 9001, Beer-Sheva 84190 (Israel).

solely electron capture processes (electrons are the only negatively charged reactive species in pure nitrogen) to other negative ion–molecule reactions, including charge transfer (dissociative and non-dissociative), clustering and new reaction channels. The relative response of ECD to methylchloride and carbontetrachloride (vida supra) was altered quantitatively and differed by a factor of 18 with addition of only 0.2% oxygen to the nitrogen carrier instead of 10^4 found in pure nitrogen [9]. Addition of oxygen to a heated ECD source induced an equilibrium between electrons and thermally dissociated oxygen ions, which can undergo charge transfer reactions [9]:

$$e^- + O_2 \leftrightarrow O_2^- \quad (1)$$

Likewise, addition of nitrous oxide leads to formation of O^- ions, which are highly reactive:

$$N_2O + e^- \rightarrow O^- + NO \quad (2)$$

These ions can react with carbon monoxide, hydrogen or hydrocarbons; i.e., compounds not normally detected by ECD [11].

Intentional changes in the gas composition in the ionization source of IMS, to enhance sensitivity or selectivity, are also well established [12–15]. For example, reactant chloride ions, from a suitable dopant, increase the sensitivity of the IMS toward vapors of explosives, such as ethyleneglycoldinitrate (EGDN) [12–14]. Doping the ion source of the IMS with acetone improves its selectivity toward organophosphorus compounds, including nerve agents as used in chemical agent monitors [15].

Systematic studies of the quantitative response of the IMS to various substances have been limited [16]. The effects that other compounds in a sample have on the response of the IMS to the target analyte, the "matrix effect", complicate the interpretation of data. One way to overcome this complication is to separate a sample into components prior to its introduction into the ion source of the IMS. Effective preseparation methods include chromatographic techniques, such as supercritical fluid chromatography (SFC) [17], liquid chromatography (LC) [18] and gas chromatography (GC) [19]. This is reminiscent of the original idea of the developers of IMS to utilize the ion mobility spectrometers as sophisticated detectors for GC [1].

Hill and co-workers [20–22] have studied the response of their ion mobility detector (IMD) for capillary gas chromatography to halogenated compounds. Oxygen doping was used [20], so that the response of the detector could be evaluated by either monitoring the increase in the product ion peak or by monitoring the decrease in the reactant ion peak. Calibration curves for hexachloroethane [20] and 2,4-dichlorophenoxyacetic acid [21] were given and the minimum detectable level (MDL) for some halogenated compounds were reported (see below).

Monitoring the presence of halocarbons in general, and substituted methanes in particular, is important in environmental analytical chemistry in discussions of air and water quality. Several of these compounds create a serious health hazard even at relatively low concentrations. For example, the threshold limit values – time weighted average (TLV-TWA) for CBr_4, $CHBr_3$, CCl_4, $CHCl_3$, and $CHCl=CCl_2$ are 0.1, 0.5, 5, 10, and 50 ppm, respectively [23].

Ionization mechanisms in ECD and IMS

In IMS, halogen substituted methanes are ionized through dissociative processes, involving either dissociative electron attachment (Eqn. 3) or dissociative charge transfer (Eqn. 4):

$$e^- + RX \rightarrow [RX]^{*-} \rightarrow X^- + R \quad (3)$$

$$Y^- + RX \rightarrow [RX]^{*-} \text{ or}$$

$$[RXY]^{*-} \rightarrow X^- + R + Y \quad (4)$$

where $R = CH_{3-n}X_n$; X = Cl or Br and $Y = O_2$, $CO_2 \cdot O_2$, etc. In pure nitrogen, there are no negatively charged reactant ions and all ionization processes occur via electrons, as shown in Eqn. 3. In a recent ab initio study, this has been shown to proceed via a concerted electron transfer bond breaking process [24]. Thus, Eqn. 3a may be a better representation of the ion formation process in these compounds:

$$e^- + RX \rightarrow X^- + R \quad (3a)$$

Addition of oxygen or carbon dioxide to nitrogen results in formation of negatively charged

reactant ions, such as O_2^- and O_4^- in oxygen, CO_3^- and CO_4^- in carbon dioxide, and clusters of these ions with water, nitrogen or additional oxygen or CO_2 molecules. Changes in reactant ion species modify the ionization chemistry of nitrotoluene compounds, as demonstrated by Spangler and Lawless [25]. In nitrogen, negative molecular ions (M^-) were formed through electron capture processes and in air, $(M-H)^-$ ions from proton abstraction were dominant. The two types of ions were shown to possess different reduced mobilities and gave distinct mobility spectra. Knighton and Grimsrud [26] have recently proposed that the reaction of negative ions with halogenated methanes proceeds via a "cluster assisted dissociative electron transfer" (CADET) mechanism with a double well potential. According to this hypothesis, the reactant ion (A^-) approaches the halogenated methane (RX), forms a cluster ($A^- \cdot RX$), undergoes internal rearrangement to ($A \cdot X^- \cdot R$) and finally dissociates to ($A \cdot X^- + R$). The product cluster ion is in equilibrium ($A \cdot X^- \leftrightarrow A + X^-$) and yields X^- ions. The factors that control the rates of such reactions include the structure of the reactants and their orientation in the transition complex, the dipole moment and polarizability of the halogenated methane, and thermodynamic factors [26].

Ionization of halomethanes proceeds via either a concerted electron transfer bond breaking mechanism [24], or via an intermediate $[RX]^{*-}$ or $[A \cdot X^- \cdot R]$ [26] ion. If one of the latter is formed, it is short-lived, rapidly dissociates and is not detected in the IMS time scale. Thus, the product ion in both mechanisms is Cl^- from chloromethanes and Br^- from bromomethanes, which can be resolved using IMS. In contrast, resolution of various chloromethanes by IMS is currently impossible since all yield the same product ion. This complicates interpretation of the response of a stand-alone IMS to different halomethanes. On the other hand, chlorometh-

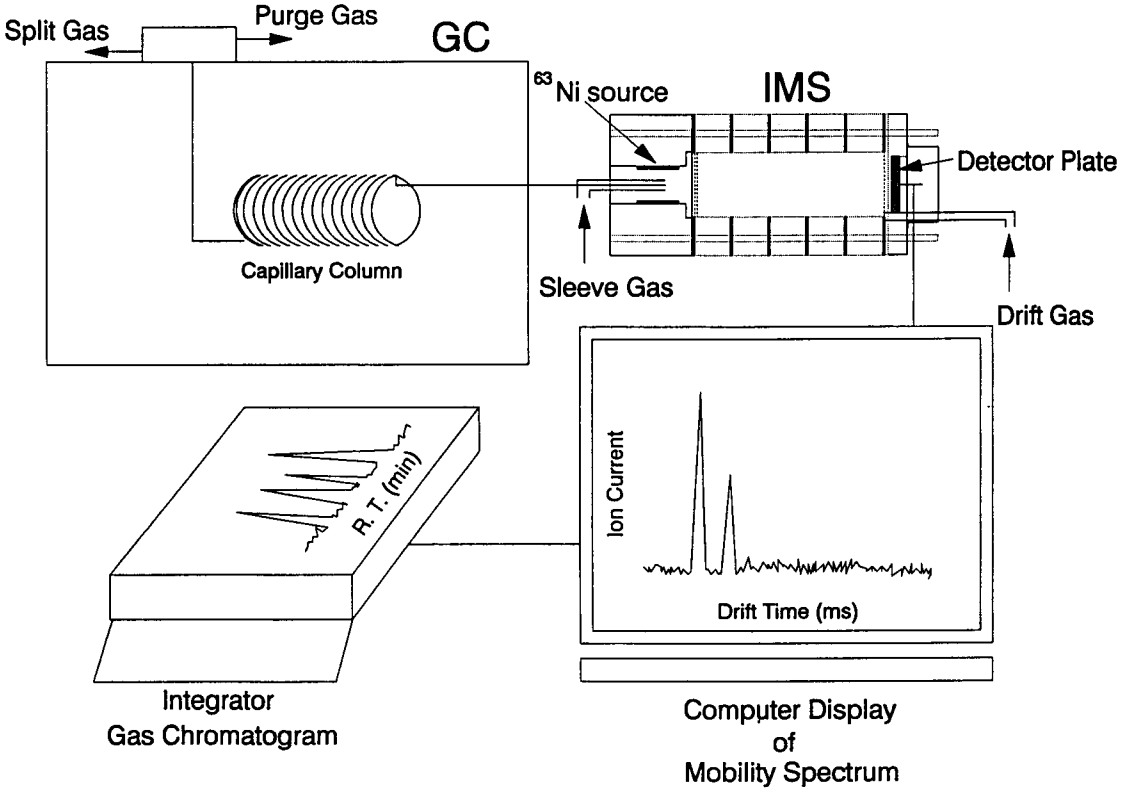

Fig. 1. Schematic of GC/IMS system.

anes may be separated by gas chromatography, so that the different GC retention times, combined with the IMS response, may serve as a means of identifying the substituted halomethanes. The same arguments presented here for halogenated methanes also apply to other halogenated alkanes and alkenes.

The main objective of the present work was to characterize the qualitative and quantitative response of the GC/IMS system with halogen-substituted alkanes and alkenes in selected gases. The effect of changing the reactant ion chemistry was especially interesting, as the sensitivity of the IMS to different compounds of a chemical family might be modified to create a selective detector, or a nondiscriminant detector, by proper control of the ionization processes. Another objective was to gain a better understanding of the reaction mechanisms that govern atmospheric pressure ionization of halocarbons and the formation of negative ions.

EXPERIMENTAL

Apparatus

The apparatus used in this study consisted of Hewlett-Packard Model 5890 gas chromatograph with an ion mobility spectrometer detector, as shown schematically in Fig. 1. The GC was equipped with an injector with a splitting ratio of 1:50 and with a capillary column 26 m long. The IMS cell was thermally insulated with glass pack material, and temperature was controlled using MINCO heaters and a controller (Model CT137). The effluent from the capillary column was introduced with an on-axis design into the center of the ^{63}Ni ionizer ring of the IMS. The end of the capillary column was placed in a concentric glass tube through which a "sleeve gas", with the same composition as the drift gas, helped carry the effluent into the ionization source. A WASP (Graseby Ionics, UK) software and hardware package was used to acquire, average and store the mobility spectra. Gas chromatograms reflected the change in product ion intensity and were recorded by a Hewlett-Packard Model 3390A integrator. Thus, for every gas chromatogram several mobility spectra were acquired. The instrumental and operating parameters of the apparatus are summarized in Table 1.

Reagents and materials

The following chemicals were obtained in high commercial purity and used without further treatment: hexane (Chromopure, Fisher Scientific), methylene chloride, 1,2-dichloroethane and tetrachloroethylene (Baker Analyzed); pentachloroethane (Baker); bromomethane, dibromomethane, bromoform, carbontetrabromide, chloro-

TABLE 1

Instrumental parameter for GC/IMS analysis of halogenated compounds

Gas chromatograph			
Initial temperature:	30°C	Final temperature:	120°C
Initial time:	5 min	Final time:	20 min
Program rate:	5°C/min	Average column flow:	100 mm/s
Injector temperature:	200°C	Split ratio:	50:1
Carrier gas:	Nitrogen		
Ion mobility spectrometer			
Source: 10 mCi ^{63}Ni		Reaction region length: 1 cm	
Drift region length: 3.8 cm		Temperature: 90°C	
Drift region field: 215 V/min		Shutter pulse: 180 μs	
Drift gas flow: 360 ml/min		Drift gas: air, N_2, CO_2/N_2	
Day system			
Scans averaged: 8		Points per spectrum: 512	
Frequency: 40 KHz			

methane, chloroform, carbontetrachloride, 1,1,1-trichloroethane and 2,3-dichloro-1-propene from Aldrich; 1,1,2-trichloroethane and 1,1,2,2-tetrachloroethane (Alltech); trichloroethylene (MCB); carbon dioxide (regular), oxygen, nitrogen (prepurified) and air.

Procedure

Stock solutions of 1 μg/ml were prepared by dissolving the appropriate quantity of the halocarbon compound in hexane. The stock solution was then diluted by hexane to lower concentrations for the experiments. The desired quantity of the sample was taken by injecting the suitable volume (1–10 μl) of the analyte solution (0.5–1000 ng/ml) into the GC inlet port with a 10 μl microsyringe (Hamilton, Reno, NV). Gaseous samples of chloromethane and bromomethane were injected directly into the GC inlet with a 100 μl gas tight syringe (Hamilton).

The optimal operating conditions were determined by a series of preliminary tests and the results are summarized in Table 1. The behavior of chloromethane and bromomethane and their very low response differed from that of the other compounds and they will be studied separately with other gases. This initial work also involved determination of the retention time of each of the compounds on the capillary column at the selected operating conditions, as summarized in Table 2.

The quantitative response of the GC/IMS system was determined by injecting known amounts of each sample, or mixture of easily separable samples, and the recording the integrated GC peak area. The total ion current in a preset region, or window, of the mobility spectrum was integrated. As the product ion from all the chlorinated compounds was the chloride ion and the bromide ion for the brominated compounds, the boundaries of this window were set for each family of chemicals. The quantity of the sample could also be determined from measurement of the maximum product ion signal in the IMS, thus providing a means of verifying the integrator results. Calibration curves of IMS response to the different chemicals were prepared according to this procedure as described in the Results and Discussion section, below.

TABLE 2

Molecular weight, retention time on the capillary column and dipole moment of the halogenated alkanes and alkenes used in the study

	M.W. (amu)	Retention time (min)	Dipole moment [a] (Debye)
Chloromethanes			
CH_3Cl	50.49	0.76	1.87
CH_2Cl_2	84.93	0.94	1.60
$CHCl_3$	119.38	1.20	1.01
CCl_4	153.82	1.70	0
Bromomethanes			
CH_3Br	94.94	0.81	1.81
CH_2Br_2	173.83	1.85	1.43
$CHBr_3$	252.73	5.12	0.99
CBr_4	331.63	11.44	0
Chloroethanes			
CH_2ClCH_2Cl	98.96	1.40	2.06
$CHCl_2CH_2Cl$	133.4	2.54	
CH_3CCl_3	133.4	1.72	1.78
$CHCl_2CHCl_2$	167.85	6.48	1.32
$CHCl_2CCl_3$	202.29	8.64	0.92
Chloroethylenes			
$CHClCCl_2$	131.39	1.88	1.45
CCl_2CCl_2	165.83	3.22	0
Chloropropene			
$CH_2ClCCl{=}CH_2$	110.97	1.92	1.66

[a] From Ref. 32.

RESULTS AND DISCUSSION

The quantitative response of the ion mobility spectrometer was established from measurement of the peak area by the integrator. The product ions, chloride or bromide, have higher mobilities than the reactant ions in air or CO_2, and appeared in the mobility spectrum before the reactant ion peak (RIP), i.e. with shorter drift times. An example of this may be seen in Fig. 2, where the chloride ion produced from CCl_4 (Fig. 2b) had a shorter drift time than the reactant ions present in 2.5% CO_2 in nitrogen (Fig. 2a). The area of the product ion peak formed from injec-

tion of a given amount of the target analyte in the GC port was recorded as each compound eluted from the GC column. Necessarily there is a transient of concentration (pulse or spike) and IMS spectra acquired during the elution of each compound reflected this. An example of this is shown in Fig. 3, where at first only the RIP is seen (frame a), but as the sample (bromoform in this case) elutes from the column, the product ion (Br^-) appears (frame b) and increases to a maximum intensity (frame c) before it begins to decrease (frame d) and disappears (frame e). As the product ion signal increases the RIP decreases and vice versa. In the above example, this process took 19 s for the whole of the bromoform spike to pass through the IMS detector. The largest product ion peak height (or area) as in Fig. 3c was also used in some cases to quantify the response of IMS to that amount of analyte.

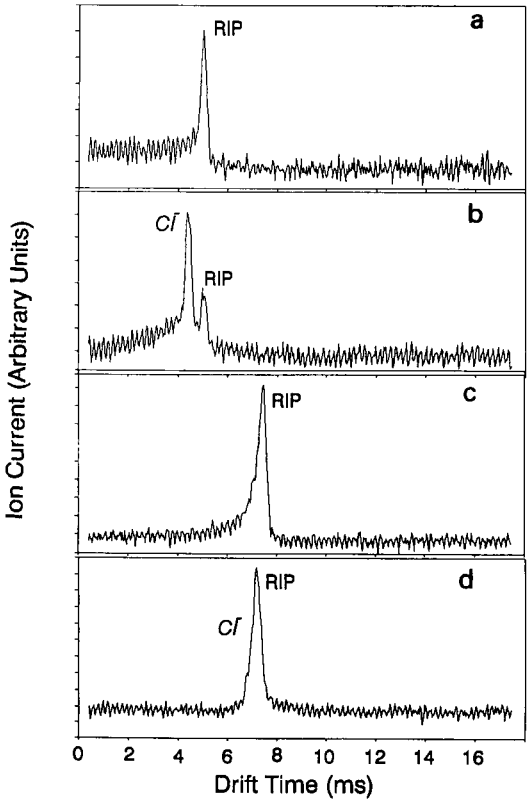

Fig. 2. Mobility spectra in CO_2/N_2 mixtures. (a) the RIP in nitrogen with 2.5% CO_2; (b) RIP and chloride ions in 2.5% CO_2 after injection of 160 ng CCl_4; (c) The RIP in nitrogen with 8.8% of CO_2; (d) RIP and chloride ions (overlapping) in 8.8% CO_2 after injection of 160 ng CCl_4.

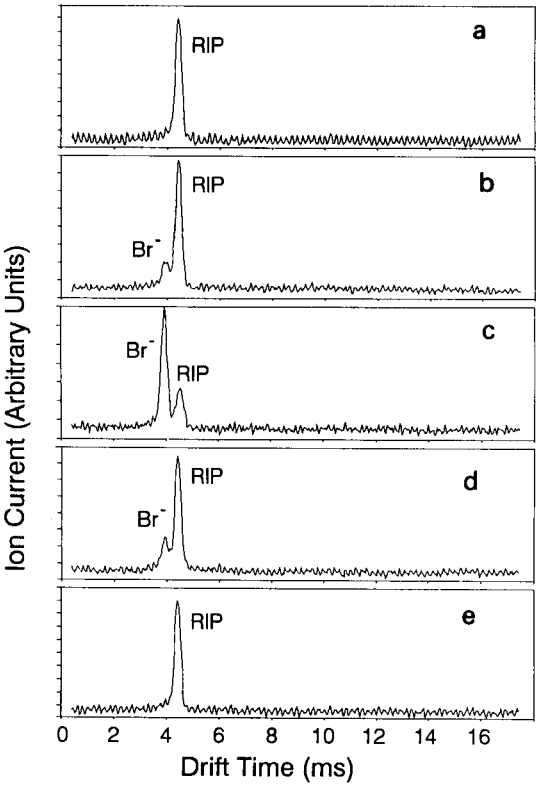

Fig. 3. Mobility spectra recorded as a spike of bromoform eluted from the GC column. (a) reactant ion, at time t; (b) Br^- ions begin to form ($t+3$ s); (c) Br^- reaches maximum intensity ($t+9$ s); (d) Br^- begins to decay ($t+15$ s); (e) RIP as bromoform completely eluted ($t+19$ s).

The qualitative response of the IMS to a given chemical was determined from the drift time of the product ion peak arising from the analyte. As mentioned above, all chloromethanes yielded only chloride ions and all bromomethanes formed only bromide ions. However, the drift time of the reactant and product ions depended on the composition of the drift gas. For example, in nitrogen the drift times were 3.525 ms for the chloride ion and 3.70 ms for the bromide ion, while in 2.5% CO_2/N_2 they were 4.075 and 4.125 ms, respectively. This was due mainly to the formation of clusters between the product ion and drift gas molecules. The same factors affected the drift time of the reactant ions, so there may be cases,

like using an 8.8% mixture of CO_2/N_2, when the reactant (Fig. 2c) and product ions cluster so heavily that their drift times coincide (Fig. 2d).

In a previous IMS study of some halogenated alkanes in air at nearly ambient temperature, halothane ($CF_3CHClBr$), enflurane ($CHClFCF_2OCHF_2$) and isoflurane ($CF_3CHClOCHF_2$), were observed to form chloride or bromide ions at low concentrations. However, at higher concentrations they readily clustered to form MX^- ions, where M is one of the above mentioned molecules and X = Cl or Br [27]. Raising the temperature to 90°C dissociated the halothane cluster ions. In the present work MX^- cluster ions, where M is one of the compounds from Table 2, were not observed at 90°C. This is probably due to lack of attractive sites for nucleophilic attack in these compounds as well as to properties such as the dipole moment and polarizability of the compounds.

Effect of temperature

The effect of drift tube temperature on IMS response to several halogen substituted methanes was examined in different reagent gases. As seen in Fig. 4, there was no significant temperature dependence for the peak area of the product ion from bromoform in nitrogen between 60 and 100°C. In contrast, with 3.2% of carbon dioxide were added to nitrogen or when air was used, the response of the IMS increased with temperature (Fig. 4). These results reflect the effect of the different product ion formation processes shown above in Eqns. 3 and 4. In nitrogen, product ion formation through electron attachment processes was not significantly affected by drift tube temperature. However, when product ion formation occurred through ion–molecule processes, the effect of temperature was pronounced. This may be due to the additional kinetic energy of the reactants to overcome activation energy barriers or to increasing the collision frequency. The major effect, however, was because the reactant ions were not only core ions (O_2^- or CO_4^-, for example), and were a mixture of clustered ions. Raising the temperature reduces the extent of clustering, enabling the reactant ion to approach the analyte

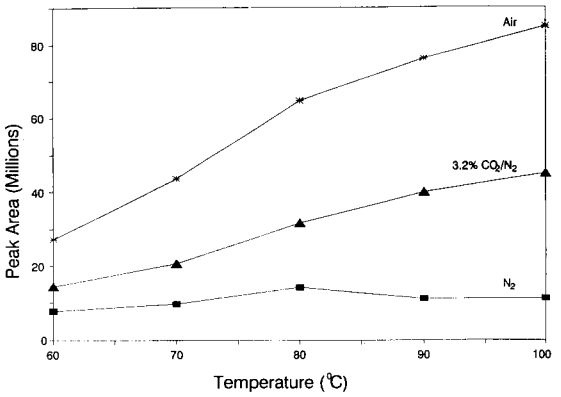

Fig. 4. Temperature effect in nitrogen, CO_2–nitrogen and air, for injection of bromoform.

molecule more closely and to transfer its charge with greater effectiveness (Eqn. 4).

This hypothesis can be tested directly by mass spectrometric ion identifications. Unfortunately this technique was not available to us, so a somewhat less direct way, based on the temperature dependence of the reduced mobility, was employed. The mobility, K, of an ion is determined from Eqn. 5:

$$K = d/(Et) \tag{5}$$

where d is the length of the drift region (distance between the shutter grid and collector plate), t is the time needed for the ion to traverse this distance and E is the electric field strength in the drift region. The reduced mobility, K_0, is obtained by normalizing the mobility to standard temperature (T, 273K) and pressure (P, 760 Torr) conditions, and should therefore not depend on the temperature.

$$K_0 = K(273/T)(P/760)$$
$$= d/(Et)(273/T)(P/760) \tag{6}$$

A change in the reduced mobility with temperature is indicative of a change in the ion identity. If raising the drift tube temperature causes declustering, as assumed above, it should be accompanied by an increase in the reduced mobility. The measured drift times of the reactant ions in CO_2–N_2 mixtures with 2.5% and 8.8% CO_2 in the temperature range 60–110°C and the calculated reduced mobilities taking $P = 660$ Torr, d

= 3.8 cm and $E = 215$ V/cm, and calculated according to Eqn. 6, are shown in Table 3. The reduced mobility increased in both mixtures by about 5% with the temperature in this range, supporting the assumption that the enhanced response of the IMS at higher temperatures arose from declustering of the reactant ions. A similar line of reasoning was used by Rokushika et al. [28] to explain changes in the reduced mobility of their reactant ions in pure carbon dioxide.

Naturally, in pure nitrogen, where free electrons are the reactant species, changes in drift tube temperature are irrelevant to declustering, and should not significantly influence the quantitative response of the IMS, as observed.

Effect of CO_2 concentration

Clustering of the reactant ions is also manifested in the effect that the CO_2 concentration has on the drift time of the reactant ions, as seen in Fig. 5b. In their drift tube–mass spectrometric study, Ellis et al. [29] have shown that in CO_2 at 25°C and 762 Torr two families of cluster ions were formed: $CO_4^- \cdot (CO_2)_n$ and $CO_4^- \cdot (CO_2)_n \cdot H_2O$, with maximum abundances for $n = 6$ and $n = 5$, respectively. CO_4^- can probably be better represented by $CO_2 \cdot O_2^-$. Increasing the temperature to 150°C changed the cluster size distribution, totally eliminating the water clusters and giving a maximum at $n = 0$ for the former type of clusters. As CO_2 is more polarizable than nitrogen or oxygen (α_p = 2.59, 1.76 and 1.60 cm^{-24}, respectively), the ion-induced dipole interactions of the reactant ions with the drift gas containing

TABLE 3

Reduced mobiltiy of the reactant ions in CO_2/nitrogen mixtures as a function of IMS cell temperature (calculation based on $E = 215$ V/cm, $d = 3.8$ cm, $P = 660$ Torr)

Temp. (°C)	K_0	
	2.5% CO_2	8.8% CO_2
60	2.54	2.01
70	2.52	1.99
80	2.55	2.03
90	2.61	2.05
100	2.64	2.07
110	2.68	2.13

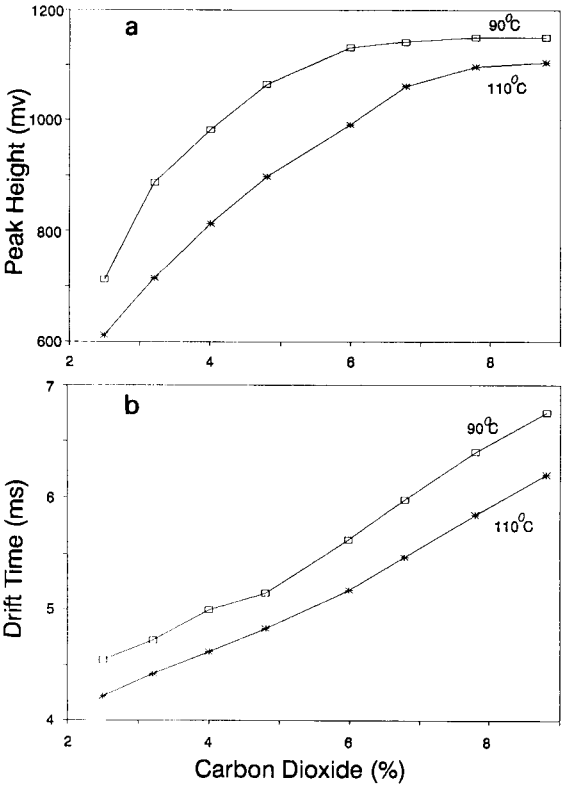

Fig. 5. Effect of CO_2 concentration on (a) RIP peak height; (b) RIP drift time.

CO_2 are stronger, forming clusters that hinder the movement of all ions along the drift region of the IMS [30]. Here too the effect of temperature on the drift time of the reactant ions is seen in the difference between the drift times at 90 and 110°C. Thus, the drift time is affected by a temperature increase of 20°C to the same extent that decreasing the CO_2 concentration by about 1.5%. Concomitant with the change in drift time, increasing the CO_2 concentration also affected reactant ions formation, until saturation was reached at about 8% CO_2 in nitrogen (Fig. 5a).

Response of GC / IMS to halogenated alkanes and alkenes

The quantitative response of the GC/IMS was determined for fourteen halogenated compounds in nitrogen, air and nitrogen doped with carbon dioxide (2.5–8.8%). The list of compounds, chlorinated and brominated methanes, chlorinated

ethanes and ethylenes and 2,3-dichloropropene, their molecular weight, retention times and dipole moments are shown in Table 2.

Nitrogen. The quantitative response in nitrogen of the IMS detector to the compounds listed in Table 2 is shown in Fig. 6. As a first approximation, there appears to be a correlation between the number of chlorine atoms in the molecule and the response of the GC/IMS to compounds of the latter group, in accordance with the response of an ECD detector [9]. The response to dichloromethane and 1,2-dichloroethane was not measurable even with injection of 1000 ng (delivery of 20 ng to IMS) of the compound and they were not shown in Fig. 6. The trichloroethanes gave a weaker response than other trichloro compounds like chloroform or trichloroethylene (TCE). In a compilation of ECD [6,9] and flowing afterglow Langmuir probe (FALP) [31] responses to chlorinated compounds similar incongruities were noted, and rationalized as arising from kinetic and thermodynamic factors. It is interesting to note that the strong response of the GC/IMS system to CCl_4 and CH_2Br_2 is in accordance with the ECD [6,9] and FALP [31] responses to these compounds. This is probably due to their large cross section for electron capture, as electrons are the only reactive species in nitrogen.

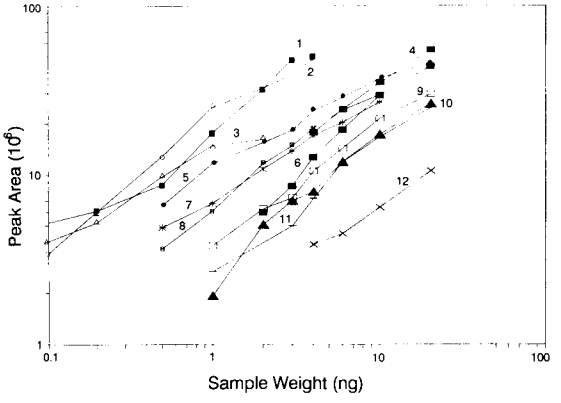

Fig. 6. Quantitative response of IMS to chlorinated alkanes and alkenes in nitrogen. The numbers correspond to (1) CCl_4, (2) CH_2Br_2, (3) $CHCl_2CCl_3$, (4) CH_3CCl_3, (5) CCl_2CCl_2, (6) $CHCl_3$, (7) $CHBr_3$, (8) CBr_4, (9) $CHCl_2CHCl_2$, (10) $CHClCCl_2$, (11) $CH_2ClCCl{=}CH_2$, (12) $CHCl_2CH_2Cl$, (13) CH_2ClCH_2Cl, (14) CH_2Cl_2.

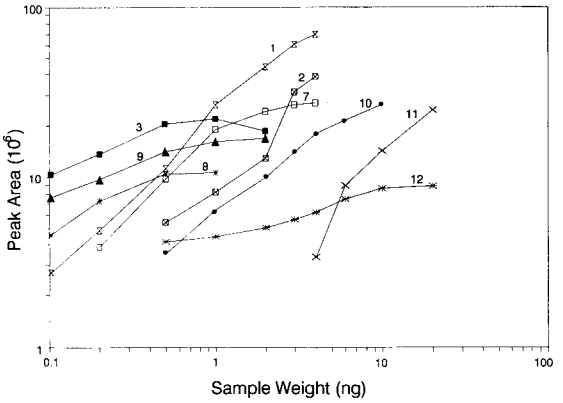

Fig. 7. Quantitative response of IMS to chlorinated alkanes and alkenes in nitrogen/CO_2. The numbers correspond to (1) CCl_4, (2) CH_2Br_2, (3) $CHCl_2CCl_3$, (4) CH_3CCl_3, (5) CCl_2CCl_2, (6) $CHCl_3$, (7) $CHBr_3$, (8) CBr_4, (9) $CHCl_2CHCl_2$, (10) $CHClCCl_2$, (11) $CH_2ClCCl{=}CH_2$, (12) $CHCl_2CH_2Cl$, (13) CH_2ClCH_2Cl, (14) CH_2Cl_2.

Nitrogen with carbon dioxide. Addition of carbon dioxide to nitrogen changes the reactant species from free electrons to negative ions derived from CO_2. The response of the GC/IMS to the halogenated compounds changed, as shown in Fig. 7 for a gas mixture containing 3.2% of CO_2. Some compounds gave a better response in nitrogen/CO_2 than in pure nitrogen (e.g. $CHBr_3$ and CBr_4), while the response of the GC/IMS to other compounds was adversely affected by addition of CO_2 (e.g. CH_2Br_2). Without detailed knowledge of the reaction cross-sections for electron attachment and charge transfer it is difficult to quantitatively account for these observations. However, these changes must be related to the different mechanisms responsible for product ion formation in pure and doped nitrogen.

As mentioned above, the amount of CO_2 added to the nitrogen influenced the reactant ion peak (RIP) and the formation of product ions. Fig. 2 demonstrates this: frame a shows the RIP in nitrogen with 2.5% CO_2 and frame b shows the spectrum with injection of 3.2 ng of CCl_4. Frames c and d show the same as a and b, respectively, with 8.8% CO_2 in nitrogen. The product ion in frame b is well separated from the RIP and has a slightly shorter drift time, while in frame d the RIP and product ion are practically indistinguish-

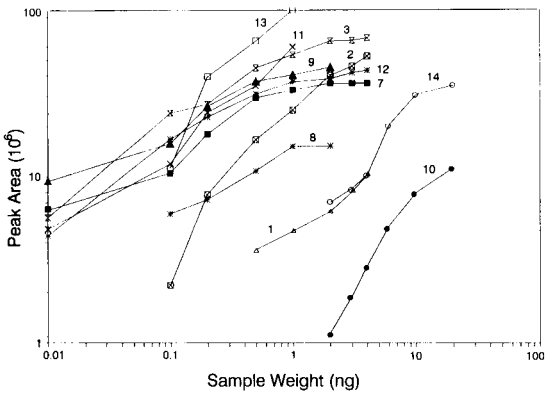

Fig. 8. Quantitative response of IMS to chlorinated alkanes and alkenes in air. The numbers correspond to (1) CCl_4, (2) CH_2Br_2, (3) $CHCl_2CCl_3$, (4) CH_3CCl_3, (5) CCl_2CCl_2, (6) $CHCl_3$, (7) $CHBr_3$, (8) CBr_4, (9) $CHCl_2CHCl_2$, (10) $CHCl$-CCl_2, (11) $CH_2ClCCl{=}CH_2$, (12) $CHCl_2CH_2Cl$, (13) CH_2Cl-CH_2Cl, (14) CH_2Cl_2.

able. Naturally, operating the IMS detector with concentrations above about 5% adversely affects it.

Air. The response of the GC/IMS system to the halogenated compounds when air is used as the reagent and drift gas in the IMS is shown in Fig. 8. A specially interesting case is that of chloroform, where a change in the shape of the reactant ion peak was observed, but the product ion could not be separated and measured. The response of the GC/IMS to some of the compounds was dramatically different in air than in nitrogen or even N_2/CO_2 mixtures. The most noted example is that of 1,2-dichloroethane to which the GC/IMS gave no response in nitrogen or N_2/CO_2 mixtures but gave the a largest response in air. A similar result, albeit less dramatic, was observed for dichloropropene. These two compounds are notable also for another characteristic of their effect on the instrument, that is the shape of the response curve. While, the response to most other compounds gradually increases until it reaches saturation, for these two compounds the response to increased quantities was sharp, and saturation was not observed.

In their study on the effect of oxygen doping on ECD response to halogenated compounds, Miller and Grimsrud [9] noted that oxygen doping did relatively little to enhance the response to highly chlorinated compounds, such as CCl_4. They attributed this to the fact that these had a large ECD response in nitrogen (i.e. large electron capture cross sections) rather than to slowness of their reaction with oxygen ions.

Conclusions

The response of the GC/IMS to several halogenated compounds depended on the composition of the bath gas in the reaction and drift regions of the IMS detector. This is mainly due to the resultant change in the reactive charged species. In nitrogen, where free electrons are the only reactive species, compounds that have a large cross section for electron capture, like CCl_4 and CH_2Br_2, gave large responses, while compounds like CH_2Cl_2 and CH_2ClCH_2Cl did not give a measurable product ion peak even when 20 ng entered the detector. When CO_2 was added to the nitrogen, the nature of the reactant species changed, so that instead of product ion formation solely through electron capture processes, charge transfer reactions also took place. As a result, the response of the GC/IMS to some compounds was enhanced, while other compounds gave a somewhat lower response. The overall effect of addition of small amounts of CO_2 was therefore beneficial. However, once the CO_2 concentration in nitrogen exceeded 5–6%, the performance of the IMS was seriously degraded, and the product ions were practically inseparable from the reactant ions. This was due to formation of ion clusters with CO_2 molecules, as evident from the increase in RIP drift time with increased CO_2 concentration and from the effect that the IMS temperature had on the drift time of the reactant ions. As mentioned above, use of air as the bath gas brings about changes in the response of the GC/IMS to some compounds. Particularly dramatic is the enhanced response to the compounds containing two chlorine atoms, a response which was practically negligible in nitrogen and nitrogen with 3.2% CO_2. The response to CCl_4 in air is much smaller than in nitrogen and N_2/CO_2 mixtures. These phenomena are all due to the changing over from electron capture processes to ion–molecule charge transfer reactions. Unfortu-

nately, it is difficult to directly compare these results with ECD experimental observations, as 0.2% of oxygen (1% of the concentration in air) was the highest dopant concentration attempted in the ECD study [6]. Furthermore, the high operating temperature of the ECD (above 300°C) ensures that (unclustered) O_2^- ions as well as free electrons coexist as reactive species. In contrast, in the IMS with air, only negative ions are formed and below 100°C they are certainly clustered to some extent. It is interesting to compare these results with GC/IMD study by Baim and Hill [20], who found that addition of small amounts of oxygen (0.5%) to nitrogen enhanced the response of their ion mobility detector. However, they observed that at oxygen concentrations above 5%, similar to our results with CO_2, the RIP broadened and complicated spectra interpretation due to overlap with the chloride ion peak.

The minimum detectable level (MDL) of the halogenated compounds by the GC/IMS in nitrogen, nitrogen/CO_2 and air may be estimated from the calibration curves presented in Figs. 6–8, as summarized in Table 4. The best MDL values of 10 pg were found for bromoform, 1,1,2-trichloroethane, 1,1,2,2-tetrachloroethane and for pentachloroethane in air. These results are comparable with the MDL values reported by Hill and co-workers [20,21], of 0.6 pg for CCl_4 and 6 pg for hexachloroethane [20] and 6 pg for 2,4-dichlorophenoxyacetic acid [21] for oxygen doped nitrogen in an IMD operated at 200°C. The best MDL values found here for pure nitrogen or CO_2/N_2 mixtures were 100 pg.

One of the most striking results is the difference between the MDL values of the two trichloroethane isomers (Table 4). While both have similar MDL values in nitrogen, the addition of CO_2, and especially oxygen (air) dramatically changed this. In air the 1,1,1-isomer was not detected even at the 20 ng level, while the 1,1,2-isomer had a low MDL of 10 pg. This is one of the most outstanding illustrations of the difference between the reaction cross section of electron capture and ion–molecule processes. A somewhat similar effect was noted by Miller and

TABLE 4

Minimum detectable level (MDL), in pg, of halogenated compounds in nitrogen, 3.2% CO_2 in nitrogen and air by the GC/IMS system

	Nitrogen	N_2/3.2% CO_2	Air
Chloromethanes			
CH_2Cl_2	> 20000	> 20000	4000
$CHCl_3$	200	> 20000	6000
CCl_4	100	100	500
Bromomethanes			
CH_2Br_2	200	500	100
$CHBr_3$	500	200	10
CBr_4	500	100	100
Chloroethanes			
CH_2ClCH_2Cl	> 20000	> 20000	200
$CHCl_2CH_2Cl$	4000	500	10
CH_3CCl_3	4000	> 20000	> 20000
$CHCl_2CHCl_2$	1000	100	10
$CHCl_2CCl_3$	100	100	10
Chloroethylenes			
$CHClCCl_2$	1000	> 20000	2000
CCl_2CCl_2	500	500	> 20000
Chloropropene			
$CH_2ClCCl{=}CH_2$	1000	4000	100

Grimsrud [9] in their ECD study of chlorinated compounds. The response to the *cis*-dichloroethylene isomer was 100 times larger than that to the *trans* isomer in nitrogen, but only 3 times larger in nitrogen doped with 0.2% oxygen. They attributed this lack of relative enhancement with oxygen doping to the absence of a hydrogen atom on the alpha-carbon of a mono- or dichlorinated molecule [9]. The same argument may be used to rationalize the differences observed here in the MDL of trichloroethylene and tetrachloroethylene in nitrogen and air. The former has a hydrogen atom on the alpha-carbon and efficiently reacts with oxygen ions, while the latter does not have a hydrogen atom and the reaction is hindered. The fact that tetrachloroethylene has no dipole moment, while trichloroethylene has 1.45 Debye (Table 2) may also effect their relative reaction rates according to the CADET mechanism [26]. However, it is difficult to interpret the relative MDL values, and the changes in them caused by doping nitrogen with CO_2 or oxygen, and attribute them to a single factor. It appears that a combination of reaction enthalpies, appropriate electronic states for resonant charge transfer, dipole moments and polarizabilities of the neutral, the extent and type of clustering of the ion, as well as its ability to participate in cluster-assisted dissociative electron transfer transition states, affect the response of the IMS detector.

The ability to selectively modify the response of the GC/IMS system has practical applications. For example, use of nitrogen will give a more or less uniform response to several of the compounds (Fig. 6) over quite a broad concentration range. On the other hand, in air, sensitivity towards several compounds, such as bromoform, 1,1-dichloroethane, tertachloroethane and pentachloroethane is selectively enhanced, while 1,1,1-trichloroethane and tetrachloroethane are not detected. Thus, it is possible to tailor the response of the GC/IMS detector according to the desired matrix.

We gratefully acknowledge the technical assistance by Dan Hampton and financial support of KRUG Life Sciences under subcontract No. 70149 and of the Environmental Protection Agency under award No. R-815991-01-0. The information in this paper does not necessarily reflect the views of the Agency and no official endorsement should be inferred.

REFERENCES

1 M.J. Cohen and F.W. Karasek, J. Chromatogr. Sci., 8 (1970) 331.
2 (a) F.W. Karasek and D.M. Kane, Anal. Chem., 45 (1973) 576; (b) F.W. Karasek and G.E. Spangler, in A. Zlatkis and C.F. Poole (Eds.), Electron Capture: Theory and Practice in Chromatography, Elsevier, Amsterdam, 1981, chap. 15, pp. 377–406.
3 E.P. Grimsrud and D.A. Miller, Anal. Chem., 50 (1978) 1141.
4 C.A. Clemons and A.P. Altshuller, Anal. Chem., 38 (1966) 133.
5 E.C.M. Chen, W.E. Wentworth, E. Desai and C.F. Batten, J. Chromatogr., 399 (1987) 121.
6 E.P. Grimsrud, Mass Spectrom. Rev., 10 (1992) 457.
7 H.J. Van De Wiel and P. Tommassen, J. Chromatogr., 71 (1972) 1.
8 E.P. Grimsrud and R.G. Stebbins, J. Chromatogr., 155 (1978) 19.
9 D.A. Miller and E.P. Grimsrud, Anal. Chem., 51 (1979) 851.
10 E.P. Grimsrud, in A. Zlatkis and C.F. Poole (Eds.), Electron Capture: Theory and Practice in Chromatography, Elsevier, Amsterdam, 1981, Chap. 5, pp. 91–117.
11 F.C. Fehsenfeld, P.D. Goldan, M.P. Phillips and R.E. Sievers, in A. Zlatkis and C.F. Poole (Eds.), Electron Capture: Theory and Practice in Chromatography, Elsevier, Amsterdam, 1981, Chap. 4, pp. 69–90.
12 C.J. Proctor and J.F.J. Todd, Anal. Chem., 56 (1984) 1794.
13 A.H. Lawrence and P. Neudorfl, Anal. Chem., 60 (1988) 104.
14 L.L. Danylewych-May, Paper C-10, Proc. 1st Intl. Symp. Explos. Detec. Technol., FAA Center, Atlantic City, Nov. 13–15, 1991.
15 G.E. Spangler, D.N. Campbell and J.P. Carrico, Acetone Reactant Ions for Ion Mobility Spectrometry", Pitt. Conf. Anal. Chem. Appl. Spectrosc., Atlantic City, NJ, 1983.
16 (a) V.J. Vandiver, C.S. Leasure and G.A. Eiceman, Int. J. Mass Spectrom. Ion Proc., 66 (1985) 223; (b) Z. Karpas and Y. Pollevoy, Anal. Chim. Acta, 249 (1991) 503.
17 (a) R.L. Eatherton, M.A. Morrissey, W.F. Siems and H.H. Hill, Jr., J. High Resolut. Chromatogr. Chromatogr. Commun., 9 (1986) 154; (b) S. Rokushika, H. Hatano and H.H. Hill, Jr., Anal. Chem., 59 (1987) 8; (c) M.A. Morrissey and H.H. Hill, Jr., J. Chromatogr. Sci., 27 (1989) 529.
18 (a) F.W. Karasek and D.W. Denny, Anal. Lett., 6 (1973) 993; (b) C.B. Shumate and H.H. Hill, Jr., Anal. Chem., 61 (1989) 601.

19 H.H. Hill, Jr. and M.A. Baim, in T.W. Carr (Ed.), Plasma chromatography, Plenum Press, New York, 1984, pp. 143–176.
20 M.A. Baim and H.H. Hill, Jr., J. High Resolut. Chromatogr. Chromatogr. Chromatogr. Commun., 6 (1983) 4.
21 M.A. Baim and H.H. Hill, Jr., J. Chromatogr., 279 (1983) 631.
22 R.H. St. Louis and H.H. Hill, Jr., J. High Resolut. Chromatogr. Chromatogr. Commun., 13 (1990) 628.
23 American Conference of Governmental and Industrial Hygienists, Threshold Limit values for Chemical Substances in the Work Environment, Cincinnati, OH, 1990–91.
24 J. Bertran, I. Gallardo, M. Moreno and J.M. Saveant, J. Am. Chem. Soc., 114 (1992) 9576.
25 G.E. Spangler and P.A. Lawless, Anal. Chem., 50 (1979) 884.
26 W.B. Knighton and E.P. Grimsrud, J. Am. Chem. Soc., 114 (1992) 2336.
27 G.A. Eiceman, D.B. Schoff, C.S. Harden, A.P. Snyder, P.M. Martinez, M.F. Fleischer and M.L. Watkins, Anal. Chem., 61 (1989) 1093.
28 S. Rokushika, H. Hatano and H.H. Hill, Jr., Anal. Chem., 58 (1986) 361.
29 H.W. Ellis, R.Y. Pai, I.R. Gatland, E.W. McDaniel, R. Wernlund and M.J. Cohen, J. Chem. Phys., 64 (1976) 3935.
30 (a) Z. Karpas and Z. Berant, J. Phys. Chem., 93 (1989) 3021; (b) Z. Berant, Z. Karpas and O. Shahal, J. Phys. Chem., 93 (1989) 7527.
31 D. Smith, C.R. Herd and N.G. Adams, In. J. Mass Spectrom. Ion Proc., 93 (1989) 15.
32 D.L. Lide, Handbook of Chemistry and Physics, CRC Press, Boca Raton, FL, 71st edn., 1990–1.

Analytica Chimica Acta, 282 (1993) 33–45
Elsevier Science Publishers B.V., Amsterdam

Stationary phase degradation in reversed-phase liquid chromatography: a possible cause of bad predictions in experimental design

B. Bourguignon and D.L. Massart

Vrije Universiteit Brussel, Farmaceutisch Instituut, Laarbeeklaan 103, B-1090 Brussels (Belgium)

(Received 29th January 1993; revised manuscript received 29th May 1993)

Abstract

The degradation in function of time of cyanopropyl- and octadecyl-modified silica stationary phases, a polymer coated silica phase and a polymer phase is investigated as this could be a cause of bad predictions in experimental design. By simulating routine conditions on both types of silica columns, considerable changes of retention, peak width and asymmetry in function of time were observed when switching mobile phase pH but also when mobile phase pH is held constant. The initial column performance was best maintained on the polymer coated silica column. On most of the other columns, changes in elution characteristics are rapid enough to make them a major cause of bad predictions in experimental design.

Keywords: Chromatography; Liquid chromatography; Experimental design; Stationary phase degradation

Experimental designs have been introduced in liquid chromatography because they provide a means to optimize separations with few experiments. Although successful optimizations with the pH as one of the parameters have been achieved, in some cases the "optimum" conditions predicted with an accurate model did not lead to a satisfactory chromatogram [1]. One possible cause of bad predictions could be column ageing during the experimental design, resulting in insufficiently reproducible retention times and peak widths. It is known that the life of silica based stationary phases, even when modified with di- or trifunctional silanes, may be seriously reduced in the presence of aqueous buffer–mobile phase systems with $pH < 2$ or $pH > 7.5$. It has also been shown that even at a constant pH in the range between 2 and 7.5, capacity factors decrease continuously [2,3]. When the pH is one of the experimental variables in a design, the sequential use of several mobile phases with a different pH is required and it is feared that this switching of pH might enhance the ageing process. In the literature, this has not been studied yet. With the exception of one study about the effect of pH in reversed-phase liquid chromatography [4], the results of which became known to use while writing this article, the evaluation of column performance in function of time is limited to experiments at constant pH on conventional silica phases, for instance [5,6]. Moreover, in some published experiments [7,8] normal chromatographic conditions are not respected by feeding back the waste to the eluent reservoir which may cause a saturation of the solvent in degradation products. This recycling could have a protecting effect on the column.

This paper aims to investigate whether deterioration of reversed-phase stationary phases could

Correspondence to: D.L. Massart, Vrije Universiteit Brussel, Farmaceutisch Instituut, Laarbeeklaan 103, B-1090 Brussels (Belgium).

be the cause of prediction problems. Particularly, we were interested in (i) the evolution of retention, peak width and asymmetry in function of time when sequentially using mobile phases with a different pH on cyanopropyl and octadecyl modified silica stationary phases, (ii) comparing those results with the evolution of column performance when mobile phase pH is kept constant and, (iii) investigating also the stability of recently developed stationary phases such as a polymer coated silica gel and a polystyrene phase. Both types of phases are described to have a greater chemical stability and could be an appropriate alternative to silica columns.

EXPERIMENTAL

Chromatographic equipment and parameters

Experiments were carried out with a Varian 5000 or with a Merck Hitachi liquid chromatograph equipped with respectively a Perkin Elmer LC 90 UV detector or with a Merck Hitachi L-4000 UV detector. Detection was performed at 254 nm and the attenuation was set at 0.04 AUFS. Both chromatographs were provided with a Rheodyne injection valve (50 μl sample loop). The chromatograms were recorded with a Vista CDS 401 data system, with a Shimadzu CR6A Chromatopac data system or with a Merck Hitachi D2500 Chromato-Integrator. The columns used in this study were Lichrosorb CN (25×0.4 cm i.d.) (Merck, Darmstadt), Lichrosorb RP-18 (25×0.4 cm i.d.) (Merck), Spherisorb S5 PC18 (20×0.46 cm i.d.) (Euro-Scientific) and Polyspher RP-18 (15×0.46 cm i.d.) (Merck). All stationary phases had a particle size of 5 μm. The flow-rate was maintained at 1 ml min^{-1} and at 0.5 ml min^{-1} during the experiments on respectively the silica-based columns and on the polymer column. Overnight flow-rate was set at 0.5 ml min^{-1} on the former type of columns and at 0.2 ml min^{-1} on the latter type. During chromatography, the column temperature was maintained at 30°C to assure reproducible conditions. Retention time (t_R) and peak widths at the half of the peak height ($w_{1/2}$) are the average of at least two determinations. pH measurements of buffer solutions were carried out with an Orion Research digital ionalyzer. Depending on the range investigated, the electrode was calibrated with standard solutions of pH 3 and 7.

Standards and reagents

All test compounds are of reference grade. Stock solutions prepared in methanol and containing 500 mg l^{-1} were daily diluted with water to concentrations between 1 and 10 mg l^{-1}. The water used was deionized in a Milli-Q system. Methanol, acetonitrile, tetrahydrofuran, citric acid, phosphoric acid, sodium dihydrogenphosphate monohydrate and disodium hydrogenphosphate dihydrate of pro analysis quality were obtained from Merck. Buffer solutions of pH 3, 4, 5 and 6 and ionic strength of 0.05 mol l^{-1} were prepared with doubly distilled water and filtered through a 0.2-μm membrane filter after controlling the pH.

Procedure

To study the degradation of the four types of phases, the evolution of retention, peak width and asymmetry in function of time of pentoxifylline, indomethacin and papaverine is investigated. On the polymer phase the test mixture also contains aniline, a polar and basic analyte, and naphthalene, which is neutral.

The following procedures were adopted to simulate continued use of the stationary phase, either at constant pH or when switching pH of the mobile phase. Mobile phase was pumped continuously for several weeks, eluent being renewed every two days. At appropriate intervals, namely twice or three times a day standard solutions of each compound were injected. To simulate the sequential use of mobile phases with different pH when pH is one of the experimental variables in an experimental design a Lichrosorb CN and C_{18} column each were sequentially subjected to mobile phases with pH 6 and pH 4 during periods long enough to equilibrate the phase and perform the injections. After each experiment pH was changed and the column was thoroughly cleaned and equilibrated during at least 2 h with the other mobile phase. To investigate if a deterioration of the stationary phase is

due only to the pH-switching an analogous experiment at constant pH 5, is carried out on two other Lichrosorb stationary phases, one modified with cyanopropyl and another one with octadecyl ligands. During the experiments on the Spherisorb column, pH of the mobile phase was maintained at 5. The eluent consisted of 30 or 65% of methanol respectively on the cyanopropyl modified columns and on the octadecyl modified ones (both Lichrosorb and Spherisorb) in order to keep capacity factors in the same range.

It was not possible to apply the same experimental conditions on the Polyspher phase as on the silica-based column. Since polymer-based packing material shows better performance in a mobile phase containing tetrahydrofuran than in methanol–water [9], the mobile phase applied on the Polyspher phase consisted of 10% tetrahydrofuran and different volume fractions of acetonitrile and buffer. The experiment to study the degradation was performed at pH 6 and with 46% of acetonitrile but was alternated by experiments of a central composite design with pH values varying from 7 to 10 and with different concentrations of acetonitrile between 38 and 54%.

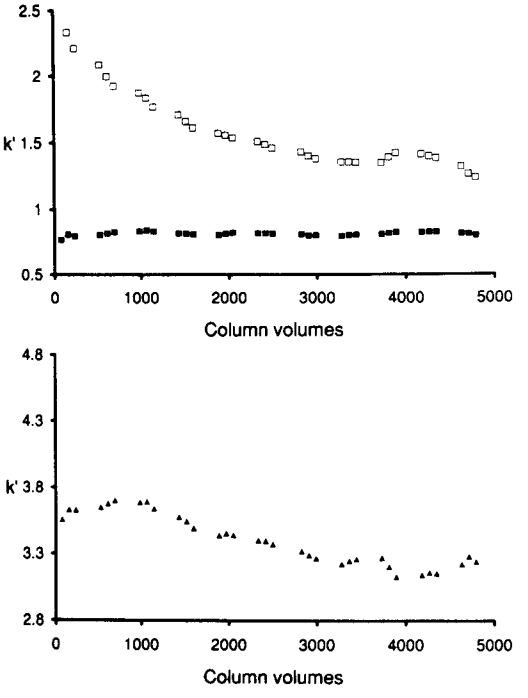

Fig. 1. Capacity factor (k') as a function of volume of mobile phase passed through the Lichrosorb CN column at pH 5. ■ = pentoxifylline, ▲ = papaverine, □ = indomethacin.

Evaluation

Capacity factors (k') are calculated with the following standard relationship:

$$k' = (t_R - t_0)/t_0$$

where t_0 = dead volume time. Dead volume time was determined by measuring the first baseline distortion after injection of mobile phase enriched with water or with organic modifier. Asymmetry factors (As) are calculated as the ratio of the leading half of the peak to the trailing half measured at 10% of the peak height.

To better perceive trends in measured values (x_n) of retention, peak width and asymmetry from fluctuations caused by experimental error, curves are smoother by applying the following equation:

$$x_n = (x_{n-2} + x_{n-1} + x_n + x_{n+1} + x_{n+2})/5$$

RESULTS

On the cyanopropyl column, already after 1435 column volumes (i.e., 8 experiments in 84 h), capacity factors of indomethacin are decreased with 25% at constant pH (Fig. 1). By hydrolysis of bonded ligands, retention times decrease as solute retention in function of alkylligand density follows a linear relationship up to a certain value [10]. When pH is varied on the cyanopropyl column, retention also decreases for the experiments at pH 4 and a decrease of 25% is obtained after 1845 column volumes (Fig. 2). However for the experiments at pH 6, k' values of indomethacin remain almost constant so that the different evolution of retention of indomethacin ($pK_a = 4.5$) at different pH only partially can be explained by an increase in silanol functions. The largest decrease of retention occurs at pH 5. As retention decreases most at pH 5, peak width also does (Fig. 3). The opposite phenomenon occurs at pH 4 while changes in peak width are almost

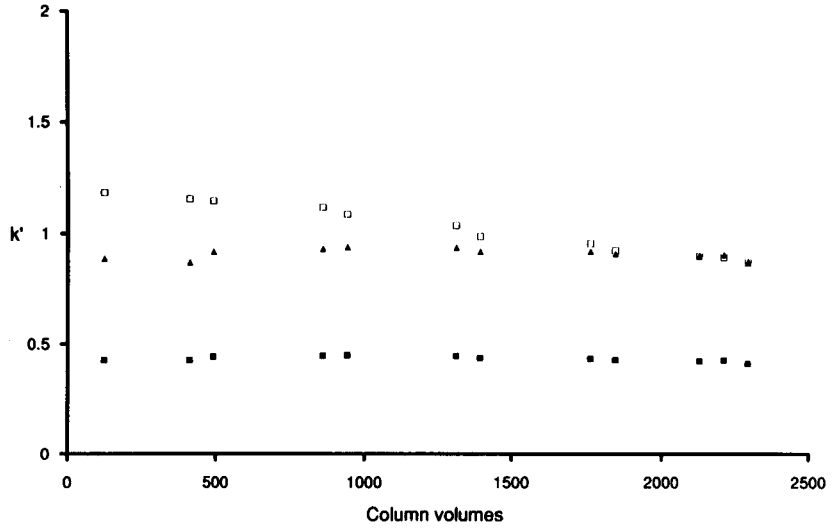

Fig. 2. Capacity factor (k') as a function of volume of mobile phase passed through the Lichrosorb CN column, when switching pH at pH 4. ■ = pentoxifylline, ▲ = papaverine, □ = indomethacin.

negligible at pH 6 (Fig. 4). Different amounts of residual silanols may explain the discrepancy at pH 5. Asymetry factors increase at pH 4 and 5 but not at pH 6 (Figs. 5 and 6).

When applying a constant pH on the Lichrosorb RP-18 column, a considerable peak broadening is observed after 3000 column volumes of mobile phase (Fig. 7). When varying the pH on the Lichrosorb RP-18 column, chromatograms with doubled peaks and bad peak shapes are observed after six days, so that experiments had to be stopped. During these six days

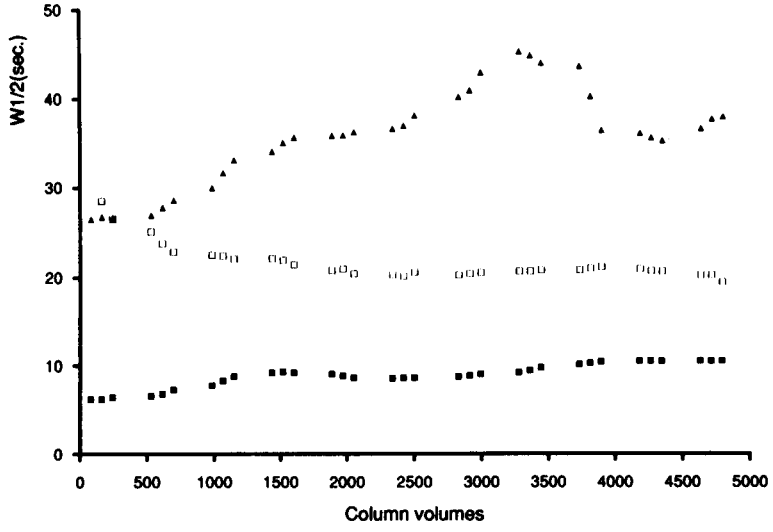

Fig. 3. Peak width at the half of the peak height ($w_{1/2}$) as a function of volume of mobile phase passed through the Lichrosorb CN column at pH 5. ■ = pentoxifylline, ▲ = papaverine, □ = indomethacin.

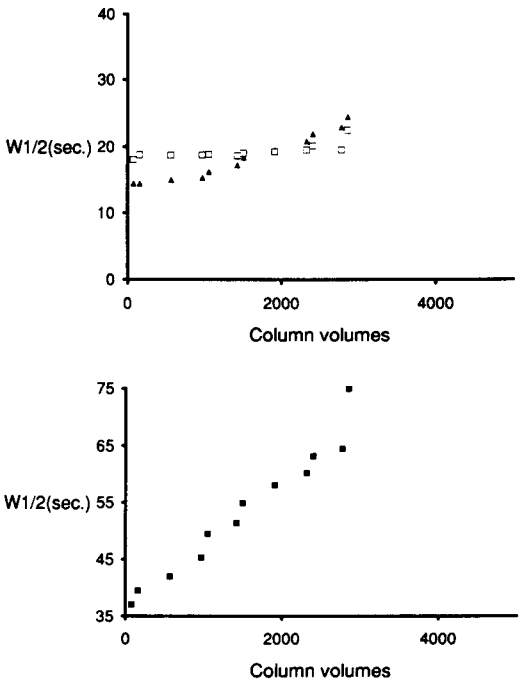

Fig. 4. Peak width at the half of the peak height ($w_{1/2}$) as a function of volume of mobile phase passed through the Lichrosorb CN column, when switching pH at pH 6. ▲ = pentoxifylline, ■ = papaverine, □ = indomethacin.

retention and peak width remain almost constant and asymmetry increases a little.

On the Spherisorb stationary phase initial values of retention, peak width and peak symmetry are almost maintained after 6400 column volumes (Figs. 8–10).

Capacity factors of indomethacin on the Polyspher phase decrease with about 40% within 2500 column volumes and increase again to their initial value after 3800 column volumes (Fig. 11). Both peak width and asymmetry increase in course of time (Figs. 12 and 13).

For pentoxifylline retention remains constant on all types of columns at constant pH but also when varying pH on the silica stationary phases (Figs. 1, 2, 8 and 14). At constant pH a slight peak broadening is observed on the CN column but when mobile phases with different pH are switched the initial peak width of pentoxifylline is almost doubled within 2000 column volumes (Fig. 4). When varying the pH but also when pH is kept constant, peaks become more asymmetric in function of time (Figs. 5 and 6). On the Lichrosorb RP-18 column a doubling of the peak width was observed at constant pH after 3800 column vol-

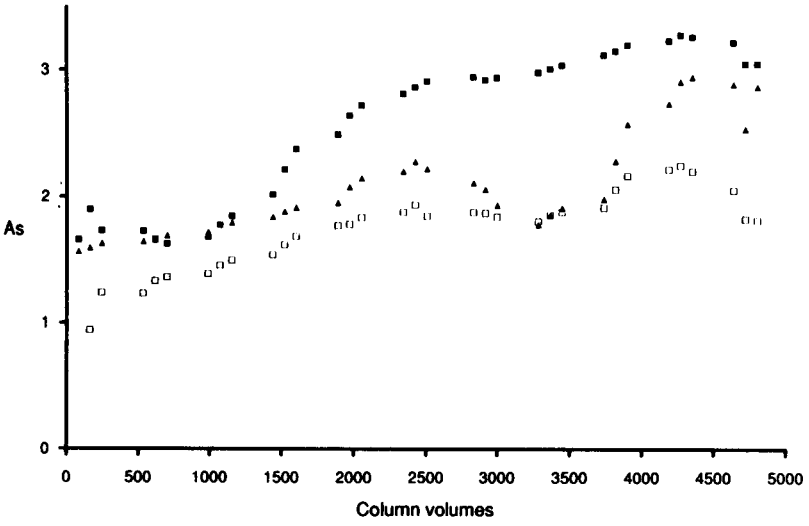

Fig. 5. Asymmetry factors (As) as a function of volume of mobile phase passed through the Lichrosorb CN column at pH 5. ■ = pentoxifylline, ▲ = papaverine, □ = indomethacin.

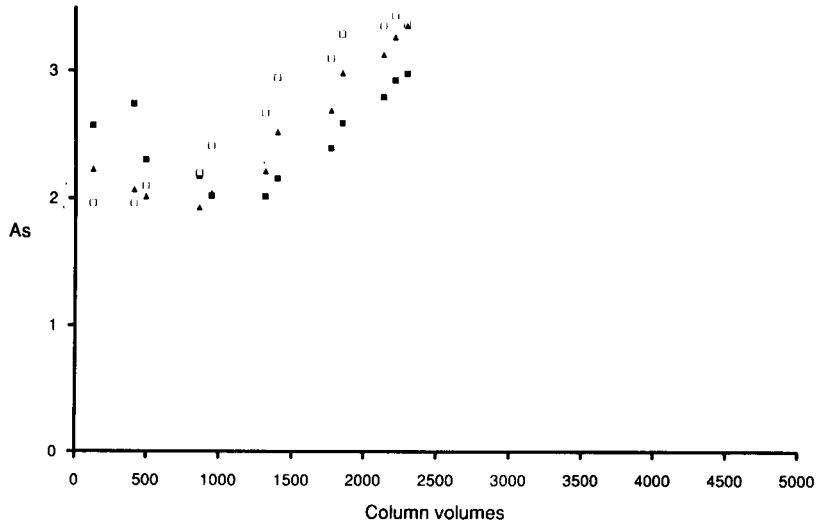

Fig. 6. Asymmetry factors (*As*) as a function of volume of mobile phase passed through the Lichrosorb CN column, when switching pH at pH 4. ■ = pentoxifylline, ▲ = papaverine, □ = indomethacin.

umes (Fig. 7). Peak asymmetry fluctuates considerably at pH 5 and increases at pH 4. On the polymer coated silica gel asymmetry factors decrease in function of time (Fig. 10). Values of the asymmetry factor are not reproducible on the polymer phase (Fig. 12).

k' values of papaverine on the CN column decrease in function of time at constant pH and when varying pH at pH 6 but almost not at pH 4 (Figs. 1 and 2). Compared with pH 6, the basic papaverine ($pK_a = 6.4$) is almost completely positively charged at pH 4, which results in increased

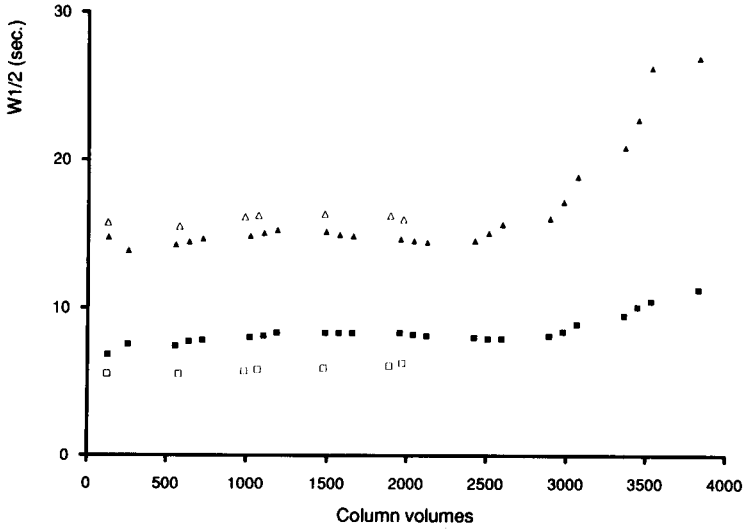

Fig. 7. Peak width at the half of the peak height ($w_{1/2}$) as a function of volume of mobile phase passed through the Lichrosorb RP-18 column, at constant pH 5 (■,▲) and when switching pH at pH 4 (□,△). ■,□ = pentoxifylline, ▲,△ = indomethacin.

acidic–basic interactions with the stationary phase and thus also in a smaller decrease of k' values. On the CN column, peak width increases considerably during both series of experiments and $w_{1/2}$ is even doubled after 2200 column volumes of mobile phase with a different pH (Figs. 3 and 4). The increased *As* also indicates a loss of bonded alkyl ligands (Figs. 5 and 6). On the Lichrosorb RP-18 column capacity factors of papaverine increase slightly at constant pH (Fig. 8). The increasing affinity for the stationary phase suggests that the silanol groups are responsible for this phenomenon. The evolution of peak width and peak symmetry shows large fluctuations at pH 5 and when varying pH (Fig. 9). Retention, peak width and peak symmetry remain constant on the Spherisorb column, even after a period of 21 days (Figs. 8–10). On the polymer phase, peak width only changes a little in function of time (Figs. 12, 14 and 15).

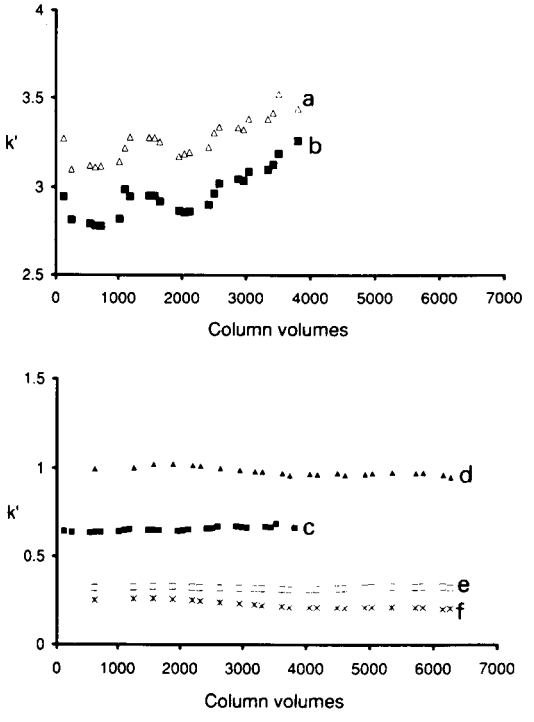

Fig. 8. Capacity factor (k') as a function of volume of mobile phase passed through (a–c) the Lichrosorb RP-18 column and (d–f) the Spherisorb S5P C_{18} column at pH 5. c,e = pentoxifylline, b,f = indomethacin, a,d = papaverine.

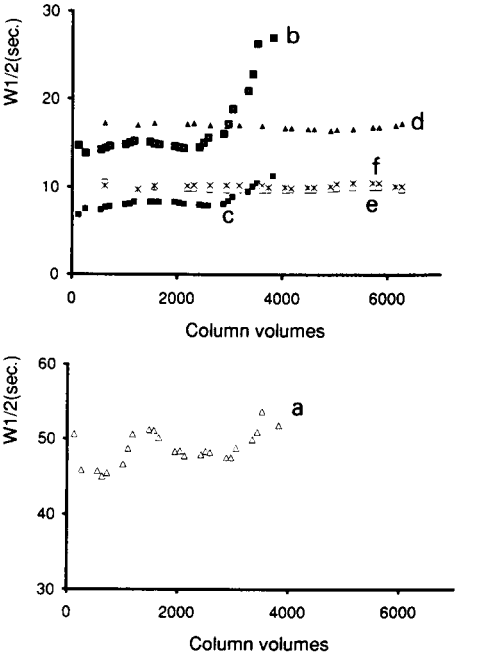

Fig. 9. Peak width at the half of the peak height ($w_{1/2}$) as a function of volume of mobile phase passed through the Lichrosorb RP-18 column and the Spherisorb S5P C_{18} column at pH 5. a–f as in Fig. 8.

Retention of aniline does not change on the Polyspher RP-18 column but asymmetry and peak width increase (Figs. 12, 14 and 15).

For naphthaline none of the three variables remain constant on the polymer phase (Figs. 11, 12 and 15).

DISCUSSION

For certain responses changes in function of time are larger when varying pH than when holding pH constant but the opposite is true for other responses. For indomethacin on the cyanopropyl column for instance larger changes of capacity factors are observed when pH is kept constant but for the *As* the opposite is true. Considerable changes of the peak width occur during both series of experiments.

When pH is varied, deterioration of a C_{18} modified stationary phase occured within six days so that this type of column seems less stable than

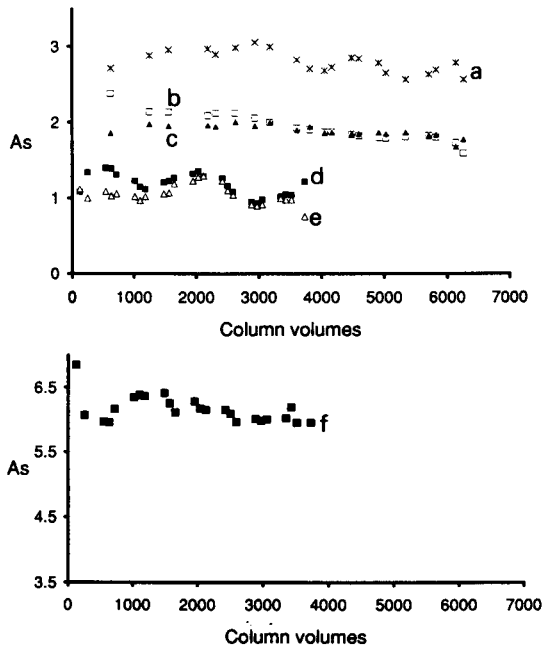

Fig. 10. Asymmetry factors (As) as a function of volume of mobile phase passed through (d,e,f,) the Lichrosorb RP-18 column and (a,b,c) the Spherisorb S5P C_{18} column at pH 5. d,b = pentoxifylline, c,e = indomethacin, a,f = papaverine.

the cyanopropyl modified one. One can argue that the C_{18} modified stationary phase used in the experiments with varying pH occasionally could have been a bad one. However, very recently Schoenmakers et al. [4] also reported a considerable degradation of an octadecyl-modified silica column when varying pH and concentration of organic modifier during an experimental design. In a period of 19 working-days retention times of some of the compounds were reduced to half of their initial value.

Considering column degradation in this study, at constant pH and when varying pH, for the two types of silica columns, there is no convincing evidence that sequentially using mobile phases with a different pH does enhance the ageing process.

When comparing the stability of CN and C_{18} columns, several factors have to be taken into account. Chromatographic characterization methods, ^{29}Si CP-MAS NMR measurements and elemental analysis indicate that longer alkyl ligands better isolate the silica surface from substrate hydrolysis than short-chain ligands [3,6,8,11,12].

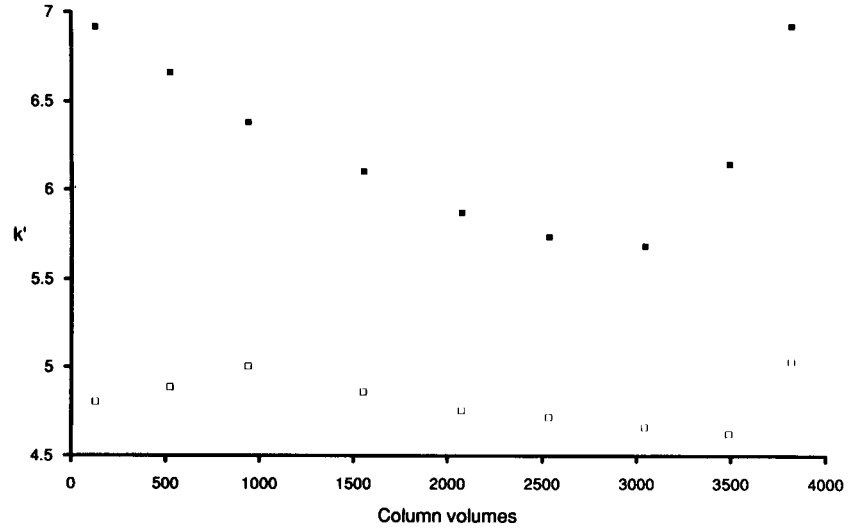

Fig. 11. Capacity factor (k') as a function of volume of mobile phase passed through the Polyspher RP-18 column at pH 6. ■ = indomethacin, □ = naphthalene.

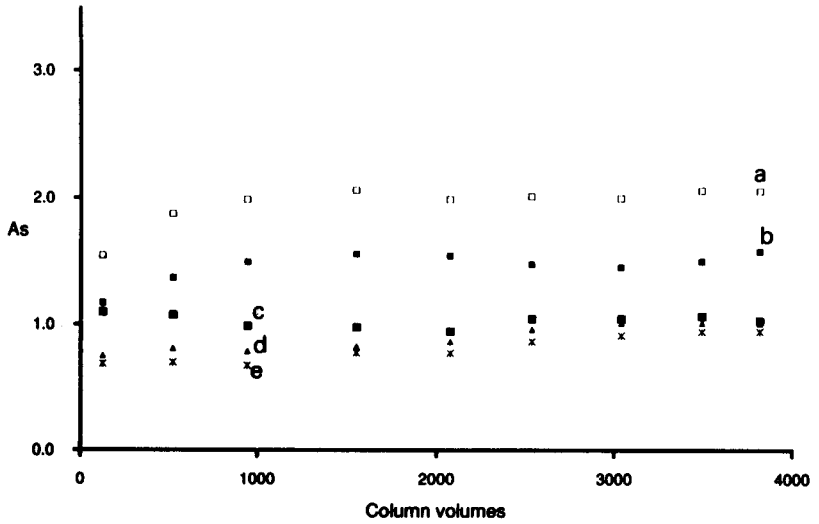

Fig. 12. Asymmetry factors (*As*) as a function of volume of mobile phase passed through the Polyspher RP-18 column at pH 6. a = indomethacin, e = naphthalene, b = pentoxifylline, c = papaverine, d = aniline.

Considering only the length of the alkyl ligand, one might expect the C_{18}-modified silica column to be more stable than the cyanopropyl modified one. For papaverine for instance changes in peak width and in *As* are indeed larger on the cyanopropyl column. Though on the Lichrosorb RP-18 column, changes in retention, peak width and asymmetry are reduced, yet considerable fluctuations of the values of these three variables are observed in a period of thirteen days.

As mobile phases with a greater percentage of organic modifier have some protecting effect due to a better solvatation of the ligands by the organic modifier [7,8,11–13], the C_{18} column is

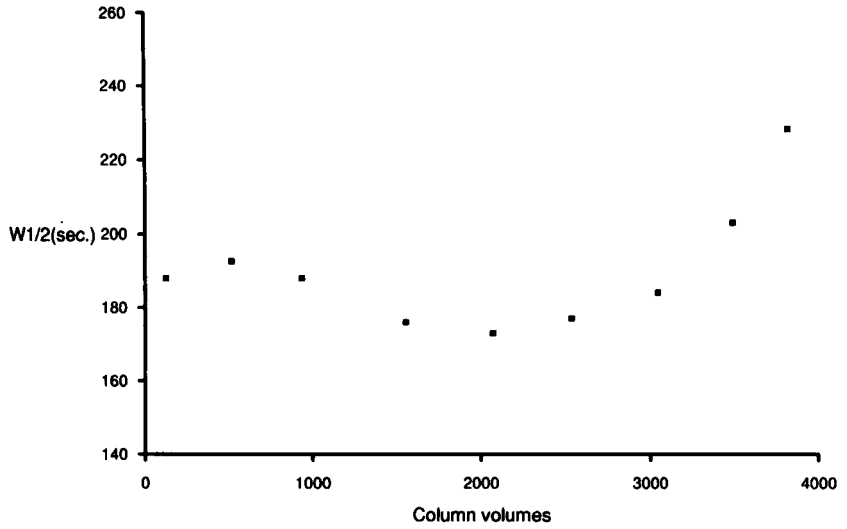

Fig. 13. Peak width at the half of the peak height ($w_{1/2}$) of indomethacin as a function of volume of mobile phase passed through the Polyspher RP-18 column at pH 6.

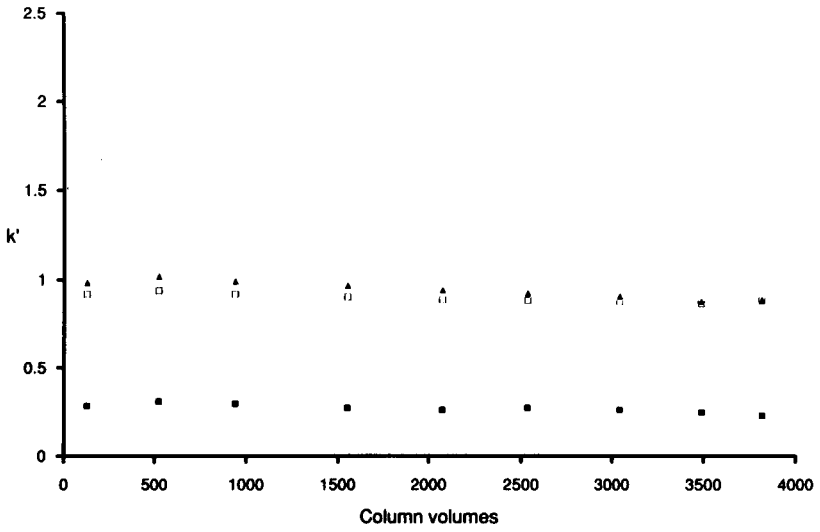

Fig. 14. Capacity factor (k') as a function of volume of mobile phase passed through the Polyspher RP-18 column at pH 6. ■ = pentoxifylline, □ = papaverine, ▲ = aniline.

expected to exhibit a better stability in this study, since different percentages of methanol, namely 30 and 65%, respectively, were applied on the cyano column and on the C_{18}-column. Yet, other workers [3] observed a column degradation problem when methanol-rich mobile phases were used. If 30% of methanol is considered as a low concentration and 65% as a high concentration, then the effect of the modifier concentration opposes the effect of the length of the alkylligand, which might explain that in this study the C_{18} column was not found to be more stable than the CN column.

On the Polyspher RP-18 column retention of

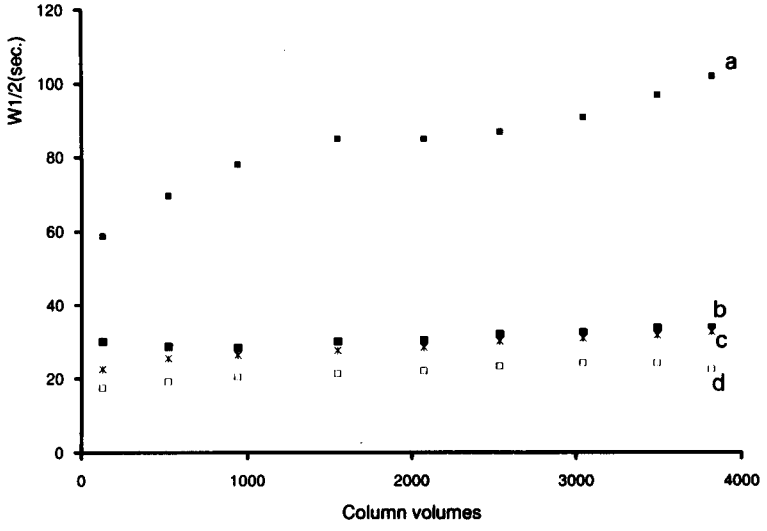

Fig. 15. Peak width at the half of the peak height ($w_{1/2}$) as a function of volume of mobile phase passed through the Polyspher RP-18 column at pH 6. a = naphthalene, d = pentoxifylline, b = papaverine, c = aniline.

all compounds except indomethacin and naphthalene remains quite constant. The Polyspher RP-18 column contains a polymer of crosslinked polystyrene divinylbenzene, derivatized with covalently bonded octadecylchains, which swells and shrinks with the volume fraction of organic modifier in the mobile phase [14,15]. During the experiments that alternate the degradation experiment, the organic modifier content of the mobile phase was changed. By sequentially varying this content it might be that after some time the initial column performance is not maintained and/or the polymer no longer completely swells or shrinks to its initial form. A changed structure of the polymer resin may cause a change in the mass transfer dispersion mechanism which may influence the π–π interactions between solutes and π orbitals of the benzene rings [15] and induce variation of retention, peak width and asymmetry. These parameters may also vary by the creation of new adsorption sites for cations (or repulsion sites for anions as indomethacin) or by the burrying in the polymer matrix of existing sites in micropores which become less accessible [14]. This might explain the irreproducible chromatographic behaviour of indomethacin and naphthalene. However a steric factor could also play a role as for papaverine, which at the applied pH is also ionized, results were more reproducible.

On the Spherisorb RP-18 stationary phase retention and peak width remained essentially unchanged for papaverine, pentoxifylline and indomethacin during 6400 column volumes, which corresponds to a period of 21 working-days with a flow-rate of 1 ml and 0.5 ml during respectively 9 h and 15 h each day. The reproducibility of results contrasts favourably with the large changes of the variables that were obtained on the Lichrosorb RP-18 column, under the same experimental conditions (Figs. 8–10) and is in agreement with results of Engelhardt et al. [2] and Ohmacht et al. [16]. This improved stability is due to the physical protection from the eluent by a polymeric coating, which should also extend the working range of pH.

The reproducibility of measurements was determined in those cases where this was possible for apparently stable columns. The relative standard errors for the three parameters on the Spherisorb RP-18 stationary phase and for the different compounds are represented in Table 1. For pentoxifylline for instance with k' values of the order of 0.3 the relative standard error was 0.02. The reproducibility of k' values on unstable columns could of course not be measured.

To show that there are trends in the different figures obtained on the traditional silica stationary phases (Lichrosorb columns) and on the polymer stationary phase no statistics are required. The observed changes in retention, peak width and asymmetry in function of time make it very difficult to gather accurate data, an essential requirement in the application of experimental design. As an example, a central composite design, with pH of the mobile phase and volume fraction of acetonitrile as experimental variables, was performed on the Polyspher RP-18 stationary phase, to optimize the separation of a mixture of five basic pharmaceuticals, namely diazepam, papaverine, doxepin, mianserin and metaclopramide. A quadratic model [1] was selected to model retention and peak width. Quadratic models are not the most appropriate models when pH is involved. We use it here only for demonstration purposes. To simulate changes in the phase, the values of k' and $w_{1/2}$ obtained in the experiments of the design were respectively decreased or increased with a percentage that increased linearly in function of time. The data of the first experiment were not changed. The values of k' and $w_{1/2}$ obtained in the ninth experiment were changed with the largest percentage which is respectively 5.6% and 9.6%, as one expects changes of the phase to become more important with increasing use of the phase. When simulating degradation by introducing such a shift, the retention times of the five solutes at the optimal

TABLE 1

Relative standard deviations of k', $w_{1/2}$ and As values on the Spherisorb RP-18 stationary phase

	Pentoxifylline	Indomethacin	Papaverine
k'	0.017	0.089	0.021
$w_{1/2}$	0.019	0.019	0.015
As	0.092	0.04	0.051

experimental conditions decrease at least by 3.0% and at most by 3.9%. This is not dramatic, but, added to other sources of inaccuracy in the prediction it is sufficiently large to make predictions in experimental design less reliable than one would hope.

As the evolution of retention in function of time is different for all compounds, the method of calculating relative retentions, i.e., referring retentions of each compound to the retention of a carefully selected other one, offers no solution to bad predictions by column ageing.

In order to model retention and take into account column deterioration, an exponential column-decay factor has been proposed [4]. Such an exponential model might be appropriate for instance for indomethacin at constant pH on a CN column (Fig. 1) but not for papaverine on the Lichrosorb RP-18 column (Fig. 8).

The remarkable changes in column performance do not only appear during the first days the column is in use but continue over the whole investigated period. Obviously, applying conventional silica columns after an "ageing period" does not guarantee results to become reproducible.

When one takes the trouble to perform a design, then everything possible should be done to guarantee results to remain reproducible. Stationary phase problems as the ones described in this study should be avoided by selecting a robust phase such as polymer-coated silica columns which were shown to have a longer column lifetime. If for certain reasons one prefers to use traditional silica phases then column performance should be monitored in function of time by means of a simple test, a variety of which was published [17–22]. These tests can be of help to trace a degradation of the stationary phase leading to unreliable results and to decide whether or not a column should be discarded. Very recently alumina based columns, became available [23]. They might be a solution that is as good as polymer-coated silica phases. Another precaution might be the use of a precolumn. This is a guard column, also called a saturation column, which is placed upstream from the injector to pretreat the mobile phase so that it is less damaging to the column. Furthermore it has been shown that buffers or mobile phase additives in concentrations less than ca. 10 mM may lead to results that are more susceptible to reproducibility problems than if the additive concentrations are ≥ 20 mM. On the other hand, concentrations > 50 mM are seldom advantageous in reversed-phase liquid chromatography as, especially with high organic solvent concentrations, they greatly increase the chance of buffer precipitation.

Conclusion

The observed fast deterioration of conventional silica columns when using a constant pH or sequentially applying mobile phases with a different pH can be a cause of bad predictions in experimental design, because it leads to irreproducible data. In fact, this was shown experimentally to be the case for the polymer phase. This phase is less sensitive to changes in pH than the silica phases but is considerably more sensitive to changes in the organic modifier content of the mobile phase. Sequentially varying the concentration of organic modifier may induce changes in the structure of the polymer resin which can be a cause of the bad prediction.

The polymer coated phase was found to have a superior stability; measurements were still reproducible after 21 days and nights of continuous use. As the performance in terms of separation quality of this type of phase was similar to the performance obtained on conventional silica phases, polymer coated phases have to be preferred. The stability of this type of columns when varying pH should be investigated.

The authors thank the National Fund for Scientific Research for financial support and Karine Verbiest for assistance during the experimental work.

REFERENCES

1 B. Bourguignon, F. Marcenac, H.R. Keller, P.F. de Aguiar and D.L. Massart, J. Chromatogr., 628 (1993) 171.
2 H. Engelhardt, H. Low, W. Eberhardt and M. Maub. Chromatographia, 27 (1989) 535.

3 J.L. Glajch, J.C. Gluckman, J.G. Charikofsky, J.M. Minor and J.J. Kirkland, J. Chromatogr., 318 (1985) 23.
4 P.J. Schoenmakers, S. van Molle, C.M.G. Hayes and L.G.M. Uunk, Anal. Chim. Acta, 250 (1991) 1.
5 A. Wehrli, J.C. Hildenbrand, H.P. Keller, R. Stampfli and R.W. Frei, J. Chromatogr., 149 (1978) 199.
6 J.J. Kirkland, J.L. Glajch and R.D. Faller, Anal. Chem., 61 (1989) 2.
7 B. Law and P.F. Chan, J. Chromatogr., 467 (1989) 267.
8 M.J.J. Hetem, J.W. de Haan, H.A. Claessens, L.J.M. van de Ven, C.A. Cramers and J.N. Nickel, Anal. Chem., 62 (1990) 2288.
9 N. Tanaka, T. Ebata, K. Hashizume, K. Hosoya and M. Araki, J. Chromatogr., 475 (1989) 195.
10 K.D. Lork and K.K. Unger, Chromatographia, 26 (1988) 115.
11 M.J.J. Hetem, J.W. de Haan, H.A. Claessens, L.J.M. van de Ven, C.A. Cramers and J.N. Nickel, Anal. Chem., 62 (1990) 2296.
12 A. Burcinova, J.W. de Haan, H.A. Claessens, L.J.M. van de Ven, C.A. Cramers, A. Bolck, P.M.J. Coenegracht, A.K. Smilde, D.A. Doornbos, F. Eisenbeiss and D. Lubda, 15th International Symposium on Column Liquid Chromatography, 1991, Switzerland.
13 M.J.J. Hetem, L. van de Ven, J. De Haan, L. Cramers, K. Albert and E. Bayer, J. Chromatogr., 479 (1989) 269.
14 L.D. Bowens and S. Pedigo, J. Chromatogr., 371 (1986) 243.
15 H.W. Stuurman, J. Kohler, S.O. Janssen and A. Litzen, Chromatographia, 23 (1987) 341.
16 R. Ohmacht, M. Kele and Z. Matus, Chromatographia, 28 (1989) 19.
17 T. Daldrup and B. Kardel, Chromatographia, 18 (1984) 81.
18 H. Engelhardt, B. Dreyer and H. Schmidt, Chromatographia, 16 (1985) 11.
19 P.C. Sadek and P.W. Carr, J. Chromatogr. Sci., 21 (1983) 314.
20 M.J. Walters, J. Assoc. Off. Anal. Chem., 70 (1987) 465.
21 L.C. Sander, J. Chromatogr. Sci., 26 (1988) 380.
22 P.A. Bristow and J.H. Knox, Chromatographia, 10 (1977) 279.
23 D. Lubda, K. Czerny, K. Cabrera, R. Bender and G. Jung, 15th International Symposium on Column Liquid Chromatography, 1991, Switzerland.

Analytica Chimica Acta, 282 (1993) 47–54
Elsevier Science Publishers B.V., Amsterdam

Aspects of quantitative determinations with polarimetric detectors in liquid chromatography [1]

Richard Däppen and Peter Voigt

Central Analytical Department, Ciba-Geigy AG, 4002 Basel (Switzerland)

François Maystre and Alfredo E. Bruno

Analytical Research, Ciba-Geigy AG, 4002 Basel (Switzerland)

(Received 23rd March 1993)

Abstract

The overall performance of polarimetric detectors for liquid chromatography has substantially improved in the last few years. Results show relative standard deviations of 0.50% and as good as 0.25% can be obtained using present models. Under reversed-phase conditions using achiral columns, pseudo-rotation due to refractive index related effects preclude these detectors from performing equally well when operated under static conditions. This situation becomes critical when analyzing compounds having small specific rotations or mixtures with small enantiomeric excess. Due to such pseudo-rotations, the calibration factors of the polarimetric detectors for two *R* and *S* enantiomers are not necessarily identical. Although the response functions are linear, the negative and positive parts do not coincide at zero enantiomeric excess.

Keywords: Liquid chromatography; Polarimetric detectors

Polarimetric detectors in liquid chromatography (LC) are useful tools to specifically analyze natural compounds in a matrix or to directly determine the ratio of two enantiomers of a sample relative to a reference compound of known enantiomeric composition. Previous reports in liquid chromatography have introduced general purpose polarimeters modified to accept a suitable flow cell [1,2] as well as dedicated research (not commercially available) polarimetric detectors [3]. The results reported here were obtained using a well documented technique [4,5] employing mono- and polychromatic polarimetric detection.

Correspondence to: R. Däppen, Central Analytical Department, Ciba-Geigy AG, 4002 Basel (Switzerland).

[1] This paper was presented at the *3rd International Symposium on Chiral Discrimination* in Tübingen, FRG, October 5–8, 1992.

In the last few years, several new commercial polarimetric LC detectors have been made available permitting the routine analysis of chiral samples. These instruments posses the potential of analyzing samples that cannot be analyzed accurately on chiral columns, primarily because the minor enantiomer elutes poorly resolved near the major peak leading to inaccurate integrations. In this regard it is also desirable to be able to use polarimetric detection to analyze, e.g., *R* samples taking the *S* component as reference and vice versa.

In order to determine simultaneously the content of the major substances, the impurities and the enantiomeric composition of the major compound with a single LC method, the possibilities of combining polarimetric detection with an existing, validated LC method on an achiral stationary phase and a standard detector [6] were explored.

This approach, not requiring an additional LC or GC method with a chiral column, is of great importance for the pharmaceutical industry [7] seeking for applications of polarimetric LC detectors in routine analysis.

In general, most present LC methods are based on a reversed-phase stationary phase, and aqueous eluents composed of organic modifiers, buffer, and ion-pairing additives to elute the compounds. For this reason, a simple reversed phase was chosen to optimize the chromatographic parameters best suited for the polarimetric detection mode selected.

EXPERIMENTAL

The schematic arrangement of the chromatographic system employed is shown in Fig. 1. It consists of an LC instrument (Hewlett-Packard 1090 with diode array UV absorption detector) interfaced to a polarimetric detector (also known as an optical activity detector) featuring a Faraday rotator between a polarizer/analyzer set [6].

As polarimetric detectors, either a commercially available Polarmonitor (IBZ, Hannover) using polychromatic light and a 40-μl flow cell, or a self-designed instrument using an IR-laser diode as light source and a 16-μl z-type flow cell (referred to thereafter as ARES-LD 10) were used. Preliminary evaluation tests were also performed on other commercial polarimetric detectors which are reported in detail in Ref. 6.

The polarimetric signal is proportional to the excess concentration of one enantiomer in a mixture of chiral compounds. By measuring the concentration of both enantiomers with the UV detector, the enantiomeric ratio of the sample can be determined. The entire system was calibrated using reference samples with known enantiomeric ratio. The enantiomeric excess, *ee*, of a sample is given by:

$$ee = \left\{ C_p \times \left[\frac{P}{UV} \right] \right\} \quad (1)$$

where C_p is a calibration factor and P/UV is the ratio of the polarimetric (P) to the UV signal (UV).

Data were collected with a Hewlett-Packard two channel A/D-converter and processed with the Pascal-Chemstation software package. The two channels of the converters collected the positive and the negative parts of the polarimetric output, respectively. As the differences on the

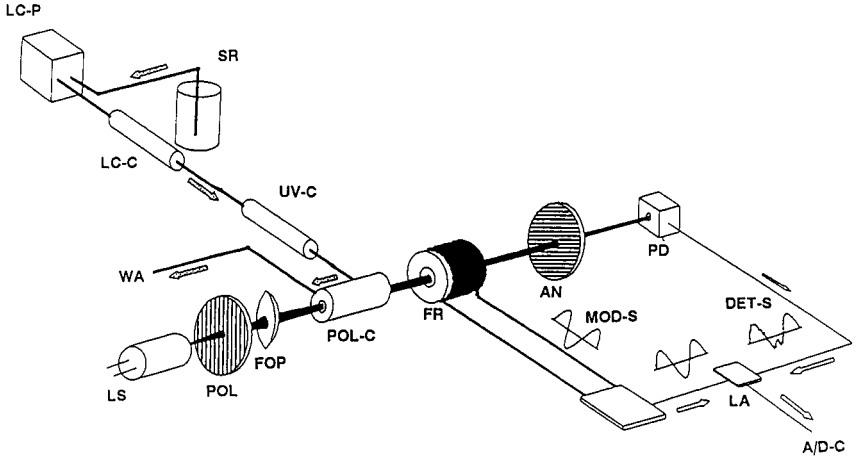

Fig. 1. Experimental setup including the main parts of the polarimetric detector employed. SR = Solvent reservoir; LC-P = LC pump; LC-C = separation column; UV-C = UV cell; POL-C = polarimetric cell; WA = waste; LS = light source; POL = polarizer filter; FOP = focussing optics; FR = faraday rotator; AN = polarizer analyzer; PD = photodiode; MOD-S = modulated signal; DET-S = polarimentric signal; LA = lock-in amplifier; A/D-C = A/D converter.

integrations between the two channels was constant and smaller than 0.5% its influence in the data reported in Table 1 has been neglected.

A 5-μm Nucleosil 100 RP-18 reversed phase, packed into a 125 × 4.6 mm i.d. column, with methanol–water (50:50) was used.

RESULTS

To evaluate the chromatographic conditions needed for optimization of the polarimetric detectors, constant amounts of $R(+)$- and S(−)-1-phenylethanol ($[\alpha]_D^{20} = 47°$) were injected on a C_{18} reversed-phase column with various methanol/water mixtures as mobile phase. Figure 2 shows the dependence of the signal to noise ratio (S/N) with flow-rate for various sample retentions, k'. It is apparent from this figure that small flow rates and small k' values result in better S/N ratios.

Alternatively, optically pure $R(+)$- and $S(-)$-1-phenylethanol samples were analyzed at various flow rates and temperatures for constant composition of the mobile phase near $k' \approx 2$. Table 1 reports the percentage relative standard deviations (%R.S.D.) for three series of five injections each calculated from the area and the peak

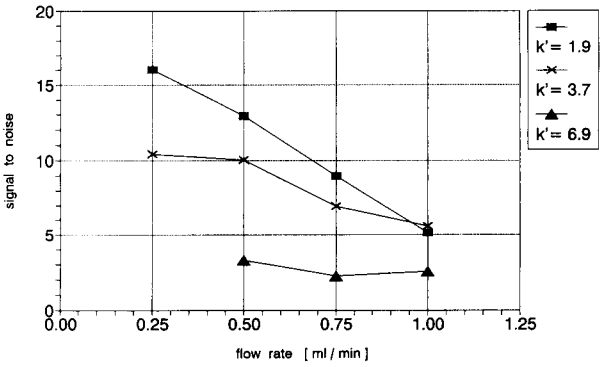

Fig. 2. S/N ratio of the polarimetric detector as a function of the flow rate for three retention values (k') using the Polarmonitor instrument and standard conditions (see text).

heights at 35°C and 50°C, respectively. In order to improve S/N ratios in the polarimetric signal, the column was chromatographically overloaded such that the peak profile was not severely degraded. In addition, the calibration factors for the $R(+)$ and $S(-)$ samples, $C_p(+)$ and $C_p(-)$ were calculated, adjusting the results for chemical and enantiomeric composition of the test samples. The percent differences of the calibration factors (ΔC_p) were calculated (see Table 1) as follows:

$$\Delta C_p = 100 \times \frac{[C_p(+) - C_p(-)]}{C_p(+)} \qquad (2)$$

TABLE 1

Relative standard deviations (in%) and differences of calibrations factors (see text for definitions) using the Polarmonitor detector and a sample injected of ca. 200 μg 1-phenylethanol under standard conditions (see text)

Sample	Flow rate (ml/min)	Area/height %R.S.D. (min)	Area/height %R.S.D. (max)	Area/height ΔC_p
Temp. = 35°C				
R-(+)	1.00	0.59/0.58	2.65/1.01	0.59/6.58
S-(−)	1.00	1.23/0.55	2.53/1.34	0.59/6.58
R-(+)	0.50	0.64/0.42	1.59/0.85	8.98/7.34
S-(−)	0.50	1.19/0.46	2.01/1.05	8.98/7.34
R-(+)	0.25	0.63/0.36	0.72/0.61	1.62/1.82
S-(−)	0.25	0.61/0.38	0.85/0.55	1.62/1.82
Temp. = 50°C				
R-(+)	1.00	0.62/0.40	1.20/0.90	−5.22/1.15
S-(−)	1.00	0.59/0.24	2.30/4.89	−5.22/1.15
R-(+)	0.50	0.95/0.13	1.24/0.72	5.63/6.37
S-(−)	0.50	0.28/0.35	1.21/0.40	5.63/6.37
R-(+)	0.25	1.33/0.58	2.83/1.39	0.90/5.13
S-(−)	0.25	0.59/1.39	0.93/1.76	0.90/5.13

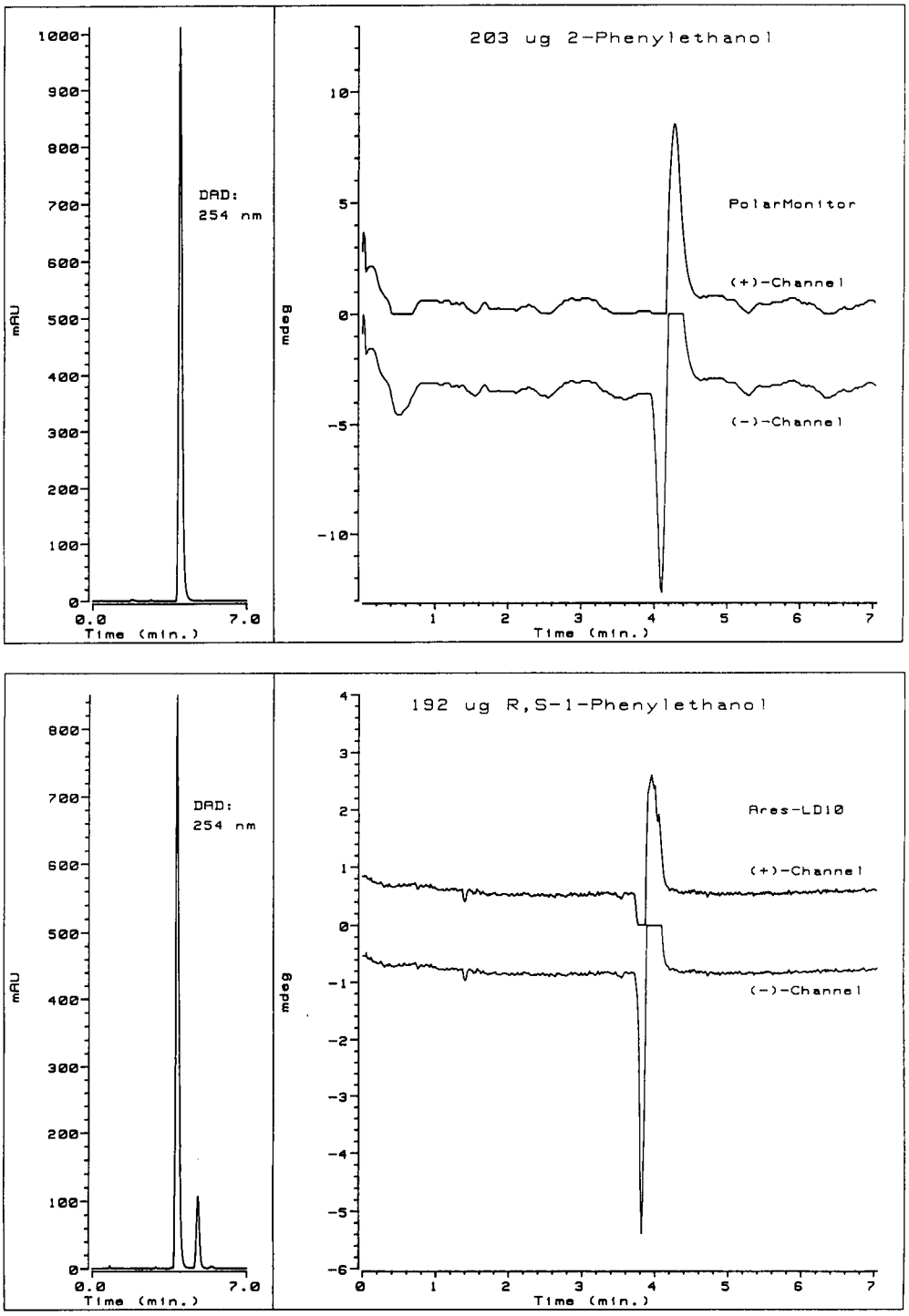

Fig. 3. Chromatogram of (top) 203 μg of 2-phenylethanol and (bottom) 192 μg of (±)1-phenylethanol displaying pseudo-rotations. Standard conditions, except for the flow rate which was 1 ml/min, were employed.

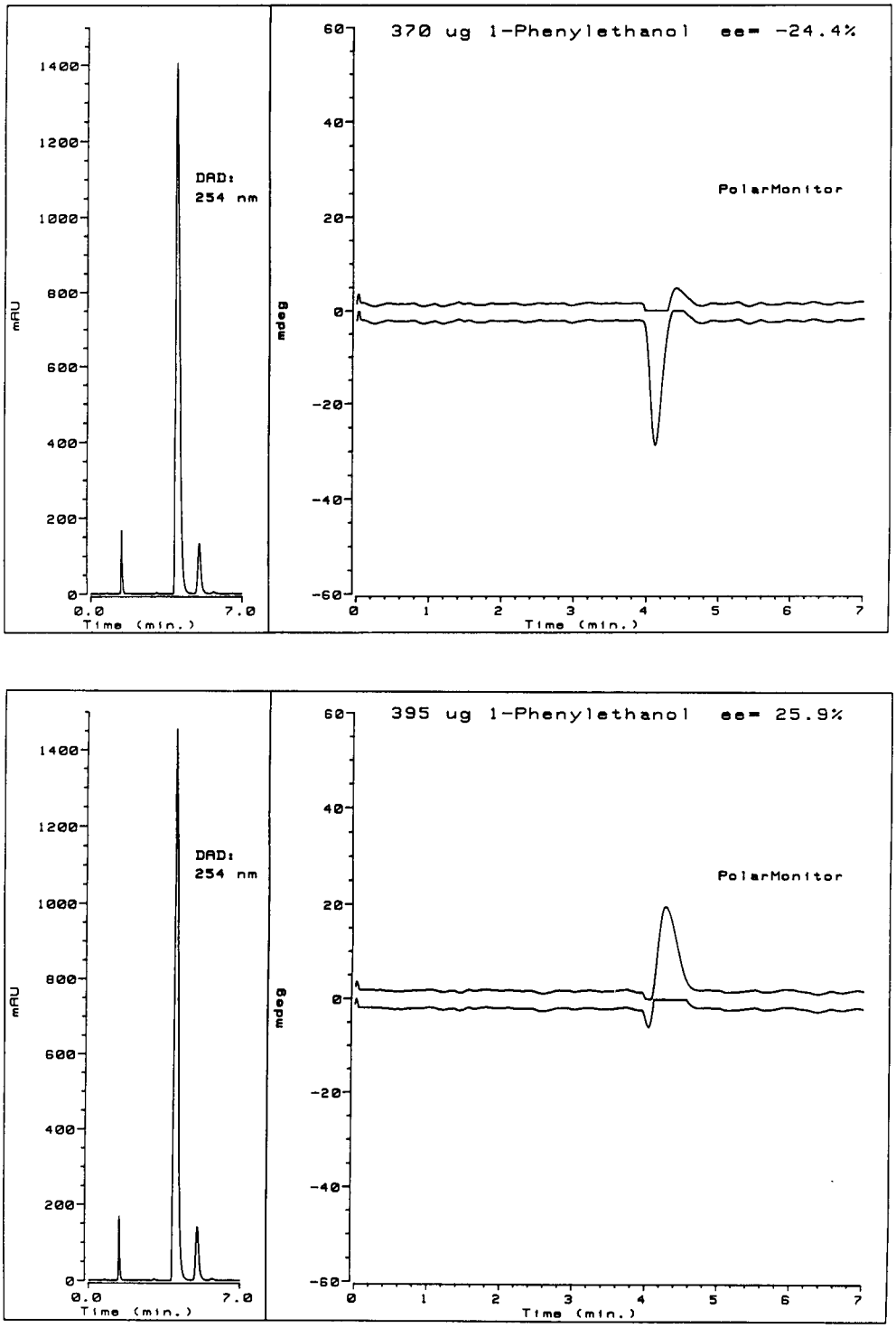

Fig. 4. Chromatogram of 375 μg of 1-phenylethanol having small enantiomeric excess. The chromatogram was recorded under standard conditions except for the flow rate of 1 ml min^{-1}.

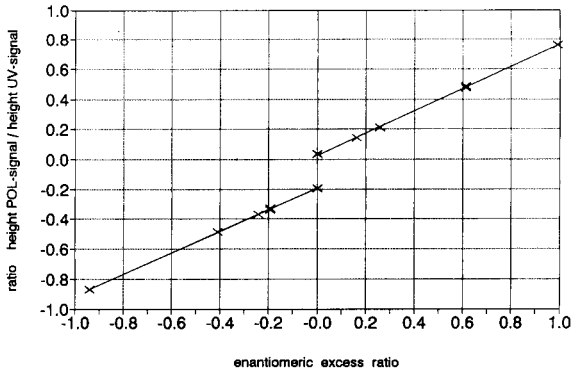

Fig. 5. Calibration curve of the Polarmonitor injecting ca 375 μg 1-phenylethanol at a flow rate of 0.5 ml min^{-1} and standard conditions.

The data presented in Table 1 show, as expected according to the results presented in Fig. 2, that lower flow rates, associated with better S/N ratios, produced the higher reproducibility for polarimetric detection. The increase in temperature from 35°C to 50°C did not significantly improve the reproducibility. Table 1 also shows, that the difference in calibration factors, ΔC_p (Eqn. 2), for the $R(+)$ and the $S(-)$ samples do change with the flow rate. Not only is there a change in the absolute value of ΔC_p, but also in its sign (see Eqn. 2). Similar results were found when methanol is replaced by acetonitril or THF in the eluent.

Figure 3 displays the polarimetric and UV signal of racemic (±) 1-phenylethanol and achiral 2-phenylethanol, injected into the LC system. The unexpected strong signal produced by the polarimeter is an artifact due to refractive index related effects generated by the eluting peaks. This pseudo-rotation seems to be a general problem for LC polarimetric detectors particularly in the presence of aqueous mobile phases [8–10] explaining the fluctuations in ΔC_p reported in Table 1, the refractive index induced artifacts shown in Fig. 3 and the observed distortions on the chromatographic peaks shown in Fig. 4.

Pseudo-rotations manifest also in anomalous calibration curves as the one shown in Fig. 5. In this regard it must be noted that a similar calibration curve to that shown in Fig. 5 has already been documented (see Fig. 17 in Ref. 1) but not interpreted.

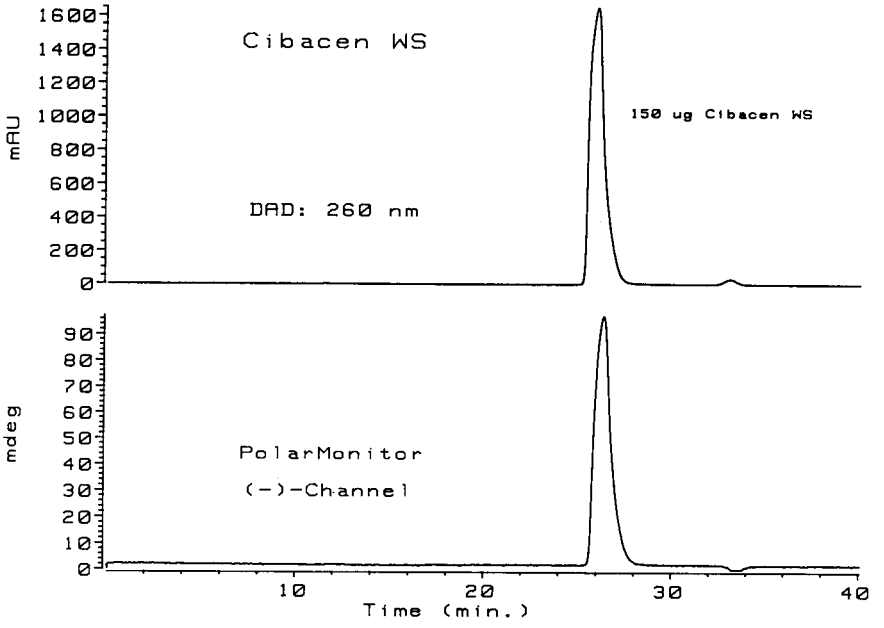

Fig. 6. Chromatogram of Cibacen WS using polarimetric detection (lower trace) and UV absorption detection (upper trace) eluted from Nucleosil RP-18 using as eluent Veibel buffer (17%) + water (25%) + methanol (58%). The Veibel buffer is made of 90 mM KCl + 10 mM HCl at pH 2.06. The flow rate was 0.25 ml min^{-1} and the temperature 35°C.

TABLE 2

P/UV ratios for pure and spiked Cibacen samples. (The chromatographic conditions are identical to those of Fig. 6)

Sample	Area/height P/UV	Area/height %R.S.D.	Area/height P/UV (min)	Area/height P/UV (max)
Cibacen WS (= *SS*)	0.626/0.578	0.23/0.10	0.624/0.577	0.628/0.580
Cibacen WS + 0.50% *RR*	0.620/0.572	0.12/0.08	0.619/0.572	0.621/0.572
Cibacen WS + 0.25% *RR*	0.623/0.576	0.24/0.08	0.622/0.576	0.624/0.576

Pharmaceutical applications

The above described method has been employed in the analysis of two optically active compounds of importance to the pharmaceutical industry, Cibacen WS and 10-EDAM WS. Cibacen WS is a pure enantiomer with *SS*-configuration and a high specific rotation of $[\alpha]_D^{20} = 140°$. Its diastereomers are separated from Cibacen WS using reversed-phase conditions. Based on an existing LC method the flow rate and the injected amount were optimized for polarimetric detection. The resulting chromatograms are shown in Fig. 6 and the corresponding reproducibility data are reported in Table 2. By adding a defined amount of the other enantiomer its detection limit was determined to be better than 0.5% with respect to the major component

10-Edam WS consists of two diastereomers that cannot be separated on a reversed-phase column. The two diastereomers have opposite specific rotations leading to an overall specific rotation of the 1:1 mixture adding only to $[\alpha]_D^{20} = -14.8°$, resulting in a poor polarimetric signal as shown in Fig. 7. In this case, due to pseudo-rotations, the width of the peak of the polarimetric trace is even smaller than the UV signal. By

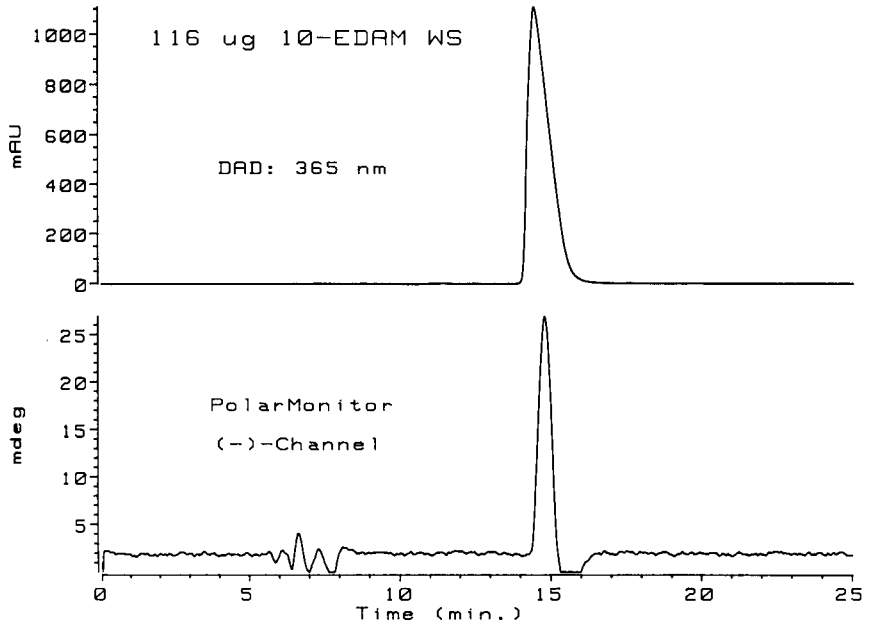

Fig. 7. Chromatogram of 10-EDAM WS using polarimetric detection eluted from a 10-μm Nucleosil RP-18; 250 × 4.6 mm i.d. column using as eluent a 50% ion-pairing solution–50% methanol mixture (ion-pairing solution = 20 mM $CH_3(CH_2)_5SO_3Na$ + 20 mM H_2SO_4); flow rate, 0.25 ml min^{-1}; temperature, 35°C.

adding the pure diastereomers with specific rotations of −206° and 240°, respectively, the detection limit of the diastereomers in the 1 : 1 mixture was found to be 1%.

Conclusions

Present polarimetric instruments may be routinely used to analyze enantiomeric ratios of chiral compounds with detection limits better than 1% depending on the specific rotation of the samples. Due to refractive index induced pseudo-rotations, distorted peak shapes are often observed. These effects are particularly strong when dealing with chromatographically overloaded reversed-phase conditions in the presence of samples displaying small enantiomeric excess or low specific rotations together with aqueous mobile phases. Care should be taken when employing deconvolution techniques as those discussed in Ref. 11.

One possibility to overcome the quantitative problems caused by pseudo rotations was recently proposed [9,10] and is referred to as a *refractive index equalizer*. This device consist of a servo-controlled system which equalizes the refractive index of the eluent to a constant value placed after the column and before the polarimeter.

We would like to thank S. Barnard for critically reviewing the manuscript.

REFERENCES

1 J.L. DiCesare and L.S. Ettre, J. Chromatogr., 251 (1982) 1.
2 W. Boehme, G. Wagner, U. Oehme and U. Priesnitz, Anal. Chem., 54 (1982) 709.
3 E.S. Yeung, L.E. Steenhoek, S.D. Woodruff and J.C. Kuo, Anal. Chem., 52 (1980) 1399.
4 A. Mannschreck, Chirality, 4 (1992) 163.
5 D.M. Goodall, Trends Anal. Chem., 12 (1993) 177; D.K. Loyd and D.M. Goodall, Chirality, 1 (1989) 251.
6 P. Voigt, Diplomarbeit Fachhochschule Reutlingen, Germany and Ciba-Geigy AG Basel, Switzerland, January 1992.
7 S.C. Stinson, C&EN, 70 (1992) 46.
8 M. Kamahori, Y. Watanabe, H. Miyagi, H. Ohki and R. Miyabe, J. Chromatogr., 549 (1990) 101.
9 F. Maystre and A. E. Bruno, Proceeding of HPLC'92, Boston, MA, p. A-67.
10 F. Maystre and A. E. Bruno, Refractive Index Equalizer for HPLC, European patent application, No. 91810991.9, December 1991.
11 A. Mannschreck and L. Kiessl, Chromatographia, 28 (1989) 263.

Analytica Chimica Acta, 282 (1993) 55–61
Elsevier Science Publishers B.V., Amsterdam

Analytical method for white phosphorus residues in munitions-contaminated sediments

Marianne E. Walsh and Susan Taylor

U.S. Army Cold Regions Research and Engineering Laboratory, Hanover, NH 03755-1290 (USA)

(Received 10th March 1993; revised manuscript received 20th April 1993)

Abstract

An analytical method is described to determine white phosphorus (P_4) in sediments contaminated by smoke munitions. Experiments were performed to promote the extraction of P_4 from saturated sediment with a nonpolar solvent. P_4 extraction was enhanced by adding water to form a sediment–water slurry prior to shaking with isooctane for up to 24 h. P_4 was determined with a portable capillary gas chromatograph equipped with a nitrogen–phosphorus detector. A certified reporting limit of 0.88 $\mu g\ kg^{-1}$ was estimated.

Keywords: Gas chromatography; Munitions; Phosphorus; Sediments

White phosphorus (P_4) has been used extensively in smoke-producing munitions by the United States and European militaries since World War I. Until recently, long-term environmental contamination from the explosion of projectiles containing P_4 was considered unlikely due to the thermodynamic instability of P_4 in the presence of atmospheric oxygen. However, when a catastrophic waterfowl die-off at Eagle River Flats, AK, a U.S. Army training site, was traced to the presence of P_4 in the salt marsh sediments [1], an investigation was initiated to determine the spatial distribution of P_4 contamination. This investigation required the analysis of over 1000 sediment samples. Although there is no standard method for the determination of P_4 in soil or sediment, Addison and Ackman [2] have published a packed-column gas chromatographic method developed to analyze sediments contaminated by the effluent from a P_4 production facility. The method we optimized to analyze P_4 munitions-contaminated sediments was based on the work of Addison and Ackman [2], but it was modified as required by the different mode of contamination and the different sediment characteristics of our samples. We also optimized the method for detection of very low (less than 1 $\mu g\ kg^{-1}$) P_4 concentrations, and used a capillary-column gas chromatograph, which was portable and could be used in a field lab.

Correspondence to: M.E. Walsh, U.S. Army Cold Regions Research and Engineering Laboratory, Hanover, NH 03755-1290 (USA).

EXPERIMENTAL

An analytical standard for P_4 was obtained from Aldrich (Milwaukee, WI). A stock solution was prepared under nitrogen by dissolving 250 mg of P_4 in 0.50 l isooctane (Aldrich). Calibration standards over the concentration range 3.6 to 72 $\mu g\ l^{-1}$ were prepared by diluting the stock solution with isooctane.

Various experiments, as described below, were performed to enhance the extraction of P_4 from the wet sediments. We found the best procedure

to be as follows: wet sediment samples were extracted by placing a 20-cm^3 (30- to 40-g) subsample into a 120-ml jar containing 10.0 ml of isooctane and 10.0 ml of degassed reagent-grade water. (The 20-cm^3 subsample was obtained using a 20-cm^3 plastic syringe with the tapered end cut off. This procedure was used to minimize oxidation of P_4 by contact between the subsample and air while the subsample was added to the solvent.) Each jar was tightly sealed with a PTFE-lined cap and vortex-mixed for 1 min, and then placed horizontally on a platform shaker for 18 h. The sample then was allowed to stand undisturbed for 15 min to permit phase separation. If a clear isooctane layer failed to form, approx. 35 ml of the sample was centrifuged for 1 min at 2500 rpm.

P_4 was determined by injecting a 1.0-μl aliquot of the isooctane extract on-column into an SRI Model 8610 gas chromatograph equipped with a nitrogen–phosphorus detector. The methylsilicone fused silica column (J&W DB-1, 15 m × 0.53 mm i.d., 3.0 μm film thickness) was maintained at 80°C. The carrier gas was nitrogen set at 30 ml min^{-1}. Under these conditions, white phosphorus eluted at 2 min.

RESULTS AND DISCUSSION

Extraction conditions

The method developed by Addison and Ackman [2] was designed to detect P_4 in sediments contaminated with colloidal P_4 from a production plant in Long Harbour, Placentia Bay, Newfoundland. Up to 5 g of wet sediment was extracted with 50 ml of isooctane by swirling with 5-mm glass beads in a stoppered flask for 10–15 min. The samples were filtered and the isooctane layer was collected for analysis by GC-FPD. Analyte recoveries ranging from 77 to 90% were estimated based on spiked, wet sediment. Since the extraction kinetics for spiked samples can be significantly faster than for field-contaminated samples [3], we performed experiments using field-contaminated sediments collected at Eagle River Flats to study the effects of extraction conditions such as sediment-to-solvent ratio and extraction time.

A major difference between the sediments analyzed by Addison and Ackman and the sediments from Eagle River Flats was that the Eagle River Flats sediments did not mix with the nonpolar isooctane despite vigorous agitation. This poor mixing was attributed to the small particle sizes typical of the Eagle River Flats sediments. Hydrometer analyses of these sediments showed that the silt and clay fractions were always greater than 97%. In contrast, the Newfoundland sediments analyzed by Addison and Ackman [2] consisted mainly of mixed gravel, sand, silt and clay [4]. We found that adding enough water to the wet Eagle River Flats sediments to form a soil–water slurry appeared to enhance the mixing. We tested the effect of adding water to a dense clay field-contaminated sediment from Eagle River Flats on the concentration of P_4 determined from the extract. First, we extracted eight sediment samples following the procedures of Addison and Ackman and analyzed a small portion of the extract. P_4 was detectable in only three samples (Table 1). We then added 10 ml of degassed reagent-grade water to each sample and continued to shake the samples overnight. Repeat analyses of the isooctane extracts showed P_4 was detectable in all eight samples. For the three samples where P_4 was detected originally, estimated concentrations were two orders of magni-

TABLE 1

Effect of adding water and additional shaking on estimates of P_4 concentration in eight field-contaminated sediment samples

P_4 concentration ($\mu g\ kg^{-1}$)	
Method of Addison and Ackman	Modified method [a]
Not detected	73
Not detected	84
Not detected	170
Not detected	270
Not detected	270
75	540
89	11000
150	27000

[a] 10 ml water added to each sample, and samples shaken for 12 h.

tude higher following the addition of water and additional shaking (Table 1).

Next, we tested the effect of adding water on the estimate of P_4 concentration obtained with a greatly reduced solvent-to-sediment ratio. A small solvent-to-sediment ratio reduces waste and improves detection capability, provided the partitioning of P_4 between the solvent and sample is favorable. Since the octanol–water partition coefficient for P_4 is high (greater than 1000), partitioning should be not be a limiting factor for this extraction. We chose 10 ml of isooctane as an adequate volume for good extraction without solvency limitations. A series of 20-cm^3 (30- to 40-g) subsamples from a field-contaminated sample were mixed with 0, 10, or 20 ml of water plus 10 ml of isooctane and shaken overnight. Five replicates were prepared to permit comparison using nonparametric statistics [5]. We used nonparametric statistics because the P_4 is not homogeneously distributed throughout the sample; rather, it occurs as particles of various sizes [1]. (Microscopic examination of some sediments revealed P_4 particles ranging in size from less than 0.1 mm to greater than 5 mm.) We found significantly higher concentrations of P_4 in the extracts from samples to which water was added (Table 2). Adding 20 ml as compared to 10 ml of water did not significantly improve the extraction of P_4, so we chose the smaller volume. In general, the addition of sufficient water to form a water–sediment slurry greatly enhanced mixing with the nonpolar isooctane, and consequently improved the extraction of P_4 from the dense day sediments.

TABLE 2

Effect of volume of added water on estimates of P_4 concentration in a field-contaminated sediment sample

Water volume (ml)	Replicates	P_4 concentration ($\mu g\ kg^{-1}$ wet sediment)	Rank [a]
0	1	89	5
	2	75	2
	3	75	3
	4	80	4
	5	66	1
10	1	240	8
	2	220	7
	3	120000	15
	4	1510	13
	5	480	12
20	1	390	11
	2	260	9
	3	280	10
	4	210	6
	5	11000	14

[a] $H = 9.5$. $\chi^2_{0.95}$ $(df = 2) = 5.99$. Since 9.5 exceeds 5.99, there is a significant difference among the three groups. Wilcoxon-Mann-Whitney test shows no difference between the groups having 10 and 20 ml of water.

Extraction kinetics

Additional experiments were performed to determine the optimum shaking time for extraction. Four field-contaminated sediment samples with estimated P_4 concentrations ranging from 1 (barely detectable) to 1000 $\mu g\ kg^{-1}$ were used. Sediments with a wide range of analyte concentration were tested, since extraction kinetics can vary with concentration [6]. Each sample was vortex-mixed for 1 min with water and isooctane, and a Pasteur pipette was used to withdraw a 0.1-ml subsample of the isooctane layer. Then the samples were shaken horizontally on a platform for 48 h, with subsamples of the isooctane layer taken at 0.5, 1, 1.5, 4, 7.75, 24 and 48 h. Prior to sampling the isooctane, each sample was briefly centrifuged, and after sampling each sample was vortex-mixed to resuspend the sediment prior to being placed back on the platform shaker.

For the sample with the lowest analyte concentration, the highest concentration was measured after extended shaking (48 h); P_4 was undetectable in the sample shaken less than 7.75 h (Fig. 1). For the two samples at intermediate P_4 concentrations, the highest recovery was at 24 and 7.75 h (Fig. 1). Extending shaking of these samples resulted in analyte loss from the isooctane extract, presumably by oxidation. For the sample with the highest P_4 concentration, P_4 was detectable after 1 min of vortex-mixing and reached a maximum value after 4 h of shaking (Fig. 1).

Based on these results, a shaking time between 7.75 and 24 h is a reasonable compromise. It may not be sufficient to extract all the P_4 from very low-concentration samples, but extended extraction times can lead to some analyte loss for

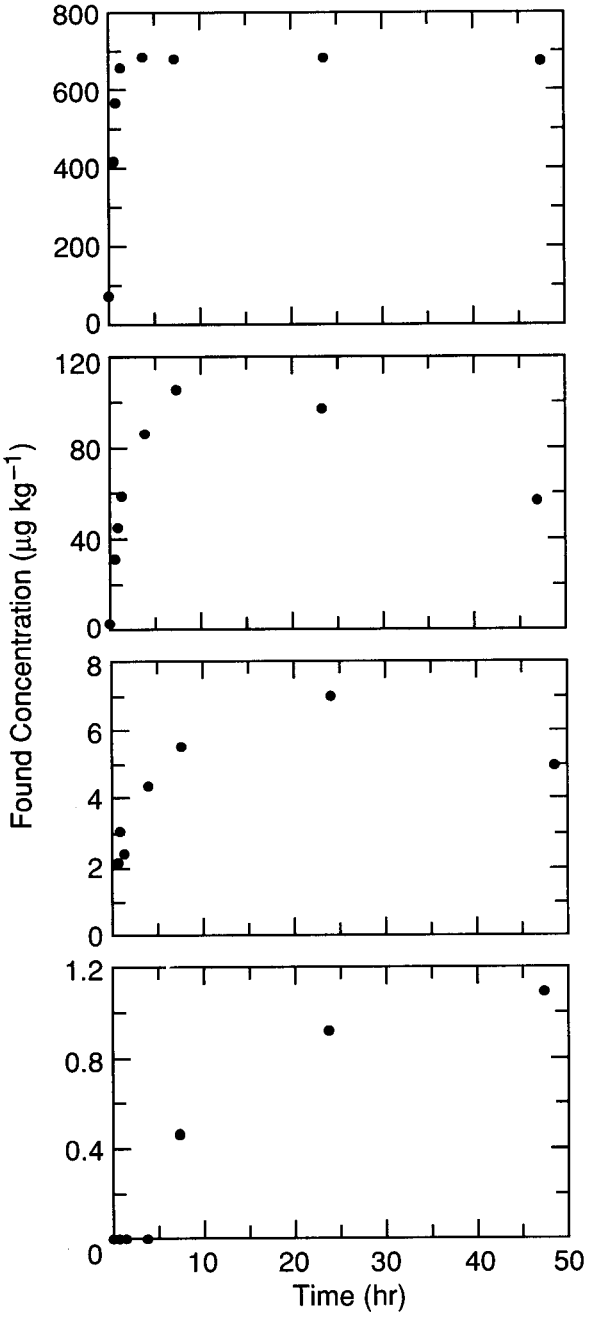

Fig. 1. Results of extraction kinetics experiment that tested four field-contaminated sediments of different estimated concentrations.

intermediate concentrations. For practical reasons, a shaking time of approximately 18 h is convenient, since samples that are prepared for extraction in the afternoon can be shaken overnight and are ready for analysis the following morning.

Sample volume

We examined whether changing the subsample size would systematically change the concentration estimates obtained. Five replicate 5-, 10- and 20-cm^3 subsamples from a field-contaminated sediment were extracted by adding 10 ml of degassed water and 10 ml of isooctane to each subsample in 120-ml glass jars. The remaining 288 g (approximately 150 cm^3) of sediment were extracted by adding 300 ml of degassed water and 100 ml of isooctane in a 1-l glass jar. Samples were shaken overnight.

A nonparametric rank test was used to compare the five replicates in each group [5]. The results indicate that sample size does not significantly ($\alpha = 0.05$) alter the estimate of P_4 concentration (Table 3). The large variation among subsamples reflects the fact that P_4 occurs as heterogeneously distributed particles of different sizes. A 20-cm^3 subsample size was chosen to minimize

TABLE 3

Effect of sample volume on estimated concentration of P_4 in a field-contaminated sediment

Sample volume	Concentration ($\mu g\ kg^{-1}$)	Geometric mean ($\mu g\ kg^{-1}$)	Rank [a]
5	12	33	1
	45		10
	31		8
	120		12
	20		6
10	17	40	4
	22		7
	920		14
	16		3
	19		5
20	16	110	2
	1900		15
	53		11
	43		9
	200		13
150	34		

[a] $H = 1.58$. $\chi^2_{0.95}$ ($df = 2$) = 5.99. Since 1.58 does not exceed 5.99, the average concentrations of the three groups are not significantly different at the 95% confidence level.

the risk of false negatives. A larger subsample would require larger extraction jars, reducing the batch size that could be simultaneously extracted on a single platform shaker and adding to the expense of the analysis.

Sources of subsampling error

Because P_4 is present in the sediments as particles of different sizes, the mass of P_4 detected in a 20-cm^3 subsample from a bulk sample would depend on the number and size of the particles in the subsample. We were concerned that if a bulk sample contained only a few heterogeneously distributed particles of P_4, a negative result (i.e., no P_4 or below detection) might be obtained from a subsample. To test this possibility we first subsampled five sediment samples (collected in the vicinity of contaminated samples at Eagle River Flats) that were negative when analyzed initially. Five subsamples from each of these bulk samples all tested negative. When the remainder (200–300 cm^3) of each bulk sample was extracted, no P_4 was found. These results suggest that the risk is low of reporting a bulk sample as blank when in fact P_4 particles are present. We also took multiple subsamples from bulk samples that we found were positive when analyzed initially. None of the replicates from these samples gave a below-detection (or negative) results, which also supports the conclusion that, using our subsampling protocol, the risk is low of reporting the absence of P_4 in a bulk sample where it is actually present.

Comparison with method of Addison and Ackman

We compared estimates of P_4 concentrations obtained using the extraction parameters described by Addison and Ackman [2] with those described in the Experimental section that we found enhanced extraction. Five subsamples of eleven sediment samples collected in Eagle River Flats representing different areas of the salt marsh (i.e., mudflat, pond bottom, bulrush areas) and a wide range of P_4 concentrations were extracted by both procedures. Using our method, we detected P_4 in every subsample in all 11 samples. Following the original procedure [2], P_4 was consistently detectable in only one sample (Table 4). This sample had the highest P_4 concentration as determined by our procedure; we found a median concentration of 12 000 $\mu g\ kg^{-1}$, almost two orders of magnitude greater than that found by the procedure of Addison and Ackman [2].

TABLE 4

Estimates of P_4 concentration obtained by improved extraction conditions compared to those obtained by method of Addison and Ackman [2]

Optimized procedure		Method of Addison and Ackman [2]	
Range of concentrations [a] found ($\mu g\ kg^{-1}$)	Median ($\mu g\ kg^{-1}$)	Range of concentrations [a] found ($\mu g\ kg^{-1}$)	Median ($\mu g\ kg^{-1}$)
0.74–47	1.5	Not detected	
1.5–7.4	4.5	Not detected	
1.6–4.1	2.4	Not detected	
2.4–5.2	3.2	Not detected	
4.2–10	9.2	Not detected	
6.9–12	11	Not detected	
9.9–27	17	Not detected, 24 800 [b]	
11–9 900	83	Not detected	
100–200	160	Not detected	
76–360	220	Not detected	
8 000–67 000	12 000	150–230	200

[a] Five replicates. [b] P_4 detected in one out of five replicates.

TABLE 5

P_4 concentrations found in separate subsamples taken after an extended time interval

First analysis concentration ($\mu g\ kg^{-1}$)	Days between analyses	Second analysis concentration ($\mu g\ kg^{-1}$)	Number of repeat analyses	Median ($\mu g\ kg^{-1}$)
3.6	274	5.5–260	8	7.8
11	265	11–550	8	14
62	267	7.6–32	8	11
150	271	70–520	8	97
420	313	210–120000	10	340

Stability of extracts and standards

After analyzing over 1000 samples within 24 h of collection from Eagle River Flats and then reanalyzing selected samples weeks later, we found that P_4 was stable in sediment samples that were refrigerated at 4°C and capped tightly to prevent desiccation. In fact, P_4 was stable for at least 9 to 10 months (Table 5). The isooctane extract in contact with the sediment is relatively stable also, provided the sample is not shaken continuously. For example, three sample extracts had estimated P_4 concentrations of 0.5, 1.0, and 92 mg l^{-1} when analyzed initially. These samples were left for six weeks at room temperature and resampled. Estimated P_4 concentrations were 0.7, 0.6 and 87 mg l^{-1}, respectively, indicating that even at room temperature P_4 is not subject to rapid degradation once a subsample is mixed with solvent for 18 h and then left undisturbed.

Calibration standards over the concentration range 3.6 to 72 $\mu g\ l^{-1}$ are stable for months stored in ground glass stoppered flasks in the dark at 4°C. However, the stock standard, with a P_4 concentration of 500 mg l^{-1}, was not stable; a water soluble, whitish-yellow precipitate formed within 24 h after preparation. Thus dilutions for the calibration standards should be made as soon as the P_4 dissolves in the stock solution.

Method performance demonstration

A spike-recovery study was conducted to allow estimation of a detection limit [7]. Subsamples (40 g) of wetted (50% moisture on a wet-weight basis) standard sediment (U.S. Army Environmental Center, Aberdeen Proving Ground, MD) were spiked with isooctane solutions of P_4 to yield sediment concentrations over the range of 0.8 to 16.9 $\mu g\ kg^{-1}$. Samples were prepared and extracted on four consecutive days (Table 6). A certified reporting limit was calculated using 90% confidence bands about a linear least-squares regression model for found concentrations versus spiked concentrations [7]. A reporting limit of 0.88 $\mu g\ kg^{-1}$ (wet weight) was calculated, and mean recovery was 97.2%.

Interferences

Using the procedure described in this paper, we have analyzed over 1000 sediment samples and have not observed any interferences, probably due to the selective nitrogen–phosphorus detector. White phosphorus can be confirmed, if necessary, using gas chromatography–mass spectrometery. The mass spectrum of P_4 has a base peak at mass/charge 124 amu corresponding to the molecular ion. The molecular ion also fragments into P^+, P_2^+ and P_3^+, which have peaks at mass/charge (relative abundance) 31 amu (12%), 62 amu (20%), and 93 amu (10%), respectively [1].

TABLE 6

Data for method performance validation

	Spike concentration ($\mu g\ kg^{-1}$)	Found concentration ($\mu g\ kg^{-1}$)			
		Day 1	Day 2	Day 3	Day 4
0.5×	0.845	0.819	1.10	1.03	1.04
1×	1.69	1.93	1.90	1.53	1.82
2×	3.38	3.48	3.51	3.42	3.76
5×	8.45	8.16	8.58	7.73	8.42
10×	16.9	16.4	17.2	17.6	16.1

Conclusions

White phosphorus (P_4), which is used by the military to produce smoke screens, combusts in air to produce a mixture of polymeric phosphoric acids with oxidation states of +1 to +5. These acids may be analyzed by high-performance liquid chromatography [8,9]. The method described in this report is for the determination of the unoxidized residue, P_4, which has an oxidation state of zero. Prior to the development by Addison and Ackman of a gas chromatographic method for the determination of P_4, P_4 was analyzed after oxidation to phosphate, which then was determined by standard methods. The Addison and Ackman [2] approach was a vast improvement over classical procedures for P_4 analysis since it does not suffer from interference from naturally occurring phosphates. However, the extraction procedure is inadequate for sediments high in silts and clays. Using field-contaminated sediments, we found P_4 extraction was enhanced by adding water to form a sediment–water slurry prior to shaking with isooctane for up to 24 h. Detection capability was improved by using a small solvent-to-sediment ratio. A certified reporting limit of 0.88 $\mu g\ kg^{-1}$ was estimated. Since P_4 has been widely used in smoke munitions at least since World War I, military training areas that contain wetlands and are undergoing site investigations should be screened for P_4 contamination. The procedure we describe here should meet the analytical needs of site investigators for this analysis.

The authors gratefully acknowledge Dr. Thomas F. Jenkins and Dr. C.L Grant for technical review of this manuscript. Dr. Charles H. Racine led the site investigation at Eagle River Flats. He and Charles M. Collins provided the samples and offered useful suggestions. Laboratory assistance was provided by Elizabeth Nadeau. Funding for this research was provided by the U.S. Army Environmental Center, Aberdeen Proving Ground, MD, Martin H. Stutz and Steve Bird, Project Monitors, and the U.S. Army Engineer Waterways Experiment Station, Vicksburg, MS, Ann Strong, Project Monitor. This publication reflects the personal views of the authors and does not suggest or reflect the policy, practices, programs, or doctrine of the U.S. Army or Government of the United States.

REFERENCES

1 C.H. Racine, M.E. Walsh, B.D. Roebuck, C.M. Collins, D. Calkins, L. Reitsma, P. Bucli and G. Goldfarb, J. Wildlife Diseases, 28 (1992) 669.
2 R.F. Addison and R.G. Ackman, J. Chromatogr., 47 (1970) 421.
3 T.F. Jenkins, M.E. Walsh, P.W. Schumacher, P.H. Miyares, C.F. Bauer and C.L. Grant, J. Assoc. Off. Anal. Chem., 72 (1989) 890.
4 D.L. Peer, in P.M. Jangaard (Ed.), Effects of Elemental Phosphorus on Marine Life: Collected Papers Resulting from the 1969 Pollution Crisis Placentia Bay, Newfoundland, Fisheries Research Board of Canada, Halifax, 1972, pp. 181–186.
5 M.G. Natrella, Experimental Statistics, National Bureau of Standards Handbook 91, 1966, pp. 16–13.
6 T.F. Jenkins and C.L. Grant, Anal. Chem., 59 (1987) 1326.
7 A. Hubaux and G. Vos, Anal. Chem., 42 (1970) 840.
8 R.S. Brazell, R.W. Holmberg and J.H. Moneyhun, J. Chromatogr., 290 (1984) 163.
9 R.S. Ramsey, Adv. Chromatogr., 25 (1986) 219.

Analytica Chimica Acta, 282 (1993) 63–74
Elsevier Science Publishers B.V., Amsterdam

Determination of picomolar concentrations of titanium, gallium and indium in sea water by inductively coupled plasma mass spectrometry following an 8-hydroxyquinoline chelating resin preconcentration

Kristin J. Orians

Departments of Oceanography and Chemistry, University of British Columbia, Vancouver, British Columbia V6T 1Z4 (Canada)

Edward A. Boyle

Department of Earth, Atmospheric and Planetary Sciences, Massachusetts Institute of Technology, Cambridge, MA 02139 (USA)

(Received 11th January 1993; revised manuscript received 1st April 1993)

Abstract

Picomolar concentrations of dissolved titanium, gallium and indium in sea water are measured using inductively coupled plasma mass spectrometry (ICP-MS) after concentration and separation from the major ions in sea water via an 8-hydroxyquinoline chelating ion exchange resin (TSK-8HQ). Detection limits of 5–10 pM (0.2–0.4 part per trillion, ppt), 0.5 pM (0.02 ppt) and 0.1 pM (0.01 ppt) were found for Ti, Ga and In, respectively, after a 400-fold (Ti) or 3000-fold (Ga and In) concentration. The detection was blank limited for Ti, due primarily to background interferences from the HNO_3 matrix, and sensitivity limited for Ga and In. Open ocean sea water concentrations for these elements are in the range of 6–300 pM for Ti, 2–60 pM for Ga, and 0.1–2.0 pM for In. Sampling and analytical precision of 7–10% was generally found for concentrations greater than twice the detection limit.

Keywords: Flow injection; Mass spectrometry; Gallium; 8-Hydroxyquinoline; Indium; Sea water; Titanium; Waters

Many trace elements exist at extremely low concentrations in sea water, relative to their crustal abundance, due primarily to their rapid removal from solution by adsorption onto the surfaces of sinking particles. Ti, Ga and In, with crustal abundances or 0.57%, 15 parts per million (ppm), and 0.1 ppm, respectively [1], are thought to be limited to their sub-nanomolar (nM) sea water concentrations ($\leq$ 0.02 ppb) by this scavenging removal mechanism [2–5]. These elements are potentially analogous to the more abundant hydroxide-forming elements, aluminum and iron (crustal abundances 8.2% and 5.6%, respectively) [1], which have been more extensively studied [6–10]. Rapid removal from sea water leads not only to low concentrations, but also to tremendous spatial and temporal variability, as these elements are not in the oceans long enough to become thoroughly mixed ($\leq$ 500 years). Concentration ranges of up to 3 orders of magnitude are found for some hydroxide-forming trace elements, with distributions which reflect a complex combination of external sources, variations in removal intensities [2–4,9–14], and for some elements (Ga and Fe), involvement in nutrient-type

Correspondence to: K.J. Orians, Departments of Oceanography and Chemistry, University of British Columbia, 6270 University Boulevard, Vancouver, British Columbia V6T 1Z4 (Canada).

cycling (surface uptake and mid-depth release) as well [4,9,10]. Their large dynamic range makes these elements potentially useful as tracers of marine processes.

Our ability to accurately measure trace levels of metals in sea water has been enhanced by developments in two separate areas: advances in analytical instrumentation, providing for more sensitive elemental detection, and advances in trace metal clean sampling strategies, allowing collection of contamination-free sea water samples. The recent development of inductively coupled plasma mass spectrometry (ICP-MS), first made commercially available in 1983, is a prime example of an instrumental advance which is enabling further exploration into the cycles of trace metals in the oceans. Recent studies on gold [15], barium [16,17], and thorium [18], for example, would have been much more difficult without this new technique. Another advantage of ICP-MS determination is its multi-elemental capability, as demonstrated for the first row transition metals in sea water (after concentration/separation using a chelating resin) by a group at the National Research Council of Canada [19,20]. This manuscript describes the development of ICP-MS methods for the determination of ultra-trace levels of titanium, gallium and indium in sea water.

There are few published methods for the reliable determination of Ti, Ga and In in sea water. Titanium in sea water has recently been measured by an electrochemical method, using cathodic adsorption stripping voltammetry, with a detection limit of 0.03 nM [21]. This method has been successfully used in estuarine regions where Ti concentrations are higher [22], but does not presently have low enough detection limits for the open ocean levels, determined using the method presented here [2]. Early workers used coprecipitation with $Al(OH)_3$, followed by spectrophotometric detection, but found all measurements to be below their detection limit (≤ 20 nM) [23]. Gallium in sea water has recently been analyzed by graphite furnace atomic absorption spectroscopy (GFAAS) after similar concentration procedures to those described here [3,4,11]. Early workers used coprecipitation with $Fe(OH)_3$ followed by spectrophotometric detection [24], but found Ga levels an order of magnitude higher than we now believe occur in the ocean. There are no recent publications on indium in sea water, but early investigations using expensive and time-consuming methods, such as isotope dilution mass spectrometry (thermal source) [25] or neutron activation analysis [26], showed low picomolar levels. A sensitive, multi-elemental technique for the trace analysis of Ti, Ga and In in sea water will enable further investigations into the marine geochemical cycles of these elements.

EXPERIMENTAL

Materials and reagents

Sea water. Sea water samples were collected by two methods which have been shown to be contamination free for a number of trace metals: clean methods developed by Bruland et al. [27], using Teflon®-lined, General Oceanics "Go Flo" bottles, suspended on a Kevlar® line; and methods developed at the Massachusetts Institute of Technology (MIT), using modified Niskin bottles (all O-rings replaced with silicone O-rings and the internal rubber device replaced by an epoxy coated spring), suspended on hydrowire. All samples were filtered through acid-leached 0.4 μm Nuclepore® polycarbonate membrane filters, using 10 psi filtered N_2 over-pressure, and stored in acid-leached polyethylene bottles. White polypropylene lids or spigots were avoided, as the white pigmentation was found to be high in titanium. Samples were acidified to pH 1.5–2.0 with 2 ml 6 M HCl/liter sea water for preservation until further processed.

Reagents. For ultra-trace level work, it is important that all reagents be as clean as possible. Reagents were purified by: (1) double distillation in a sub-boiling quartz still (used for hydrochloric acid, nitric acid, acetic acid and water), (2) vapor phase transition into quartz-cleaned H_2O (used for ammonium hydroxide), or (3) passing the concentrated reagent through a chelating resin column (used for potassium acid phthalate, KHP). Ammonium acetate was prepared by slowly mixing clean HAc and NH_4OH, in stoichiometric

amounts, over ice. Reagent blanks were tested, and found to be minimal.

Standards. Metal standards (Ti, Ga and In) were prepared from accurately weighed pure solids and/or purchased as atomic absorption (AA) standards. An isotopically enriched titanium-49 standard (96.25% ^{49}Ti) was prepared from $^{49}TiO_2$ supplied by Oak Ridge National Laboratories. A 10 ppm primary standard was prepared by dissolving approximately 2 mg ^{49}Ti (~ 3.3 mg $^{49}TiO_2$) with 4 ml HF–HCl–HNO_3 (25 : 25 : 50) in a sealed Teflon® microwave digestion vessel, heated for one hour at power level 2 (20% of maximum), then transferred to an acid-cleaned polyethylene bottle and diluted to 200 ml (final matrix 0.5% HF–0.5% HCl–1% HNO_3). From this primary standard, a 50 ppb standard (~ 1000 nM) in dilute HNO_3 (pH 1.5) was prepared, and used to spike the sea water samples. The exact concentration of the spike solution, 956.8 nM Ti, was determined via calibration against the known titanium standards of natural abundance, as the original 3.3 mg of TiO_2 was difficult to weigh accurately.

Resins and columns. An 8-hydroxyquinoline resin, TSK-8HQ (synthesized in-house on a polymeric vinyl solid support, after the methods of Landing et al. [28]), was used for trace metal concentration/separation. The solid support used was Toyopearl® TSK-75F, purchased from Supelco, as Fractogel® is no longer available. All reagents used in the synthesis were filtered prior to use, and the final resin was initially cleaned by alternating rinses with reagent grade acid (1 M HCl) and base (1 M NaOH). Resin capacities varied from batch to batch, as the synthesis is

TABLE 1

ICP-MS hardware and operating conditions typically used for analysis of Ti, Ga and In

	V.G. Plasma Quad (PQ1) (MIT)	V.G. PQ2 Turbo Plus (UBC)
Nebulizer	Meinhard concentric glass	Meinhard concentric glass
Spray chamber	Glass, water cooled (15°C)	Glass, water cooled (8°C)
ICP RF:		
Forward power	~ 1300 W	1350 W
Reflected power	≤ 15 W	≤ 10 W
Gas Flows (Ar):		
Nebulizer	0.8 l/min	0.80 l/min
Auxiliary	0.5 l/min	0.50 l/min
Cool	12 l/min	13.75 l/min
Cones:		
Sampler	Nickel, ~ 1.0 mm orifice	Nickel, 1.2 mm orifice
Skimmer	Nickel, ~ 0.7 mm orifice	Nickel, 0.4 mm orifice
Operating pressures:		
Analyser	2×10^{-6} mbar	2.2×10^{-6} mbar
Intermediate	$\leq 0 \times 10^{-4}$ mbar	$\leq 0 \times 10^{-4}$ mbar
Extraction	2.8 mbar	2.8 mbar
Ion lens settings:	(optimized daily)	(optimized daily)
Extraction	~ −180 V	~ −118 V
Collector	~ 0 V	~ 0 V
Lens 1	~ 0 V	~ 0 V
Lens 2	~ −30 V	~ −48 V
Differential aperture	~ −120 V	~ −120 V
Lens 3	~ 3 V	~ 6 V
Lens 4	~ −40 V	~ −48 V
Quadrupole	12-125	SX300
Channel electron multiplier	Pulse count mode	Pulse count mode
Sensitivity		
In, 115 (cps/ppm)	3×10^6	12×10^6

problematic; the batches used in this study had capacities of 10–30 μmoles Cu^{2+}/gram resin (2–7 μmoles/ml). A commercially available resin, Chelex-100, was also tested as its capacity is 100 times higher (700 μmoles Cu^{2+}/ml resin) [29] and does not require in-house synthesis. Although recoveries for Ti and Ga (In not tested) were comparably good, difficulties were found in adequately separating out Ca^{2+}, Mg^{2+} and SO_4^{2-}, which interfere with the titanium determination. A larger volume of eluent was also needed for complete recovery using Chelex-100, thus reducing the concentration factor. Columns constructed of mostly Teflon® parts (5 cm × 8 mm i.d. Teflon tubing with 0.3 μm polyethylene frits held on by jam-fit end caps), were loaded with 2 ml TSK-8HQ resin, thoroughly cleaned by elution with 20 ml clean 2.4 M HNO_3, and pH adjusted to 4.0 (the optimum extraction pH) with dilute NH_4OH before use. Samples were then pumped through the resin columns using a Masterflex® peristaltic pump with acid-cleaned C-Flex® pump tubing (a fluorinated flexible pump tubing from Cole Parmer). The pump was upstream of the resin column to minimize leaks (water leaks are more readily eliminated than air leaks), as the fine-sized resin (≤ 30 μm particle size) compacted easily, leading to high resistance.

Instrumentation

ICP-MS. Initial studies were carried out on a VG "Plasma Quad" (PQ1) at MIT and followed up on a VG "PQ2 Turbo Plus" at the University of British Columbia (UBC). Both instruments were equipped with flow injection (FI) sample introduction mechanisms (all Teflon 6-way valve, assembled in-house) to allow for reproducible injection of small samples (100–500 μl) into the dilute HNO_3 carrier stream. The later instrument, primarily due to improved ion optics, provided higher sensitivity, enhanced short-term stability, and reduced oxide interference levels, thus improving the analytical results. Typical operating conditions for each instrument are presented in Table 1.

The column eluent was analyzed for Ti by ICP-MS in continuous aspiration (flow rate 0.8 ml/min), mass-scan mode (45.4–49.6 amu, software limitations did not allow a smaller range), with isotope dilution. Tuning and torch box position were optimized for maximum signal to background ratios, to minimize oxides and doubly charged species without lowering the atomic Ti sensitivity by more than 20% (tested with a ^{49}Ti enriched standard in 2.4 M HNO_3, by optimizing the 49/48 count ratio). Signals were acquired for 42 s (250 μs dwell time/channel, 512 channels over the 4.2 amu range, 300 sweeps, 10 ms quad settle time between sweeps), starting 15–20 s after the signal reached the detector.

The evaporated eluent was analyzed for Ga and In using flow injection (FI) with a 300 μl sample loop, pulling the sample through the loop with a syringe to avoid contamination. Peak jump mode (PJ) was used with standard additions for these elements. Matrix effects, from varying concentrations of dissolved salts or acids, have a significant effect on the sensitivity of ICP-MS analysis, thus requiring either isotope dilution, an internal standard or standard additions. Signals were acquired for 30 s (5 peaks, at 48, 49, 69, 71 and 115 amu), 7 points/peak, 1000 μs dwell time/point, 350 sweeps, 10 ms quad settle time between peaks), starting just before the signal reached the detector.

Atomic absorption. A Perkin Elmer 5000 graphite furnace atomic absorption spectrophotometer (GFAAS) was used for comparison on samples where gallium and titanium concentrations were sufficiently high for detection by GFAAS (≥ 0.2 ppb for Ga and ≥ 2 ppb for Ti in column eluent). For Ti analysis, 30 μl sample volumes were deposited on a pyrolytic graphite tube (no platform), dried at 160°C for 40 s, thermally pre-treated at 800°C for 20 s, atomized at 2700°C for 4 s, and cleaned at 2800° for 4 s. Absorbance was measured using the 365.3 nm Ti line, a 0.2 nm slit, and continuum source background correction. Ga analysis was performed as described previously [4]. A Perkin Elmer 403 flame atomic absorption spectrophotometer was used to check for Ca interference. Operating conditions similar to those recommended by the manufacturer were used.

Ion chromatography. A WESCAN ion chromatograph with a Model 213A conductivity de-

tector and a "WESCAN Anion" column was used to check for sulfate concentrations after separation. The eluent (4 mM KHP in methanol–water (1 : 99), adjusted to pH 4.6 with 0.1 M potassium hydroxide and vacuum-filtered prior to use) was pumped at a flow rate of 2 ml/min. A 500-μl sample injection loop was used.

General procedure. Acidified sea water samples (4 l) were spiked with ^{49}Ti for isotope dilution analysis, equilibrated for at least two hours (2–24 h), adjusted to the extraction pH with dilute NH_4OH and buffered with NH_4OAc. Conditions for maximum recovery and separation during the concentration step were optimized by adjusting the flow rate, pH, buffer concentration, column rinses and eluent volume and strength. Optimal conditions were found at 3–5 ml/min, pH 4.0 $\pm$ 0.3, and 0.05% NH_4Ac (0.5 ml NH_4Ac/liter sea water). After pumping, the resin was resuspended with 8 ml H_2O, rinsed with 3 ml of 0.02 M KHP and then 15 ml H_2O to remove Ca^{2+}, Mg^{2+} and SO_4^{2-} from the resin prior to elution with 10 ml (5 $\times$ 2 ml) 2.4 M HNO_3. The eluent was then split into two 5-ml portions, one for direct analysis (Ti, 400-fold concentration) and one for further evaporative concentration (Ga and In, 3000-fold concentration). Analysis was performed by ICP-MS in continuous aspiration mass-scan mode with isotope dilution (Ti), or using flow-injection analysis (FIA) in peak jump mode (PJ) with standard additions (Ga and In).

RESULTS AND DISCUSSION

Optimization of extraction conditions

Isotope dilution; spiking and equilibration. Isotope dilution (ID) analysis was used to correct for matrix effects, variable instrumental sensitivity, changes in extraction efficiency, and any minor sample losses during handling in the determination of dissolved titanium, using a ^{49}Ti enriched standard (96.25% ^{49}Ti, 2.71% ^{48}Ti). Problems from contamination or background interference during analysis, however, are not corrected for by this method, and were carefully monitored by other means. Gallium has an unfavorable ratio of its two stable isotopes, mass 69 (60%) and 71 (40%), and indium has interference problems at its minor isotope from ^{113}Cd, which appears to be significantly retained on the TSK-8HQ resin throughout the concentration/separation procedure. This prohibited the use of ID analysis for Ga and In, which were therefore determined by standard additions.

Optimum precision for isotope ratio measurement by mass spectrometry is found for ratios near 1.0, whereas optimum conditions for ID calculations are found when the measured ratio equals the square root of the product of the ratios of the spike and natural isotopes (due to counting statistics and error propagation) [30], ^{49}Ti /^{48}Ti = 1.6 in this case. For best results, therefore, some estimate of the concentration in the sample is needed before analysis. The large dynamic range of titanium in sea water, and the sparsity of data available on this element in the oceans, required that a few samples from each profile be run by conventional analysis (by comparison with a standard curve) to obtain an estimate of the concentration prior to adding the ID spike. This precluded adding the spike immediately upon collection, which would have allowed for maximum equilibration time. The filtered sea water samples (4 l), acidified upon collection to pH 1.5–2.0, were spiked back in the shore-based laboratory with 50–500 μl of the 50 ppb ^{49}Ti enriched standard, and equilibrated for two to twenty-four hours. Equilibration times of one hour to one week were tested, with no significant changes. The exchange kinetics for titanium appear to be sufficiently rapid on these times scales at pH 2.

pH. The effect of pH on extraction efficiency for titanium and gallium was investigated from pH 3.0 to 8.3, by stable spike recovery tests. Indium recoveries were verified only at the conditions chosen for Ti and Ga, and were fortuitously good. Quantitative extraction of all three metals was found from pH 3.0–4.5. Gallium recoveries are 98 $\pm$ 9% (n = 33) from pH 3.0 to 6.5, and drop off above pH 7.0 (down to 75% at pH 8.3, n = 5). Titanium recoveries are 98 $\pm$ 10% (n = 13) between pH 3.0 and 4.5, and drop off above pH 5.5 (down to 50% at pH 7.0, n = 3). Indium recoveries at pH 4.0 $\pm$ 0.3 were 100 $\pm$ 8% (n = 7).

As pH below 3.0 was not investigated, it is possible that good recoveries would have been found at lower pH as well. The conditions chosen for all samples was pH 4.0 ± 0.3, buffered with 0.05% NH_4Ac (0.5 ml NH_4Ac/liter sea water).

Flow rate. Due to the large volume of sample needed, it was desirable to pump at maximum flow rates without sacrificing the recoveries. Flow rates from 1 to 8 ml/min were investigated, with optimal conditions found at 3–5 ml/min. Above 5 ml/min, the metal recoveries decreased (50–75% at 8 ml/min); below 3 ml/min, the sample processing time was excessive (> 22 h). Due to the small size of the resin beads (≤ 30 μm) the

TABLE 2

Potential isobaric interferences in ICP-MS for titanium, gallium and indium

Element	Isotope	%Abundance	Possible interference	Natural abund. of interference (if ≤ 20%)
Titanium	46	8.0	$^{14}N^{16}O_2^+$	
			$^{46}Ca^+$	0.003
			$^{40}Ar^6Li^+$	7.5 (^{6}Li)
			$^{92}Zr^{2+}$	17.1
			$^{92}Mo^{2+}$	14.8
	47	7.5	$^{31}P^{16}O^+$	
			$^{40}Ar^7Li^+$	
			$^{28}Si^{19}F^+$	
			$^{94}Zr^{2+}$	17.5
			$^{94}Mo^{2+}$	9.3
	48	73.7	$^{96}Mo^{2+}$	16.7
			$^{48}Ca^+$	0.19
			$^{96}Ru^{2+}$	5.5
			$^{96}Zr^{2+}$	2.8
			$^{32}S^{16}O^+$	
			$^{24}Mg_2^+$	
			$^{31}P^{16}OH^+$	
			$^{40}Ar^7LiH^+$	
			$^{29}Si^{19}F^+$	4.7 (^{29}Si)
			$^{14}N^{18}O^{16}O^+$	0.2 (^{18}O)
	49	5.5	$^{32}S^{16}OH^+$	
			$^{33}S^{16}O^+$	0.75 (^{33}S)
			$^{35}Cl^{14}N^+$	
			$^{40}Ar^9Be^+$	
			$^{30}Si^{19}F^+$	3.1 (^{30}Si)
			$^{98}Mo^{2+}$	
			$^{98}Ru^{2+}$	1.9
	50	5.3	$^{50}V^+$	0.25
			$^{50}Cr^+$	4.35
			$^{34}S^{16}O^+$	4.2 (^{34}S)
			$^{40}Ar^{10}B^+$	20.0 (^{10}B)
			$^{100}Mo^{2+}$	9.6
			$^{100}Ru^{2+}$	12.6
Gallium	69	60.0	$^{138}Ba^{2+}$	
			$^{138}La^{2+}$	0.09
			$^{138}Ce^{2+}$	0.25
	71	40.0	$^{142}Ce^{2+}$	11.1
			$^{142}Nd^{2+}$	
Indium	113	4.3	$^{113}Cd^+$	12.3
	115	95.7	$^{115}Sn^+$	0.35

resin compacted over time, increasing the resistance and causing a decrease in the flow rate. Flow rates were set at 4.5–5.0 ml/min at the start of pumping, and often slowed to 3.0–3.5 ml/min after a few hours. Pumping time for 4 l was typically 16–20 h.

Rinses and eluent

In addition to the concentration factor required to get detectable levels of trace metals from their low level in sea water, it is also necessary to separate the trace elements from the major ions in sea water which can cause interferences. The total dissolved salt content of solutions aspirated into the ICP-MS is best kept below 0.1% to avoid clogging of the sample cone orifice [31]. Sea water contains 3.5% dissolved salts, with Na^+, Mg^{2+}, K^+ and Ca^{2+} being the dominant cations. For the ICP-MS detection of Ti, Ga and In, at masses 48, 49, 69, 71 or 115, possible interference can come from a number of sources, including Ca^{2+}, SO_4^{2-}, HPO_4^{2-}, Mg^{2+}, Ba^{2+} or Sn, as shown in Table 2, and discussed in the next section. Due to their high concentrations in sea water and significant interference risk, separation from Ca^{2+} (10.3 mM in sea water) and SO_4^{2-} (28.2 mM in sea water) was of particular concern. Before elution, therefore, it was necessary to remove these species. Water rinses alone were found to be ineffective at removing Ca^{2+} and SO_4^{2-} from the 8HQ resin. To optimize the removal of Ca^{2+} and SO_4^{2-}, rinsing with NH_4Ac or KHP (potassium acid phthalate) in addition to H_2O was investigated, all under gravity flow rate of approximately 0.1 ml/min.

Sulfate was measured in the eluent via anion chromatography after evaporation to dryness to remove the HNO_3 matrix, as the NO_3^- peak overlaps with SO_4^{2-} when present at a 10^6-fold excess. Sulfate was readily redissolved in water after evaporation, giving a quantitative recovery. Optimizing for low levels, the detection limit of this technique for sulfate could be set to 0.15 μM (with an upper limit of 8 μM), which would lead to a signal below the detection limit of the ICP-MS for SO^+ and SOH^+ at masses 48 and 49. Preliminary studies were conducted at instrumental settings with a detection limit of 3 μM SO_4^{2-}, or a signal at 48 amu equivalent to 1.3 ± 0.5 nM Ti (3 pM Ti in original sea water). At high buffer concentrations, 5 ml of KHP removed $\geq 98\%$ of the sulfate which remained after water rinses alone (≤ 3 μM vs. 190 μM in eluent), whereas 5 ml of NH_4Ac removed only 96% of the sulfate (7.5 μM remained). Neither effected the recoveries of Ti, Ga or In. Optimization of the method required using the minimum amount of KHP needed for separation, as KHP had a significant

TABLE 3

Column separation and recovery experiments, using spiked seawater samples [Note: 3 μM SO_4^{2-} ⇒ signal at mass 48 equivalent to 1.3 ± 0.5 nM Ti (3 pM Ti in sea water), 0.15 μM SO_4^{2-}, equivalent to ~0.06 nM Ti (below detection limit). Each entry is an average of two experiments]

Rinses			SO_4^{2-}		Ti (%)		Ga (%)	In (%)
H_2O	Other (N × 1 ml)	H_2O	μM	% Removed [a]	GFAAS	ICP-MS	ICP-MS	ICP-MS
2 × 7 ml	5 ml 0.2 M KHP	2 × 3 ml	≤ 3	≥ 98	91	100	93	101
2 × 7 ml	5 ml 20% NH_4Ac	2 × 3 ml	7.5	96	104	102	89	93
2 × 7 ml	5 ml H_2O	2 × 3 ml	190	0	91	114 [b]	100	106
3 × 4 ml	5 ml 0.2 M KHP	3 × 5 ml	≤ 3	≥ 98	95	106	108	
3 × 4 ml	5 ml 0.05 M KHP	3 × 5 ml	≤ 3	≥ 98	100	105		
3 × 4 ml	5 ml 0.01 M KHP	3 × 5 ml	80	50	99	110 [b]		
3 × 4 ml	5 ml H_2O	3 × 5 ml	180	0	105	97 [b]		109
2 × 4 ml	3 ml 0.2 M KHP	5 × 3 ml	≤ 0.15	≥ 99.9	94	116	96	106
2 × 4 ml	3 ml 0.02 M KHP	5 × 3 ml	≤ 0.15	≥ 99.9	104	120		109
2 × 4 ml	3 ml 0.002 M KHP	5 × 3 ml	≫ 8	≪ 95	106	116 [b]		

[a] Assuming water rinse only removes no SO_4^{2-}. [b] Large process blank measured by ICP-MS only ($\geq 15\%$ of 100 ng spike), presumably from SO_4^{2-} interference.

effect on the blank and therefore the detection limit, even after thorough cleaning. Table 3 shows the effect of varying amounts and concentrations of KHP rinse on the resulting SO_4^{2-} concentration. Resuspending the resin with 8 ml H_2O (2×4 ml) then rinsing with 3 ml of 0.02 M KHP (3×1 ml) followed by 15 ml H_2O (5×3 ml) to remove residual KHP, was found to remove the interferences from the resin prior to HNO_3 elution.

Calcium was measured by flame atomic absorption in the 2.4 M HNO_3 acid and the column eluents after a 4-fold dilution with a releasing agent (La, final concentration 1000 ppm). The acid alone did not have detectable levels of Ca (< 0.05 μM), but some of the column eluents did contain significant levels of Ca (up to 4 μM Ca). The maximum level, 4 μM Ca, is equivalent to 8 nM ^{48}Ca which could erroneously be interpreted as up to 20 pM Ti in the original sea water. Obviously this needed to be monitored for each sample, and corrected for if high levels were found. In cases where the Ca concentration in the eluent was found to be high, reprocessing was required. The eluent was rediluted in 500 ml distilled water, pH adjusted, pumped through the resin a second time, with all the appropriate rinses. The eluent for these reprocessed samples was found to be free of significant Ca interferences.

Evaporation. Evaporation was performed slowly, so as to avoid splattering, in 5 ml Teflon® PFA conical vials on a modified, cup-style hot plate (to increase heat transfer from the sides) under a filtered air environment. Samples were then re-dissolved in 0.3 ml 2.4 M HNO_3 and diluted to 0.55 ml with H_2O. The recovery of Ga and In by this method was quantitative. These elements were determined in the redissolved eluent without filtration or further processing. Titanium, however, was not easily resolubilized after evaporation without the use of HF, which caused additional problems during analysis (SiF^+ interferences, see Table 2). Ti was therefore analyzed in the non-evaporated eluent instead. Standard additions resulted in an additional 1 : 1.2 dilution, giving a final matrix of 1.1 M HNO_3 with a 3000-fold concentration for Ga and In.

Mass spectral interferences

One of the key benefits of ICP-MS, in comparison to ICP optical emission spectroscopy (ICP-OES), is often stated to be the spectral simplicity of ICP-MS. All elements, except indium, have at least one isotope free from elemental isobaric interferences. There are, however, many molecular species which can form in the plasma and/or en route to the quadrupole vacuum chamber, the importance of which is sometimes understated. These species are more common in the mid and low mass range, and are often a problem in the analysis of first row transition elements. The stated spectral simplicity is more evident at higher masses.

Titanium. Spectral interferences for titanium are a potential problem at each of its five isotopes (46, 47, 48, 49 and 50 amu), as shown in Table 2. The most likely interferences in sea water concentrates, at 48 and 49 amu [the isotopes of choice for isotope dilution (ID) analysis], are calcium-48 (0.19% natural abundance), the molecular oxide species of phosphorus (POH^+), sulfur (SO^+) and nitrogen (NO_2^+), and possibly diatomic Mg^{2+}. The oxides and molecular species form in the ICP-MS from HPO_4^{2-}, SO_4^{2-} and Mg^{2+} in the sea water matrix, or from the HNO_3 acid eluent.

To help identify interfering species present, a high resolution ICP mass spectrum (HR-ICP-MS) from 47.90–48.02 amu was obtained for 5 ppb Ti in 20% HNO_3 (Merck, ultrapure) at the VG factory in Manchester (UK). Exact masses for the possible species at 48 amu are shown in Table 4. The spectrum, shown in Fig. 1, shows three resolvable peaks: 47.948 ± 0.005, 47.967 ± 0.003, and 47.997 ± 0.004 amu. The first peak is due to $^{48}Ti^+$; interferences from Mo^{2+}, Ca^+, Ru^{2+} and Zr^{2+} would not be resolvable, but would show up as asymmetry in this peak. The second peak is due to SO^+, verified by adding H_2SO_4 to the HNO_3 matrix; any contribution from Mg_2^+ would not be resolvable, but would show up as asymmetry in this peak. The presence of significant amounts of SO_4^{2-} in this ultrapure HNO_3 acid demonstrates how difficult it is to fully separate out SO_4^{2-}. The third peak can only be due to NO_2^+, showing the importance of this species at

TABLE 4

Exact masses of each potential interference at mass 48

Species	Isotope	Atomic mass of isotope	Mass of species
$^{48}Ti^+$	Ti	47.94795	47.9479
$^{96}Mo^{2+}$	Mo	95.90467	47.9523
$^{48}Ca^+$	Ca	47.95253	47.9525
$^{96}Ru^{2+}$	Ru	95.90760	47.9538
$^{96}Zr^{2+}$	Zr	95.90827	47.9541
$^{32}S^{16}O^+$	S	31.97207	47.9670
	O	15.99491	
$^{24}Mg_2^+$	Mg	23.98504	47.9701
$^{29}Si^{19}F^+$	Si	28.97650	47.9749
	F	18.99840	
$^{31}P^{16}OH^+$	P	30.97376	47.9765
	O	15.99491	
	H	1.00783	
$^{40}Ar^7LiH^+$	Ar	39.96238	47.9862
	Li	7.01600	
	H	1.00783	
$^{14}N^{18}O^{16}O^+$	N	14.00307	47.9971
	^{16}O	15.99491	
	^{18}O	17.99916	

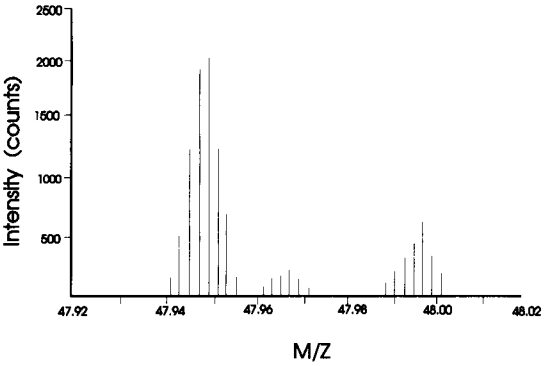

Fig. 1. High resolution (HR) ICP-MS analysis of 5 ppb titanium in 20% Merck ultrapure HNO_3. Peak identification: (1) 47.948 ± 0.005 amu, $^{48}Ti^+$ (or Mo^{2+}, Ca^+, Ru^{2+}, Zr^{2+}); (2) 47.967 ± 0.003 amu, SO^+ (or Mg_2^+); (3) 47.997 ± 0.004 amu, NO_2+. Spectrum obtained at the VG Elemental factory in Manchester.

48 amu in a strong HNO_3 matrix. No peaks are seen at masses corresponding to SiF^+, POH^+ or $ArLiH^+$ in this solution. HR-ICP-MS and conventional ICP-MS instruments have different ion optics, which could easily lead to differing degrees of formation of oxides and other molecular species. Use of HR-ICP-MS, however, does help to illustrate the potential importance of some molecular interferences.

Sea water contains high levels of Ca^{2+}, Mg^{2+}, SO_4^{2-} and HPO_4^{2-} relative to the picomolar levels of titanium. A chemical separation to remove these species was performed via selective rinsing of the TSK-8HQ resin with KHP and H_2O, as

TABLE 5

Interference checks, ICP-MS signal (peak jump, CPS, blank corrected)

Mass	Species	Acid Blk [a]	Col. Blk [b]	Sea water [c] sample	Mix std. [d] 10 ppb	Mo [e] 4.8 ppm
7	Li	67	16	13	55	12
9	Be	64	−1	0	0	−4
46	Ti/NO_2	3130	−21	130	2260	−280
48	Ti	260	460	3320	20700	−110
49	Ti	66	460	2560	1540	−1
69	Ga	66	44	220	15900	−14
71	Ga	45	31	150	11400	−7
90	Zr	30	40	90	25	−6
96	Mo	23	1.8×10^4	1.1×10^6	9	1.2×10^6
98	Mo	21	2.8×10^4	1.6×10^6	13	1.8×10^6
102	Ru	17	3	1	2	−8
115	In/Sn	66	2	10	35900	−9

[a] Acid Blk: 2.4 M HNO_3 (represents a typical matrix blank, subtracted from column blank, seawater sample and mixed standard). [b] Col. Blk: 2.4 M HNO_3 passed through resin columns ($N = 3$), note added Ti-49 spike. [c] Sea water sample: column eluent, in 2.4 M HNO_3, from V7T7 2000 meters depth, not evaporated (400 × concentration), note added Ti-49 spike. [d] Mix std. 10 ppb: standard of 10 ppb Ti, Ga and In in 2.4 M HNO_3. [e] Mo 4.8 ppm: standard in pure water (blank correction therefore different).

described previously. This eliminated most interferences from Ca^+, Mg_2^+, SO^+, SOH^+, and POH^+, as verified by testing for Ca and Mg by flame atomic absorption spectroscopy (≤ 4 μM), SO_4^{2-} by ion chromatography (≤ 0.15 μM), and HPO_4^{2-} by colorimetric detection [32] (0.2 ± 0.2 μM). Other potential interferences at masses 48 and 49, from $ArLiH^+$, $ArBe^+$, ClN^+, SiF^+, Mo^{2+}, Zi^{2+}, Ru^{2+} species, were not significant. For Li, Be, Mo, Zr, and Ru this was verified by checking the elemental concentrations at their major masses in the sea water extracts, as shown in Table 5. Li, Be and Ru were undetectable, and Zr was too low to impose any problems (in a worst case scenario, with a Zr^{2+}/Zr ratio of 0.01, only 0.08% of the signal at mass 48 could be due to Zr^{2+}). Though Mo was found at quite high levels in the sea water concentrates (3–5 ppm), Mo^{2+} was still not a interference problem at masses 48 and 49. The amount of doubly ionized, Mo^{2+}, in a solution with comparable Mo levels (4.78 ppm) was found to be undetectable, as shown in Table 5. Due to the HNO_3 acid eluent, NO_2^+ was an unavoidable species in the background signal, and was carefully monitored and accounted for. Improved ion optics in the VG PQ2 Turbo Plus resulted in a significant reduction in oxide levels over that found on the VG PQ1, thus lowering the instrumental detection limit for Ti in 2.4 M HNO_3 acid from approximately 0.2 ppb (5 nM) down to approximately 0.02 ppb, both variable from day to day.

Gallium. Spectral interferences for gallium are possible at mass 69 from doubly-ionized Ba, La and Ce, and at mass 71 from doubly-ionized Nd and Ce, as shown in Table 2, but were not found to be significant in the sea water extracts. Levels of La, Ce and Nd are not significantly higher than Ga in sea water (all in the low picomolar range) [33,4], and the degree of doubly ionization in the ICP-MS is minimal ($\leq 1\%$). Ba is present in sea water at nanomolar levels [34], and could therefore present a significant problem if quantitatively retained and 1–10% doubly ionized, but Ba appears to be removed by the methods designed to remove Ca and Mg. Ga concentrations calculated using mass 69 versus mass 71 were indistinguishable, and both agreed well with those determined by GFAAS on the same samples, as shown in Fig. 2.

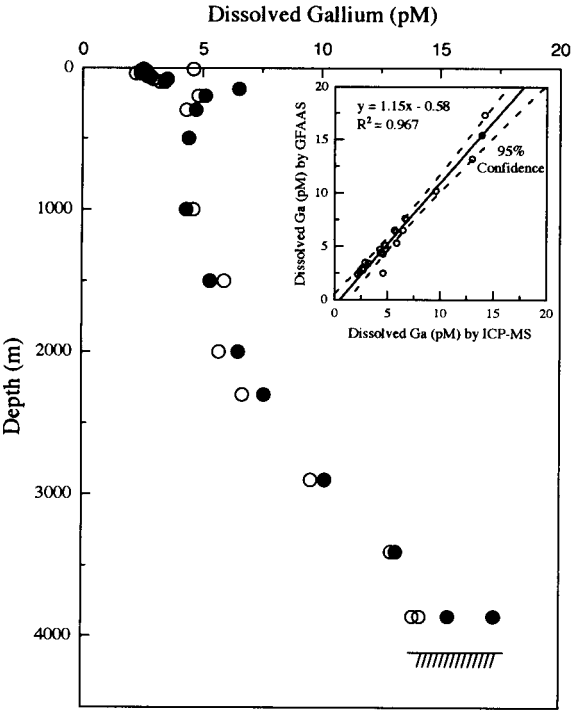

Fig. 2. Dissolved gallium concentration versus depth in the Subarctic North Pacific (VERTEX 7, Station T7, 50°N, 145°W), analysed by graphite furnace atomic absorption [4] (closed circles), and by inductively coupled plasma mass spectrometry (open cirlces), after concentration with an 8-hydroxyquinoline resin.

Indium. Interferences for indium are possible at mass 115 (95.7% In) from tin-115 (0.35% Sn) and at mass 113 (4.3% In) from cadmium-113 (12.2% Cd). The cadmium interference at mass 113 was found to be significant, as Cd appears to be significantly retained on the TSK-8HQ resin throughout the In concentration procedure, thus eliminating the possibility of ID analysis for indium. The potential for interference from Sn at mass 115 was determined to be of low significance. With a maximum concentration of Sn in sea water of 20 pM [35], a 100% recovery of Sn during processing could result, in a worst case scenario, in a 50% interference for In at 0.1 pM levels. Recovery tests for Sn by this method indicate $\leq 20\%$ recovery, which leads to $\leq 10\%$ interference, within the error of the technique.

Analytical figures of merit

Detection limits. The detection limit for dissolved titanium in sea water by this method is 5–10 pM (0.2–0.4 ppt) using 4 l sample volumes concentrated into 10 ml, a 400-fold concentration. Detection limit is defined here as 3 times the standard deviation of replicate process blanks. If Ti concentrations are higher than 10 pM, then smaller sample sizes could be used. For the low levels found in the surface waters of the North Pacific Ocean, however, 4-l sea water samples are required for this method. The detection is limited primarily by the background signal at mass 48. Clean laboratory conditions keep the metal blanks sufficiently low, but background interference from polyatomic species are limiting. This background signal at mass 48 is suggested to be primarily NO_2^+ (with ^{18}O and ^{16}O, a large peak was observed at mass 46 from standard NO_2^+, with ^{16}O only) and was minimized by optimizing the torch position for low oxide formation. Other limiting factors are the interferences from Ca^{2+} and SO_4^{2-}, which are difficult to remove completely and attempting to do so requires substantial sample handling, thus raising process blanks. These factors result in a variable detection limit from one run to another. In some cases, samples had to be processed through the separation/concentration procedure twice to adequately remove the Ca interference. We now question the reliability of the Atlantic Ocean data, published in Ref. 2, due to higher Ca levels in these eluents. Errors of up to 25% may be present in these data, particularly in the surface waters where Ti levels are lower. Detection limits for dissolved gallium and indium are 0.5 pM (0.02 ppt) and 0.1 pM (0.01 ppt), respectively, for 2 l sample volumes concentrated into 0.65 ml (3000-fold concentration), and are limited by instrumental noise and counting statistics. Process blanks and interference problems are minimal for these elements.

Precision. The reproducibility of the method is demonstrated by repeated spike recovery tests and replicate analysis of sea water samples. Because of the large volume needed, replicate sea water samples required separate sampling casts, and only three depths were sampled in duplicate. The precision for both sampling and analytical procedures was generally 6–10% for concentrations greater than twice the detection limit, and up to 15–20% for values near the detection limit (particularly a problem for the low values seen for In). Without the isotope dilution (ID) for the Ti analysis, the precision for Ti would have been worse; $\pm 15\%$ rather than $\pm 7\%$.

Accuracy. Accuracy is more difficult to determine, as there are no accepted values for these elements in sea water standard reference materials. A comparison with other more established detection methods, such as GFAAS, for Ga, however, shows excellent agreement, as shown in Fig. 2. The same samples and initial processing were used for both these analyses, with the ICP-MS determination performed after two years storage, then diluting and re-processing the column eluent to add the KHP rinse necessary for Ti analysis. The minor differences between the two sets of data most likely a result from additional sample handling. The few samples with sufficiently high levels of Ti for detection by GFAAS also show good agreement with ICP-MS results, although there is considerable uncertainty in the GFAAS data as the values are close to the 2 ppb detection limit. Samples from 1000 and 1400 m in the central North Pacific (without the ^{49}Ti spike) show 2.5 ± 1.0 ppb Ti by GFAAS and 2.3 ± 0.2 ppb by ICP-MS in the column eluent, after a 400-fold concentration (120 pM in original sea water). Accuracy for indium cannot easily be verified. The 0.1–2.0 pM levels measured by this technique, however, are in general agreement with early results from isotope dilution mass spectrometry (thermal source) [25] and neutron activation analysis [26], which showed low picomolar levels.

Conclusions

The method described here demonstrates the use of ICP-MS, after a chelating resin concentration/separation procedure, for analysing ultra-trace concentrations of Ti, Ga and In in sea water samples. The detection limits achieved (5–10 pM, 0.5 pM and 0.1 pM, for Ti, Ga and In, respectively) are sufficiently low for most open ocean samples. Open ocean sea water concentrations for these elements are in the range of 6–300 pM

for Ti, 2–60 pM for Ga, and 0.1–2.0 pM for In. The accuracy of this method is verified by comparison with accepted values. Sampling and analytical precision of 7–10% was generally found for concentrations greater than twice the detection limit. This method will allow investigation of the marine biogeochemistry of these difficult to analyze elements.

The authors thank Kelly Falkner and John Edmond for use of and training on the ICP-MS facility at MIT. This work was funded by the U.S. Office of Naval Research and the Natural Science and Engineering Research Council of Canada.

REFERENCES

1 S.R. Taylor, Geochim. Cosmochim. Acta, 28 (1964) 1273.
2 K.J. Orians, E.A. Boyle and K.W. Bruland, Nature, 348 (1990) 322.
3 K.J. Orians and K.W. Bruland, Nature, 332 (1988) 717.
4 K.J. Orians and K.W. Bruland, Geochim. Cosmochim. Acta, 52 (1988) 2955.
5 M. Whitfield and D.R. Turner, in W. Stumm (Ed.), Aquatic Surface Chemistry, Wiley, New York, 1987, pp. 457–494.
6 D.J. Hydes, Science, 205 (1979) 1260.
7 C.I. Measures, J.M. Edmund and T.D. Jickells, Geochim. Cosmochim. Acta, 50 (1986) 1423.
8 K.J. Orians and K.W. Bruland, Earth Planet. Sci. Lett., 79 (1986) 397.
9 J.H. Martin and R.M. Gordon, Deep Sea Res., 35 (1988) 177.
10 J.H. Martin, R.M. Gordon and S.E. Fitzwater, Nature, 345 (1990) 156.
11 A.M. Shiller, Geochim. Cosmochim. Acta, 52 (1988) 1879.
12 D.J. Hydes, G.J. de Lange and H.J.W. de Baar, Geochim. Cosmochim. Acta, 52 (1988) 2107.
13 C.I. Measures and J.M. Edmund, J. Geophys. Res., 93 (1988) 591.
14 K.J. Orians and K.W. Bruland, Nature, 316 (1985) 427.
15 K.K. Falkner and J.M. Edmond, Earth Planet. Sci. Lett., 98 (1990) 208.
16 G.P. Klinkhammer and L.H. Chan, Anal. Chim. Acta, 232 (1990) 323.
17 D.W. Lea and E.A. Boyle, Nature, 338 (1989) 751.
18 T.J. Shaw and R. Francois, Geochim. Cosmochim. Acta, 55 (1991) 2075.
19 J.W. McLaren, A.P. Mykytiuk, S.N. Willie and S.S. Berman, Anal. Chem., 57 (1985) 2907.
20 D. Beauchemin and S.S. Berman, Anal. Chem., 61 (1989) 1857.
21 H. Li and C.M.G. van den Berg, Anal. Chim. Acta, 221 (1989) 269.
22 S.A. Skrabal, W.J. Ullman and G.W. Luther, Mar. Chem., 37 (1992) 83.
23 J.V. Griel and R.J.J. Robinson, J. Mar. Res., 2 (1952) 173.
24 F. Culkin and J.P. Riley, Nature, 181 (1958) 179.
25 T.J. Chow and G.B. Snyder, Earth Planet. Sci. Lett., 7 (1970) 221.
26 A.D. Mathews and J.P. Riley, Anal. Chim. Acta, 51 (1970) 287.
27 K.W. Bruland, R.F. Franks, G.A. Knauer and J.H. Martin, Anal. Chim. Acta, 105 (1979) 233.
28 W.M. Landing, C. Haraldsson and N. Paxeus, Anal. Chem., 58 (1986) 3031.
29 Bio-Rad Laboratories Chelex-100 Product Information No. 2020 (1981).
30 J.D. Fassett and P.J. Paulsen, Anal. Chem., 61 (1989) 643A.
31 J.A. Olivares and R.S. Houk, Anal. Chem., 58 (1986) 20.
32 T.R. Parsons, Y. Maita and C.M. Lalli, A Manual of Chemical and Biological Methods for Seawater Analysis, Pergamon Press, Oxford, 1984.
33 H.E. Elderfield, Philos. Trans. Roy. Soc. London A, 325 (1988) 105.
34 L.H. Chan, D. Drummond, J.M. Edmond and B. Grant, Deep Sea Res., 24 (1977) 613.
35 J.T. Byrd and M.O. Andrea, Science, 218 (1982) 565.

Analytica Chimica Acta, 282 (1993) 75–80
Elsevier Science Publishers B.V., Amsterdam

Implementation of ultraviolet solid-phase spectrophotometry by use of derivative techniques

L. Fermín Capitán-Vallvey, Ignacio de Orbe and M. Carmen Valencia

Department of Analytical Chemistry, University of Granada, E-18071 Granada (Spain)

Juan J. Berzas-Nevado

Department of Analytical Chemistry and Foods Technology, University of Castilla-La Mancha, E-13071 Ciudad Real (Spain)

(Received 2nd December 1992; revised manuscript received 8th April 1993)

Abstract

A spectrophotometric method for the simultaneous determination of sulphathiazole and sulphametazine based on fourth-derivative solid-phase spectrophotometry is proposed. Both sulphonamides were fixed on a dextran-type cation-exchange gel at pH 2.5. The absorbance on the gel, packed in a 1-mm silica cell, was measured directly. The method does not require any separation step. The range of application is between 0.20 and 12.00 μg ml^{-1} for sulphathiazole and between 0.20 and 15.00 μg ml^{-1} for sulphametazine. The acuracy and precision of the method are reported. The method was applied for the determination of sulpha thiazole and sulphametazine in synthetic mixtures and pharmaceuticals.

Keywords: Spectrophotometry; Derivative spectroscopy; Pharmaceutical analysis; Solid-phase spectrophotometry; Sulphametazine; Sulphathiazole

Derivative spectrophotometry can be used to resolve mixtures of compounds whose absorption spectra overlap, although, if these are present in low concentrations a preliminary stage of preconcentration is necessary. Solid-phase spectrophotometry (SPS) is based on the direct absorptiometric measurements of fixed analytes on a solid support, usually an ion-exchange resin. The SPS methods proposed for low level species in waters [1], air [2], beverages [3] and body fluids [4] are much more sensitive and selective than the conventional spectrophotometric methods in solution.

In the past, derived signals in SPS have been used in improving the methods of determination of metallic ions but not in the resolution of mixtures overlapping spectra components. Ishii [5] used derived signals obtained by means of an analogue differentiation circuit to explore the possibilities which they offer to increase the sensitivity in the individual determination of copper, chromium and iron.

The aim of the authors in this work is to combine the SPS methodology with the use of derivative techniques in order to: (1) resolve mixtures of compounds which are found in low concentrations and which show overlapping spectra by means of their preconcentration in a solid support; (2) eliminate the necessity imposed by the SPS method of measuring at two wavelengths in order to avoid the variability in the absorbance measurements caused by the packaging of the resin [6]; and (3) explore the possibilities for the use of derived signals in SPS methodology for the

Correspondence to: L.F. Capitán-Vallvey, Department of Analytical Chemistry, University of Granada, E-18071 Granada (Spain).

resolution of mixtures of compounds in the ultraviolet.

Sulphonamides, compounds which are extensively used in medical and veterinary practice for the treatment of bacterial infections, can be analyzed by many methods. Chromatographic techniques such as TLC [7,8], GC [9,10] and LC [11,12] have been reported for the analysis of sulphonamide mixtures. By using the spectrophotometric technique, the Bratton-Marshall procedure [13] and other methods developed on the basis of this reaction [14–17] are well known and used for the determination of total sulphonamide content. It is not possible to determine mixtures of sulphonamides by direct spectrophotometric measurements, i.e. without some form of deconvolution, because they all show overlapping of the spectra in the ultraviolet.

In this study, mixture samples containing the sulphonamides sulphatiazole (ST) and sulphametazine (SM) have been resolved satisfactorily by means of derivative spectrophotometry in solid phase and the method was applied for their analysis in pharmaceuticals.

EXPERIMENTAL

Apparatus

A Beckman Instrument DU-70 spectrophotometer connected to an IBM PC-AT 286 microcomputer fitted with Beckman Data Leader Software [18] was used for all the measurements and treatment of data.

Further, an Agitaser 2000 rotating agitator, a Selecta desk centrifuge and a Crison 2002 digital pH-meter fitted with a glass-saturated calomel combined electrode for pH measurements, were used.

A liquid cromatograph (Hewlett-Packard 1090) provided with a diode array detector, an automatic injector, and a Hewlett-Packard 3392A integrator, was used for the reference method.

Reagents

All reagents were of analytical-reagent grade and the water was pretreated by inverse osmosis.

Sephadex SP C-25 cation-exchange gel (Pharmacia) was used in the sodium form and without pretreatment in order to avoid contamination.

Sulphathiazole (ST) and sulphametazine (SM) stock solutions of 1.0 mg ml^{-1} were prepared from sulphathiazole and sulphametazine Sigma R.A. chemicals in absolute ethanol. Both solutions are stable for at least 1 month at 4°C. Working solutions were prepared by appropiate dilution with absolute ethanol.

Basic procedure

An appropriate volume of sample containing between 20 and 1200 μg of sulphathiazole and between 20 and 1500 μg of sulphametazine and absolute ethanol up to 10 ml was made up to 100 ml with water and transferred into a 1-l polyethylene bottle. Then, 10 ml of 0.1 M monochloroacetic acid and 50 mg of Sephadex SP C-25 gel were added. The mixture was shaken mechanically for 5 min, then the gel beads were collected by filtration under suction and, with the aid of a pipette, packed into a 1-mm silica cell together with a small volume (about 0.2 ml) of the filtrate. A blank solution containing all the reagents except both sulphonamides was prepared and treated in the same way as described for the sample.

Absorption spectra were recorder between 200 and 400 nm with a scan speed of 600 nm min^{-1} against the blank and stored in a disk file. The fourth-derivative spectra were calculated by the Savitzky-Golay method [19,20] with a width of 72 nm.

Fourth-derivative measurements were made as the vertical distance from the fourth-derivative spectrum at 286.0 nm ($^4D_{286.0}$) to the baseline for sulphathiazole and from 266.3 nm ($^4D_{266.3}$) to the baseline for sulphametazine.

Calibration graphs were constructed in the same way using sulphathiazole and sulphametazine solutions of known concentrations.

Procedure for pharmaceutical formulations

The above-mentioned reagents were added to a volume of treated pharmaceutical sample containing an adequate amount of sulphathiazole and sulphametazine, made up to 100 ml with

water and placed into a 1-l polyethylene bottle, as described under *Basic Procedure*. The standard additions method was used for calibration.

Sample treatment

1 g of the commercial product Respig (Syva) was pulverized and homogenized and a weight of 0.2 g of this powder was extracted with absolute ethanol by means of a mechanical shaker or an ultrasonic bath, then filtered through common filter paper and made up to 100 ml with absolute ethanol.

Reference method

A determination of sulphathiazole and sulphametazine by LC was used as a reference method. Chromatography was performed on a high-speed Hypersyl ODS analytical column (100 mm × 2.1 mm i.d.). The loop of the sample-injection valve was 2.0 μl and the mobile phase was water–acetonitrile (88:12, v/v). The flow-rate was set at 0.3 ml min^{-1} and the wavelength of measurement was 280.4 nm for sulphathiazole and 265.4 nm for sulphametazine, respectively [21].

RESULTS AND DISCUSSION

Spectral characteristics and effect of experimental variables

The UV absorption spectra in solution of sulphathiazole and sulphametazine are both characterized by two broad absorption bands in the 205–215 and 250–290 nm regions, with maxima at 256 and 284 nm for sulphathiazole and 243 and 301 nm for sulphametazine, respectively.

Contrarily, their spectra when fixed on Sephadex SP C-25 gel, only show a band for sulphathiazole centered at 280 nm and two bands for sulphametazine with maxima at 244 and 302 nm (Fig. 1). Of the solid supports assayed for retention purposes of both sulphonamides, the strong cation-exchange gel Sephadex SP C-25 was the most effective.

On the other hand, several sulphonamides (sulphanilamide, sulphadiazine, sulphamethoxazole and sulphaquinoxaline) are not fixed on

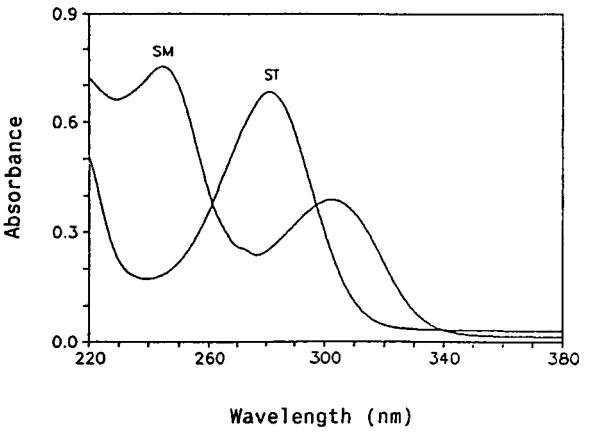

Fig. 1. The UV absorption spectra of sulphathiazole (ST) and sulphametazine (SM) fixed on Sephadex SP C-25 gel.

Sephadex SP C-25. Sulphamerazine and sulphamethoxipyridazine, are fixed only partially on this gel.

The resolution of ST–SM mixture can be accomplished using the derivative techniques. Derivative spectra of different orders were obtained from conventional spectra of ST, SM and ST–SM. The first- and third-order derivative spectra were excluded, but the second- or fourth-order derivative spectra can be used for the quantitative analysis of ST and SM mixture. Detection limits for ST and SM were 0.07 and 0.08 μg ml^{-1} respectively for the second derivative and 0.05 and 0.06 μg ml^{-1} respectively for the fourth derivative. As the use of the fourth-order derivative spectra led to better recovery percentages and detection limits, this order of derivative was selected in order to propose a method for resolving this mixture.

The pH influence is critical in the ion-exchange process because the species fixed on the gel are the corresponding monoprotonated sulphonamides [21]. The absorbance of both sulphonamides fixed on Sephadex SP C-25 are slightly modified in the pH interval of 1.5–3. For sulphathiazole at pH values below 1.5 or above 3.0 the absorbance decreases significantly. The absorbance values are the highest at pH 2.5 for sulphathiazole and pH 2.8 for sulphametazine. In order to obtain an absorbance signal for both

sulphonamides simultaneously a pH of 2.5 was selected.

The best buffer solution for fixation purposes is the monochloroacetic acid/monochloroacetate buffer (pH 2.50). A pH value which in practice is obtained by the addition of 10 ml of 0.1 M monochloroacetic acid solution, and which is due to the exchange of the monochloroacetic H^+ with counterion (Na^+) of the cation-exchange gel. The absorbance of both sulphonamides decreases when the monochloroacetic acid concentration is increased. A 0.009 M concentration of monochloracetic acid was selected to obtain an adequate buffering capacity without an excessive decrease in sensitivity.

An increase in the percentage of ethanol decreases the proportion of sulphonamides in the cation-exchange gel and hence the absorbance. With the idea of maintaining a sufficient margin of ethanol, the solutions were prepared in this solvent, 10% (v/v) ethanol was used even though this implied a slight loss of sensitivity.

The stirring time necessary for maximum absorbance development was 5 min for both sulphonamides. This fact indicates that the fixation process can be seen to have rapid kinetics which is usually common in ion-exchange processes where no previous chemical reaction has taken place.

Conversely, in ion-exchange the stirring time is usually considerably faster (3–6 times) where there has been a previous complexation stage or other type of chemical reaction.

In order to decant adequately it is necessary to leave the gel in the cell for 1 min before taking the measurement. Absorbance measurements remained stable for at least 24 h after equilibration. The order of addition of the reagents did not affect the results obtained.

The use of a large amount of resin reduces the absorbance. The minimum amount of dry resin yields the highest absorbance and greatest ease of handling is obtained using 50 mg.

Instrumental parameters

The smoothing operation of the UV spectra using the Savitzky-Golay method [19,20] does not give appreciable variation in the derivative signal

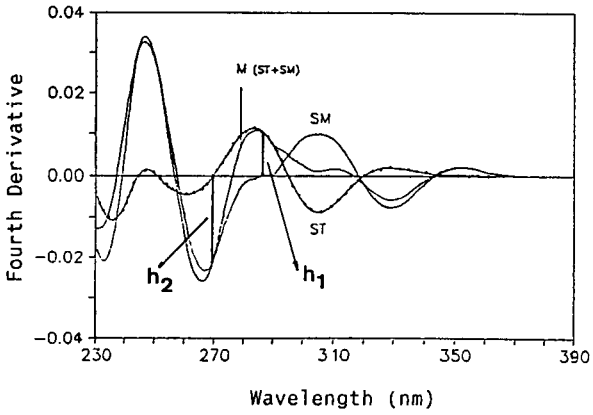

Fig. 2. Fourth-derivative spectra of sulphathiazole (ST), sulphametazine (SM) and sulphathiazole–sulphametazine mixture (M) fixed on Sephadex SP C-25 gel.

from 5 to 25 experimental points for either of the sulphonamides studied. The spectra were therefore not smoothed. A scan speed of 600 nm min^{-1} was selected after verifying that this parameter hardly affects the derivative signal obtained, because the differentiation is attained numerically and not electronically.

For the calculation of the fourth-derivative spectra, a width of 72 nm was selected as giving the best signal-to-noise ratio.

The technique used to choose suitable wavelengths to take measurements proportional to the sulphathiazole and sulphametazine concentrations for the preparation of calibration graphs was the "zero-crossing". Using this technique the height h_1 at wavelength 286.0 nm is proportional to the sulphathiazole concentration, whereas h_2 at 266.3 nm is proportional to sulphametazine concentration (Fig. 2).

Analytical parameters

In order to test the mutual independence of the analytical signals for sulphathiazole and sulphametazine i.e. to show that h_1 and h_2 are independent of sulphametazine and sulphathiazole concentrations, respectively, four calibration graphs were obtained from the height (h) measurements for standards containing between 0.20 and 12.00 $\mu g\ ml^{-1}$ of sulphathiazole, in the absence of sulphametazine and in the presence of 4.0, 8.0 and 12.0 $\mu g\ ml^{-1}$ of sulphametazine,

TABLE 1

Statistical analysis of the determination of sulphathiazole (0.20–12.00 μg ml^{-1}) and sulphametazine (0.20–15.00 μg ml^{-1}) in mixtures by fourth-derivative solid-phase spectrophotometry

Sulphonamide determined	Other sulphonamide		Slope $\times 10^3$	Intercept $\times 10^3$	r
	Name	Concentration (μg ml^{-1})			
ST	SM	–	2.57	0.5	0.9997
		4.00	2.62	1.6	0.9998
		8.00	2.56	1.7	0.9999
		16.00	2.68	0.4	0.9998
SM	ST	–	2.17	0.5	0.9998
		4.00	2.21	1.1	0.9999
		8.00	2.33	0.2	0.9999
		16.00	2.18	0.6	0.9999

respectively. Following the same procedure four calibration graphs were prepared for standards containing between 0.20 and 15.00 μg ml^{-1} of sulphametazine in the absence of sulphathiazole and in the presence of 4.00, 8.00 and 12.00 μg ml^{-1} of sulphathiazole, respectively.

The analytical parameters for all the calibration graphs are summarized in Table 1, from which it can be deduced that the amplitude of the derivative signal of the mixture at the zero-crossing point of the derivative spectrum of one of two components is a function only of the concentration of the other component. Also, the values of the correlation coefficients and the low values for the intercepts indicate good linearity for all the calibration graphs obtained for the fourth-derivative measurements.

The detection limits ($k = 3$) according to IUPAC [22] were 0.05 μg ml^{-1} for sulphathiazole and 0.06 μg ml^{-1} for sulphametazine and the quantification limits ($k = 10$) [23] were 0.16 μg ml^{-1} for sulphathiazole and 0.19 μg ml^{-1} for sulphametazine. The relative standard deviations (R.S.D.) ($P = 0.05$, $n = 10$) were 0.6% for 5 μg ml^{-1} of sulphathiazole and 1.5% for 5 μg ml^{-1} of sulphametazine.

Determination of sulphathiazole and sulphametazine in synthetic samples

The proposed method was applied to the analysis of several synthetic mixtures of sulphathiazole and sulphametazine in different ratios. Table 2 summarizes the results calculated from the calibration graphs, showing that the accuracy is acceptable in all instances.

Determination of sulphathiazole and sulphametazine in pharmaceutical preparations

Sulphathiazole and sulphametazine were determined in a zoosanitary pharmaceutical (Respig from Syva Laboratory), using the procedure de-

TABLE 2

Determination of sulphathiazole and sulphametazine in synthetic mixture by fourth-derivative solid-phase spectrophotometry

ST/SM ratio	[ST]			[SM]		
	Theoretical (μg ml^{-1})	Found [a]	Recovery (%)	Theoretical (μg ml^{-1})	Found [a]	Recovery (%)
1:5	2.00	2.00	100.00	10.00	10.19	101.90
	3.00	3.06	102.00	15.00	15.34	102.27
1:2	4.00	3.97	99.25	8.00	8.04	100.50
	8.00	8.07	100.88	16.00	16.00	100.00
1:1	3.00	2.95	98.33	3.00	3.00	100.00
	5.00	5.07	101.40	5.00	5.08	101.60
	8.00	8.00	100.00	8.00	7.83	97.88
	10.00	10.22	102.20	10.00	9.96	99.60
2:1	4.00	4.05	101.25	2.00	2.04	102.00
	8.00	8.18	102.25	4.00	4.00	100.00
5:1	10.00	10.16	101.60	2.00	1.96	98.00
	15.00	15.18	101.20	3.00	2.94	98.00

[a] Data are based on the average obtained from three determinations.

TABLE 3

Determination of sulphathiazole and sulphametazine in Respig

Composition [a] (%)		Found [b] (%)	
		Proposed method	LC method
Sulphathiazole	(20.0)	19.2±0.1	19.3±0.1
Sulphametazine	(20.0)	20.4±0.1	20.6±0.1
Guaiacol glyceryl ether	(2.5)		
KI	(0.8)		
Sodium ascorbate	(1.5)		
Vitamin K	(0.1)		

[a] Composition indicated by the supplier. [b] Average value ± standard deviation of five determinations.

scribed above. Table 3 summarizes the results obtained. There is good agreement between the LC method [21] and the proposed method, with the latter having superior detection limits for both ST (0.05 μg ml^{-1} compared with 2.0 μg ml^{-1}) and SM (0.06 μg ml^{-1} compared with 2.0 μg ml^{-1}).

In conclusion, a practical application of derivative spectrophotometry in combination with solid phase spectrophotometry to multicomponent analysis has been described. The combination of both techniques allows for the simultaneous determination of sulphatiazole and sulphametazine at low levels in mixtures, without previous preconcentration or separation.

This study was funded by the Managing Committee of Technical and Scientific Research (DGICYT) of the Ministery of Science and Education (Spain) (Project No. PS88-0101).

REFERENCES

1 F. Capitán, F.L. Capitán-Vallvey, M.C. Valencia, J.M. Bosque-Sendra, F. Molina and I. de Orbe, Analusis, 19 (1991) 177.
2 J.M. Bosque-Sendra, F. Molina and E. López, Analyst, 116 (1991) 871
3 M.C. Valencia, J. García and L.F. Capitán-Vallvey, Anal. Lett., 23 (1990) 1095.
4 F. Molina, M.C. Valencia, J. de la Torre and L.F. Capitán-Vallvey, J. Pharm. Biomed. Anal., 7 (1989) 843.
5 H. Ishii, Fresenius' Z. Anal. Chem., 319 (1984) 23.
6 K. Yoshimura, H. Waki and S. Ohasi, Talanta, 23 (1976) 449.
7 O. Parks, J. Assoc. Off. Anal. Chem., 65 (1982) 632.
8 M.H. Thomas, R.L. Epstein, R.B. Ashworth and H. Marks, J. Assoc. Off. Anal. Chem., 66 (1983) 884.
9 S.J. Stout, W.A. Steller, A.J. Manuel, M.O. Poeppel and A.R. Da Cunha, J. Assoc. Off. Anal. Chem., 67 (1984) 142.
10 R.M. Simpson, F.B. Suhre and J.W. Schafer, J. Assoc. Off. Anal. Chem., 68 (1985) 23.
11 N. Haagsma and C. Van de Water, J. Chromatogr., 333 (1985) 256.
12 M.N.L. Aerts, W.M.J. Beek and U.A.Th. Brinkman, J. Chromatogr., 435 (1988) 97.
13 A.C. Bratton and E.K. Marshall, J. Biol. Chem., 128 (1939) 537.
14 J. Rieder, Chemotherapy (Basel), 17 (1972) 1.
15 A. Bye and A.F.J. Fox, Clin. Chem., 20 (1974) 288.
16 M.A. Koupparis and P.I. Anagnostopoulou, Anal. Chim. Acta, 204 (1988) 271.
17 F. Salinas, A. Espinosa Mansilla and J.J. Berzas-Nevado, Anal. Chim. Acta, 233 (1990) 289.
18 Beckman Instruments, Spectroscopy, 2 (1987) 16.
19 A. Savitzky and M.J.E. Golay, Anal. Chem., 36 (1964) 1627.
20 J. Steiner, Y. Termonia and J. Deltour, Anal. Chem., 44 (1972) 1906.
21 I. de Orbe, PhD Thesis, University of Granada, 1991.
22 IUPAC, Nomenclature, Symbols, Units and Their Usage in Spectro-chemical Analysis, Pure Appl. Chem., 45 (1976) 105.
23 Guidelines for Data Acquisition and Data Quality Evaluation in Environmental Chemistry, Anal. Chem., 52 (1980) 2242.

Analytica Chimica Acta, 282 (1993) 81–85
Elsevier Science Publishers B.V., Amsterdam

UV–visible spectrum of nitrous acid in solution: pK_a determination and analytical applications

Maria das Graças Gomes and Simone da S.S. Borges

Departamento de Química Analítica e Físico Química, Universidade Federal do Ceará, Fortaleza-CE (Brazil)

Luiz G.F. Lopes and Douglas Wagner Franco

Universidade de São Paulo–USP, Instituto de Física e Química de São Carlos, Caixa Postal 369, 13560-970 São Carlos, SP (Brazil)

(Received 22nd December 1992; revised manuscript received 1st April 1993)

Abstract

The UV–visible spectra of nitrous acid in four different solvents were obtained. The hyperfine structure observed in all these spectra was tentatively attributed to vibrational coupling. The unique characteristics of the nitrous acid spectrum in acidic solution allowed the detection and determination of 3.0×10^{-4} mol l^{-1} nitrite in the presence of 0.1 mol l^{-1} nitrate solution. Through spectrophotometric and potentiometric measurements, the pK_a value for nitrous acid was calculated to be 2.3 ± 0.2.

Keywords: UV–Visible spectrophotometry; Dissociation constants; Nitrate; Nitrite; Nitrous acid

The simultaneous analytical determination of nitrate and nitrite has been performed by many methods [1–4]. One of these methods [4] does not involve the addition of any reagent to the sample, and takes advantage of the fact that aqueous $NaNO_2$ exhibits an absorption band at 355 nm whereas aqueous $NaNO_3$ shows no absorption at this wavelength. Wetters and Uglum [4] also mentioned that at pH < 5.0, the spectrum of nitrous acid begins to appear in $NaNO_2$ aqueous solutions. Although recognizing the unique characteristics of the nitrous acid spectrum, they did not consider this aspect further.

In this work, the UV–visible spectra of nitrous acid in aqueous solutions and in other solvents were obtained and a specific method for NO_2^- detection was developed. The dissociation constant of nitrous acid was redetermined by two independent methods.

Correspondence to: D.W. Franco, Universidade de São Paulo–USP, Instituto de Física e Química de São Carlos, Caixa Postal 369, 13560-970 São Carlos, SP (Brazil).

EXPERIMENTAL

Apparatus

Spectrophotometric measurements were made with a Hewlett-Packard HP 8452A diode-array spectrophotometer and a Hitachi U-3210 spectrophotometer utilizing 1-cm quartz cells.

All pH measurements were made on a Corning Model 130 pH meter equiped with a Corning Model 476541 semi-micro electrode.

Reagents

All the reagents used (Merck and Aldrich) were of analytical-reagent grade. Nitrite and nitrate solutions were standardized spectrophotometrically by Wetters and Uglum's method [4].

The solvents employed (Merck) were purified according to the literature [5] just before use. Doubly distilled water was used throughout.

Procedure

The UV–visible spectra of nitrous acid solutions were obtained in CF_3COOH–CF_3COONa solutions in the pH range 0.24–4.00. For pK_a calculations, all the measurements were made 5 min after the addition of sodium nitrite solution to CF_3COOH–CF_3COONa solution. CF_3COONa was used as a background electrolyte for maintaining the ionic strength constant.

An uncertainty of ca. ± 1.0 nm (ca. 66 cm^{-1}) could be assigned to the attribution of λ_{max} in the spectra.

From absorbance measurements at 347, 358, 372 and 386 nm it was possible to calculate the dissociation constant of nitrous acid (HONO) by using the equation [6]

$$pK = pH + \log\left(\frac{A_o - A_{NO_2^-}}{A_{HONO} - A_o}\right)$$

where A_o is the absorbance at the chosen wavelength for the mixture of the two forms at a particular pH and $A_{NO_2^-}$ and A_{HONO} are the absorbance of the basic and acidic forms, respectively.

The pK_a for HONO was also calculated from pH measurements on HONO–$NaNO_2$ aqueous solutions. In these experiments the ionic strength was maintained at 1.0.

The pH meter was calibrated using 1.00×10^{-3} mol l^{-1} CF_3COOH solutions in CF_3COONa medium ($\mu = 0.10$–1.00). Therefore, the pH measurements are referred to hydrogen ion concentration and not activity.

RESULTS AND DISCUSSION

In aqueous solutions HONO exhibits four distinct absorption peaks at 386, 372, 358 and 347 nm. In addition to these peaks, two shoulders can be easily observed at 337 and 325 nm (see Table 1 and Fig. 1).

Similarly to the absorptions observed in the UV–visible spectra of $NaNO_2$ solutions [4], the above absorptions for HONO solutions are of low intensity and probably originate from forbidden transitions of the nitrous acid molecule. The hyperfine structure of the HONO spectrum is probably a consequence of a vibrational coupling [7].

This hyperfine structure is also present in the UV–visible spectra of HONO in methanol, acetonitrile and benzene (Fig. 1). In addition to the six peaks mentioned above, a seventh absorption process is observed in methanol and in water.

The molar absorptivities of the transitions increase as the polarity of the solvent decreases. Also, the energy of the transition increases as the polarity of the solvent decreases. The major shift in energy observed in the HONO spectra on changing from water to benzene medium corresponds to only to 0.8 kcal (1 kcal = 4.184 kJ) (337–334 nm).

The average energy difference between the peaks present in the hyperfine structure in Fig. 1

TABLE 1

Molar absortivities of HONO in different solvents

Solvents	Parameter	Values						
Water	λ(nm)	386	372	358	347	337	325	318
	ε(l mol^{-1} cm^{-1})	31.3	52.0	51.2	38.6	25.0	~ 15	~ 11
Methanol	λ(nm)	386	366	353	341	330	320	312
	ε(l mol^{-1} cm^{-1})	15.0	54.8	81.4	77.7	58.8	37.3	24.9
Acetonitrile	λ(nm)	388	373	360	348	337	327	[a]
	ε(l mol^{-1} cm^{-1})	36.6	61.3	58.0	38.5	23.1	13.2	–
Benzene	λ(nm)	387	371	357	345	334	323	[a]
	ε(l mol^{-1} cm^{-1})	91.4	257.1	372.0	356.3	374.4	179.8	–

[a] It is difficult to observe this band in these solvents owing to their strong absorption in this region.

is about 1.0×10^3 and 9.3×10^2 cm^{-1} for benzene and water as solvent, respectively. Benzene is not a polar solvent, hence little influence of the solvent on the characteristics of the spectra [8] is expected and the UV–visible spectra of HONO in benzene and in the gaseous phase are expected to be similar.

In the gaseous phase the HONO molecule exhibits *cis* and *trans* configurations that are easily interconvertible as the difference in energy between the forms is only about 0.51 kcal mol^{-1} [9]. Both the *cis* and *trans* forms of nitrous acid absorb near 850 cm^{-1} due to the N–O stretch ν_4 [9,10]. The nitrite ion does not exhibit absorption bands in this region.

Taking into account the experimental uncertainties in the attribution of λ_{max} in the UV–visible spectra and in the NO_2^- and HONO vibrational spectra [4,10], it is reasonable to ascribe the hyperfine structure to the coupling of the electronic transition with the vibrational component ν_4 [9]. The value of 850 cm^{-1} corresponds to the energy gap between two vibrational levels at the ground state and as in the vibronic–electronic coupling the differences are between the vibrational levels of the excited states, 850 cm^{-1} should be considered only as a reference value.

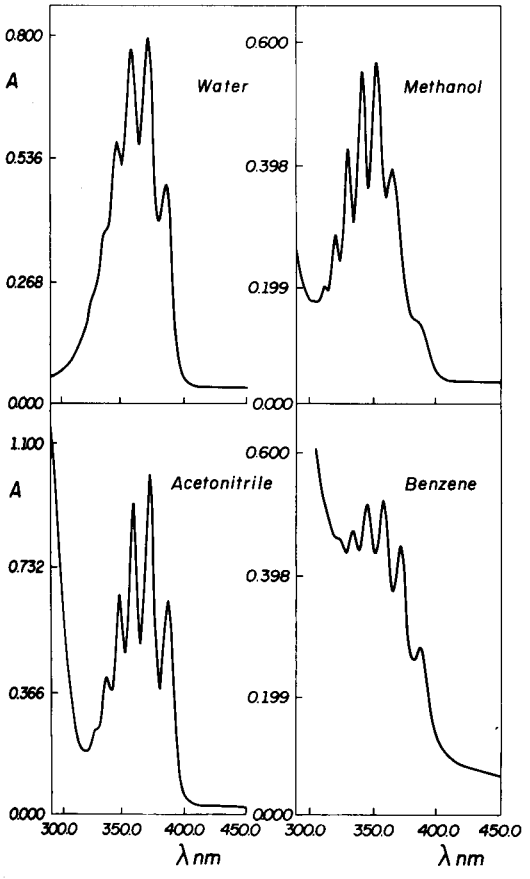

Fig. 1. UV–visible spectra of HONO in different solvents.

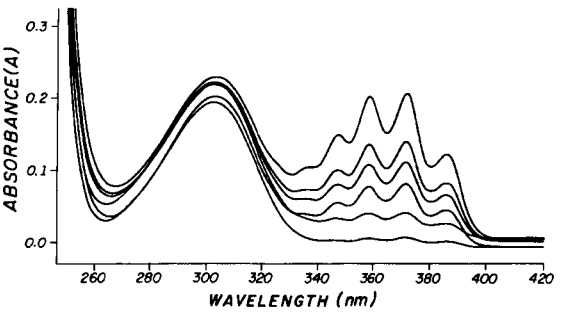

Fig. 2. UV–visible spectra of nitrite and nitrate mixtures at pH 1.0. Concentrations: $NaNO_3 = 0.03$ mol l^{-1}; $NaNO_2 = 3.0 \times 10^{-4}$, 7.5×10^{-4}, 1.5×10^{-3}, 2.3×10^{-3} and 4.5×10^{-3} mol l^{-1}.

Owing to the unique characteristics of the UV–visible spectra of HONO acidic solutions, it provides a selective and useful method for detecting nitrite contamination in samples. It is possible to identify and determine $NaNO_2$ at concentrations down to 3.0×10^{-4} mol l^{-1} in 0.1 mol l^{-1} $NaNO_3$ solution (see Fig. 2), provided that the hydrogen ion concentration is properly adjusted with CF_3COOH. This limit would be decreased by one order of magnitude if a 10-cm path-length cell were to be employed. The NO_2^- detection can be performed without interference in the presence of 1.0×10^{-1} mol l^{-1} of the following ions: ClO_4^-, $CF_3SO_3^-$, Cl^-, BF_4^-, Br^-, CH_3COO^-, SO_4^{2-}, PO_4^{3-} and PF_6^-.

This procedure has proved useful in detecting $NaNO_2$ impurities in isolated nitrosyl ruthenium complexes of the type *trans*-$[Ru(NH_3)_4LNO](PF_6)_3$ (see Fig. 3).

The absorbance of aqueous HONO solution changes with time. A decrease in absorbance is observed for the peaks corresponding to the nitrous acid. For $\lambda_{max} = 372$ nm, the molar absortivity is 52.0, 49.9, 48.0, 46.8 and 46.0 l mol^{-1} cm^{-1}

after 5, 10, 15, 20 and 25 min, respectively. In spite of the absorbance changes, very good straight lines were obtained for plots of absorbance versus NO_2^- concentration when the data were referred to the same measured time. For all the plots, the correlation coefficient was never worse than 0.990. For instance, for absorbance measurements at 372 nm carried out 5 min after acidification of nitrite solution, the correlation coefficient was 0.999; the slope and the standard deviation of the slope were 52.0 and 2.22 ($n = 6$), respectively, and the intercept and the standard deviation of the intercept were 8.20×10^{-4} and 7.70×10^{-3} ($n = 6$), respectively. Therefore, this spectrophotometric method can be also used for quantitative purposes.

The pK_a of HONO is another point that deserves comment. Spectrophotometric measurements of the absorption peaks of nitrous acid for solutions of different hydrogen ion concentrations allowed the calculation [6] for the pK_a value for HONO as 2.4 ± 0.1 at 25°C and $\mu = 0.10$ (CF_3COONa). As observed from the results in Table 2, all the measurements led to very close pK_a values for the HONO. This observation is consistent with the fact that all these peaks correspond to the spectrum of the same species.

There is much controversy in the literature about the pK_a of HONO, with reported values varying from 2.80 to 5.22 [11–15]. The pK_a value of 2.4 given in Table 2 is the smallest value reported so far and is one order of magnitude smaller than the first value (3.35) reported [11].

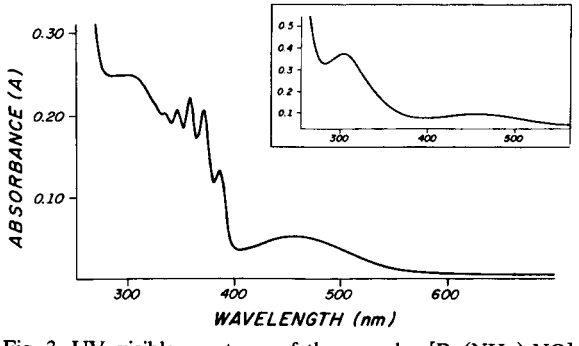

Fig. 3. UV–visible spectrum of the complex $[Ru(NH_3)_5NO](PF_6)_3$ with nitrite impurity. Inset: UV–visible spectrum of the same complex free of nitrite.

TABLE 2

pK_a values for nitrous acid determined by spectrophotometry [a]

λ (nm)	pK_a
347	2.38 ± 0.08
358	2.42 ± 0.09
372	2.4 ± 0.1
386	2.4 ± 0.1
Mean [b]	2.4 ± 0.1

[a] $\mu = 0.10$ (CF_3COOH–CF_3COONa); temperature = 25 ± 1°C.
[b] Mean ± standard deviation ($n = 4$).

Potentiometric measurements in $NaNO_2$–HONO solutions allowed the pK_a value of HONO to be calculate as 2.2 ± 0.1 at 25°C and $\mu = 1.0$ (CF_3COONa). In spite of the difference in ionic strength in the two methods, this value strongly supports the pK_a value obtained from spectrophotometric data. From the above arguments, it is reasonable to accept a mean pK_a value of 2.3 ± 0.2 for HONO.

The authors are very grateful to Dr. Celso Ulysses Davanzo for helpful discussions and Dra. Heloise de O. Pastore for language correction. They also thank the Brazilian agencies CNPq, CAPES and FAPESP for financial support.

REFERENCES

1 H. Hammaguchi, R. Kuroda and E. Endo, Bunseki Kagaku, 7 (1958) 409; C.A., 54 (1960) 7421e.
2 G. Meerman, Diss. Abstr., 20 (1960) 4507.
3 L. Haddad and J.C. MacDonald, presented at the Pittsburgh Conference on Analytical Chemistry and Applied Spectroscopy, Cleveland, OH, March 1969.
4 H.J. Wetters and K.L. Uglum, Anal. Chem., 42 (1970) 335.
5 D.D. Perrin, W.L. Almarege and D.R. Perrin, Purification of Laboratory Chemicals, Pergamon, New York, 1983.
6 A. Albert and P.E. Serjeant, The Determination of Ionization Constants, Chapman and Hall, Edinburgh, 2nd edn., 1971.
7 A.B.P. Lever, Inorganic Electronic Spectroscopy, Elsevier, New York, 1984.
8 D.A. Skoog, Principles of Instrumental Analysis, Saunders College Publishing, Philadelphia, 3rd edn., 1985.
9 R.T. Hall and G.C. Pimentel, J. Chem. Phys., 38 (1963) 1889.

10 K. Nakamoto, Infrared and Raman Spectra of Inorganic and Coordination Compounds, Wiley, New York, 3rd edn., 1977.
11 M. Schümann, Chem. Ber., (1900) 527.
12 D.D. Perrin, Ionisation Constants of Inorganic Acids and Bases in Aqueous Solution, Pergamon, New York, 2nd edn., 1982.
13 F.A. Cotton and G. Wilkinson, Advanced Inorganic Chemistry, Wiley, New York, 4th edn., 1980.
14 D.A. Sookg, D.M. West and F.J. Holler, Fundamentals of Analytical Chemistry, Saunders College Publishing, New York, 5th edn., 1988.
15 The Merck Index, Merck, Rahway, NJ, 11th edn., 1989.

Analytica Chimica Acta, 282 (1993) 87–94
Elsevier Science Publishers B.V., Amsterdam

Catalytic determination of iodide by a maximum absorbance method using the oxidation reaction of chlorpromazine with hydrogen peroxide

Bing Liang, Susumu Kawakubo, Masaaki Iwatsuki and Tsutomu Fukasawa

Department of Applied Chemistry and Biotechnology, Faculty of Engineering, Yamanashi University, Takeda-4, Kofu 400 (Japan)

(Received 28th January 1993; revised manuscript received 4th May 1993)

Abstract

Chlorpromazine is oxidized catalytically in the presence of iodide with 1 M hydrogen peroxide in 1 M sulphuric acid medium to form a red radical, which is further oxidized to a colourless sulphoxide. The plot of absorbance at 528 nm vs. reaction time shows an absorbance maximum proportional to the concentration of iodide ions in the range 0–7 ng ml^{-1}. The method has the advantage that careful control of the reaction time and temperature is not needed; the reaction temperature has little influence on the determination in the range 20–40°C. The method also gives a higher sensitivity and shows less influence of the concentrations of hydrogen peroxide and sulphuric acid than the tangent method using the initial reaction. The limit of detection is about 0.1 ng ml^{-1} (0.5 ng in 5 ml of measured solution). The effects of foreign ions were investigated. The mechanism of the reaction is discussed.

Keywords: Catalytic methods; UV–Visible spectrophotometry; Iodide

Many methods have been studied for the determination of traces of iodide and the following have been reported as highly sensitive methods. A limit of detection (LOD) of 1 ng ml^{-1} was obtained by cathodic stripping voltammetry using mercury [1], and LODs of 2–10 ng ml^{-1} have been reported for ion chromatographic methods [2–4], which often required preconcentration. Catalytic analysis has also been studied as a highly sensitive method that can be carried out simply and easily using an inexpensive instrument such as a simple spectrophotometer. Two catalytic methods, based on the reduction of cerium(IV) ion with arsenious ion [5] and the decomposition of thiocyanate ions with nitrite ion [6] are especially sensitive with LODs of ca. 0.1 ng ml^{-1}. However, because the reaction rate or parameters related to the rate are measured, these catalytic methods are very susceptible to the influence of reaction conditions such as reaction temperature, reaction time and reactant concentrations, as shown by the Arrhenius and rate equations.

Chlorpromazine, one of the redox indicators, in acidic media is first oxidized reversibly to a coloured free radical or semiquinone, and further oxidized irreversibly to a colourless sulphoxide [7]. The oxidation of chlorpromazine with potassium bromate in phosphoric acid medium has been reported for the catalytic determination of iodide in the range 5–70 ng ml^{-1} by the tangent method [8], which is also susceptible to the influence of reaction conditions, as described above. In this study, it was found that the oxidation of chlorpromazine with hydrogen peroxide in sulphuric acid solution gave an absorbance maxi-

Correspondence to: T. Fukasawa, Department of Applied Chemistry and Biotechnology, Faculty of Engineering, Yamanashi University, Takeda-4, Kofu 400 (Japan)

mum that is proportional to the concentration of iodide included in the reaction solution. The measurement of the maximum absorbance, i.e., the maximum absorbance method, allows iodide to be determined down to 0.1 ng ml^{-1} (0.5 ng in 5 ml of the reaction solution used) and has the advantages of a lack of influence of reaction temperature and of no need for control of the reaction time, in addition to a low influence of reactant concentrations. The effects of foreign ions were also studied. The maximum absorbance method was compared with the tangent method, which is based on measurement of the reaction rate in the initial reaction. The mechanism of the reaction is discussed.

EXPERIMENTAL

Reagent solutions and apparatus

All chemicals were of analytical-reagent grade and deionized, distilled water was used throughout. Chlorpromazine hydrochloride (CPH) solution (0.12 M) was prepared by dissolving the compound (Wako) in water. The solution was kept in a refrigerator and diluted with water to prepare working solutions just before use. An iodide stock standard solution (1.0 mg I^- ml^{-1}) was prepared by dissolving potassium iodide in water. Working iodide solutions were prepared by diluting the stock standard solution with water. Hydrogen peroxide reagent (30%) was used without dilution.

All spectrophotometric measurements were done using a Hitachi Model 100-10 spectrophotometer equipped with a chart recorder. The temperature of the cell and cell chamber was kept at constant by circulating the water from a thermostated water-bath at the reaction temperature.

Recommended procedure

Maximum absorbance method. Transfer sample solution or iodide solution (less than 3.5 ml) containing less than 35 ng of I^- into a 20-ml glass test-tube with a ground-glass stopper. Add 0.5 ml of 10 M sulphuric acid and water to make the solution volume exactly 4.0 ml. After adding 0.5 ml of 0.06 M CPH to the test-tube, add 0.5 ml of 30% hydrogen peroxide and immediately mix well the solution to start the reaction. Transfer part of it into 10-mm cell and set the cell in the cell chamber. All solutions can be in the temperature range 20–40°C. Record the absorbance at 528 nm vs. reaction time curve on the chart until the maximum absorbance (A_{max}) appears after several minutes. Construct a calibration graph of A_{max} vs. iodide concentration.

Tangent method. Experimental procedures are carried out in the same manner as for the maximum absorbance method except for the following. A sample or iodide solution containing less than 1 μg of I^- and 0.5 ml of 0.03 M CPH solution are used, and all solutions are kept previously in a water-bath thermostated at 25°C. Calculate the tangent (k), which is a pseudo-zero-order reaction constant, from the slope of a linear portion of the absorbance vs. reaction time curve within 2 min. Construct a calibration graph of k vs. iodide concentration.

RESULTS AND DISCUSSION

Preliminary experiment

Experiments were first carried out under the reaction conditions of 1×10^{-4} M CPH, 5×10^{-4} M bromate, 1.5 M phosphoric acid and 40°C, as proposed by Vinas et al. [8]. The calibration graph of the tangent method was severely curved at iodide concentrations below 20 ng ml^{-1}, and A_{max} was not proportional to iodide concentration. Sulphuric acid medium gave results similar to those of the phosphoric acid medium.

Instead of bromate, hydrogen peroxide was tried for oxidizing CPH in sulphuric acid medium. In this reaction system, the catalytic effect of iodide was more significant and sensitive, and linear calibration graphs were obtained by both the maximum absorbance method and the tangent method. Therefore, the detailed experimental conditions described in the recommended procedure were studied on the same system as follows.

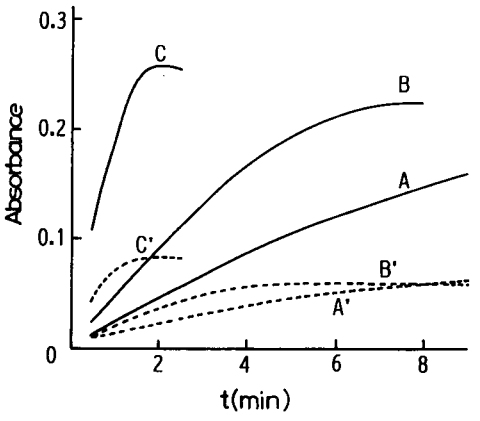

Fig. 1. Effect of sulphuric acid concentration on the absorbance vs. reaction time curve. Conditions: 0.5 M (A, A'), 1 M (B, B') and 2 M (C, C') H_2SO_4; 6×10^{-3} M CPH; 1 M H_2O_2; 25°C. Dashed lines, blank; solid lines, 5 ng I^- ml^{-1}.

Effect of sulphuric acid concentration

Figure 1 shows the effect of sulphuric acid concentration on the absorbance vs. reaction time curve. Both the catalytic and non-catalytic (blank) reactions were accelerated and A_{max} appeared earlier with increase in sulphuric acid concentration. The linearity of the absorbance vs. reaction time curve in the initial reaction was good in 1 M sulphuric acid, which was used in the tangent method, and became poor at higher sulphuric acid concentrations. Figure 2 shows the effect of sulphuric acid concentration on A_{max} and k. A_{max} in both the catalytic and non-catalytic reactions varied little in the range of 1.0–2.0 M. However, k varied greatly in the catalytic reaction but little in the non-catalytic reaction.

Effect of hydrogen peroxide concentration

Figure 3 shows that A_{max} appeared earlier and the linearity of the absorbance vs. reaction time curve became poor with increase in hydrogen peroxide concentration. Figure 4 shows that A_{max} in both the catalytic and non-catalytic reactions was almost constant in the range 1.0–2.0 M hydrogen peroxide, although k changed greatly in the catalytic reaction and little in the non-catalytic reaction. A hydrogen peroxide concentration of 1 M was used in the recommended procedure for both methods.

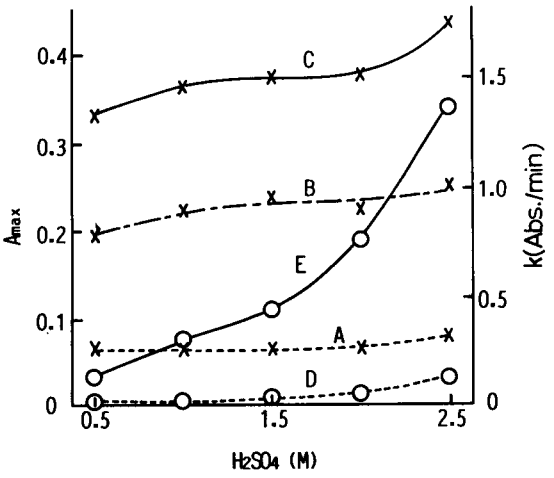

Fig. 2. Effect of sulphuric acid concentration on A_{max} and k. Conditions: 1 M H_2O_2; 25°C. × = Curves for A_{max}, 6×10^{-3} M CPH (A = blank, B = 5 ng I^- ml^{-1}, C = 10 ng ml^{-1} I^-); ○ = curves for k, 3×10^{-3} M CPH (D = blank, E = 50 ng I^- ml^{-1}).

Effect of CPH concentration

Figure 5 shows that increased CPH concentration gave accelerated reaction and better linearity of the absorbance vs. reaction time curve in both the catalytic and non-catalytic reactions, but A_{max} appeared later. Figure 6 shows that both A_{max} and k were approximately proportional to CPH concentration.

A CPH concentration of 6×10^{-3} M was selected for the recommended A_{max} procedure be-

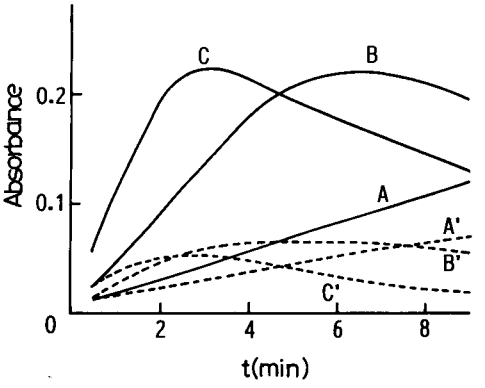

Fig. 3. Effect of hydrogen peroxide concentration on the absorbance vs. reaction time curve. Conditions: 1 M H_2SO_4; 0.2 M (A, A'), 1 M (B, B') and 2 M (C, C') H_2O_2; other conditions and symbols as in Fig. 1.

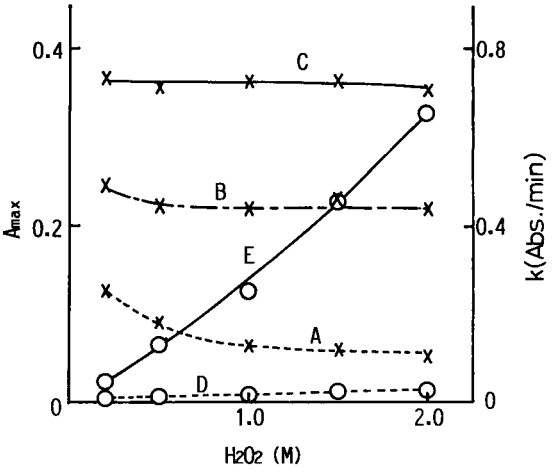

Fig. 4. Effect of hydrogen peroxide concentration on A_{max} and k. Conditions: 1 M H_2SO_4; other conditions and symbols as in Fig. 2.

cause it gave a calibration graph of maximum absorbance vs. iodide concentration over a wider range. The use of higher CPH concentrations gave bubbles in mixed solutions when hydrogen peroxide solution was added, and the bubbles interfered with the measurement of absorbance

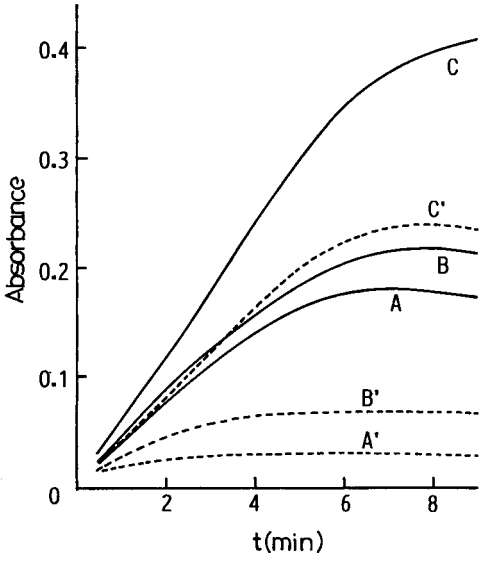

Fig. 5. Effect of CPH concentration on the absorbance vs. reaction time curve. Conditions: 1 M H_2SO_4; 3×10^{-3} M (A, A'), 6×10^{-3} M (B, B') and 18×10^{-3} M (C, C') CPH; other conditions and symbols as in Fig. 1.

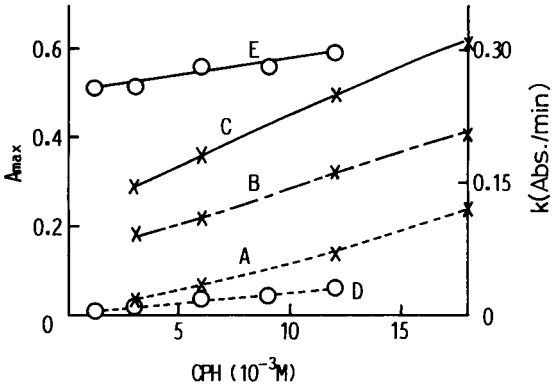

Fig. 6. Effect of CPH concentration on A_{max} and k. Conditions: 1 M H_2SO_4; other conditions and symbols as in Fig. 2.

in the initial reaction. Therefore, a lower CPH concentration of 3×10^{-3} M was chosen for the tangent method.

Effect of reaction temperature

A_{max} appeared earlier with elevation of the reaction temperature, as shown in Fig. 7, but Fig. 8 shows that A_{max} in both the catalytic and non-catalytic reactions was nearly constant irrespective of the reaction temperature. On the other hand, the linearity of the absorbance vs. reaction time curve became poor with elevation of reaction temperature, as shown in Fig. 7, and the k

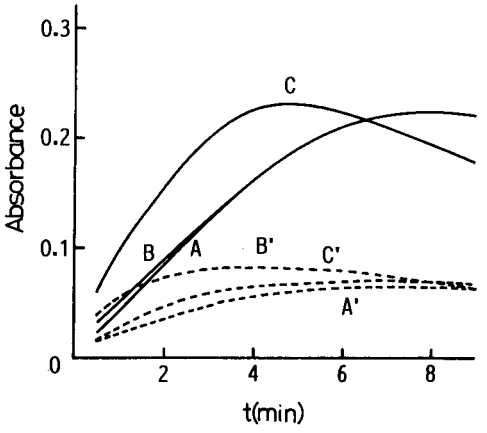

Fig. 7. Effect of reaction temperature on the absorbance vs. reaction time curve. Conditions: 1 M H_2SO_4; Temperature 20°C (A, A'), 25°C (B, B') and 40°C (C, C'); other conditions and symbols as in Fig. 1.

value of the catalytic reaction was greatly affected by temperature. A temperature at 25°C was adopted considering the linearity of the absorbance vs. reaction time curve for the tangent method.

Calibration

Ten standard solutions ranging in concentration from 0 to 8 ng I^- ml^{-1} were used to construct the calibration graph for the maximum absorbance method. A linear calibration graph was obtained up to 7 ng I^- ml^{-1}; the equation of the line was $A_{max} = 2.98 \times 10^{-2}[I^-] + 0.072$ and the correlation coefficient was $r = 0.989$. The standard deviations (σ) and the relative standard deviations (R.S.D.) for repeated determination ($n = 6$) of 0.5 and 1 ng I^- ml^{-1} were 0.03 ng ml^{-1} and 6% and 0.05 ng ml^{-1} and 5%, respectively. The LOD was about 0.1 ng I^- ml^{-1}.

The calibration graph was rectilinear up to 200 ng I^- ml^{-1} in the tangent method: $k = 4.97 \times 10^{-3}[I^-] + 0.0164$, $r = 0.998$; σ and R.S.D. ($n = 6$) for 1 and 5 ng I^- ml^{-1} were 0.2 ng ml^{-1} and 20% and 0.5 ng ml^{-1} and 10%, respectively. The

TABLE 1

Effects of foreign ions on the determination of 5 ng I^- ml^{-1}

Ion	Amount added ($\mu g\ ml^{-1}$)	Added as	Error (%)	Ion	Amount added ($\mu g\ ml^{-1}$)	Added as	Error (%)
EDTA	6000	Disodium salt	−7	PO_4^{3-}	15 000	Na_3PO_4	33
	5000		−5		1250		5
Citrate	800	$(NH_4)_2HC_6H_5O_7$	10	SO_4^{2-}	1150	Na_2SO_4	2
	400		5	$C_2O_4^{2-}$	300	$Na_2C_2O_4$	5
CH_3COO^-	4500	CH_3COOK	16	CO_3^{2-}	600	K_2CO_3	9
	1000		5		200		7
Tartrate	1600	$(NH_4)_2C_4H_4O_6$	14	F^-	1200	NaF	9
	400		3		400		3
ClO_4^-	400	$NaClO_4$	6	CyDTA [a]	200	CyDTA [a]	16
	300		4		250		4
Zn^{2+}	1200	$Zn(NO_3)_2$	9	K^+	2000	KNO_3	−6
	400		2		100		−2
Ni^{2+}	600	$Ni(NO_3)_2$	8	NH^{4+}	1000	NH_4NO_3	7
	400		3		500		0
Cd^{2+}	550	$Cd(NO_3)_2$	−3	Na^+	1500	$NaNO_3$	10
Ca^{2+}	1200	$Ca(NO_3)_2$	14		1000		4
	200		0	Cl^-	200	NaCl	12
Al^{3+}	200	$Al(NO_3)_3$	25		100		6
	10		5	SO_3^{2-}	250	Na_2SO_3	19
Co^{2+}	20	$Co(NO_3)_2$	15		60		7
	10		5	Mn^{2+}	50	$MnCl_2$	11
Mg^{2+}	400	$Mg(NO_3)_2$	18		5		2
	4		3	SeO_3^{2-}	16	H_2SeO_3	−11
Cr^{3+}	5	$K_2Cr(SO_4)_4$	11		6.4		−8
	2.5		3	Cu^{2+}	200	$CuSO_4$	80
Ba^{2+}	0.8	$Ba(NO_3)_2$	8		0.8		4
Pb^{2+}	1	$Pb(NO_3)_2$	10	Br^-	2	NaBr	32
	0.75		5		0.4		3
VO_3^-	0.039	NH_4VO_3	8	NO_2^-	0.02	$NaNO_2$	10
Fe^{3+}	0.1	$Fe(NO_3)_3$	22		0.01		4
	0.01		9	SCN^-	0.1	NaSCN	100
IO_3^-	5×10^{-4}	KIO_3	13		0.005		12
	2×10^{-4}		4				

[a] CyDTA = *trans*-1,2-cyclohexanediaminetetraacetic acid.

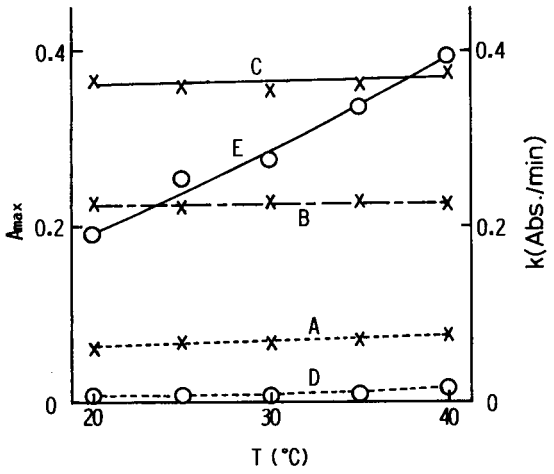

Fig. 8. Effect of reaction temperature on A_{max} and k. Conditions: 1 M H_2SO_4; other conditions and symbols as in Fig. 2.

LOD was about 0.5 ng ml^{-1}, which was inferior to that of the maximum absorbance method.

Effects of foreign ions on the maximum absorbance method

The effects of foreign ions on the determination of 5 ng I^- ml^{-1} by the maximum absorbance method were investigated (Table 1). Many kind of ions were tolerated, although Fe^{3+}, V(V), NO_2^-, SCN^- and IO_3^- interfered with the determination.

Mechanism of the reaction

The iodide-catalysed oxidation of CPH by excess of hydrogen peroxide in acidic medium is a consecutive reaction:

$$\underset{\text{colourless}}{\text{CPH}} \rightarrow \underset{\text{red}}{\text{CPH}^*} \rightarrow \underset{\text{colourless}}{\text{CPH}'}$$

There have been some discussions [9,10] about consecutive reactions or processes leading to a maximum signals which can be used for determination. One discussion [9] however, was not concerned with catalytic reactions. In the other [10], although the maximum signal (absorbance) of a catalysed consecutive reaction was used, it was not for the determination of the catalyst.

In this instance, the total rate of generation of the red intermediate, CPH* can be expressed by Eqns. 1 and 2 for the non-catalytic reaction and for the reaction including both the non-catalytic and catalytic modes, respectively.

$$d[CPH^*]/dt = k_b[H^+]^j[H_2O_2]^l[CPH]^m - k_2[H^+]^n[H_2O_2]^p[CPH^*]^q \quad (1)$$

$$d[CPH^*]/dt = k_b[H^+]^j[H_2O_2]^l[CPH]^m + k_1[H^+]^f[H_2O_2]^g[CPH]^h[I^-]^i - k_2[H^+]^n[H_2O_2]^p[CPH^*]^q \quad (2)$$

where k_b and k_1 represent the rate constants of non-catalytic and catalytic reactions of the first step, respectively, and k_2 is the rate contant for the second reaction.

In the initial period of the reaction, because the concentration of CPH* is very low, the $k_2[H^+]^n[H_2O_2]^p[CPH^*]^q$ term is very small compared with the other two terms, and can be ignored:

$$d[CPH^*]/dt = k_b[H^+]^j[H_2O_2]^l[CPH]^m \quad (3)$$

$$d[CPH^*]/dt = k_b[H^+]^j[H_2O_2]^l[CPH]^m + k_1[H^+]^f[H_2O_2]^g[CPH]^h[I^-]^i \quad (4)$$

Because the absorbance of the reaction system is proportional to [CPH*], the exponents can be determined by measuring the rate of change of absorbance when the concentration of one reagent was varied while the others were fixed. The results of $f = 1$, $g = 1$, $h = 0$, $i = 1$, $j = 1$, $l = 1$ and $m = 1$ were obtained. Hence Eqns. 1 and 2 become

$$d[CPH^*]/dt = k_b[H^+][H_2O_2][CPH] - k_2[H^+]^n[H_2O_2]^p[CPH^*]^q \quad (5)$$

$$d[CPH^*]/dt = k_b[H^+][H_2O_2][CPH] + k_1[H^+][H_2O_2][I^-] - k_2[H^+]^n[H_2O_2]^p[CPH^*]^q \quad (6)$$

When the absorbance reaches its maximum, $d[CPH^*]/dt = 0$, so

$$[CPH^*]^q_{max}(\text{non-catalytic}) = (k_b/k_2)[H^+]^{1-n}[H_2O_2]^{1-p}[CPH] \quad (7)$$

$$[CPH^*]^q_{max}(\text{catalytic}) = (k_b/k_2)[H^+]^{1-n}[H_2O_2]^{1-p}[CPH] + (k_1/k_2)[H^+]^{1-n}[H_2O_2]^{1-p}[I^-] \quad (8)$$

Because the maximum absorbance was proportional to the concentration of iodide, as shown above, q was reasonably considered to be 1:

$$[CPH^*]_{max}(\text{non-catalytic}) = (k_b/k_2)[H^+]^{1-n}[H_2O_2]^{1-p}[CPH] \quad (9)$$

$$[CPH^*]_{max}(\text{catalytic}) = (k_b/k_2)[H^+]^{1-n}[H_2O_2]^{1-p}[CPH] + (k_1/k_2)[H^+]^{1-n}[H_2O_2]^{1-p}[I^-] \quad (10)$$

The maximum absorbance remained almost constant despite changes in the concentration of sulphuric acid in the range 1.0–2.0 M, and with concentrations of hydrogen peroxide above 1.0 M, so both n and $p = 1$ under the conditions used:

$$[CPH^*]_{max}(\text{non-catalytic}) = (k_b/k_2)[CPH] \quad (11)$$

$$[CPH^*]_{max}(\text{catalytic}) = (k_b/k_2)[CPH] + (k_1/k_2)[I^-] \quad (12)$$

Replacing $[CPH^*]$ with absorbance A, Eqns. 11 and 12 become

$$A_{max}(\text{non-catalytic}) = \epsilon(k_b/k_2)[CPH] \quad (13)$$

$$A_{max}(\text{catalytic}) = (\epsilon k_b/k_2)[CPH] + (\epsilon k_1/k_2)[I^-] = A_{max}(\textit{non-catalytic}) + (\epsilon k_1/k_2)[I^-] \quad (14)$$

where ϵ is the molar absorptivity of CPH^*.

According to the discussion above, the decreasing rate of concentration of CPH can be expressed as

$$d[CPH]/dt = -k_b[H^+][H_2O_2][CPH] - k_1[H^+][H_2O_2][I^-] \quad (15)$$

Integration of Eqn. 15 gives

$$[CPH] = \{(k_1[I^-] + k_b[CPH]_0) \times \exp(-k_b[H^+][H_2O_2]t) - k_1[I^-]\}/k_b \quad (16)$$

where $[CPH]_0$ is the original concentration of CPH. Substituting $n = 1$, $p = 1$, $q = 1$ and Eqn. 16 into Eqn. 6 and integrating gives

$$[CPH^*] = \{\exp(-k_b[H^+][H_2O_2]t) - \exp(-k_2[H^+][H_2O_2]t)\} \times (k_1[I^-] + k_b[CPH]_0)/(k_2 - k_b) \quad (17)$$

By applying the condition $d[CPH^*]_{max}/dt = 0$ to En. 17, the expression of the time required for the maximum absorbance to appear is obtained:

$$t_{max} = \{1/(k_2 - k_b)[H^+][H_2O_2]\} \ln(k_2/k_b) \quad (18)$$

Equation 18 agrees well with the experimental results that t_{max} was independent of the concentration of iodide and was proportional to the reciprocal of the concentrations of sulphuric acid and hydrogen peroxide. However, it cannot explain why t_{max} increased slightly when the concentration of CPH increased.

By combining Eqns. 17 and 18, Eqn. 19 is obtained, which explains theoretically that $[CPH^*]_{max}$ is independent of the concentrations of sulphuric acid and hydrogen peroxide.

$$[CPH^*]_{max} = \{\exp(-k_b \ln(k_2/k_b)/(k_2 - k_b)) - \exp(-k_2 \ln(k_2/k_b)/(k_2 - k_b))\} \times (k_1[I^-] + k_b[CPH]_0)/(k_2 - k_b) \quad (19)$$

It was found that in this reaction, k_2 is far larger than k_b; the experimental values of K_b, K_1 and K_2 were 4×10^{-4}, 54 and 0.14 $(\text{mol l}^{-1})^{-2}\,\text{min}^{-1}$, respectively. Then Eqn. 19 becomes

$$[CPH^*]_{max} \approx (k_b/k_2)[CPH]_0 + (k_1/k_2)[I^-] \quad (20)$$

which indicates that $[CPH^*]_{max}$ increases linearly with increasing iodide concentration and also the

initial concentration of CPH (as shown in Fig. 6). Substituting the Arrhenius equation $k = A' \exp(-E/RT)$ into Eqn. 20 and by differentiating it with respect to temperature gives

$$\begin{aligned} d[CPH^*]_{max}/dT &= \{A'_b(E_b - E_2)[CPH]_0/A'_2RT^2\} \\ &\times \exp[(E_2 - E_b)/RT] \\ &+ \{A'_1(E_1 - E_2)[I^-]/A'_2RT^2\} \\ &\times \exp[(E_2 - E_1)/RT] \end{aligned} \quad (21)$$

The fact that dA_{max}/dT or $d[CPH^*]_{max}/dT$ was very small implies that the values of E_b, E_1 and E_2 are very similar. In practice, the experimental values of E_b, E_1 and E_2 were 30.1, 22.3 and 21.3 kJ mol^{-1}, respectively.

The second term on the right-hand side of Eqn. 6 does not include the CPH concentration, and is proportional to the concentrations of hydrogen ion (i.e., sulphuric acid), hydrogen peroxide and iodide. Therefore, the catalytic reaction of the generation of CPH* may be considered to proceed by the following two steps, and CPH joins in the fast step only:

$$H^+ + H_2O_2 + I^- \xrightarrow{\text{slow}} H_2O + I^+(HOI) \quad (22)$$

$$CPH + I^+(HOI) \xrightarrow{\text{fast}} CPH^* + I^- \quad (23)$$

where Eqn. 22 is the rate-determining step.

This work was supported by a Grant-in-Aid (No. 02650538) for Scientific Research from the Ministry of Education, Science and Culture, Japan.

REFERENCES

1 R. Bilewicz and Z. Kublok, Anal. Chim. Acta, 171 (1985) 205.
2 K. Han, W.F. Koch and K.W. Pratt, Anal. Chem., 59 (1987) 731.
3 E.C.V. Butler and R.M. Gershey, Anal. Chim. Acta, 164 (1984) 153.
4 R.D. Rocklin and E.L. Johnson, Anal. Chem., 55 (1983) 4.
5 P.W.F. Fischer, M.R. L'Abbe and A. Giroux, J. Assoc. Off. Anal. Chem., 69 (1986) 687; Anal. Abstr., 48 (1986) 12F7.
6 J. Tusl, Chem. Listy, 77 (1982) 513; Anal. Abstr., 45 (1983) 5F5.
7 H.P. Tarasiewicz, Phenothiazines and 1,4-Benzothiazines, Vol. 4, Elsevier, Amsterdam, 1988, p. 861.
8 P. Vinas, M.H. Cordoba and C.S. Pedreno, Talanta, 34 (1987) 351.
9 H.A. Mottola and A. Hanna, Anal. Chim. Acta, 100 (1978) 167.
10 P.V.S. Rao, G.S.R.K. Rao, K. Ramakrishna and P.S.N. Murthy, Indian J. Chem., 30A (1991) 239.

Analytica Chimica Acta, 282 (1993) 95–100
Elsevier Science Publishers B.V., Amsterdam

On-line photochemical derivatization and flow-injection spectrophotometric determination of ergonovine maleate

A. Mellado Romero and G. Gomez Benito

Departamento de Química, Colegio Universitario CEU, Universitat de Valencia, Moncada, Valencia (Spain)

J. Martínez Calatayud

Departamento de Química Analítica, Universitat de Valencia, c/. Dr. Moliner 50, 46100 Burjasot, Valencia (Spain)

(Received 7th December 1992; revised manuscript received 16th April 1993)

Abstract

A flow-injection manifold is proposed for the on-line photochemical derivatization of ergonovine maleate with application to pharmaceutical formulations. The procedure is based on the reaction with *p*-dimethylaminobenzaldehyde in presence of iron(III) and sulphuric acid medium. The reaction rate is improved by irradiation of the solution with a mercury lamp (254.0 nm). The calibration graph is linear over the range 3–74 μg ml^{-1} ergonovine, with a mid-range R.S.D. of 1.7% and a sample throughput of 34 h^{-1}. The influence of foreign compounds was tested.

Keywords: Flow injection; UV–Visible spectrophotometry; Alkaloids; Ergonovine maleate; Pharmaceuticals; Photochemical derivatization

Ergonovine is an alkaloid isolated from ergot. This and similar alkaloids have varying degrees of α-adrenergic blocking activity, a direct stimulating action on smooth muscle, especially that of the blood vessels and the uterus, and antiserotonin effects. They may be used in obstetrics to prolong uterine contractions in the later stages of labour and to check post-partum haemorrhaging [1].

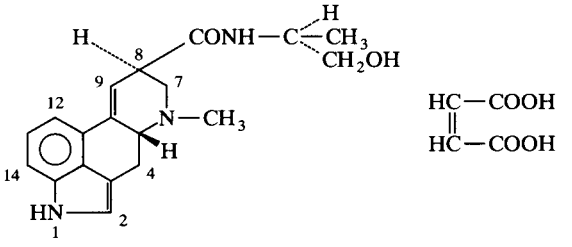

$C_{19}H_{23}N_3O_2 \cdot C_4H_4O_4$ Mol.wt. = 441.48

Ergonovine maleate

Most of the currently used procedures for the determination of ergot alkaloids, including official recommendations in some pharmacopoeias

Correspondence to: J. Martínez Calatayud, Departamento de Química Analítica, Universitat de Valencia, c/. Dr. Moliner 50, 46100 Burjasot, Valencia (Spain).

and in the AOAC Official Methods of Analysis [2], are based on reaction of the alkaloid with *p*-dimethylaminobenzaldehyde (PDAB), also known as the Van Urk reaction [3]. Many modifications have been proposed to the original procedure. Smith [4] modified the reagent by dissolving PDAB in concentrated sulphuric acid instead of acidified ethanol and also found that exposure to light was necessary for full colour development. This exposure was unnecessary if a small amount of iron(III) chloride [5] or hydrogen peroxyde was added to the reagent [6]. Michelon and Kelleher

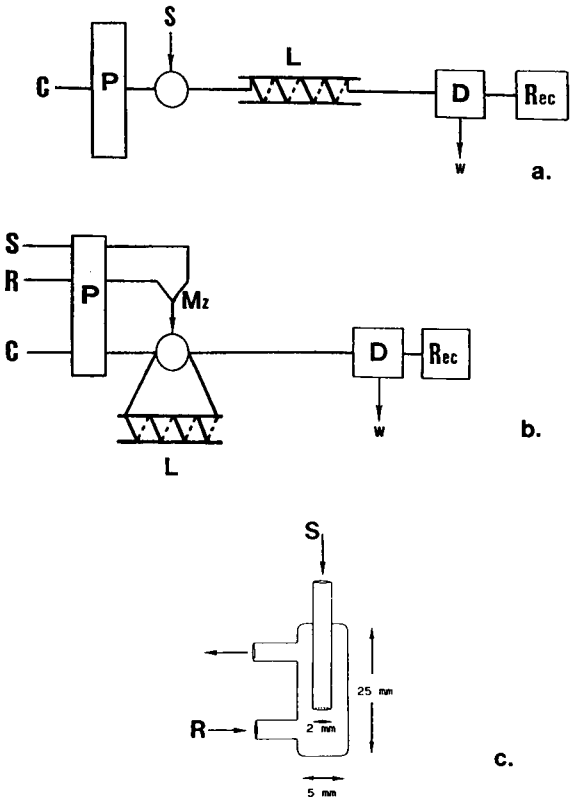

Fig. 1. Flow manifolds. (a) Assembly for preliminary experiments. L, 315 cm; S, 312.5 μl; C, 3.4 ml min^{-1}. (b) Proposed FI assembly for ergonovine determination. C, carrier [4.2×10^{-3} M PDAB–4.47×10^{-2} M Fe(III) in 30% sulphuric acid]; R, reagent [8.4×10^{-3} M PDAB–8.95×10^{-2} M Fe(III) in 30% sulphuric acid]; S, sample (ergonovine maleate in 30% sulphuric acid); Mz, mixing chamber; L, irradiation source (mercury lamp); P, peristaltic pump; D, spectrophotometric detector; Rec, recorder; W, waste. (c) Selected merging device.

[7] reported that nitrite enhanced the colour produced by the reaction between PDAB and ergot alkaloids. The system ergonovine–PDBA in sulphuric acid medium was applied to the kinetic–spectrophotometric determination of nitrite ions [8]; the reaction rate was strongly enhanced by the presence of nitrite or iron(III). Linear calibration graphs were obtained for nitrite concentrations in the range 0.66–6 $\mu g\ l^{-1}$.

The analytical potential of photochemical reactions arises from the inherent advantages of this type of reaction over ordinary chemical reactions. The advantages include the facility to change the nature of the reagent (the photon) by simply modifying the working wavelength; some reaction conditions, such as the lamp power or reactor configuration, can be easily changed to speed up the process concerned. There are a large number of light-sensitive pharmaceutical compounds and it would therefore be of interest to develop methods for their determination exploiting the features of photochemical processes. Implementing a continuous-flow assembly with photo-derivatization is an interesting trend [9,10]; the flow-injection (FI) determinations of reserpine [11] and diferent phenothiazines [12–14] have been achieved with the drug derivatized on-line by photoreaction.

This paper deals with the FI spectrophotometric determination of ergonovine on the basis of the reaction with PDAB in the presence of iron(III) in an FI manifold provided with an on-line irradiation source.

EXPERIMENTAL

Reagents and apparatus

Analytical-reagent grade chemicals were used unless indicated otherwise.

Ergonovine maleate (Sigma), *p*-dimethylaminobenzaldehyde (PDAB) (Scharlau), sulphuric acid (Panreac), sodium nitrite (Probus), iron(II) chloride hexahydrate (Probus, pure), phosphoric acid (Probus), sodium chloride (Panreac, ar), hydrochloride acid (Panreac), caffeine (Merck, pure), lactose (Poulenc) phenobarbital acid (Lasa, pure) cyclicine hydrochloride (Gayoso

Wellcome, pure), paracetamol (Guinama, pure) and maleic acid (Doesder) were used.

The stability of ergonovine and PDAB aqueous solutions was tested by means of periodic recording of absorption spectra. A 9.22×10^{-6} M ergonovine maleate aqueous solution, kept in a closed vessel, showed unchanged spectra during 45 days. In 30% sulphuric acid medium it remained stable during for about 2.5 h. The stability of the reagent solution (8.95×10^{-2} M iron(III) plus 8.37×10^{-3} M PDAB in 30% sulphuric acid medium) was studied over 6 days and no changes were observed.

The action of UV irradiation on the system was studied by using the manifolds depicted in Fig. 1. The sample was irradiated whilst being circulated through a tube coiled around the lamp. The sample solution merged with a mixture of PDAB in sulphuric acid medium and iron(III), both at a flow-rate of 2.05 ml min^{-1}; the mixing chamber produced a homogeneous solution which, in turn, was injected, via a Rheodyne Model 5051 injection valve, into the carrier stream flowing at 4.85 ml min^{-1}. The carrier was a solution with the same composition as the reagent solution but with different concentrations. The sample–reagent mixture was irradiated with a Philips T UV mercury lamp (6 W) in the sample loop, the volume of which was 2008 μl. After 1 min of irradiation the sample passed to the flow-cell of a Hewlett-Packard Model 8452A diode-array spectrophotometer. Outputs at 542.0 nm were recorded. The PTFE tubing was of 0.8 mm i.d. and the peristaltic pump used was a Gilson Minipuls Model 2.

RESULTS AND DISCUSSION

Preliminary experiments were carried out by a batch procedure; the lamp was placed on a beaker containing the reaction mixture and spectra (from 380 to 820 nm) were recorded at different time intervals up to 20 min; the influence of the medium on the reaction rate was tested with sulphuric and phosphoric acid. Both acidic media were studied in the presence and absence of iron(III) or nitrite ions; all results were obtained by comparing experiments carried out with irradiation with experiments without irradiating the mixture. Some of results obtained are shown in Fig. 2. All the recorded spectra showed the same profile, differences only being observed in the absorbance values.

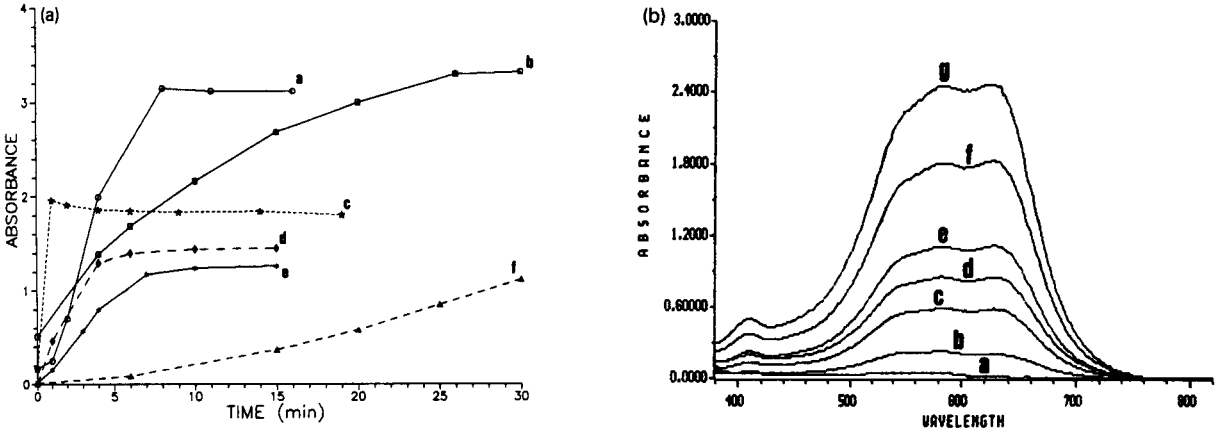

Fig. 2. Development of the blue colour with time in the batch procedure. (a) Plot of absorbances at 554.0 nm: a = irradiation and 32.5% sulphuric acid; b = irradiation, 2.24×10^{-2} M Fe(III) in 15% sulphuric acid; c = no irradiation, 1.81×10^{-2} M nitrite in 32.5% sulphuric acid; d = irradiation and 32.5% phosphoric acid; e = irradiation and 15% sulphuric acid; f = irradiation, 2.24×10^{-3} M Fe(III) in 32.5% phosphoric acid. (b) Spectra of the ergonovine–PDAB system vs. irradiation time: a = 0; b = 10; c = 20; d = 25; e = 30; f = 40; g = 50 min. Concentration of Fe(III), 2.24×10^{-2} M; 32.5% phosphoric acid. Ergonovine and PDAB final concentrations were 2.3×10^{-4} and 4.18×10^{-3} M, respectively, for all solutions.

Sulphuric was found to be the more suitable acidic medium; the recorded absorbances were clearly higher than those ones obtained with solutions containing phosphoric acid. The comparison of absorbances in sulphuric acid against the corresponding in phosphoric acid were 22% and 5% higher in the presence of nitrite and iron(III) ions, respectively. Some results are compared in Fig. 2b.

Using the sulphuric acid medium, the absorbances were higher with irradiation alone than with irradiation in the presence of nitrite. The best results were observed in 15% sulphuric acid medium at 2.2×10^{-2} M iron(III) and with irradiation; the absorbance was about 56% lower in the absence of iron(III).

The influence on the reaction rate and absorbances at the steady state was also tested by changing the order in which the reagents (and irradiation) were added. Systems in which iron(III) and ergonovine (in that order) were sucessively added to a solution of PDAB in sulphuric acid medium, the photon being the last added "reagent", showed the best results. Two different lamps were tested (with the main wavelengths at 254 and 365 nm, respectively); the results were about 16% higher at 254 nm.

The above results led to the following optimum conditions: sulphuric acid concentration, ca. 15%; main wavelength of irradiation, 254 nm; iron(III) present, ca. 2.2×10^{-2} M; and PDAB concentration, ca. 4.18×10^{-3} M.

Unsegmented continuous-flow experiments

Two different unsegmented continuous-flow manifolds were tested (see Fig. 1). Preliminary studies on the influence of various parameters were carried out: sulphuric acid was tested over the range 20–30%, the manifold conditions were varied and the irradiation time was changed from 0 to 5 min.

The concentrations of iron(III) and sulphuric acid had a marked effect. For instance, with 8.95×10^{-2} M Fe(III) the peak height absorbances were 0.30 and 0.15 for 30 and 20% sulphuric acid, respectively; when the iron(III) concentration was decreased to 1.79×10^{-2} M the corresponding absorbances were 0.23 and 0.11.

Some conclusions were drawn from the former continuous-flow experiments (the stopped-flow mode was considered): stopped flow for 1 min with and without irradiation resulted in absorbances of 0.29 and 0.14, respectively. The transient outputs increased with the time of irradiation; the stopped-flow interval (irradiation time) resulted in an increase in the transient signal [30% sulphuric acid and 8.95×10^{-2} M Fe(III)]; the absorbances were 0.21, 0.29 and 0.35 for stopped-flow intervals of 0, 1 and 5 min, respectively.

An increase in the lamp power from 6 to 30 W did not result in an increase in peak height.

The FI manifold in Figure 1b was selected for further work. The sample solution in the proposed manifold merges with the reagent stream [PDAB and iron(III) in sulphuric acid medium], the resulting mixture is exposed to irradiation (mercury lamp, 254 nm, 6 W) in the sample loop, then the carrier leads the sample to the spectrophotometer flow cell. The optimization of both chemical and FI manifold parameters was carried out in a sequential procedure.

Temperature was found not to be a critical parameter; the absorbances obtained varied from 0.50 to 0.54 when the temperature was increased from 6 to 46°C.

The irradiation time was tested by varying the irradiation interval and the length of tubing coiled around the lamp. Figure 3 shows that irradiation times over 1 min are not critical.

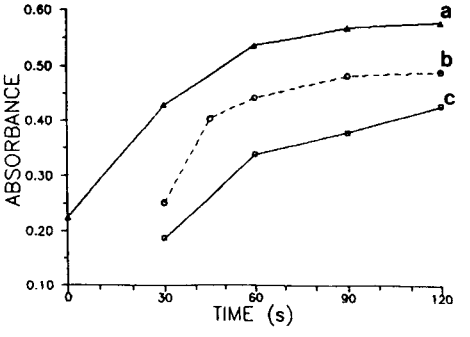

Fig. 3. Influence on absorbance of varying the irradiation time by changing the length of the coiled tubing around the lamp: a = 351; b = 198; c = 90 cm.

TABLE 1

Optimization of chemical and FI parameters

Parameter	Studied range	Selected value
Temperature (°C)	6–46	Ambient
Reagent concentrations:		
PDAB (M)	3.4×10^{-3}–1.3×10^{-2}	8.4×10^{-3}
Fe(III) (M)	1.79×10^{-2}–35.8×10^{-2}	8.95×10^{-2}
Sulphuric acid (%, w/v)	10–50	30
Irradiation time (min) [a]	0.5–2	1
Irradiated coil length (cm)	90–351	351
Injection valve–detector distance (cm)	22–122	22
Carrier flow-rate (ml min^{-1})	1.4–4.8	4.8
Wavelength (nm)	540.0–528.0	542.0

[a] The reported stopped-flow intervals were studied for each irradiated coil length tested.

Different sets of experiments were carried out in order to test the influence of flow rate, the type of merging device and the compositions of the reagent and carrier solutions. The compositions of the reagent and carrier solutions should be the same in order to avoid absoption differences due to the yellow colour developed in the mixture of reagents (without ergonovine). Owing to dilution of the reagent solution when it merges with the sample solution, the prepared concentrations in the reagent solution were twice those in the carrier. The selected values of concentrations given in Table 1 are those corresponding to the reagent solution.

The merging device selected is depicted in Fig. 1c. Bearing in mind the profile of the absorption spectra without a clear maximum absorption band, the monitoring wavelength was also optimized. The results of the optimization experimentes are given in Table 1.

Analytical application

The procedure was applied to the determination of ergonovine in pharmaceutical formulations. The calibration graph was linear over the range 3–74 $\mu g\ ml^{-1}$ ergonovine. The calibration was carried out by means of three independent experiments on different days; the average equation was

$$\text{absorbance} = (-1.7 \times 10^{-2}) + 1.35 \times 10^{-2} \times [\text{ergonovine } (\mu g\ ml^{-1})]$$

were the absorbance is the corrected (from reagent absorbances) value; Mean results of three experiments were obtained and the calculated R.S.D. for the slope was 3.6%; the mean correlation coefficient was 0.9999 ($n = 3$).

The reproducibility of the method and the sample throughput were studied by using a sample solution containing 29 $\mu g\ ml^{-1}$ of ergonovine. The calculated R.S.D. (17 replicates) was 1.7% and sample throughput was 34 h^{-1}.

The tolerance of the method to foreign substances formulated together with the ergonovine was studied with sample solutions containing 29 $\mu g\ ml^{-1}$ ergonovine and various amounts of foreign compounds up to 1000 $\mu g\ ml^{-1}$ or giving a relative error (in comparison with the output for pure ergonovine in distilled water) of up to about 3% (see Table 2).

TABLE 2

Influence of foreign compounds

Compound	Concentration ($\mu g\ ml^{-1}$)	Relative error (%)
Paracetamol	750	0.2
Caffeine	1000	1.9
Lactose	1000	2.3
Maleic acid	1000	0.9
Sodium chloride	1000	0.1
Phenobarbital	500	0.1
Chloride acid	750	0.3
Cyclicine (10% in ethanol)	750	0.4

Samples (injectable solutions) were prepared according to [1]: (a) sterile solutions of the drug at pH 3.0, adjusted potentiometrically with maleic acid; and (b) solutions of ergonovine maleate containing NaCl and HCl. Errors were calculated by comparing the results obtained with the amount added: (a) added, 200.0 μg ml^{-1} obtained 194 μg ml^{-1} and (b) added, 200.0 μg ml^{-1}, obtained 202 μg ml^{-1} calculated relative error, 3% and 1%, respectivelly.

Conclusions

A procedure for the determination of ergonovine (probably with application to other ergot alkaloids) in pharmaceutical formulations was developed. The procedure use milder conditions than the batch process (the sulphuric acid concentration was 65% in the former procedure). The present method allows the determination of ergonovine at lower concentrations than in a previously published non-selective FI procedure for ergonovine (linear calibration graph over the 150–250 μg ml^{-1}), based on the oxidation of the drug by the combined action of sodium periodate and hydrogen peroxide and spectrophotometric measurement [15].

REFERENCES

1 Martindale, The Extra Pharmacopoeia, Pharmaceutical Press, London, 6th edn., 1972.
2 S. Williams (Ed.) Official Methods of Analysis, of the Association of Official Analytical Chemists, Association of Official Analytical Chemistry, Washington, DC, 14th edn., 1985.
3 H.W. van Urk, Pharm. Weekbl., 66 (1929) 473.
4 M.I. Smith, Public Health Rep., 45 (1930) 1466.
5 N.L. Allport and T.T. Cocking, Q.J. Pharm. Pharmacol., 5 (1932) 341.
6 E. Schulek and G. Vastag, Dan. Tidsskr. Farm., 13 (1939) 101.
7 L. Michelon and W.J. Kelleher, Lloydia, 26 (1963) 192.
8 J. Martinez Calatayud and C. Medina Hernandez, Michrochem. J., 43 (1991) 143.
9 J. Martinez Calatayud and C. Gomez Benito, Cienc. Pharm., 2 (1992) 57.
10 M.C. Mahedero and J.J. Aaron, Anal. Chim. Acta, 269 (1992) 193.
11 J. Martinez Calatayud and C. Gomez Benito, Anal. Chim. Acta, 245 (1991) 101.
12 J. Martinez Calatayud and C. Gomez Benito, Anal. Chim. Acta, 256 (1992) 105.
13 A. Mellado Romero, C. Gomez Benito and J. Martinez Calatayud, Anal. Lett. 25 (1992) 1289.
14 D. Chen, A. Rios, M.D. Luque de Castro and M. Valcarcel, Analyst, 116 (1991) 171.
15 J. Martinez Calatayud and S. Sagrado Vives, Pharmazie, 44 (1989) 614.

Analytica Chimica Acta, 282 (1993) 101–108
Elsevier Science Publishers B.V., Amsterdam

Apparent differences in binding site distributions and aluminum(III) complexation for three molecular weight fractions of a coniferous soil fulvic acid

Sukla Lakshman, Ryan Mills and Howard Patterson
Department of Chemistry, University of Maine, Orono, ME 04469 (USA)

Christopher Cronan
Department of Plant Biology and Pathology, University of Maine, Orono, ME 04469 (USA)

(Received 1st December 1992; revised manuscript received 15th April 1993)

Abstract

A soil fulvic acid isolated from a northern coniferous forest (NCFA) was fractionated into three different molecular sizes ranging from less than 500 to 10000 daltons by ultrafiltration and the fractions were studied by synchronous scan fluorescence spectroscopy (SSFS). The SSFS gives three distinct emission peaks (I, II and III) for these fractions of NCFA, which are attributed to different fluorophores. The lower-wavelength peaks (315 and 370 nm) are attributed to fluorophores that consist of a single aromatic ring with carboxyl and/or hydroxyl groups attached to it, whereas the longest-wavelength peak (470 nm) is associated with a fluorophore containing three or four condensed aromatic rings with substituted groups. The ratio of the intensity of peak III to II increases from the lower to higher molecular weight fraction which indicates a higher content of condensed aromatic rings in the high molecular weight fraction. This study also included aluminum(III) binding experiments with the different molecular weight fractions of NCFA. Results showed that the high molecular weight fraction has a stronger affinity for aluminum(III) than the low molecular weight fraction.

Keywords: Fluorimetry; Aluminium; Fulvic acids; Metal complexes

In acidic water, ionic inorganic aluminum exerts toxic effects on some aquatic and terrestrial life forms [1]; in contrast, complexes of aluminum with naturally occurring organic ligands, such as humic substances, are apparently non-toxic [2]. Humic substances play an important regulatory role in determining the availability, speciation and hence toxicity of aluminum to plants and aquatic organisms [1,3]. Although several studies have described the interaction of aluminum(III) with naturally occurring inorganic ligands [4,5], relatively little research has been performed to quantify the aluminum(III) complexes of naturally occurring organic ligands like fulvic acids [6–9].

Fluorescence spectroscopy is a sensitive technique for the study of metal binding to fulvic acid. While several other techniques measure the free metal concentration, fluorescence spectroscopy observes the bound ligand concentration directly [10]. Recently, the technique of synchronous scan fluorescence spectroscopy (SSFS) has been used to characterize humic materials

Correspondence to: H. Patterson, Department of Chemistry, University of Maine, Orono, ME 04469 (USA).

from diverse terestrial and aquatic sources [6,11,12]. SSFS involves recording the fluorescence intensity and locking the excitation and emission wavelength drives together at a constant wavelength difference ($\Delta\lambda$). In this study the SSFS technique has been utilized for estimating stability constants of different binding sites.

Fulvic acids are complex and heterogeneous mixtures of highly oxidized organic substances that result from microbial decomposition of plant residues. Fulvic acids range in weight from 500 to 2000 daltons as obtained by different methods and from different sources [13–15]. Hence, one might hypothesize that fulvic acids contain different sizes of molecules having different binding site(s) for aluminum(III). To define the structural chemistry and metal binding properties of fulvic acids, it is necessary to fractionate the fulvic acid macromolecules into size groups and to study these groups individually.

The aims of this present investigation were (1) to fractionate a soil fulvic acid from a northern coniferous forest (NCFA) into different molecular sizes using ultrafiltration; (2) to characterize these fractions of NCFA using SSFS; and (3) to study the binding of aluminum(III) with these fractions at pH 3.5, where the dominant equilibrium aluminum species is the free trivalent cation.

EXPERIMENTAL

Materials and instrumentation

The NCFA was isolated from the surface O Horizon beneath a coniferous forest stand located in the Pancake-Hall watershed in the west-central Adirondack Mountains of New York. This site has been described in detail elsewhere [11]. The soil sample was extracted for 3 h on a shaker using a 1:10 ratio of soil to distilled water. The resulting slurry was centrifuged, pressure filtered through a Gelman A/E glass fiber filter, and the filtrate was centrifuged a second time. The extracted solution was then acidified to pH 1 with concentrated HCl in order to remove humic acid. The fulvic acid was purified by the XAD-8 adsorption chromatographic method of Leenheer [16]. Cation-exchange chromatography using acid-washed Rexyn 101 resin was used to produce fulvic acid in fully protonated form. Finally the fulvic acid sample was isolated by lyophilization and stored in a desiccator in the dark. The residual metal content was determined using plasma emission spectroscopy and found to be less than 0.01% on a dry weight basis. Stock solutions of aluminum(III) were prepared from analytical reagent grade $Al(NO_3)_3 \cdot 9H_2O$. Doubly deionized water was used in all experiments.

An Amicon Model 8050 ultrafiltration cell was used in conjunction with Amicon filter membranes PM10, YM2, YC05, which had molecular cut-offs of 10000, 1000 and 500 daltons, respectively. In an earlier study Wang et al. [17] used molecular weight cut-offs ranging from 1000 to 30000 daltons for the ultrafiltration fractionation of a Laurentian fulvic acid. However we used the range 500 to 10000 daltons because the molecular weight of fulvic acids has been reported as 1000–2000 by analytical ultracentrifugation [14], as 860 by flow field-flow fractionation [15] and as 740 by vapor-pressure osmometry [18]. The filter membranes were prepared by soaking in deionized water for at least 6 h with three water changes. The membranes were stored in ethanol–water (1:10, v/v) and were refrigerated when not in use. Prior to use, stored membranes were rinsed with deionized water to remove ethanol. During filtration, the solution in the cell was stirred constantly with a magnetic stirrer.

The fluorescence measurements were made on a Perkin Elmer MPF-4 fluorescence spectrophotometer. Both slits were set at 7 nm and the signal gain was set at 3 or 10, depending on the recorded spectrum intensity. The chart speed was set at 60 nm min^{-1}. A Beckman Φ 71 pH meter was used for adjustment of pH. The stability constants were calculated by a Fortran nonlinear regression analysis program. This program uses a least-squares technique to calculate the best fit of the experimental data.

PROCEDURE

A 50-ml volume of fulvic acid stock solution adjusted to a concentration of 150 μg ml^{-1} was

passed sequentially through PM10, YM2, YC05 filter membranes under a pressure of 55 p.s.i. of nitrogen. Three filtrate fractions were collected and freeze-dried to yield sub-fraction fulvic acid samples. Each fraction was diluted to 10 μg ml^{-1} by adding distilled deionized water and adjusted to pH 3.5 with 0.1 M or 1.0 M HCl and/or NaOH solution. The synchronous scan excitation spectra of these fractions were obtained by recording the fluorescence intensity while synchronously scanning over both the excitation and emission wavelengths. The wavelength difference $\Delta\lambda$ was maintained constant (25 nm) as the spectrum was recorded.

The aluminum(III)–fulvate binding experiments were done at room temperature (22 ± 2°C) by adding aliquots of aluminum(III) stock solution (1×10^{-2} M) to 25 ml of 10 μg ml^{-1} fulvic acid fractions; both solutions were adjusted to pH 3.5. Following addition of each aliquot of aluminum(III), the fulvic acid solution was stirred vigorously for 10 min and allowed to equilibrate for 5 min. Subsequently, fluorescence intensities were recorded at three wavelengths settings (F^a, F^b and F^c). F^a, F^b and F^c are the intensities at λ_{ex} 315, 370 and 470 nm, and λ_{em} 340, 395 and 495 nm, respectively. The total concentration of aluminum(III) added was 4×10^{-6} M to 4×10^{-4} M. At these concentrations of aluminum(III), no precipitation of aluminum(III)–fulvate occurred as confirmed by scattered light measurements. The whole procedure of ultrafiltration and aluminum(III) binding to fractions of NCFA was repeated twice with separate batches of sample.

RESULTS AND DISCUSSION

Synchronous scan fluorescence data for fulvic acid fractions

The synchronous scan fluorescence spectra (SSFS) of unfractionated NCFA at pH 3.5 and the molecular size fractions A, B and C of NCFA are shown in Figs. 1 and 2. All of these spectra exhibit three peaks: one at 315 nm, a second relatively broad peak at 365–395 nm and a third

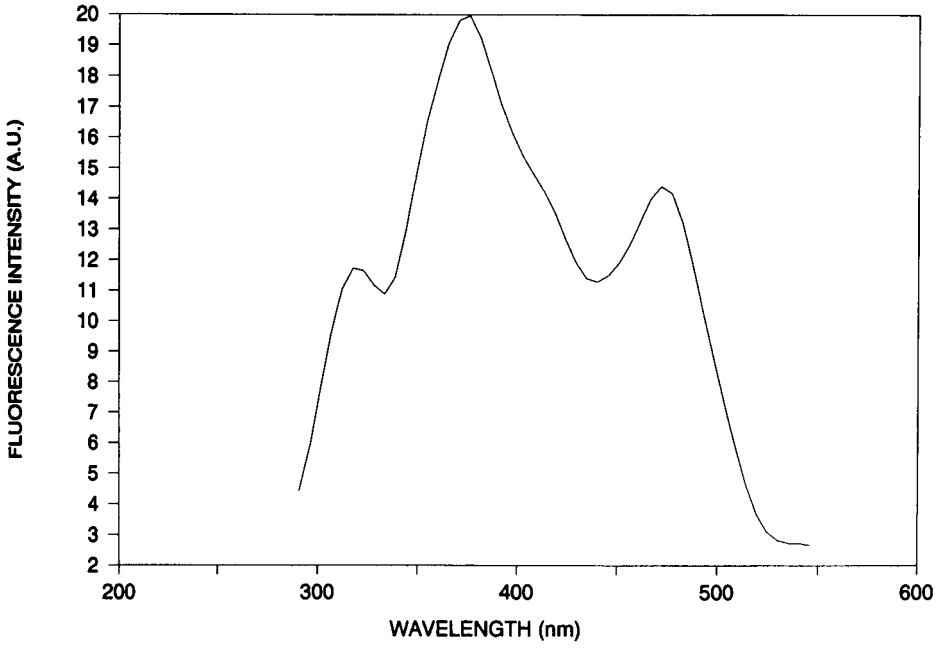

Fig. 1. SSFS of unfractionated NCFA at pH 3.5.

one at 470 nm. These three peaks, referred to as type I, II and III, are attributed to three different fluorophores. Although it is very difficult to identify the structural components of fulvic acid which are responsible for this type of fluorescence, some possible structures can be suggested based on the available data of fluorescence properties of various fluorophores. The lower-wavelength type I and type II peaks (315 and 370 nm) are due to simple aromatic compounds with attached carboxyl and/or hydroxyl groups as in syringic acid, salicylic acid, 3-hydroxybenzoic acid, catechol, phthalic acid [19]. The presence of simple aromatic carboxylic acids like salicylic acid and phthalic acid in fulvic acid is well known from the literature. The longest-wavelength type III peaks (470 nm) are attributed to fluorophores with extended π-conjugation, which decreases the energy difference between the ground state and the first excited state, thus shifting the fluorescence to longer wavelength. These types of fluorophores consist of three or four condensed aromatic rings with attached carboxyl and/or hydroxyl group (e.g. flavanoid). Alternatively, the structure could include one aromatic ring with a long conjugated aliphatic chain.

The ratio of intensities of the type III peak to the type II peak increased from the lower to the higher molecular weight fractions (Fig. 2). These results suggest that the lower molecular weight fraction of fulvic acid has a higher content of simple aromatic compounds with attached carboxyl and/or hydroxyl groups, whereas the higher molecular weight fractions have a greater aromatic character and/or π-conjugation. These findings support recent observations of Wang et al. [17] from Fourier transform infrared (FT-IR) data.

Aluminum(III)-binding study of fulvic acid

The changes in the synchronous scan fluorescence spectra of NCFA fraction B upon addition of aluminum(III) at pH 3.5 are shown in Fig. 3. The addition of aluminum(III) produces an in-

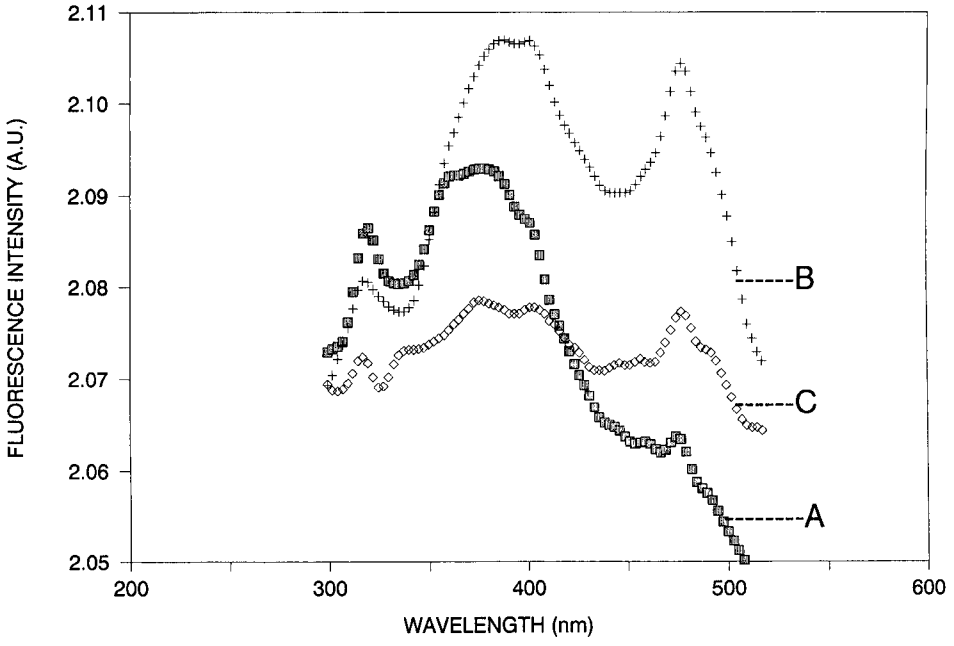

Fig. 2. SSFS of molecular size fractions of NCFA. (A) fraction of MW below 500; (B) fraction of MW between 500 and 1000; (C) fraction of MW between 1000 and 10000. pH = 3.5.

crease in the fluorescence intensities of all peak types (I, II and III) as a result of metal–organic ligand complexation. This complexation increases the structural rigidity of the fulvic acid macromolecule, thus reducing the degree of interaction of these molecules with the solvent. This in turn reduces the rate of internal conversion resulting in an increase in fluorescence intensity [20]. This type of fluorescence enhancement was also observed by Shotyk and Sposito [21] in pine leaf litter extract and by Cabaniss [22] in fulvic acid at pH < 5.

The titration curves of NCFA and aluminum (III) at three wavelengths (315, 370 and 470 nm) are shown in Fig. 4. At this pH (3.5), fulvic acid has some deprotonated aromatic carboxylic sites where aluminum(III) binds to form Al–organic complexes which are more fluorescent than the original fluorophores. The increment of intensity is highest for the type II peaks, intermediate for type III peaks and lowest for type I peaks which suggests that the aluminum(III) complexes involving type II fluorophores are more fluorescent than complexes with type III or type I fluorophores.

Conditional stability constants at pH 3.5 were calculated for NCFA and its three fractions. The model used for the binding study was similar to that reported in our previous paper [11], except that we modified the single binding site model to include two binding sites. Several other reports also suggest two binding sites for copper with fulvic acid [23,24]. Backes and Tipping [8] also reported a similar observation for aluminum binding to humic substances at a pH above 3.5.

In order to describe completely the binding of fulvic acid, every individual binding site must be mathematically accounted for. Hence the total intensity at any point of the titration may be expressed by summing the contribution from each site as

$$I = \sum_{k=1}^{n} C_k I_k \qquad (1)$$

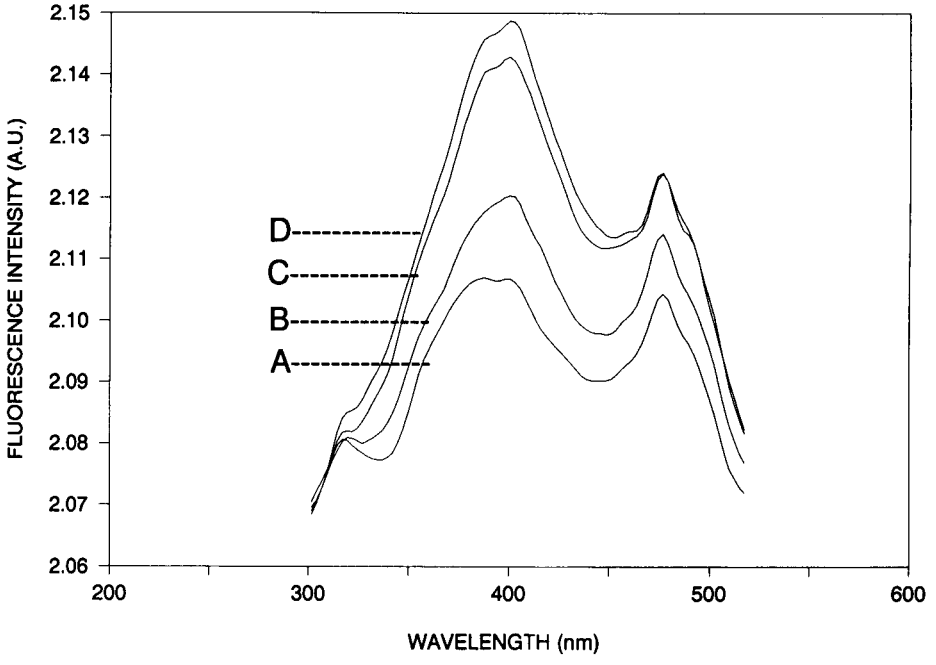

Fig. 3. Effect of aluminum(III) on SSFS spectra of B fraction of NCFA. (A) 0 μM Al(III); (B) 4 μM Al (III); (C) 40 μM Al(III); (D) 400 μM Al(III). The concentration of NCFA was 10 μg ml^{-1} and pH = 3.5.

where I = fluorescence intensity at any point of the titration, n = total number of sites, and C = fraction of a site bound to metal at saturation.

We have assumed that there are two classes of binding sites n_1 and n_2 in NCFA (where each class consists of several similar type of microscopic binding sites). Each class of binding site n_1 and n_2 represents an average of the total number of microscopic sites of a similar type. The intensity obtained from fluorescence enhancement is a linear combination of the intensities from each class of binding site.

We can write the fluorescence intensity

$$I = C_1 I_1 + C_2 I_2 \quad (2)$$

where I_1 and I_2 are the intensities of each class of binding site and C_1 and C_2 are the fractions of each class of binding site bound to aluminum(III) at saturation.

The intensity obtained from the fluorescence enhancement of a ligand by complexation with the aluminum(III) ion at any point is proportional to the fraction of total ligand bound.

$$I = ([\mathrm{ML}]/C_\mathrm{L}) I_\mathrm{ML} \quad (3)$$

where $[\mathrm{ML}]/C_\mathrm{L}$ is the fraction of total ligand bound and I_ML is the increased fluorescence intensity at saturation. For a simple 1:1 equilibrium, the conditional binding constant (K) can be expressed as:

$$K = [\mathrm{ML}]/([\mathrm{M}][\mathrm{L}]) \quad (4)$$

where [M] and [L] are the concentrations of free metal ion and ligand respectively. Using the mass balance equation for aluminum(III) ion and ligand, the fraction of total ligand bound can be expressed in terms of the conditional binding constant and free aluminum(III) ion concentration from Eqns. 3 and 4

$$[\mathrm{ML}]/C_\mathrm{L} = (K[\mathrm{M}])/(K[\mathrm{M}] + 1) \quad (5)$$

Replacing $[\mathrm{ML}]/C_\mathrm{L} = A$, the above equation can be written as

$$A = [K(C_\mathrm{M} - AC_\mathrm{L})]/[K(C_\mathrm{M} - AC_\mathrm{L}) + 1] \quad (6)$$

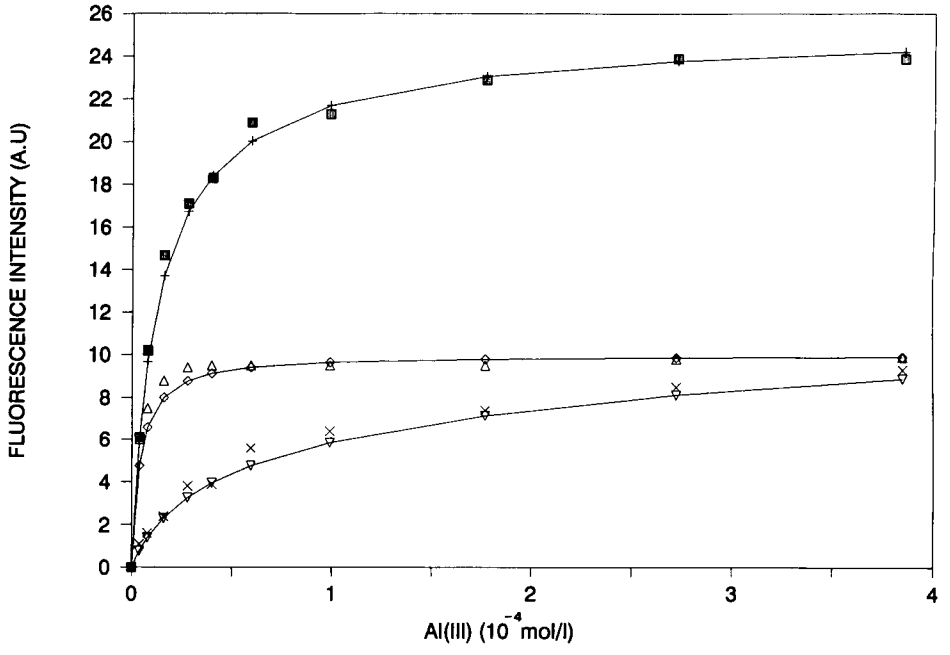

Fig. 4. Change of fluorescence intensity of NCFA at three different wavelengths on addition of aluminum(III) at pH 3.5. For upper curve λ_{ex} = 370 nm and λ_{em} = 395 nm, for middle curve λ_{ex} = 470 nm and λ_{em} = 495 nm and for lowest curve λ_{ex} = 315 nm and λ_{em} = 340 nm.

TABLE 1

Conditional stability constants of aluminum(III) binding to NCFA and its molecular weight fractions at pH 3.5 [a]

	A-NCFA		B-NCFA		C-NCFA		NCFA	
	Log K_1'	F_1	Log K_2'	F_1	Log K_3'	F_1	Log K'	F_1
Strong site								
Type I site	4.4	1	4.6	0.3	5.1	0.4	4.6	0.4
Type II site	4.5	1	5.0	1	5.2	0.7	5.0	0.8
Type III site	4.9	1	5.3	1	5.5	0.9	5.3	1
	Log K_1''	F_1	Log K_2''	F_1	Log K_3''	F_1	Log K''	F_1
Weak site								
Type I site	–	–	3.5	0.7	3.6	0.6	3.5	0.6
Type II site	–	–	–	–	4.4	0.3	4.2	0.2
Type III site	–	–	–	–	4.9	0.1	–	–

[a] K = Binding constant; F = fractions of binding sites. A,B,C = Fractions of NCFA with MW < 500, 500 to 1000 and 1000 to 10 000 dalton, respectively. Type I site: λ_{ex} 315 nm and λ_{em} 340 nm; type II site: λ_{ex} 370 nm and λ_{em} 395 nm; type III site: λ_{ex} 470 nm and λ_{em} 495 nm. When the experiment was repeated with a separate set of NCFA fractions, the constants were all within 5% of values in this table.

Equation 6 can be expressed in the form of a quadratic in A and after substituting this value of A in Eq. 3, the fluorescence intensity (I) can be written as

$$I = \left[(C_1)(I_{ML}/2K'C_L)\left\{(K'C_L + K'C_M + 1) - \sqrt{[(K'C_L + K'C_M + 1)^2 - 4K'^2C_LC_M]}\right\}\right] + \left[(1-C_1)(I_{ML}/2K''C_L)\left\{(K''C_L + K''C_M + 1) - \sqrt{[(K''C_L + K''C_M + 1)^2 - 4K''^2C_LC_M]}\right\}\right] \quad (7)$$

where I_{ML} = fluorescence intensity of bound ligand, K' and K'' = conditional stability constants for site 1 and site 2, C_L = concentration of total ligand, and C_M = concentration of total aluminum(III).

We have written a nonlinear regression analysis program in Fortran to calculate the best fitting aluminum(III) association binding constant K_1, K_2 and K_3 for our data from the above expression. We have calculated the binding constants log K_1, log K_2 and log K_3 for NCFA and all three fractions of NCFA at three wavelengths (315, 370 and 470 nm).

The results presented in Table 1 show one binding site at each SSFS peak for lower molecular weight fractions and two binding sites for the higher molecular weight fraction. In comparison, the unfractionated NCFA shows two binding sites for the type I peak and one binding site for the type II peak. Another observation from Table 1 is that the binding constant increases from the lower to higher molecular weight fractions and lower to longer wavelength peaks. This suggests that the type III sites are stronger binding sites for aluminium(III) than the type I and type II sites, for which both protons and aluminum(III) compete. The binding constant value increases from the lower to the higher molecular weight fraction because of the higher content of the type III sites in the heavier fraction.

The value of binding constants log $K' = 4.6$, 5.0 and 5.3 for Al–NCFA obtained at pH 3.5 were very close to other reported values in the literature. The reported stability constant (log K) of Al–fulvic acid at pH 2.35 is 3.7 obtained by the method of continuous variations [7]. The other reported values of log K of Al–leaf litter extract at pH 4.5, obtained by a fluorescence method, are 5.1 and 4.5 at 132 and 26 g m^{-3} of dissolved organic carbon, respectively [12]. Although direct comparisions of our data with other reports are not possible because of different experimental conditions, there is reason to believe that binding constants do not change significantly for fulvic acid in this pH range. Pott et al. [25] reported that in the pH range of 3 to 6, the binding

constant values of aluminum humic complex do not vary significantly.

Conclusion

A soil fulvic acid (NCFA) was separated into three separate molecular size fractions by ultrafiltration, and these fractions were examined by SSFS and were used to estimate conditional stability constants for fulvate binding with aluminum(III). The synchronous scan fluorescence spectra of NCFA showed type I, type II and type III peaks at 315, 370 and 470 nm, respectively, which are attributed to three different fluorophores. The type I and II peaks are attributed to fluorophores having a single aromatic ring with attached carboxyl and/or hydroxyl groups, and the type III peak represents a fluorophore with three or four condensed aromatic rings with carboxl, carbonyl and/or hydroxyl type of functional groups attached to these rings. All three fractions of NCFA also showed type I, II and III peaks at the same wavelength as the unseparated sample, but the ratio of the intensity of peak III to peak II increased from the lower to the higher molecular weight fraction. This result shows that the lower molecular weight fraction contains more of type II fluorophores whereas the higher molecular weight fraction has more of type III fluorophores.

Aluminum(III) binding with fulvic acid (NCFA) and its fractions at pH 3.5 gave an increase in the intensities of all SSFS peaks. The conditional stability constant values (log K) for NCFA and its fractions at pH 3.5 varied from 3.5 to 5.5. Binding constants for type III sites were always higher than the type I and type II sites for all these fractions, indicating that type III fluorophores have a stronger affinity for aluminum (III). The binding constants for all the binding sites increased from the lower to the higher molecular weight fractions due to the higher content of the strong affinity sites.

REFERENCES

1 C.T. Driscoll, J.O. Baker, J.J. Bisgoni and C.L. Schofield, Nature, 284 (1980) 161.
2 N.M. Johnson, G.E. Likens, M.C. Feller and C.T. Driscoll, Science, 225 (1984) 1424.
3 C.J. Lind and J.D. Hem, Effects of Organic Solutes on Chemical Reaction of Aluminum; US Geological Survey Water Supply Paper 1827-G, US Government Printing Office, Washington, DC, 1975 pp. 1–83.
4 W.D. Burrows, CRC Crit. Rev. Environ. Control, 7 (1977) 167.
5 N.M. Johnson, C.T. Driscoll, J.S. Eaton, G.E. Liken and W.H. McDowell, Geochim. Cosmochim. Acta, 45 (1981) 1421.
6 W. Shotyk and G. Sposito, Soil Sci. Soc. Am. J., 54 (1990) 933.
7 M. Schnitzer and E.H. Hansen, Soil. Sci., 109 (1970) 333.
8 C.A. Backes and E. Tipping, Water Res., 21 (1987) 211.
9 M.S. Shuman, Environ. Sci. Technol., 26 (1992) 598.
10 D.K. Ryan and J.H. Weber, Anal. Chem., 54 (1982) 986.
11 H.H. Patterson, C.S. Cronan, S. Lakshman, B.J. Plankey and T.A. Taylor, Sci. Total Environ., 113 (1992) 179.
12 T.M. Miano, G. Sposito and J.P. Martin, Soil Sci. Soc. Am. J., 52 (1988) 1016.
13 R. Deborger and H.C.R. Debacker, C.R. Acad. Sci., Paris, Ser. D, 266 (1968) 2052.
14 P.M. Reid, A.E. Willkinson, E. Tipping and M.N. Jones, Geochim. Cosmochim. Acta, 54 (1990) 131.
15 R. Beckett, Z. Jue and J.C. Giddings, Environ. Sci. Technol., 21 (1987) 289.
16 J.A. Leenheer, Environ. Sci. Technol., 15 (1981) 578.
17 Z.D. Wang, B.C. Pant and C.H. Langford, Anal. Chim. Acta, 232 (1990) 43.
18 G.R. Aiken, P.A. Brown, T.I. Noyes and D.J. Pinkney, in R.C. Avrett, J.A. Leenheer, D.M. McKnight and K.A. Thorn (Eds.), Humic Substances in the Suwannee River, Properties and Proposed Structures, Open File Report of the US Geological Survey, Federal Center, Denver, CO, No. 87–557, 1989, p. 168.
19 C.S. Cronan, S. Lakshman and H.H. Patterson, J. Environ. Qual., 21 (1992) 457.
20 A.F. Gutierrez and A.M. De La Pena, in P.J. Elving, J.P. Winefordner and I.M. Kolthoff (Eds.), Molecular Luminescence Spectroscopy: Methods and Applications, Part I, Chemical Analysis Series, Vol. 77, Wiley-Interscience, New York, 1985, p. 427.
21 W. Shotyk and G. Sposito, Soil Sci. Soc. Am. J., 54 (1990) 1305.
22 S.E. Cabaniss, Environ. Sci. Technol., 26 (1992) 1133.
23 M. Taga, S. Tanaka and M. Fukushima, Anal. Chim. Acta, 244 (1991) 281.
24 D.M. McKnight, G.L. Feder, M. Thurman, R.L. Wershaw and J.C. Westall, Sci. Total Environ., 28 (1983) 65.
25 D.B. Pott, J.J. Alberts and A.W. Elzerman, Chem. Geol., 48 (1985) 293.

Analytica Chimica Acta, 282 (1993) 109–115
Elsevier Science Publishers B.V., Amsterdam

Automated determination of mercury at ultra trace level in waters by gold amalgam preconcentration and cold vapour atomic fluorescence spectrometry

Chris C.Y. Chan and Ram S. Sadana

Laboratory Services Branch, Ontario Ministry of Environment and Energy, 125 Resources Road, Etobicoke, Ontario M9P 3V6 (Canada)

(Received 1st December 1992; revised manuscript received 22nd March 1993)

Abstract

Mercury in water samples is oxidized to its divalent ion form by an acid digestion procedure. The mercury is then reduced to its elemental form by a stannous chloride solution in a continuous flow system. The mercury vapour is separated and an aliquot is diverted into a gold wire absorber via a flow injection valve to form an amalgam. The mercury is then thermally desorbed and is swept with a stream of argon into a flow cell of an atomic fluorescence spectrometer where the fluorescence is measured at 253.7 nm. The operation of the analytical system is fully automated. The detection limit of the method is 2 ng l^{-1}, and the precision is 3% R.S.D. The results for standard reference materials agree closely with the certified values.

Keywords: Fluorimetry; Flow system; Cold vapour atomic fluorescence spectrometry; Amalgamation; Mercury; Waters

Mercury is a hazardous contaminant in the environment. It is toxic at low level to the biota. In waters, it is converted by bacteria to methyl mercury which is known to bioaccumulate in fish tissue. In drinking waters, its permissible criterion by the Ontario Ministry of the Environment is 1 $\mu g\, l^{-1}$. Mercury in most water bodies of Ontario is at concentrations well below the criterion. There is growing interest by biologists and environmentalists to measure and regulate its concentration at or near the background level. There are several analytical methods described in the literature for the determination of mercury at low concentrations in environmental samples. These methods are based upon a wide range of analytical techniques such as neutron activation analysis [1], inductively coupled plasma mass spectrometry [2], electrothermal atomic absorption spectrometry [3], cold vapour atomic absorption spectrometry (CVAAS) [4], and atomic fluorescence spectrometry (AFS) [5]. The CVAAS is the most widely used method because of its sensitivity, absence of spectral interference and relatively low operation costs.

The hardware used in the CVAAS generally consists of a continuous-flow vapour generator coupled with an atomic absorption spectrometer for measurement of elemental mercury. The elemental mercury vapour is generated by reducing agents such as stannous chloride or sodium borohydride in an acidic solution. The mercury vapour is stripped out of solution by using a gas–liquid separator, and swept into an absorption cell to be

Correspondence to: R.S. Sadana, Laboratory Services Branch, Ontario Ministry of Environment and Energy, 125 Resources Road, Etobicoke, Ontario M9P 3V6 (Canada).

measured at 253.7 nm. Several commercial systems are available to measure mercury by this technique. The method is simple and convenient for the determination of mercury in a variety of environmental samples such as fish, sediments, vegetation and soils. However, the method lacks ruggedness, and is not sensitive enough for the determination of background concentration of mercury in water samples.

Vermeir et al. [6] used preconcentration of the mercury on a gold absorber followed by CVAAS in order to achieve a sufficiently low detection limit for the determination of mercury in biological samples. In a subsequent publication [7], they described the use of AFS in combination with reduction aeration for the determination of mercury in this matrix and reported a detection limit of 0.9 ng l^{-1}. Temmerman et al. [8] reported a detection limit of 2 pg for air samples by using preconcentration onto a gold absorber followed by measurement with AFS.

This paper describes an automated method for the determination of low level mercury in waters using a gas-phase flow injection technique for the introduction of mercury vapour onto a gold wire to form an amalgam after its generation by a continuous flow chemical reduction reaction. The mercury is thermally released and measured by AFS. The method offers the desired sensitivity.

EXPERIMENTAL

Instrumentation

A continuous flow mercury generation apparatus consists of an auto-sampler (Gilson Model ANACOL SC30, Middleton, WI), a peristaltic pump (Model 1200, Lachat Instruments, Milwaukee, WI) to propel sample and the reducing reagents, a gas–liquid separator to separate mercury vapour from the solution, and two moisture absorbers, 50 mm high and 12 mm i.d., connected in series. A flow injection module (Model 1600, Lachat Instruments, Milwaukee, WI) with six ports (1 mm dia.) was used for collecting and transferring an aliquot of the gaseous mercury sample to the gold wire absorber (GWA) to form an amalgam. The GWA was made from a quartz tube, 4″ long and 1/4″ i.d. with Teflon joints at both ends, and loosely packed with 0.5 to 1 g of gold wire (0.1 to 0.2 mm dia.). The tube was wound with about 50 cm of 22-gauge Chromel wire, with two terminals connected to the cable of a variable transformer to provide heat for desorbing mercury.

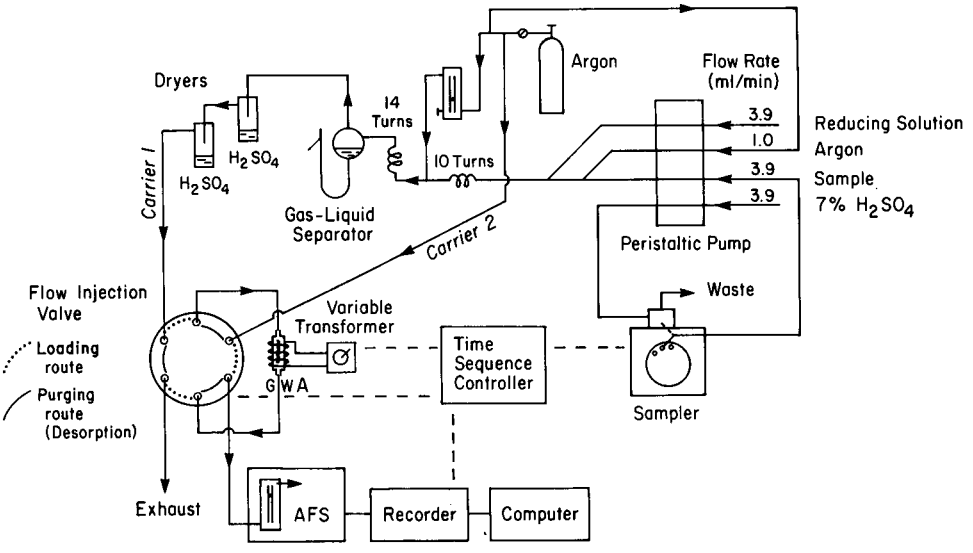

Fig. 1. Analytical system for determination of mercury.

A cold vapour atomic fluorescence spectrometer (Model-2, Brooks Rand, Seattle, WA) was used for measuring the desorbed mercury. A recorder (Model BD 111, Kipp & Zonen) was used to capture the analog fluorescence signals. A computer system (DP-1000) supplied by Labtronics (Guelph, Ontario) was interfaced with the atomic fluorescence spectrometer to digitize the signal and automate the calculation step.

A programmable sequence controller (MICRO-1, TI-Mars, Mississauga) was interfaced with the sampler, flow injection valve, variable transformer, and recorder chart-drive, to provide the appropriate time sequence for automatically switching on and off these mechanical devices.

A schematic diagram of the analytical system is shown in Fig. 1.

Reagents

All chemicals used were reagent grade and water was distilled. Mineral acids used were of high quality with low levels of residual mercury, and Mallinckrodt AR Select Plus grade was found satisfactory. Acids and reagents used were hydrochloric acid, 37%; nitric acid, 70%; sulphuric acid, 96%; potassium persulphate solution, 5% (w/v); saturated potassium dichromate solution.

Sulphuric acid solution, 7% (v/v), was prepared by diluting 70 ml of concentrated sulphuric acid in water and made up to 1 l.

Reducing solution was made by dissolving 40 g of stannous chloride in 100 ml of concentrated HCl by heating and stirring, and adding 20 g of hydroxylamine sulphate and 10 g of sodium chloride. The contents were made up to 1 l with water.

Mercury stock standard solution, 100 μg ml^{-1}: the contents of "Dilute-it" ampoule, supplied by Baker, was transferred into a 1-l volumetric flask. 10 ml of concentrated HNO_3 and 2 ml of saturated potassium dichromate solution were added as preservatives. The contents were diluted to volume with water.

Mercury stock standard solution, 1000 ng ml^{-1}: 2 ml of the 100 μg ml^{-1} mercury stock standard solution was transferred into a 200-ml volumetric flask. 2 ml of concentrated HNO_3 and 0.5 ml of saturated potassium dichromate solution were added. The contents were diluted to volume with water.

Working mercury standard solutions: 100 ml each of 0, 0.1, 0.2, and 0.3 ng ml^{-1} standard solutions in 1% HNO_3 was prepared by serial dilution of the 1000 ng ml^{-1} stock solution. 0.1 ml of the saturated potassium dichromate solution was added to each of the working standard solutions before it was made up to 100 ml.

Procedure

Sample preparation. The procedure of sample preparation is mainly based on that recommended by U.S.A. EPA [9]. 25 ml of sample solution was transferred to a borosilicate glass tube with screw cap, calibrated at 25 ml. 1.2 ml concentrated H_2SO_4, 0.5 ml concentrated HNO_3, 0.3 ml potassium persulphate solution, and 0.3 ml potassium dichromate solution were added. After the sample tube was screw capped and the contents were mixed, it was placed in a hot water bath set at 85–90°C for two hours with cap loosened. The digested sample was removed from the water bath and allowed to cool to room temperature. The final volume of the sample solution was 27.3 ml. A reagent blank was also prepared.

Determination of mercury. Mercury was determined using the analytical system as shown in Fig. 1. The instrumental parameters were selected as given in Table 1.

Prior to analysis, the sample probe was placed in the rinsing position (in reservoir) and the flow injection valve was switched to purging position (green light on). The peristaltic pump was turned on to continuously propel the reducing solution

TABLE 1

Optimum instrumental parameters

Atomic fluorescence spectrometer	
Gain	7.0
Argon flow	22 ml min^{-1} (Flowmeter setting at 40)
Variable transformer	
Setting	12 V
Recorder	
Span	0.1 mV
Chart speed	1 cm min^{-1}

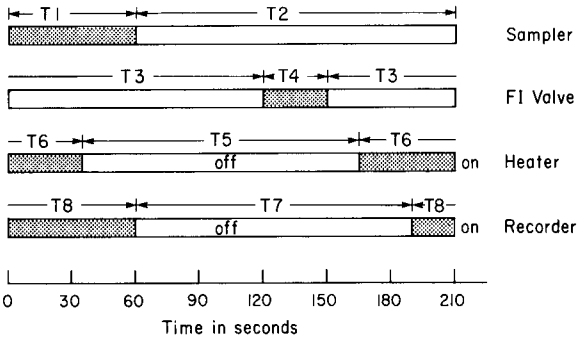

Fig. 2. Time sequence diagram.

into the reacting stream and the 7% H_2SO_4 solution into the reservoir of the sampler. The argon was introduced into the analytical system through three inlets as shown in Fig. 1. When the continuity and steadiness of these flows had been achieved, the power switch of the time sequence controller was turned to ON position. This allowed the analysis to proceed automatically. The time sequences for switching the mechanical positions and the powers of the four devices are as follows: the sample probe staying in sample tube and in reservoir for 60 s (T1) and 150 s (T2) respectively; the flow injection valve in purging and loading positions for 180 s (T3) and 30 s (T4) respectively; the heater off and on for 130 s (T5) and 80 s (T6) respectively; and the recorder off and on for 130 s (T7) and 80 s (T8) respectively. These four sequences were overlapped one another in the order as shown in Fig. 2. The entire analytical cycle took 210 s.

Acquisition of results. An optimum response of the analytical system was established by analysing a control standard solution several times until a constant signal was attained. The digested blank, the standard solutions, and the samples were run sequentially. The concentrations used for constructing the standard curve were 0, 0.1, 0.2, and 0.3 ng ml^{-1}. A standard curve of peak height vs. concentration was obtained by the computer. The curve is linear up to at least 1 ng ml^{-1}. Typical recorder tracings of a series of standards are shown in Fig. 3. The net concentrations of mercury in the sample (digested blank subtracted) were calculated automatically by computer from the curve. The analog signals were also recorded by the chart recorder for visual inspection of the peak shape.

RESULTS AND DISCUSSION

Time sequence controller optimization

Sufficient time is required for the sample solution to flow through the reaction path and for the stream of mercury vapour to reach the injection valve. If the injection valve opens (loading position) too early, the mercury has not arrived; and

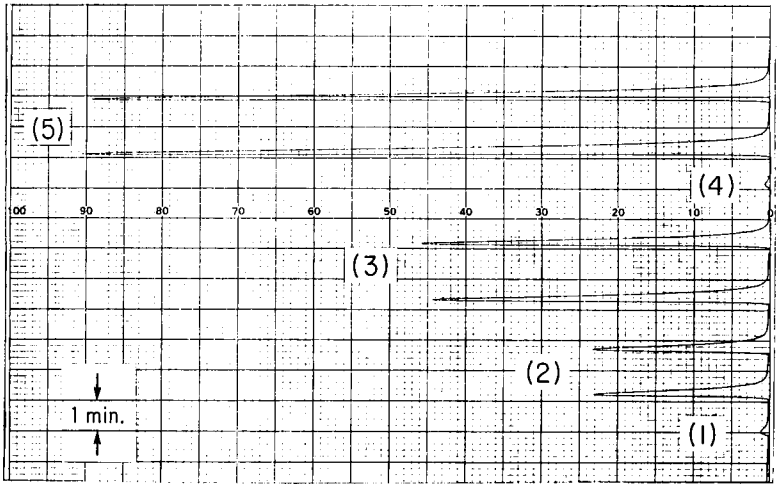

Fig. 3. Recorder tracings of Hg signals: (1) and (4) 0 ng ml^{-1}; (2) 0.1 ng ml^{-1}; (3) 0.2 ng ml^{-1}; (5) 0.4 ng ml^{-1}.

if it opens too late, the mercury would have exhausted. The optimum time lag between the start of sampling and opening injection valve was found to be 120 s which allows the middle segment of the mercury stream entering to the GWA. The minimum time for completely desorbing the mercury at the set temperature is about 80 s. After thermal desorption, sufficient time must be allowed for the gold wire to cool down before it can be reused for amalgamation. 130 s was found to be ample. Increase of the amalgamation time (T4), defined as the time allowed for the gaseous mercury stream entering the GWA, increases the amount of mercury which form amalgam. The signal response is proportional to the amalgamation time. Thus, longer amalgamation time yields higher sensitivity, but is at the expense of analytical throughput because of the longer analytical cycle. In order to maximize the analytical throughput and to retain satisfactory sensitivity, a compromise amalgamation time of 30 s was chosen.

Selection of amalgamation trap

Amalgamation is a well known technique for the preconcentration of ultra trace of mercury generated in an analytical system. There are several types of gold traps in use for preconcentration. Temmerman et al. [8] used quartz sand coated with gold for preconcentration of mercury in air samples. They believe sand gives a large surface area for trapping mercury vapour. Others found that it has a memory effect and causes non-reproducible results. Silver wire [10] has also been used for amalgamation purposes with limited absorption capacity, and it is subject to aerial oxidation and therefore not suitable as an efficient trap. In this study, gold wire with 0.1 to 0.2 mm dia., when packed in a quartz tube of 6 mm i.d. had none of the aforementioned drawbacks over a year of continuous use. The fabrication of the GWA is relatively simple.

Interferences

Oxygen, nitrogen, and moisture, in the gaseous mercury stream are known [11] to quench the atomic fluorescence signal. Precautions were taken to eliminate the above interferences. Argon was used exclusively for segmenting the combined reagent stream and for carrying the mercury vapour into the GWA and the fluorescence detector. During analysis, the sample probe moves back and forth from the sample tube to the reservoir in cycles, and a small amount of air is introduced into the system and possibly carried into the GWA. To prevent interference by air, the GWA was purged with argon before desorbing mercury. A period of 15 s purge time was found to be sufficient. The moist gaseous mercury separated from the gas–liquid separator was dehydrated by two sulphuric acid scrubbers as shown in Fig. 1. For effective removal of moisture, it is recommended that the sulphuric acid in the scrubbers be replaced daily.

Effect of argon flow rate

The argon (carrier 1) introduced into the continuous flow system should be at a sufficiently fast flow rate to carry the generated mercury vapour into the GWA, but not too fast to create back pressure which can push the waste liquid in the gas–liquid separator to the bottom of the separator, causing some mercury to bubble out with the argon. The optimum flow rate was about 20 ml min^{-1}.

The other argon flow (carrier 2) which sweep the desorbed mercury into the flow cell of the atomic fluorescence spectrometer, was controlled by the built-in flow meter in the spectrometer from 5 to 50 ml min^{-1}. Mercury sensitivity decreases with increasing flow rate due to gaseous dilution. Thus a lower flow rate will give a higher sensitivity, but at the cost of greater peak broadening. It is also difficult to maintain a steady flow at lower settings, e.g., below 15 ml min^{-1}. A compromise flow rate of 22 ml min^{-1} (flowmeter setting at 40) was adopted.

Reagent blank

The lowest possible reagent blank should be achieved in order to measure mercury at near blank levels more accurately. The main source of mercury contributing to the blank value was found to be the HCl in the reducing solution. Most of the mercury was removed from the solution by purging with mercury-free argon for half an hour.

Prolonged purging did not further reduce the amount of the residual mercury. An attempt to further purify the solution by passing it through a specific resin (Supelco Duolite GT-73) column resulted in only slight improvement. Deionized distilled water was found to contain slightly less residual mercury than distilled water. Use of distilled water for preparation of the reagents is satisfactory if deionized distilled water is not available. The small signal response from the zero Hg standard solution (see Fig. 3) is mainly due to the residual mercury in the HCl of the reducing solution. This accounts for the fact that the standard curve does not intersect the origin.

Precision, accuracy, and detection limit

The precision of the method was determined from the results of ten replicate analyses on a composite of natural water samples containing 0.06 ng ml^{-1} of mercury. The R.S.D. is 3%. The accuracy was demonstrated by the close agreement of the results with the certified values of two EPA standard reference water samples as shown in Table 2.

The detection limit is defined as three times the S.D. (3σ) from replicate analyses on a sample with the analyte concentration near the blank level. Eleven digested blank solutions were chosen for analyses. The results were used for calculation of the S.D.. The detection limit (3σ) thus obtained was 0.002 ng ml^{-1}, or 2 ppt.

A number of natural water samples with various mercury concentrations were selected and analyzed by the present method and by CVAAS. The results are in good agreement as shown in Table 3. The paired sample t-test gives a t value of -0.744. The critical value of t at 95% confidence interval ($P = 0.05$) is 2.45. Therefore, the two methods do not give significantly different values.

TABLE 2

Analytical results on SRMs (ng ml^{-1} Hg)

Sample, water	Certified value	This study		
		Mean	N	R.S.D. (%)
EPA WS378	1.6	1.58	3	1.9
EPA WS386	4.9	4.88	4	2.6

TABLE 3

Results for Hg in waters by this method vs. CVAAS

Sample	Hg (ng ml^{-1})	
	This method	CVAAS
1	24	25
2	28	29
3	23	23
4	50	53
5	90	92
6	102	101
7	61	58
8	8	< 20
9	10	< 20
10	12	< 20
11	4	< 20

GENERAL REMARKS

Optimum temperature of the GWA for rapidly desorbing mercury is provided by applying 12 V from the variable transformer across the Chromel wire, which yields approximately 500°C as indicated by the red glow of the wire. This temperature can be measured by a thermocouple. Lower temperature results in sluggish and incomplete release of mercury from the amalgam; too high a temperature may enhance the risk of damaging the GWA and also requires more time to cool it down. The diameter of the ports of the injection valve should not be less than 1 mm in order to avoid creating back pressure in the gas–liquid separator. The chamber volume of the gas–liquid separator was approximately 8 ml, and was found to be not critical. Helium can be used as a carrier [12], which is just as effective. A gold wire trap can be installed in the argon supply line to remove any residual mercury, if it exists, before the argon enters the analytical system. Installation of a mercury scrubber at the vent of the atomic fluorescence spectrometer is recommended for safety reasons. The scrubber, filled with dry moss (sphagnum) and charcoal, will serve as a mercury trap, preventing the hazardous vapour from escaping to the workspace.

The authors thank Darryl Russell for his technical assistance and George Kanert for his helpful comments.

REFERENCES

1 P.S. Tjioe, J.J.M. de Goey and J.P.W. Houtman, J. Radioanal. Chem., 37 (1971) 511.
2 M.J. Powell, E.S.K. Quan, D.W. Boomer and D.R. Wiederin, Anal. Chem., 64 (1992) 2253.
3 R.F. Sanzolone and T.T. Chao, Analyst, 108 (1983) 58.
4 J.E. Hawley and J.D. Ingle, Anal. Chem., 47 (1975) 719.
5 P.B. Stockwell, K.C. Thompson, A. Henson, E. Temmerman and C. Vandecasteele, Int. Labmate, 14 (1989) 45.
6 G. Vermeir, C. Vandecasteele and R. Dams, Anal. Chim. Acta, 220 (1989) 257.
7 G. Vermeir, C. Vandecasteele and R. Dams, Anal. Chim. Acta, 242 (1991) 203.
8 E. Temmerman, C. Vandecasteele, G. Vermeir, R. Leyman and R. Dams, Anal. Chim. Acta, 236 (1990) 371.
9 U.S.A. EPA Methods for Chemical Analysis of Water and Wastes, EPA–600/4–79–020 (1979).
10 J.P. Lodge, Jr., Methods of Air Sampling and Analysis, Lewis Publishers, Boca Raton, FL, 3rd edn., 1989, pp. 371–375.
11 K.C. Thompson and G.D. Reynolds, Analyst, 96 (1971) 771.
12 Operation Manual for the CVAFS, Model-2 Mercury Analyzer, Nov. 1, 1990, Brooks Rand Ltd., Seattle, WA.

Analytica Chimica Acta, 282 (1993) 117–124
Elsevier Science Publishers B.V., Amsterdam

Fluorescence enhancement and cofluorescence in complexes of terbium, dysprosium and europium with trimesic acid

B.S. Panigrahi, Susy Peter, K.S. Viswanathan and C.K. Mathews

Indira Gandhi Centre for Atomic Research, Kalpakkam 603102 (India)

(Received 15th December 1992; revised manuscript received 15th April 1993)

Abstract

The fluorescence of terbium, dysprosium and europium was enhanced by about two to three orders of magnitude when they were excited in the presence of trimesic acid in aqueous solutions at pH 6. The fluorescence was enhanced by a further order of magnitude when these lanthanide–trimesate complexes were treated with trioctylphosphine oxide (TOPO) and Triton X-100. The enhancement following the addition of TOPO is strongly pH dependent. An enhancement in the fluorescence of these rare earths with the carboxylate ligand is observed in the presence of ions such as La^{3+} and Gd^{3+}, due to cofluorescence. The addition of La or Gd enhances the fluorescence of the lanthanide–trimesic acid complexes by almost two orders of magnitude, leading to detection limits in the sub-ng ml^{-1} range for these rare earths.

Keywords: Fluorimetry; Dysprosium; Europium; Rare earth elements; Terbium; Trimesic acid

The technique of ligand-sensitized fluorescence has generally been employed to obtain fluorescence enhancement of the lanthanides. In this process, an organic ligand is first excited by absorption of light, followed by energy transfer to the excited energy levels of the lanthanide. It turns out that this process of indirect pumping of the excited energy levels of the lanthanide is more efficient than direct absorption of light by the lanthanide, owing to their poor absorptivities and low fluorescence quantum yields [1,2]. Several groups, using a variety of organic ligands, have shown enhancements of several orders of magnitudes in lanthanides such as Tb, Dy and Eu [3–8]. The reasons for the interest in these studies are twofold: improvement of the detection limits for the determination of these lanthanides using fluorimetry and they serve as good systems for the study of energy flow in complexes [9–11].

The fluorescence of the lanthanide complexes is further enhanced by the use of synergistic agents, such as trioctylphosphine oxide (TOPO), organic phosphates and sulphoxides. These compounds provide an insulating layer around the lanthanide complex, reducing the probability of radiationless energy transfer from the complex to the solvent [6].

It has also been shown that the presence of certain ions in solutions, such as La, Gd, Lu or Y, can lead to fluorescence enhancement of the lanthanides Tb, Eu and Dy [12–17]. This is referred to as columinescence. In this case, an intermolecular energy flow is believed to occur between the non-fluorescing donor complex (of La, Gd, Lu or Y) and the fluorescing acceptor

Correspondence to: C.K. Mathews, Indira Gandhi Centre for Atomic Research, Kalpakkam 603102 (India).

complex (of Tb, Eu or Dy). As the concentration of the donor is generally much greater than that of the acceptor complex, each acceptor is surrounded by many donor chelates, and the fluorescence of the acceptor is greatly enhanced.

Recently it has been shown that the fluorescence of Tb, Dy and Eu can be enhanced by the use of benzoate as a ligand, together with TOPO–Triton X-100 [18]. Enhancements of almost four orders of magnitude were reported in that study.

In this work, a polycarboxylic aromatic acid, trimesic acid (benzene-1,3,5-tricarboxylic acid), was chosen as the ligand for studies on the fluorescence enhancement of lanthanides. Although this system displays the expected enhancement, similar to benzoate, it also exhibits some interesting differences that will be discussed. In particular, it exhibits columinescence, a phenomenon extensively reported so far only for β-diketones such as thenoyl trifluoroacetone (TTA) [19]. This is the first report of such a phenomenon with a ligand other than the β-diketones. Interestingly, no columinescence with the benzoate ligand was observed.

EXPERIMENTAL

Apparatus

All fluorescence measurements were made with a Shimadzu RF 5000 spectrofluorimeter. The excitation source was a 150-W CW xenon lamp. The band pass for the excitation and emission monochromators were set at 5 nm. Solutions were taken in a 1-cm path-length quartz cell for fluorescence measurements. All emission spectra were blank subtracted: a blank was recorded using identical experimental conditions but without the lanthanides (Tb, Dy or Eu) in the solution.

Reagents

Stock standard solutions of rare earth nitrates were prepared from the corresponding oxides (99.9% pure, Indian Rare Earths) as described previously [18]. A stock standard solution of trimesic acid (Merck) was prepared by dissolution in distilled water and addition of the required amount of sodium hydroxide.

RESULTS AND DISCUSSION

The enhancement of the lanthanide fluorescence intensity by using trimesic acid (TMA) as the complexing agent is discussed first, followed by the effects of the synergistic agent, TOPO, and of other lanthanides such as La and Gd.

Lanthanide–trimesic acid (TMA) system

The lanthanide fluorescence was measured as a function of the pH of the solution and trimesic acid concentration. The optimum pH was found to be 6. The trimesic acid concentration was varied from 1×10^{-5} to 1×10^{-3} M. It was found that for the concentrations of the lanthanides used in this study (10^{-5}–10^{-9} M), the optimum trimesic acid concentration was 1×10^{-4} M and this concentration was used in all subsequent experiments.

Figure 1a and b show the excitation spectra for Tb^{3+} and the Tb^{3+}–TMA complex, respectively, in aqueous medium. In both instances the excitation spectra were recorded by monitoring the Tb^{3+} fluorescence at 544 nm. However, the two spectra are clearly different. Whereas the excita-

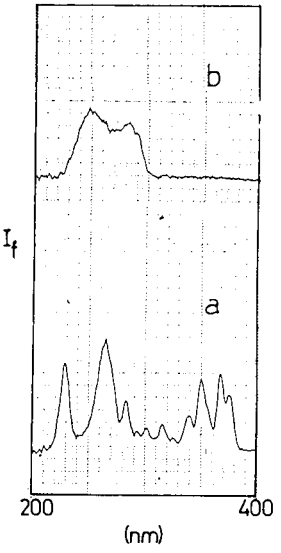

Fig. 1. Excitation spectra of (a) Tb^{3+} (4×10^{-4} M) and (b) Tb^{3+} (1.5×10^{-7} M)–TMA (1×10^{-4} M). Emission wavelength monitored, 544 nm. Intensity scales are the same for both figures.

tion spectrum shown in Fig. 1a agrees well with the absorption spectrum reported for Tb^{3+} [2], as it should, the excitation spectrum shown in Fig. 1b for the Tb^{3+}–TMA complex resembles more closely the absorption spectrum typical of aromatic carboxylic acids. Similar results were obtained with Dy^{3+}–TMA and Eu^{3+}–TMA complexes. In fact, the excitation spectra of the Tb^{3+}–TMA, Dy^{3+}–TMA and Eu^{3+}–TMA complexes are all similar (Figs. 1–3).

Figure 4a and b show the emission spectra of Tb^{3+} and the Tb^{3+}–TMA complex, respectively, both of which look identical and agree well with the emission spectrum reported for Tb^{3+} [20]. It should be noted, however, that the excitation wavelengths used to record the two spectra shown were different. For Tb^{3+} (Fig. 4a) the excitation wavelength was 350 nm, which corresponds to the absorption of Tb^{3+}. However, for the Tb^{3+}–TMA complex, the excitation wavelength used was 248 nm, which was the excitation maximum in Fig. 1b. At this excitation wavelength uncomplexed Tb^{3+} shows no perceptible fluorescence.

The Tb concentration used to record the spectra (both excitation and emission) of the Tb^{3+}–TMA complex was 1.5×10^{-7} M. At this concentration, a solution containing Tb^{3+} alone (without trimesic acid) showed no perceptible fluorescence. Hence, to record the spectrum of the bare ion, a Tb^{3+} concentration of 4×10^{-4} M was used.

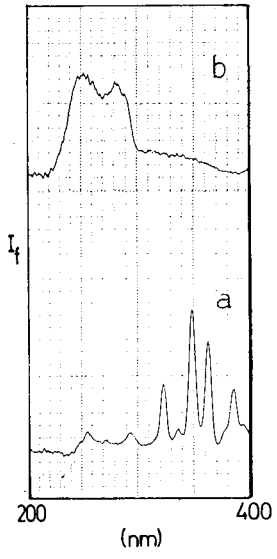

Fig. 2. Excitation spectra of (a) Dy^{3+} (3×10^{-3} M) and (b) Dy^{3+} (5×10^{-6} M)–TMA (1×10^{-4} M). Emission wavelength monitored, 477 nm. Intensity scales are the same for both figures.

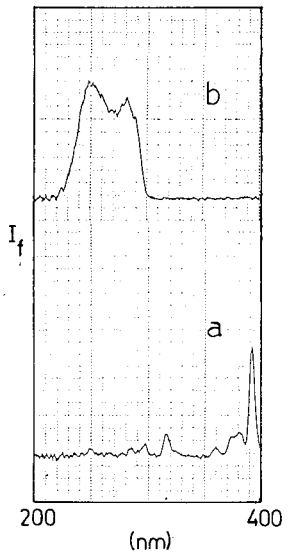

Fig. 3. Excitation spectra of (a) Eu^{3+} (2×10^{-3} M) and (b) Eu^{3+} (8×10^{-6} M)–TMA (1×10^{-4} M). Emission wavelength monitored, 592 nm. Intensity scales are the same for both figures.

It should be noted that the fluorescence intensities of the bare Tb^{3+} ion (Fig. 4a) and the Tb^{3+}–TMA complex (Fig. 4b) are comparable, even though the concentration of Tb used to record the spectrum shown in Fig. 4b was about 2000 times lower than that used for Fig. 4a. The enhancement in fluorescence due to trimesic acid is therefore obvious. Similar results were obtained with Eu and Dy (Figs. 5 and 6).

The similarity of the excitation spectra of all three lanthanide complexes of trimesic acid and their excitation maxima at 248 nm points to a common absorber in all the three instances. Further, all three excitation spectra closely resemble the absorption, spectra typical of aromatic carboxylic acids. It can therefore be concluded that trimesic acid is the common absorber, which then transfers the energy to the lanthanide ion, leading to the fluorescence of the latter. Similar re-

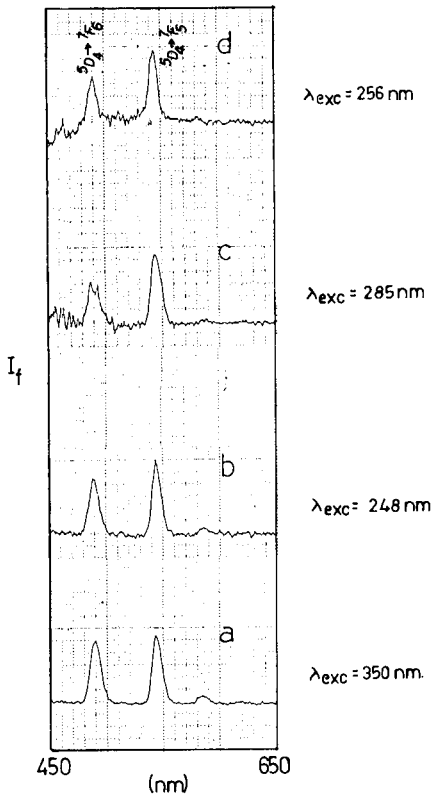

Fig. 4. Emission spectra of (a) Tb^{3+} (4×10^{-4} M) (b) Tb^{3+} (1.5×10^{-7} M)–TMA (1×10^{-4} M), (c) Tb^{3+} (1×10^{-8} M)–TMA (1×10^{-4} M)–TOPO (1×10^{-4} M) and (d) Tb^{3+} (1×10^{-9} M)–TMA (1×10^{-4} M)–La^{3+} (1×10^{-4} M). Intensity scales are same for all figures.

sults were obtained with benzoate as the complexing agent.

It must be pointed out that Brittain [21] reported that the Tb^{3+}–TMA complex was not soluble at any pH and hence its fluorescence could not be studied. However, the concentration of Tb^{3+} used in his study appears to be high (typically 10^{-3} M), and at this concentration we have confirmed that the complex precipitates. The Tb concentrations used in the present study are typically 10^{-5} M or lower, and at these low concentrations no solubility problems were encountered.

Lanthanide–trimesic acid–TOPO–Triton X-100 system

The use of TOPO as a synergistic agent to enhance the fluorescence by minimizing the collisions between rare earth ions and water molecules is well known [4–7]. Consequently, the effect of TOPO on the rare earth–trimesic acid fluorescence was studied. This was done by adding TOPO dissolved in Triton X-100 to a solution of lanthanides–trimesic acid. As in the previous studies with benzoate, the optimum concentrations of TOPO and Triton X-100 were established by measuring the rare earth fluorescence as a function of TOPO and Triton X-100 concentrations. For the concentrations of the rare earths and trimesic acid used, it was found that the optimum concentrations of TOPO and Triton X-100 were 1×10^{-4} M and 0.05%, respectively.

The fluorescence intensity of Tb was also measured as a function of the pH of the solution. It was found that with the addition of TOPO–Tri-

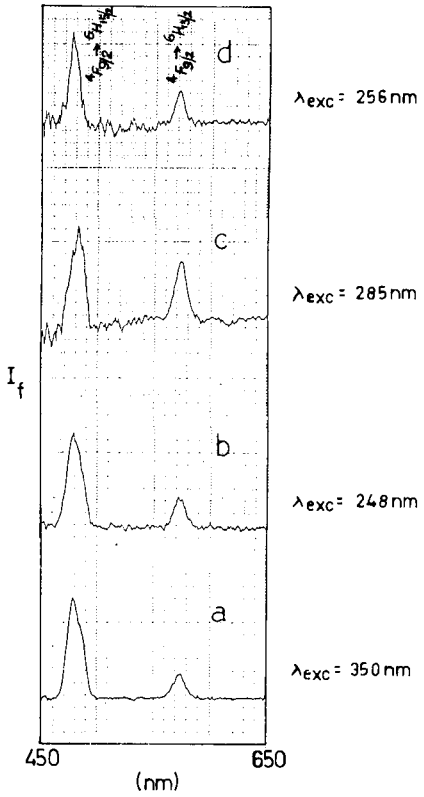

Fig. 5. Emission spectra of (a) Dy^{3+} (3×10^{-3} M), (b) Dy^{3+} (5×10^{-6} M)–TMA (1×10^{-4} M), (c) Dy^{3+} (5×10^{-7} M)–TMA (1×10^{-4} M)–TOPO (1×10^{-4} M) and (d) Dy^{3+} (5×10^{-9} M)–TMA (1×10^{-4} M)–La^{3+} (1×10^{-4} M). Intensity scales are same for all figures.

ton X-100 to the Tb^{3+}–TMA complex, the fluorescence of Tb shows a maximum at pH 4, in contrast to the value of pH 6 observed earlier without TOPO–Triton X-100. Figure 4c shows the fluorescence of the Tb^{3+}–TMA–TOPO–Triton X-100 at pH 4. It should be noted that even though the Tb concentration used in this experiment (Fig. 4c) is lower by about an order of magnitude than that used for recording the spectra of the Tb^{3+}–TMA system (Fig. 4b), the fluorescence intensities are comparable. This implies that the addition of TOPO–Triton X-100 to the Tb^{3+}–TMA system enhances the fluorescence by about an order of magnitude. Similar results were observed with Eu and Dy (Figs. 5 and 6).

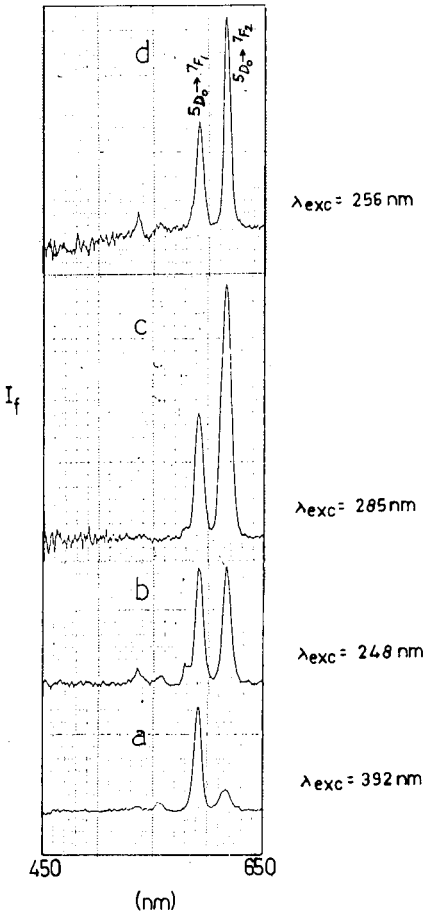

Fig. 6. Emission spectra of (a) Eu^{3+} (2×10^{-3} M), (b) Eu^{3+} (8×10^{-6} M)–TMA (1×10^{-4} M), (c) Eu^{3+} (5×10^{-7} M)–TMA (1×10^{-4} M)–TOPO (1×10^{-4} M) and (d) Eu^{3+} (1×10^{-8} M)–TMA (1×10^{-4} M)–La^{3+} (1×10^{-4} M). Intensity scales are same for all figures.

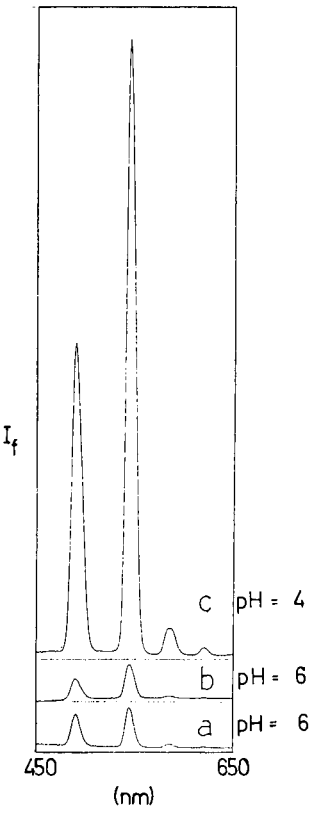

Fig. 7. Emission spectra of (a) Tb^{3+} (1×10^{-6} M)–TMA (1×10^{-4} M), pH 6, excitation wavelenght 248 nm, (b) Tb^{3+} (1×10^{-6} M)–TMA (1×10^{-4} M)–TOPO (1×10^{-4} M), pH 6, excitation wavelength 285 nm and (c) same as (b) but at pH 4.

It must be pointed out that the emission spectra of the Tb^{3+}–TMA–TOPO–Triton X-100 system are noisy, particularly at low Tb concentrations, because the emission of the blank solution (containing TMA–TOPO–Triton X-100 with no rare earth) is high and hence the subtraction of the large blank leads to noisy emission spectra.

The pH dependence of the fluorescence enhancement of the Tb^{3+}–TMA system, following the addition of TOPO–Triton X-100, is interesting. Figure 7 shows the fluorescence of the Tb^{3+}–TMA–TOPO–Triton X-100 system at pH 4 and 6. Also shown is the fluorescence of the Tb^{3+}–TMA complex for comparison (at its optimum pH of 6). It can be seen that the enhancement follow-

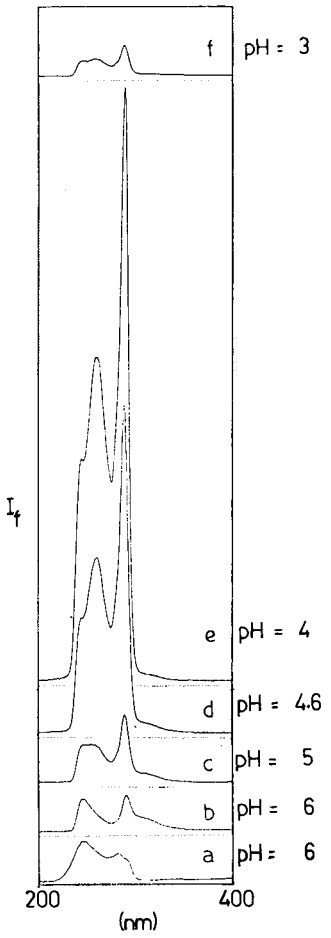

Fig. 8. Excitation spectra of (a) Tb^{3+} (1×10^{-6} M)–TMA (1×10^{-4} M), pH 6 and (b)–(f) Tb^{3+} (1×10^{-6} M)–TMA (1×10^{-4} M)–TOPO (1×10^{-4} M), pH 6–3 as indicated. Emission wavelength monitored 544 nm in all the instances. Intensity scales are the same for all figures.

ing the addition of TOPO is significant at pH 4, whereas at pH 6 the addition of TOPO has little effect on the fluorescence of the Tb^{3+}–TMA complex. As mentioned earlier, pH 4 was found to be optimum.

Figure 8 shows the excitation spectra of the Tb^{3+}–TMA–TOPO–Triton X-100 system at different pH values, obtained by monitoring the Tb emission at 544 nm. Also shown for comparison is the excitation spectrum of the Tb^{3+}–TMA system (without TOPO–Triton X-100) at its optimum pH of 6. It can be seen that at pH 6 the addition of TOPO–Triton X-100 hardly alters the excitation spectra, indicating that TOPO has yet to participate in the complexation process. As the pH of the solution is lowered, the excitation spectra begin to change, with the 285-nm peak gaining in intensity. The enhancement of the Tb fluorescence is maximum at pH 4. This is at variance with the findings using benzoate, where a pH of 6 was found to be the optimum, both with and without TOPO. This can be explained as follows. At pH 6, the trimesic acid exists predominantly in the triply ionized form (90%) and could possibly interfere with TOPO participating in the complex formation with Tb^{3+}, which is necessary for the synergy displayed by TOPO. This is seen from the fact that at pH 6, the excitation spectra of the Tb^{3+}–TMA changes very little following the addition of TOPO–Triton X-100. As the pH is lowered, the concentration of the triply ionized form decreases, with a corresponding increase in the doubly and singly ionized forms. At pH 4, trimesic acid exists largely in the singly (54%) and doubly (43%) ionized forms, with negligible contributions from the triply ionized form (as calculated from its pK_a values [22]). The decrease in the number of charged groups on the ligand might make complex formation by TOPO with Tb^{3+}–TMA more facile at lower pH values, and hence the enhancement. At pH < 4, the concentration of the Tb^{3+}–TMA complex itself would decrease; hence the optimum enhancement at pH 4. With benzoate, the charge on the ligand does not vary with pH, hence no such dependence was seen. Similar results were obtained with Dy and Eu.

A similar behaviour has been reported for Eu^{3+}–TTA complexes [23]. When phenanthroline was used as the synergistic agent, a pH of 7 was found to be optimum. However, when TOPO was used, the optimum pH was found to be 4.5.

As with benzoate, the addition of TOPO shifts the excitation maxima to 285 nm from the 248 nm seen for the lanthanide–trimesic acid complex.

The fluorescence intensities of the rare earth–TMA–TOPO–Trition X-100 complexes showed a linear dependence on their concentrations over the ranges 10^{-8}–10^{-6} M for Tb and 10^{-7}–10^{-6} M for Dy and Eu. The range is smaller than that observed with benzoate, with the upper limit be-

ing an order of magnitude lower for the trimesate than for the benzoate system.

Columinescence

The effect of Gd^{3+}, La^{3+} and Y^{3+} on the fluorescence of the rare earth–trimesate complex was also examined. A solution of, say, La^{3+}, was added to an aqeuous solution of Tb^{3+}–TMA, giving a suspension. After 30 min, the Tb^{3+} fluorescence was measured. To optimize the conditions, the Tb^{3+} fluorescence was measured as a function of the trimesic acid concentration (1×10^{-5}–1×10^{-3}M), La^{3+} concentration (1×10^{-5}–1×10^{-3} M) and the pH of the solution (3–8). In all these optimization experiments, the Tb^{3+} concentration was held at 1×10^{-7} M. The optimum concentration for both the trimesic acid and La^{3+} was 1×10^{-4} M. The fluorescence intensity was found to be independent of the pH over the range studied. A pH of 6 was used in the remainder of the study. Figure 4d shows the Tb^{3+} emission spectrum of the Tb^{3+}–TMA–La^{3+} system. The excitation wavelength used was 256 nm, which was the maximum in the excitation spectrum of the Tb^{3+}–TMA–La^{3+} system. It was found that the Tb^{3+} fluorescence in the Tb^{3+}–TMA complex was enhanced about 100 fold following the addition of La^{3+}. The La^{3+}–TMA complex itself does not show any fluorescence, but when present along with Tb^{3+}–TMA it causes a significant enhancement of the Tb fluorescence. Similar results were obtained with Dy^{3+} and Eu^{3+} following the addition of La^{3+} to the rare earth–TMA complex (Figs. 5d and 6d).

Gd^{3+} also showed columinescence, although less than La^{3+}. For example, the enhancement of the Tb fluorescence obtained when Gd^{3+} was used as the columinescent ion was about 2.5 times lower than that obtained when La^{3+} was used. Y^{3+} did not show any enhancement of the Tb^{3+} fluorescence.

Fluorescence enhancement of rare earths due to columinescence has previously been reported only with β-diketone ligands as the energy transfer agent [19]. These ligands are used together with a synergistic agent (such as TOPO) and a micellar agent (such as Triton X-100), which has been found to stabilize the system. In the experiments on cofluorescence with trimesic acid, no synergistic agent or any micelle was added. In fact, addition of TOPO was found to decrease the enhancement due to columinescence. This clearly suggests that the mechanism of cofluorescence is different in the two cases. With the β-diketone complexes, an intermolecular energy transfer is believed to occur from the enhancing chelate (say, of La) to the fluorescent chelate (say, of Tb) in the aggregated particles. In experiments with phthalic and hemimellitic acids, Brittain [24] showed energy transfer to occur from Tb^{3+} to Eu^{3+}. The energy transfer was thought to be facilitated by the formation of polynuclear complexes. It is possible that similar polynuclear complexes could have been formed in the present experiments with La^{3+} as the columinescent ion and trimesic acid as the ligand, thereby implying an intramolecular type of energy transfer. The addition of TOPO could hinder the formation of such polynuclear complexes, resulting in a decreased fluorescence. It is also relevant that with benzoate as the ligand (which cannot form polynuclear complexes), no cofluorescence was observed.

Using the TMA–La^{3+} system, it was found that the fluorescence intensity of the rare earths (Tb, Dy, Eu) showed a linear dependence on concentration over the ranges 10^{-9}–10^{-7} M for Tb and 10^{-8}–10^{-7} for Dy and Eu. Above these concentrations, saturation of the fluorescence intensity was observed. From the calibration graphs, the detection limits were then estimated by calculating the concentration corresponding to the 3σ value of the blank. It turned out that under the conditions in these experiments, the detection limits were 0.025 ng ml^{-1} for Tb^{3+}, 0.5 ng ml^{-1} for Dy^{3+} and 0.25 ng ml^{-1} for Eu^{3+}. The emission wavelengths monitored for the concentration calibrations were 544 nm for Tb^{3+}, 477 nm for Dy^{3+} and 616 nm for Eu^{3+}; for a given rare earth, these were the emissions with the highest intensity. For Eu^{3+}, even though the 616-nm transition was hypersensitive, the calibration graph was linear over the regions mentioned.

Table 1 summarizes the results of this study, giving the fluorescence enhancements of the rare earths in the different systems that were exam-

TABLE 1

Fluorescence enhancements of the rare earths with different systems

System	Relative enhancement [a]
Tb–TMA	2.7×10^3
Tb–TMA–TOPO–Triton X-100	4×10^4
Tb–TMA–La	4×10^5
Dy–TMA	6×10^2
Dy–TMA–TOPO–Triton X-100	6×10^3
Dy–TMA–La	6×10^5
Eu–TMA	2.5×10^2
Eu–TMA–TOPO–Triton X-100	4×10^3
Eu–TMA–La	2×10^5

[a] Explained in text.

ined. The enhancements are given relative to the fluorescence of the bare rare earths and are calculated as the ratios of the concentrations of the bare rare earths (Tb, Dy, and Eu) to the concentrations of the rare earths in the particular system, which gave the same fluorescence intensity. It can be seen that the Tb^{3+} fluorescence was enhanced by almost five orders of magnitude using the Tb^{3+}–TMA–La^{3+} system, in comparison with that of the bare Tb^{3+}.

From the emission spectra of Eu (Fig. 6), it can be seen that the relative intensities of the $^5D_0 \rightarrow {}^7F_J$ ($J = 1$ and 2) transitions of Eu are not the same for the four experiments shown. This is due to the fact that the $^5D_0 \rightarrow {}^7F_2$ transition in Eu is hypersensitive, the intensity being strongly dependent on the environment of the ion. Such changes have also been observed in the relative intensities of these peaks for benzoate [18].

Conclusions

Fluorescence enhancement of Tb, Dy and Eu was seen when these rare earths were complexed with trimesic acid at pH 6. The fluorescence was enhanced further when TOPO was added, as a synergistic agent. Unlike the results with benzoate, the trimesic acid–TOPO–Triton X-100 system showed an interesting pH dependence. Enhancement of the fluorescence of the above-mentioned rare earth–TMA complexes was also observed, due to cofluorescence, in the presence of ions such as La^{3+} and Gd^{3+}. Fluorescence enhancement due to cofluorescence has hitherto been reported only with β-diketone ligands. The enhancement due to cofluorescence was about five orders of magnitude relative to the fluorescence of the bare ion. This leads to detection limits in the sub-ng ml^{-1} region for the rare earths studied.

REFERENCES

1 G. Stein and E. Wurzberg, J. Chem. Phys., 62 (1975) 208.
2 W.T. Carnall, Handbook of the Physics and Chemistry of Rare Earths, Vol. 3, Elsevier, Amsterdam, 1978, Chap. 24.
3 J.-H. Yang, G.-Y. Zhu and B. Wu, Anal. Chim. Acta, 198 (1987) 287.
4 T. Taketatsu and A. Sato, Anal. Chim. Acta, 108 (1979) 429.
5 T. Taketatsu, Talanta, 29 (1982) 397.
6 G. Zhu, Z. Si, J. Yang and J. Ding, Anal. Chim. Acta, 231 (1990) 157.
7 M. Morin, R. Bador and H. Dechaud, Anal. Chim. Acta, 219 (1989) 67.
8 L.M. Perry and J.D. Winefordner, Anal. Chim. Acta, 237 (1990) 273.
9 G.A. Crosby, R.E. Whan and R.M. Alire, J. Chem. Phys., 34 (1961) 743.
10 W.R. Dawson, J.L. Kropp and M.W. Windsor, J. Chem. Phys., 45 (1966) 2410.
11 M. Kleinerman, J. Chem. Phys., 51 (1968) 2370.
12 Y.-X. Ci and Z.H. Lan, Anal. Chem., 61 (1989) 1063.
13 J. Yang, H. Zhou, X. Ren and C. Li, Anal. Chim. Acta, 238 (1990) 307.
14 Y.-Y. Xu, I. Hemmila, V.-M. Mukkala, S. Holttinen and T. Lovgren, Analyst, 116 (1991) 1155.
15 J. Georges, Spectrochim. Acta, 14 (1991) 337.
16 Y.-Y. Xu and I. Hemmila, Anal. Chim. Acta, 256 (1992) 9.
17 G. Zhu, Z. Si, X. Wang and W. Zhu, Anal. Chim. Acta, 231 (1990) 295.
18 S. Peter, B.S. Panigraphi, K.S. Viswanathan and C.K. Mathews, Anal. Chim. Acta, 260 (1992) 135.
19 Y-Y. Xu, I. Hemmila, T.N.E. Lovgren, Analyst, 117 (1992) 1061.
20 J.-C.G. Bunzli, in J.-C.G. Bunzli and G.R. Choppin (Eds.), Lanthanide Probes in Life, Chemical and Earth Sciences, Elsevier, New York, 1989, Chap. 7.
21 H.G. Brittain, J. Inorg. Nucl. Chem., 41 (1979) 567.
22 J.A. Dean, Handbook of Organic Chemistry, McGraw-Hill, Singapore, 1987, Section 8.
23 V.M. Aleksandruk, A.S. Babaev, T.A. Dem'yanova and A.V. Stepanov, Radiokhimiya, 31 (1989) 139.
24 H.G. Brittain, J. Inorg. Nucl. Chem., 41 (1979) 561.

Analytica Chimica Acta, 282 (1993) 125–132
Elsevier Science Publishers B.V., Amsterdam

Reductive potentiometric stripping analysis of manganese with potassium hexacyanoferrate(II) as reducing agent on a glassy carbon electrode

Yali Zhang

Department of Applied Chemistry, Qingdao Institute of Textile Technology, 266042 Qingdao (China)

Kui Jiao, Chengfan Liu and Xiaobin Liu

Department of Applied Chemistry, Qingdao Institute of Chemical Technology, 53 Zheng Zhou Road, 266042 Qingdao (China)

(Received 11th December 1992; revised manuscript received 5th April 1993)

Abstract

The reductive potentiometric stripping analysis (RPSA) of manganese with potassium hexacyanoferrate(II) as reducing agent on a glassy carbon electrode was investigated. This method is more sensitive, more reproducible, more precise and more convenient than the RPSA method for manganese with hydroquinone as reducing agent on a platinum working electrode. The technique was applied satisfactorily to determine micro amounts of manganese in artificial human hair sample solution and vegetables. The pretreatment of the glassy carbon electrode, the processes of anodic preconcentration and subsequent RPSA and interferences are discussed.

Keywords: Stripping voltammetry; Manganese

Potentiometric stripping analysis (PSA) has developed rapidly and has been extensively applied to determine trace elements in various samples since it was first proposed by Jagner and Graneli [1]. However, work has been focused mainly on oxidative potentiometric stripping analysis (OPSA) to determine metals that can be preconcentrated either as dilute amalgams in a mercury electrode (Zn, Cd, Pb, Cu, Bi, Tl, etc.) or directly when cathodically deposited on a glassy carbon electrode or a gold film electrode (Hg, As) [2–5]. Reductive potentiometric stripping analysis (RPSA) has been much less reported [6,7]. Christensen and co-workers described the RPSA of Mn(II) with hydroquinone as reducing agent on a platinum working electrode [6] and the RPSA of Se and S with amalgamated sodium as reducing agent and a small mercury pool as the working electrode [7].

There are some difficulties in applying RPSA. On the one hand, it is not easy to select a reducing agent considering both thermodynamic and kinetic aspects. A reducing agent for RPSA must satisfy the following conditions: its oxidation potential must be 200 mV or more cathodic than the reduction potential of the analyte to be preconcentrated; the rate of its chemical reaction with the analyte to be preconcentrated on the electrode must be appropriate—if it is too slow the stripping time is too long, and if it is too fast the analyte cannot be efficiently preconcentrated because it is reduced at the same time as it is

Correspondence to: Kui Jiao, Department of Applied Chemistry, Qingdao Institute of Chemical Technology, 53 Zheng Zhou Road, 266042 Qingdao (China).

being deposited on the electrode surface, and also the stripping is too rapid, and in both instances no good analytical signal appears; it must be stable in solution; and its overpotential of anodic oxidation must be high and the electrochemical redox reaction readily reversible. On the other hand, the analyte element must have variable oxidation states, so that its concentration anodically as a precipitate is possible, and also the plating potential must be less negative than that of oxygen evolution.

The reported RPSA procedure for Mn(II) [6] is complicated because of the requirements that the sample solution must be deaerated and kept at 50°C; the detection limit was 10^{-7} M Mn(II).

This paper reports the RPSA of Mn(II) with potassium hexacyanoferrate(II) as reducing agent and a glassy carbon electrode working electrode. It is unnecessary to deaerate or heat the test solution. The detection limit of this technique is 5×10^{-9} M Mn(II). Hence the method is more convenient and more sensitive than the previous method [6].

The preconcentration process involves anodic precipitation of Mn(II) as hydrated manganese dioxide:

$$Mn^{2+} + 2H_2O \longrightarrow MnO_2(s) + 4H^+ + 2e \quad (1)$$

($E_0 = 1.230$ V vs. SHE)

The reducing agent potassium hexacyanoferrate(II) can be anodically oxidized to form the hexacyanoferrate(III):

$$[Fe(CN)_6]^{4-} \longrightarrow [Fe(CN)_6]^{3-} + e \quad (2)$$

($E_0 = 0.356$ V vs. SHE)

As the electrode potential of the latter is 0.886 V more cathodic than that of the former, the chemical reduction reaction of MnO_2:

$$MnO_2(s) + 2[Fe(CN)_6]^{4-} + 4H^+ \longrightarrow 2[Fe(CN)_6]^{3-} + Mn^{2+} + 2H_2O \quad (3)$$

occurs very easily. Because electrode reaction 2 is very reversible and rapid, and $K_4[Fe(CN)_6]$ is fairly stable in solution, it can be predicted that potassium hexacyanoferrate(II) should be a suitable reducing agent.

EXPERIMENTAL

Apparatus

A microcomputerized Model DPSA-3 differential potentiometric stripping analyser (Shandong Electric Communication Factory No. 7) with a glassy carbon rotating disc electrode as working electrode, a platinum electrode as counter electrode and a commercial saturated calomel electrode (SCE) as reference electrode was used. With previously input parameters such as cleaning potential, plating potential, cleaning time, electrolysis time and sensitivity of the apparatus, this system can control the experimental procedure and effect data acquisition and handling. The output is a curve of dt/dE vs. E, where t is stripping time and E the potential of the working electrode. The curve can be displayed on a screen or recorded with an LZ 3-100 x–y recorder (Dahua Instrument Factory, Shanghai). The real-time sampling rate of the instrument is 5–1000 s^{-1}. Atomic absorption spectrometric measurements were made with a Shimadzu AA-670G atomic absorption spectrometer.

All glassware was thoroughly cleaned with nitric acid (1 + 1) before application. The SCE was immersed in distilled water for preservation after measurement in order to strip off manganese ions and other heavy metal ions probably present in the pores of the porous ceramic separator of the SCE. The working electrode was also preserved in distilled water after each use to prevent contamination.

Reagents

All reagents were of analytical-reagent grade and doubly distilled water was used throughout the study. Stock standard solutions (1×10^{-3} M) of manganese(II) and lead(II) were prepared from manganese(II) sulphate and lead(II) nitrate, respectively. A potassium hexacyanoferrate(II) stock standard solution (0.05 M) was prepared.

Buffer solution. In order to remove heavy metal ion impurities, 0.2 M sodium acetate was electrolysed with a platinum electrode at 3.0 V for 48 h and 0.2 M acetic acid was treated with a cation-exchange resin

RESULTS AND DISCUSSION

Pretreatment of glassy carbon electrode

In RPSA with a glassy carbon working electrode, the pretreatment of the electrode influences markedly the reproducibility, accuracy and precision of the measurements. The glassy carbon electrode can be pretreated mechanically (M), chemically (C) and electrochemically (EC). Several pretreatment methods have been compared and the following was selected. The electrode was ground on No. 700 coated abrasive and polished with a paste of powdered silicon carbide, ultrasonically cleaned in 7 M ammonia solution for 1 min, rinsed successively with ethylene dichloride, dilute nitric acid (1 + 10) and distilled water, then subjected to anodic polarization in distilled water at 800 mV (vs. SCE) for 600 s. The pretreated electrode showed good reproducibility, high sensitivity, a short stripping time and a flat baseline. Figure 1 shows the stripping potentiogram of manganese(II) on the pretreated electrode. The experimental results demonstrate that the electrode, once pretreated, can be used for several months and need not be treated again.

Influence of plating potential

In order to study the effect of the plating potential, a test solution of 2×10^{-6} M Mn(II)–4×10^{-4} M potassium hexacyanoferrate(II) in acetic acid–sodium acetate buffer (pH 6.0) was measured with an electrolysis time of 80 s at different plating potentials. The stripping potentiograms are shown in Fig. 2. At more positive or more negative potentials the stripping peak is somewhat deformed and the peak height decreases. Figure 3 shows the relationship between the height of the stripping peak and plating potential.

When the plating potential is in the range 650–800 mV the stripping peak height is basically

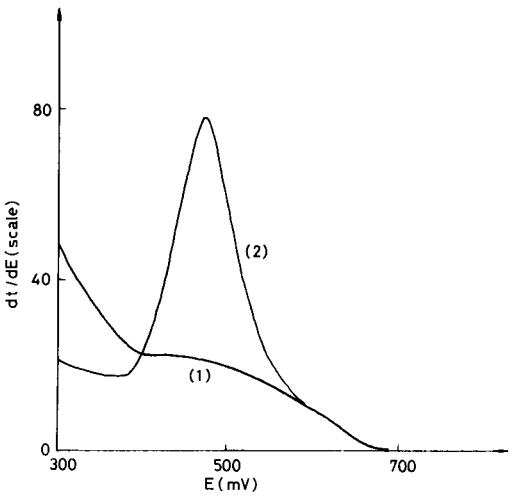

Fig. 1. Reductive potentiometric stripping potentiograms on a pretreated glassy carbon electrode. Conditions: acetic acid–sodium acetate buffer (pH 6.0); 4×10^{-4} M potassium hexacyanoferrate(II); plating at 900 mV for 80 s; recording potential, 700–300 mV; sensitivity of the apparatus, 50. Manganese(II) concentration: (1) 0 and (2) 2×10^{-6} M.

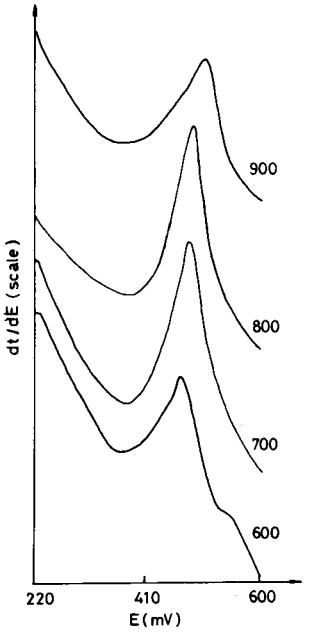

Fig. 2. Stripping curves of 2×10^{-6} M manganese(II) at different electrolysis potentials. Conditions: acetic acid–sodium acetate buffer (pH 6.0); 4×10^{-4} M potassium hexacyanoferrate(II); electrolysis time, 80 s; recording potential, 600–200 mV. Electrolysis potentials (mV) are shown on the curves.

independent of the plating potential. When the plating potential is less than 650 mV, the peak height increases with the increase in potential. This is because the electrode process is under the combined control of the charge transfer and diffusion when the overpotential is not large enough, so the current (i.e., the rate of deposition of manganese dioxide) is high at more anodic potentials and within the same interval the amount of manganese dioxide deposited on the surface of the glassy carbon working electrode is greater. When the plating potential is more anodic than 800 mV the peak height decreases with increase in potential, because the side electrode reaction, oxidation of manganese(II) to form permanganate, occurs at this large overpotential and its rate increases with increase in overpotential. When the potential is between 650 and 800 mV there is no side reaction and the electrode process is entirely under the control of diffusion, i.e., the current across the interface of the electrode depends entirely on the rate of diffusion of manganese ion from the bulk solution to the surface of the electrode. Hence the stripping peak height depends only on the concentration of manganese(II).

Choice of the concentration of potassium hexacyanoferrate(II) reducing agent

Potassium hexacyanoferrate(II) is very electrochemically reversible. Its standard oxidation potential is 886 mV more cathodic than the reduction potential of manganese dioxide. The experimental results indicated that $K_4[Fe(CN)_6]$ is a good reducing agent in the RPSA of manganese(II).

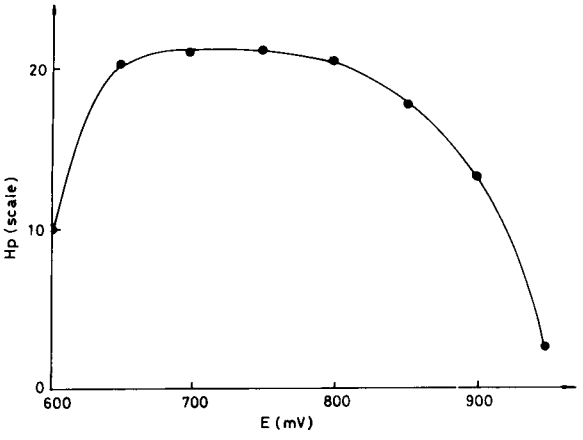

Fig. 3. Variation of stripping peak height with electrolysis potential. Experimental conditions as in Fig. 2.

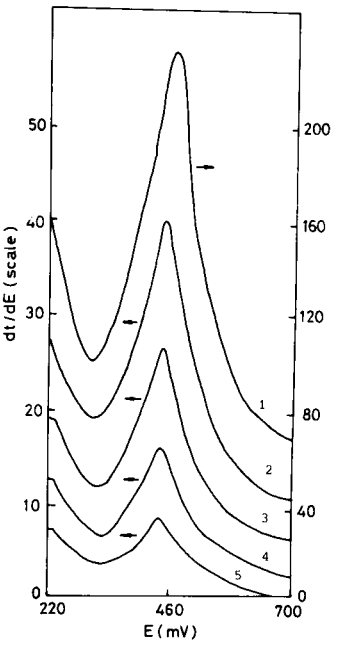

Fig. 4. Stripping curves of 2×10^{-6} M manganese(II) at different potassium hexacyanoferrate(II) concentrations. Conditions: acetic acid–sodium acetate buffer (pH 6.0); electrolysis potential, 750 mV; electrolysis time, 80 s; recording potential, 700–220 mV. Concentrations of potassium hexacyanoferrate(II): (1) 2×10^{-4}; (2) 4×10^{-4}; (3) 6×10^{-4}; (4) 8×10^{-4}; (5) 10×10^{-4} M.

Figure 4 shows the stripping curves of 2×10^{-6} M manganese(II) in pH 6 buffer containing different concentrations of potassium hexacyanoferrate(II). Figure 5 illustrates the relationship between the stripping peak height and the reciprocal concentration of potassium hexacyanoferrate(II). The stripping peak height decreases hyperbolically with increase in concentration and shows a linear relationship with the reciprocal the concentration. As the stripping time is proportional to the stripping peak height, the following equation can be obtained:

$$H = K_1 t = B' + K_2/C \qquad (4)$$

where H is the height of the stripping peak, t the stripping time, C the concentration of reducing

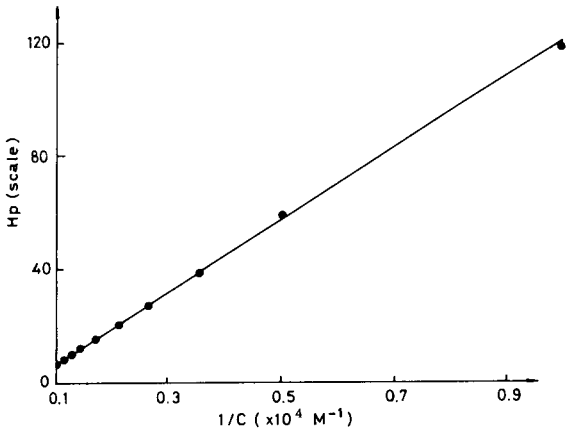

Fig. 5. Relationship between stripping peak height of 2×10^{-6} M manganese(II) and the reciprocal concentration of potassium hexacyanoferrate(II). Conditions: acetic acid–sodium acetate buffer (pH 6.0); electrolysis potential, 750 mV; electrolysis time, 80 s.

agent and B', K_1 and K_2 are constants. This equation can be rewritten as

$$1/C = -B'/K_2 + K_1 t/K_2 = B + Kt \quad (5)$$

where B and K are constants. Equation 5 is in accordance with the rate equation of the reaction of $K_4[Fe(CN)_6]$ with MnO_2 in reaction 3. According to reaction 3, the rate of the reaction is

$$-dC/dt = k'C^2C_H^4 \quad (6)$$

where, C_H is the H^+ concentration, which is a constant in a buffer. Equation 6 can be written as follows:

$$-dC/dt = kC^2 \quad (7)$$

Integrate the Eqn. 7:

$$1/C = B + Kt \quad (8)$$

Equation 8 is the same as the Eqn. 5. The result indicates that the stripping reaction may be a simple second order reaction.

The lower the concentration of $K_4[Fe(CN)_6]$, the higher is the stripping signal. However, if the $K_4[Fe(CN)_6]$ concentration is too low, the stripping time may be too long. In addition, the concentration of $K_4[Fe(CN)_6]$ must be high enough, so it may change little after some $K_4[Fe(CN)_6]$ was consumed during stripping. In our experiments the concentration of potassium hexacyanoferrate(II) is generally 4×10^{-4} M.

Influence of solution pH

Since H^+ is involved in both Eqn. 1 and Eqn. 3, solution pH may influence the RPSA of manganese. A higher pH is favourable to the formation of MnO_2(s) according to Eqn. 1 but unfavourable to the stripping of MnO_2 according to Eqn. 3. In addition, the following equilibriums in the solution are given:

$$[Fe(CN)_6]^{4-} = Fe^{2+} + 6CN^-$$
$$K' = 3.98\times10^{-36}\ (25°C) \quad (9)$$

$$H^+ + CN^- = HCN$$
$$K'' = 1.62\times10^{9}\ (25°C) \quad (10)$$

Combining the above two equations:

$$[Fe(CN)_6]^{4-} + 6H^+ \longrightarrow Fe^{2+} + 6HCN$$
$$K = 7.19\times10^{19}\ (25°C) \quad (11)$$

Hence the H^+ concentration strongly influences the stability of $K_4[Fe(CN)_6]$ in solution. The dissociation of $K_4[Fe(CN)_6]$ may increase when the pH decreases. Calculation shows that about 5% of $[Fe(CN)_6]^{4-}$ in equilibrium solution of 25°C dissociates at pH 4. The experiments also indicate that the solution changes gradually to a blue colour if pH $\not>$ 4.0. The reason is that Fe^{3+} formed in the anode owing to the oxidation of Fe^{2+} coming from the dissociation of $[Fe(CN)_6]^{4-}$ and the $[Fe(CN)_6]^{3-}$ formed in the reaction can combine with $[Fe(CN)_6]^{4-}$ and Fe^{2+} in solution to produce blue compounds. Hence the experiments must be conducted at a certain pH.

The experimental results indicate that when solution pH is in the range 5.0–7.0, the stripping peak of manganese(II) is well formed and the peak height is linearly related to the concentration of manganese(II). Although the shape of stripping peak is still good at pH 4.5, there is no longer a linear relationship between peak height and concentration of manganese(II). The shape of the stripping peak is deformed at pH < 4. Figure 6 shows the stripping curves of 2×10^{-6} M manganese(II) at different pH values.

According to electrode reaction 1, the stripping peak potential should be linearly related to the solution pH with a slope of -118 mV pH^{-1}. An experimental value of dE/dpH of -121 mV pH^{-1} was obtained, which agrees well with the theoretical value.

Linear range, detection limit and precision

In order to establish the linear range, experiments were done with acetic acid–acetate buffer (pH 6.0), 4×10^{-4} M potassium hexacyanoferrate(II) and electrolysis potentials and electrolysis times of 750 mV and 50 s, 750 mV and 200 s and 650 mV and 500 s, respectively. The results indicate that the stripping peak height versus concentration of manganese(II) relationship shows good linearity over the range 4×10^{-8}–1×10^{-5} M.

Generally, under certain experimental conditions the detection limit of potentiometric stripping analysis depends on the preconcentration time. The longer the preconcentration time, the lower is the detection limit. However, it is impossible to prolong the preconcentration time indefinitely in order to obtain a much lower detection limit. If the concentration of the analyte is too low, we cannot observe a well formed stripping peak because of the influences of interfering elements and other factors when the electrolysis time is too long. If the rate of preconcentration is not sufficiently larger than that of the reaction of the analyte deposited on the electrode with the reducing agent, no stripping signal can be detected. In the present experiments, at an electrolysis potential of 600 mV, an electrolysis time of 400 s and other conditions as above, 5×10^{-9} M manganese(II) produced a significant signal (ca. five times the standard deviation of the background), as shown in Fig. 7.

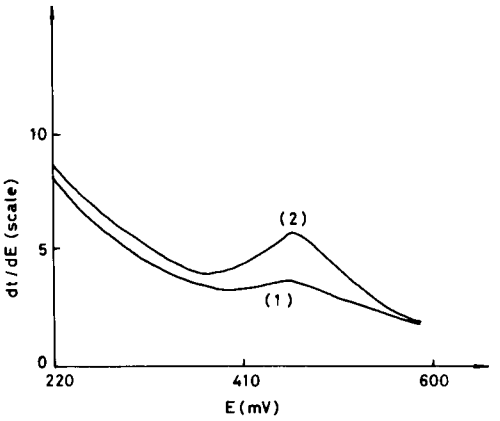

Fig. 7. Stripping curves of 5×10^{-9} M manganese(II) after plating for 400 s at 600 mV. Sensitivity of the apparatus, 5; other conditions as in Fig. 1. Mn(II) concentration: (1) 0 and (2) 5×10^{-9} M.

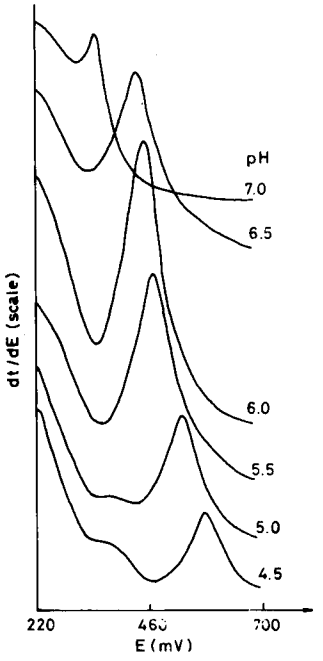

Fig. 6. Stripping potentiograms of 2×10^{-6} M manganese(II) at different pH values. Conditions: electrolysis potential, 850 mV; electrolysis time, 80 s; 4×10^{-4} M $K_4[Fe(CN)_6]$ in acetic acid–sodium acetate buffer.

The precision of the stripping procedure was evaluated by ten consecutive measurements under the conditions of 1×10^{-6} M manganese(II)–4×10^{-4} M potassium hexacyanoferrate(II), acetic acid–sodium acetate buffer (pH 6.0) and electrolysis for 50 s at 750 mV. A relative standard deviation of 0.5% was found.

Interferences

Among the metals that can be anodically plated (e.g., Pb, Ni, Ce, Fe, Tl, Co and Sb), lead is most likely to interfere because the two standard elec-

trode potentials of electrode reaction 1 and the electrode reaction

$$Pb^{2+} + 2H_2O \longrightarrow PbO_2(s) + 4H^+ + 2e \quad (12)$$

($E_0 = 1.455$ V vs. SHE)

are close to each other, with only about a 200 mV difference, and the influence of pH on both electrode potentials is the same. Hrabankova and co-workers [8,9] reported that this interference is serious in cathodic voltammetric stripping analysis. However, in RPSA this is not so because the stripping processes in the two cases are different.

When the electrolysis potential is lower than 750 mV lead does not influence the determination of manganese because at this potential lead(II) is not preconcentrated on the glassy carbon electrode. However, when the concentration of manganese increases to a certain level in the presence of a large amount of lead(II), at more negative potentials than the stripping peak potential of manganese a small stripping peak appears (Fig. 8). It is interesting that if there is only manganese or lead in solution, the small stripping peak does not appear; the reason for this is not clear. With an increase in the electrolysis potential a lead peak appears and increases with the decrease in the manganese peak; the two peaks are well separated and the manganese peak height is linearly related to its concentration.

Effect of temperature and deaeration

The stripping peak of manganese changes little if the sample solution is deaerated with pure nitrogen. With increase in the solution temperature the manganese peak decreases and at about 50°C the stripping peak disappears. This is because the rate of reaction of manganese dioxide with the reducing agent increases with increase in solution temperature, so during the preconcentration process more manganese dioxide precipitated on the electrode redissolves and diffuses into the bulk solution. At a sufficiently high temperature the redissolution rate of the analyte will reach its deposition rate, so the stripping peak may disappear.

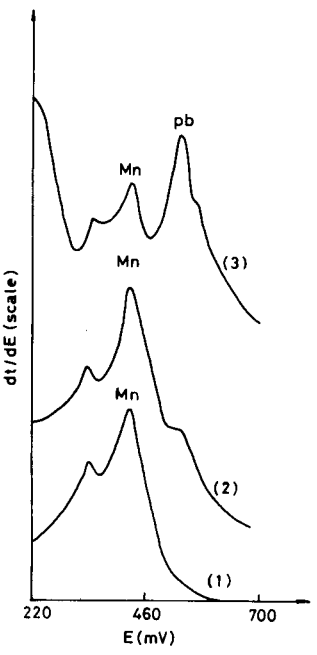

Fig. 8. Appearance of a small peak in the presence of a large amount of lead(II) and a sufficient amount of manganese(II), and the appearance of a lead peak when the plating potential is more positive than 850 mV. Conditions: 5×10^{-6} M manganese(II), 1×10^{-4} M lead(II) and 4×10^{-4} M potassium hexacyanoferrate(II) in the buffer of pH 6.0; electrolysis time, 50 s. Plating potentials: (1) 750; (2) 800; (3) 850 mV.

Analysis of artificial human hair sample solution and vegetable samples

In order to examine the practicality of this technique, an artificial human hair sample solution and two vegetable samples, cucumber and celery, were analysed.

The composition of the artificial human hair sample solution was 1×10^{-4} M Fe^{3+}, 1.5×10^{-3} M Ca^{2+}, 4×10^{-4} M Na^+, 1.6×10^{-5} M K^+, 3×10^{-4} M Zn^{2+}, 1.5×10^{-4} M Mg^{2+}, 3×10^{-5} M Cu^{2+}, 3×10^{-5} M Pb^{2+}, 2×10^{-5} M Al(III),

TABLE 1

Total manganese determined in two vegetables

Vegetable	Manganese ($\mu g\ g^{-1}$)	
	RPSA	AAS
Celery	72.6	75.4
Cucumber	98.3	96.5

Analytica Chimica Acta, 282 (1993) 133–137
Elsevier Science Publishers B.V., Amsterdam

Adsorptive stripping voltammetric behaviour of gold(III) at a hanging mercury drop electrode in the presence of 1-(2′-pyridylazo)-2-naphthol

A.Z. Abu Zuhri and M.S. El-Shahawi

Department of Chemistry, Faculty of Science, UAE University, P.O. Box 17551, Al-Ain (United Arab Emirates)

M.M. Kamal

Department of Chemistry, Faculty of Science, Assiut University, Assiut (Egypt)

(Received 18th January 1993; revised manuscript received 23rd April 1993)

Abstract

The stripping voltammetric determination of gold(III) based on the adsorptive accumulation of the Au(III)–1-(2′-pyridylazo)-2-naphthol complex on a hanging mercury drop electrode is reported. The reduction current of the adsorbed gold complex ions is measured by differential-pulse cathodic stripping voltammetry. The peak potential is at −0.8 V vs. Ag/AgCl. The effects of various parameters (pH, ligand concentration, accumulation potential and collection time) on the response in the presence of ethanol–water (30%, v/v) and 0.5 M sodium sulphate are discussed. A linear response up to 5.0×10^{-8} M and a relative standard deviation of 2.9% at 3.0×10^{-8} M were obtained. The UV–visible spectrum of the complex formed was also measured. The applicability of the method to the determination of gold(I) and mixtures of gold(I) and (III) compounds was also successfully carried out. Possible interferences by trace metals on the proposed method were examined.

Keywords: Stripping voltammetry; Gold; Waters

Several electrochemical techniques have been applied to the trace determination of gold. Jacobs [1] and Monien [2] reported the determination of gold using carbon and carbon paste electrodes, respectively. Yoshimori et al. [3] determined gold by anodic stripping voltammetry at a glassy carbon electrode. Recently, procedures have been developed for determining gold by adsorptive collection on a Rhodamine B-modified carbon paste electrode [4] and a trioctylamine-modified carbon electrode [5]. Adsorptive voltammetric measurements based on the complexing of different metal ions with various pyridylazo derivatives as complexing agents have also been investigated [6–10].

Correspondence to: A.Z. Abu Zuhri, Department of Chemistry, Faculty of Science, UAE University, P.O. Box 17551, Al-Ain (United Arab Emirates).

This paper describes an adsorptive voltammetric method for the determination of traces of gold based on differential-pulse cathodic stripping voltammetry (DPCSV) of the accumulated Au(III) complex with 1-(2′-pyridylazo)-2-naphthol (PAN) at a hanging mercury drop electrode. The optimum analytical conditions for gold determination are reported.

EXPERIMENTAL

Reagents and materials

Unless specified otherwise, all reagents were of analytical-reagent grade. All solutions were prepared from doubly distilled water and/or ethanol. A stock solution of 1 mg ml^{-1} gold (atomic absorption standard; BDH) was used and

diluted with water for standard addition whenever required. A 10^{-3} M stock solution of PAN was prepared in ethanol. Britton–Robinson buffer solutions of various pH were prepared and served as the supporting electrolyte in 0.5 M sodium sulphate. Gold(I) was prepared by reducing gold(III) by sulphur dioxide, the excess of sulphur dioxide being removed by boiling the solution for 10 min. The gold content was assayed by oxidation of the gold (I) solution with bromine water; the excess of bromine removed by boiling. The final gold(III) solution was then treated with excess of potassium iodide at pH 2 and the liberated iodine was determined by titration with 0.005 M sodium thiosulphate.

Apparatus

The voltammograms were recorded on a Metrohm 506 Polarecord with a Metrohm 663 VA stand. The working electrode was a hanging mercury drop electrode (HMDE) and Ag/AgCl and platinum wire served as reference and auxiliary electrodes, respectively. pH measurements were made with a Metrohm Model 632 pH meter. The UV–visible spectra of the solutions were recorded on a Pye-Unicam SP 8-100 spectrophotometer using a 1 cm quartz cell. All experiments were performed at room temperature (22 ± 0.5 °C).

Recommended procedure for gold determination

Determination of gold(III). Transfer 10 ml of the supporting electrolyte containing 1×10^{-7}–5×10^{-7} M PAN and 30% ethanol at pH 9.3 into the voltammetric cell. Purge cell with nitrogen for 10 min and apply an accumulation potential of -0.2 V to a fresh mercury drop for an accumulation period of 3 min with stirring. Stop the stirring and after 15 s record the voltammogram by applying a negative scan from 0.0 to -1.2 V using the differential-pulse mode. After the ground voltammogram has been obtained, repeat the adsorptive stripping with a new drop with the addition of gold sample. After each sample addition, pass nitrogen through for about 2 min.

Determination of gold(I). Transfer aliquot portions of gold(I) solution into a 100-cm^3 conical flask and add 5 cm^3 of bromine water. Allow the reaction mixture to stand for 3 min, then evaporate the solution gently on a hot-plate untill the excess of bromine has been completely removed. Determine the total content of the element by following the procedure for the determination of gold(III).

Analysis of mixtures of gold(I) and (III). Determine gold(III) in an aliquot of the mixture as described for the determination of gold(III). Then oxidize another aliquot sample with bromine water to form gold(III) as described for the determination of gold(I) and determine the total content of the element by measuring the peak current employing the procedure described for gold(III). On the basis of the proposed method, the difference between the stripping peak height in the first and second steps is equivalent to the gold(I), while the peak current in the first step is equivalent to gold(III).

RESULTS AND DISCUSSION

PAN was found to be electrochemically active in the presence of 30% ethanol–water. Therefore, different attempts employing different reduction media were used to select the optimum experimental conditions for measurement of the peak current and for the resolution of the reduction peak of PAN. In 30% (v/v) ethanol–water and with 0.05 M Na_2SO_4 as supporting electrolyte at pH 9.3, a well resolved reduction peak was observed at -0.82 V vs. Ag/AgCl and the peak current was high under the optimum experimental conditions. The solubility of PAN in ethanol is better than that in water and other common solvents. The observed reduction peak is attributed to the reduction of the azo group in the molecule [9]. In the presence of gold(III) ions, a well defined, much enhanced reduction peak is observed at the same potential of PAN reduction wave, as shown in Fig. 1. The peak current increased markedly in proportion to the Au(III) concentration and accumulation time. The enhanced peak possibly results from the adsorption of an Au(III)–PAN complex on the electrode surface.

To verify the adsorption behaviour of PAN

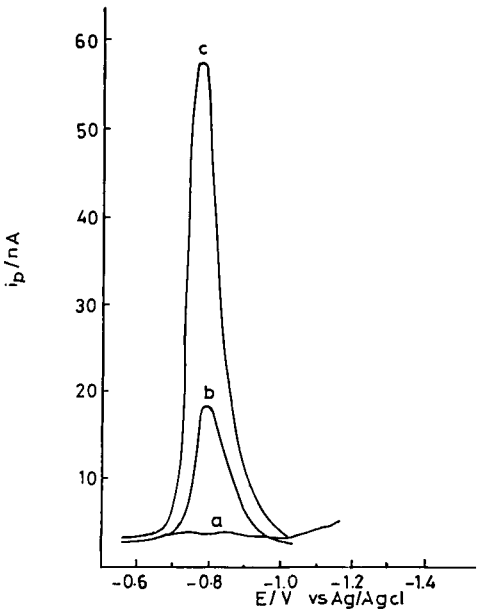

Fig. 1. Cathodic stripping voltammograms of (a) 4.0×10^{-8} M Au(III), (b) 1.5×10^{-7} M PAN and (c) 4.0×10^{-8} M Au(III)+ 1.5×10^{-7} M PAN at pH 9.35 with deposition at -0.2 V and a collection time of 3 min in the presence of 30% ethanol.

and its Au(III) complex at the electrode, electrocapillary curves were recorded. The curve of a solution containing PAN and Au(III) was similar to that of PAN itself, indicating adsorption of both the Au(III) complex and the reagent at the electrode. Using the method proposed by Gao [11], the composition of the electroactive complex formed on the electrode surface is 1 : 2 [Au(III) : PAN molar ratio].

The formation of an Au(III)–PAN chelate was confirmed from the UV–visible spectral measurements. The absorption spectrum of PAN in 30% ethanol at pH 9.3 exhibits four bands at 468, 415 (sh), 295 and 220 nm. The first three bands are assigned to $\pi \rightarrow \pi^*$ electronic transitions in the azo group, the hydrogen chelate ring and the 2-naphthol moiety [12]. The last band is due to a ^1L_a $\pi \rightarrow \pi^*$ transition characteristic of the pyridyl heterocyclic electronic system [13]. The UV–visible spectrum of gold(III) solution under the same conditions showed three well resolved bands at 316, 230 and 205 nm. On mixing gold(III) and PAN solution at pH 9.3 in 30% ethanol, the two Au(III) bands at higher wavelength disappear and the band at 468 nm of PAN becomes poorly resolved and is replaced with a shoulder at 450–470 nm, suggesting complex formation of gold(III) with PAN.

To elucidate the composition of the complex, solutions of gold(III) and reagent of 0.002 and 0.004 M were used. A series of solutions was prepared, keeping the concentration of Au(III) constant while varying the concentration of PAN and the pH values of the solutions were adjusted to 9.3 with Britton–Robinson buffer. The mixtures were allowed to stand for 20 min for completion of the reaction and the absorbance at 450 nm was measured against a blank containing no gold(III) under the same experimental conditions. The absorbance increased with up to a fourfold excess of the reagent, but increased steeply in the presence of up to a twofold excess of reagent, indicating the formation of a 1:2 gold(III)–PAN chelate [14].

To check the applicability of the adsorptive preconcentration behaviour of the Au(III)–PAN complex at the HMDE for the determination of trace amounts of gold(III) in water by DPCSV, different parameters, pH, collection time, accumulation potential and PAN and gold(III) concentrations, were investigated.

The influence of the pH of the aqueous solution on the peak height and peak potential on the adsorptive preconcentration of the Au(III)–PAN complex was examined at the HMDE. Other conditions were kept constant. The greatest peak enhancement (threefold at 3 min) and the best signal-to-background characteristics and reproducibility were obtained at pH 9.35. Therefore, pH 9.3 was adopted in subsequent work.

The dependence of the maximum stripping peak current on the collection time was examined for a sample containing 4.0×10^{-8} M Au(III) at pH 9.3 over the range 0–10 min. The maximum peak height was obtained at 3 min and was constant at longer times (Fig. 2). From the symmetrical shape of the reduction peak of the complex formed and the fact that the peak potential does not change with variation in the scan rate, it can be concluded that the electrochemical reduction of the Au(III)–PAN chelate is reversible.

The effect of the accumulation potential on the stripping peak current of the gold complex was examined over the potential range 0.0 to −0.5 V in 30% ethanol and 0.5 M Na_2SO_4 with the optimum pH and collection time. The largest peak current was obtained at a deposition potential of −0.2 V (Fig. 3). Therefore, −0.2 V was selected as the accumulation potential in the recommended procedure.

The effect of excess of the reagent was examined. The peak heights of a series of solutions containing 4.0×10^{-8} M gold(III) and various concentrations of the reagent were measured. It was found that the peak height increased linearly with increasing PAN concentration up to 5×10^{-7} M. The peak height tended to remain constant at larger excesses of the reagent. Under the optimum experimental conditions used, the maximum peak height was obtained at a ligand concentration of 5.0×10^{-7} M.

Determination of gold(III)

The greatest advantage of the determination of gold by the proposed adsorptive voltammetric method is the inherent sensitivity. Under the optimum conditions of pH 9.3 (Britton–Robinson buffer) in 30% ethanol, collection time 3 min, accumulation potential −0.2 V, negative differential-pulse scan (scan rate and amplitude) and reagent concentration 5.0×10^{-7} M, a linear relationship was obtained between the peak-height current ($I_F - I_B$) and the gold(III) concentration in the range 0–5.0×10^{-8} M, where I_F and I_B are the peak-height currents of the gold(III)–PAN complex and PAN, respectively, under the same optimum experimental conditions. The regression coefficient and detection limit were found to be 0.996 and 1.0×10^{-9} M, respectively. Reproducibility tests on ten results at 4.0×10^{-8} M Au(III) showed a relative standard deviation of 2.9%.

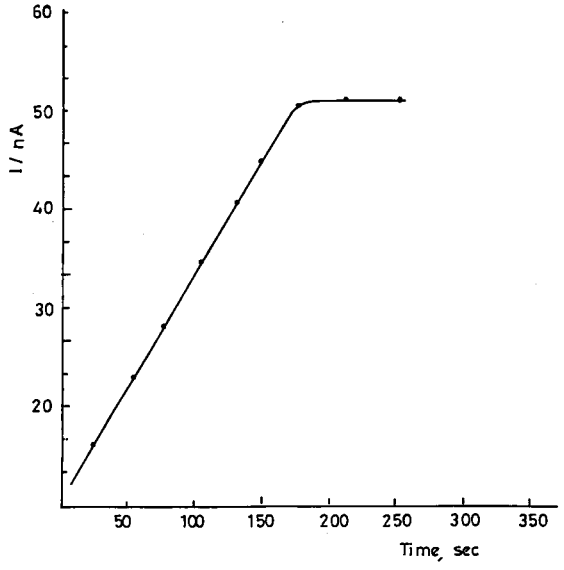

Fig. 2. Dependence of the reduction peak current on accumulation time for 4.0×10^{-8} M Au(III) with 1.5×10^{-7} M PAN at pH 9.35 with deposition at −0.2 V in the presence of 30% ethanol.

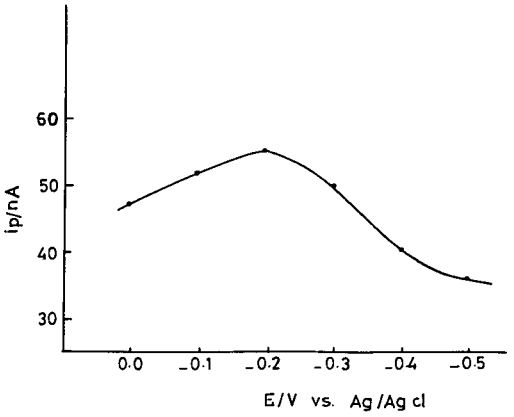

Fig. 3. Variation of peak current as a function of accumulation potential. Other conditions as in Fig. 1c.

The method was applied to the determination of gold(I), by prior oxidation to gold(III) by bromine water followed by the procedure described for the determination of gold(III). Satisfactory results were obtained and a linear calibration graph of gold concentration versus peak height was obtained.

The proposed method was also employed for the simultaneous determination of the gold(I) and gold(III) in a binary mixture in aqueous media. An aliquot of the mixture was first analysed employing the recommended procedure described for gold(III). Another aliquot was oxidized with bromine water, the unreacted bromine

was removed by boiling the solution and the peak current was measured by the procedure described for gold(III) determination. The difference between the stripping peak height was equivalent to the gold(I) concentration and the peak current in the first step was equivalent to the gold(III) concentration.

The method is also applicable to the determination of very low concentrations (less than nanomolar levels) in environmental samples. The sample is filtered through a 0.45-μm membrane followed by preconcentration of gold from a large sample volume of an acidic aqueous solution using porous polyurethane foam [15]. Elution of the sorbed gold by acetone from the foam column is possible, as reported previously [15], followed by determination using the proposed procedure.

Effect of diverse ions

The effects of diverse ions that are often present together with gold and form complexes with PAN were studied. The selectivity of the proposed method was examined by the determination of 4.0×10^{-8} M of gold(III) under the optimum experimental conditions. No interference was obtained in the presence of a relatively high excess (6.0×10^{-5} M) of Cd(II), Sr(II), Ba(II), Ca(II), Mg(II), Pd(II), Bi(III), Ni(II), Pb(II), Zn(II), La(II) and Ce(III). Bi(III), Ni(II), Pb(II), Zn(II), La(III), Cr(III) and molybdate at 1.0×10^{-7} M decreased the peak current of gold(III) by about 20–30%, while Cu(II), Fe(II) and Co(II) at 1.0×10^{-7} M interfered seriously. Ions such as molybdate may form mercury(I) salts covering the HMDE. The possible formation of mercury(I) molybdate [16,17] could explain the decrease in the reduction peak height of the Au(III)–PAN chelate. Nevertheless, the determination of gold was not affected by the presence of up to 20 g l^{-1} of Mo(VI).

REFERENCES

1 E.A. Jacobs, Anal. Chem., 35 (1963) 2112.
2 H. Monien, Fresenius' Z. Anal. Chem., 237 (1968) 409.
3 T. Yoshimori, M. Arakawa and T. Takeuchi, Talanta, 12 (1965) 147.
4 G. Koelbi, K. Kalcher and A. Voulgaropoulos, Fresenius' Z. Anal. Chem., 342 (1992) 83.
5 Q. Shi, J. Hong, R. Lu, G. Ma and Y. Zhou, Gaodeng Xuexiao Huaxue Xuebao, 11 (1990) 414; Anal. Abstr., 54 (1991) 2D21.
6 P.A.M. Farias, S.L.C. Ferreira, A.K. Ohara, M.B. Bastos and M.S. Goulart, Talanta, 39 (1992) 1245.
7 J. Zhao and W. Jin, J. Electroanal. Chem., 256 (1988) 181.
8 J. Lu, W. Jin and S. Wang, Anal. Chim. Acta, 238 (1990) 375.
9 J. Zhao and W. Jin, J. Electroanal. Chem., 267 (1989) 271.
10 P.A.M. Farias and A.K. Ohara, Electroanalysis, 3 (1991) 985.
11 X. Gao, Handbook on the Physics and the Chemistry of Rare Earths, Elsevier, Amsterdam, 1986, p. 163.
12 P.W. Alexander and R.J. Sleet, Aust. J. Chem., 23 (1970) 1183.
13 M.S. Masoud, A.A. Hasanein and A.M. Heiba, Spectrosc. Lett., 17 (1984) 441.
14 J.H. Yoe and A.L. Jones, Ind. Eng. Chem., Anal. Ed., 16 (1944) 111.
15 T. Braun and A.B. Farag, Anal. Chim. Acta, 99 (1978) 1.
16 E. Laviron, J. Electroanal. Chem., 52 (1974) 355.
17 C.H. Khan and C.M.G. van den Berg, Mar. Chem., 27 (1989) 31.

Analytica Chimica Acta, 282 (1993) 139–144
Elsevier Science Publishers B.V., Amsterdam

Voltammetric determination of tetrathiomolybdates, an effective antidote in acute intoxication by copper(II) and other toxic metal ions

Stella Th. Giroussi and Anastasios N. Voulgaropoulos

Analytical Chemistry Laboratory, Department of Chemistry, Aristotle University of Thessaloniki, 54006 Thessaloniki (Greece)

Aristomenis Ayiannidis

Chemistry Laboratory, Veterinary Faculty, Aristotle University of Thessaloniki, 54006 Thessaloniki (Greece)

(Received 5th March 1993; revised manuscript received 5th May 1993)

Abstract

A selective, sensitive and reliable voltammetric method for the determination of free tetrathiomolybdates, an antidote in acute intoxication by copper(II) and other toxic metal ions, is developed. Cyclic voltammetry of tetrathiomolybdates in aqueous solutions reveals a substantially different behaviour with respect to dimethylformamide solutions. The irreversible kinetically controlled reduction of $HgMoS_4$ in aqueous solutions is exploited to determine MoS_4^{2-} by differentical pulse voltammetry (DPV). MoS_4^{2-} and MoO_4^{2-} show quite different electrochemical behaviour and the reduction peak of $HgMoS_4$ at -0.43 V in acetate buffer at pH 4.9 is well separated from the peaks of MoO_4^{2-}; on the other hand, in phosphate buffer of pH 7.3 MoO_4^{2-} did not give any peak, while $HgMoS_4$ gave one at -0.67 V. The hydrolysis of MoS_4^{2-} is also studied. Cadmium complexes with MoS_4^{2-}, but does not interfere in the determination of free tetrathiomolybdates. The determination limit is 0.02 μg ml^{-1} for DPV and can be lowered to 1 ng ml^{-1} by employing differential pulse adsorptive stripping voltammetry; the relative standard deviation is less than 4%.

Keywords: Cyclic voltammetry; Differential pulse voltammetry; Copper(II); Molybdates; Tetrathiomolybdates; Toxic metals

In acute intoxication by copper(II) and other toxic metal ions such as nickel and zinc the most convenient and effective treatment proved to be the subcutaneous or intravenous injection of ammonium or sodium tetrathiomolybdate [1–5]. Effective control of copper poisoning in sheep was obtained by six intravenous injections of tetrathiomolybdates at three-day intervals (0.5 mg of tetrathiomolybdates/ml saline) [3]. However, above certain concentrations tetrathiomolybdates are toxic to mice (intraperitoneal $LD_{50} = 176$ mg kg^{-1}) [2]. The mechanism of toxic metals excretion is not quite clear and further investigations are needed.

The reaction of Cu(II) with tetrathiomolybdates produces an insoluble copper-containing product, that offers a plausible explanation of how molybdenum can cause copper deficiency in ruminants [6]; however, the results of the stoichiometry of the reaction between Cu(II) and MoS_4^{2-} are not in agreement with this explanation [6].

So far in the literature only spectroscopic methods for the determination of total molybde-

Correspondence to: N. Voulgaropoulos, Analytical Chemistry Laboratory, Department of Chemistry, Aristotle University of Thessaloniki, 54006 Thessaloniki (Greece).

num [5,7,8] or for the qualitative identification of MoS_4^{2-} [9] are reported.

Thus, the development of a reliable and sensitive method for the determination of tetrathiomolybdates is a matter of great importance for the elucidation of the mechanism of toxic metals excretion and for the control of tetrathiomolybdate doses. In the present paper a reliable and sensitive voltammetric method, based on the reduction of $HgMoS_4$, has been developed.

EXPERIMENTAL

Reagents

Ammonium tetrathiomolybdate was obtained from Aldrich and was used without further purification. All other reagents used were Merck pro analysis. Acetate buffer was 2 M in CH_3COOH and 2 M in CH_3COONa while phosphate buffer was 0.04 M in K_2HPO_4 and 0.01 M in KH_2PO_4.

Apparatus

Voltammetric measurements were done using a Metrohm Herisau E 506 Polarecord equipped with a Metrohm Herisau E 505 voltammetric stand. Sweep voltammograms were taken with an electrochemical system consisting of a Wenking voltage scan generator Model 72 Bank Electronic, a biopotentiostat type BI-PAD Tacussel Electronic and a Hewlett Packard 70463 *X–Y* recorder. As working electrode an EA 290 Metrohm hanging mercury drop electrode with a surface area of 2.22 mm^2 was used; the counter electrode was platinum wire and the reference electrode was Ag/AgCl saturated with KCl. All measurements were taken in a thermostated 50-ml voltammetric cell. A thermostated water circulator (Haake) was used to maintain the temperature of the solution in the voltammetric cell at 25 ± 0.05°C. The solutions were stirred by a magnetic stirrer at 55 Hz and a polyethylene-covered magnetic bar of 1.5 cm length, 3 mm diameter. Highly purified nitrogen gas was used to deoxygenate all solutions for 10 min before recording the voltammograms and its flow was maintained over the solution to prevent oxygen interference. pH measurements were taken with an Orion research Model 701 A digital ion analyzer at 25 ± 0.05°C. Eppendorf micropipettes were used to pipette μl volumes of solutions.

Procedures

Tetrathiomolybdates soluble in TCA. A volume of 1.5 ml of 20% trichloroacetic acid (TCA) was added to 1 ml of plasma. Then the mixture was centrifuged at 3000 rpm for 5 min (1000 *g*). A volume of 0.5 ml of the supernatant was introduced in a polarographic cell which contained 20 ml of phosphate buffer. The measurement was done after 10 min deoxygenation with highly purified nitrogen gas.

Tetrathiomolybdates not binding to proteins. A volume of 1 ml of the same sample of plasma was transferred to an ultrafiltration unit and was pressurized with nitrogen at 30 p.s.i. Ultrafiltration was performed with a YM2 Amicon filter, which was primarily washed with deionized water, by leaving it to stand in a beaker filled with water for 1 h. After ultrafiltration the filter was washed with an aqueous solution of 5% NaCl and three times with 2 M HCl and the washings were combined with the filtrate. A volume of 0.5 ml of the filtrate was introduced in a polarographic cell, and the measurement was done as described previously.

RESULTS AND DISCUSSION

Electrochemical behaviour of MoS_4^{2-} and MoO_4^{2-}

Very little is known about the electrochemical behaviour of MoS_4^{2-}. Thus, it was found [6] by cyclic voltammetry that MoS_4^{2-} undergoes a reversible one-electron reduction at -2.50 V, relative to the standard calomel electrode, in dimethylformamide (DMF) solutions.

However, this is not the case in aqueous solutions and in phosphate buffer, pH 7.3, as is shown in Fig. 1. The cyclic voltammogram shows an irreversible, kinetically controlled reduction, which can be used to determine MoS_4^{2-}; peak 1 corresponds to the first cycle, while peak 2 corresponds to the subsequent second cycle.

For the accurate and sensitive determination of MoS_4^{2-}, the differential pulse (DP) mode is

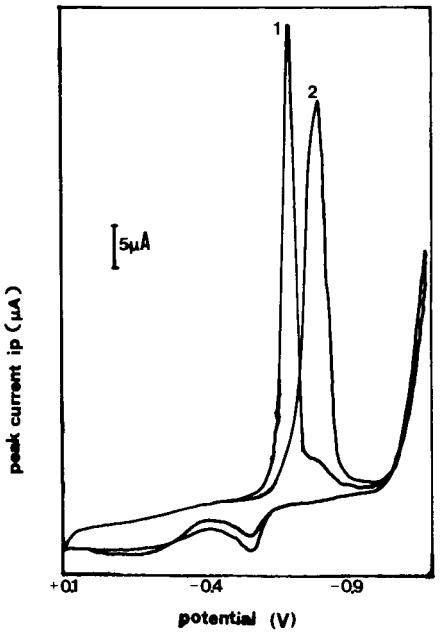

Fig. 1 . Cyclic voltammogram with HMDE of tetrathiomolybdates (4.5×10^{-4} M) in phosphate buffer, pH 7.3.

employed and the voltammograms are compared to those taken for MoO_4^{2-}, as is shown in Fig. 2. The reduction of MoO_4^{2-} takes place in two steps: Mo(VI) → Mo(V), peak A, and Mo(V) → Mo(III), peak C [10], while MoS_4^{2-} reacts with mercury to form $HgMoS_4$, which is then reduced producing a peak at −0.43 V. This mechanism is verified by the fact that the $HgMoS_4$ reduction peak is absent when glassy carbon is used as a working electrode. Note that the reduction peak of MoS_4^{2-} at −0.43 V is well separated from the peaks of MoO_4^{2-} in acetate buffer at pH 4.9. In phosphate buffer, pH 7.3, the behaviour is essentially different. MoO_4^{2-} does not give any peak, while the peak potential of MoS_4^{2-} is shifted to −0.67 V and it is considerably increased in height, as can be seen in Fig. 3. Thus, the phosphate buffer is chosen to study the DP voltammetric determination of MoS_4^{2-}. The influence of the pH on the peak height is given in Fig. 4. The optimum peak height is observed at pH 7.3.

Hydrolysis of MoS_4^{2-}

Tetrathiomolybdates are hydrolysed according to a pseudo-first order kinetic reaction described by the equation $\log(C_0/C_t) = -8.36\times10^{-3} + 2.85\ (\pm0.34)\times10^{-3}\ t$ with a rate constant, $k = 3.16\times10^{-3}\ min^{-1}$, where C_0 = initial concentration of MoS_4^{2-} and $C_t = MoS_4^{2-}$ concentration at time t. Thus, the analysis of tetrathiomolybdates has to be carried out immediately, in order to avoid significant errors.

Calibration curve

The calibration curve is linear from 0.02 to 1.60 μg ml^{-1} in accordance with the least-squares equation $y = 0.61x$. Seven replicate determinations for two different concentrations were performed to estimate the reproducibility and accuracy of the proposed method as is shown in Table 1. For concentrations from 0.02 μg ml^{-1} to 1 ng ml^{-1} DPASV should be applied. To optimize adsorption conditions the influence of adsorption potential and time on the peak current is studied. Maximum adsorption takes place at potentials from −0.4 to −0.5 V and a saturation is reached

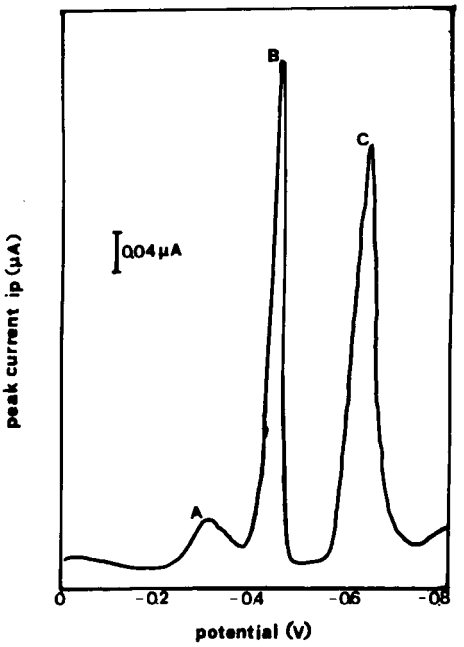

Fig. 2. Differential pulse voltammograms of tetrathiomolybdates (4.1×10^{-7} M) and molybdates (4.1×10^{-7} M) in acetate buffer, pH 4.9. (A) and (C): successive reduction of MoO_4^{2-}, Mo(VI) → Mo(V) and Mo(V) → Mo(III), respectively; (B) reduction of $HgMoS_4^{2-}$. E_{in} = 0 V; pulse amplitude = −50 mV; scan rate = 10 mV s^{-1}.

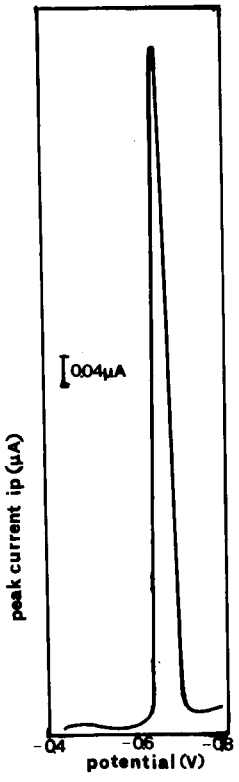

Fig. 3. Differential pulse voltammogram of tetrathiomolybdate (4.1×10^{-7} M) in phosphate buffer, pH 7.3.

after 10 min stirring at 55 Hz and 25 ± 0.05°C as is shown in Fig. 5. At optimum conditions tetrathiomolybdate as low as 1 μg ml^{-1} can be determined.

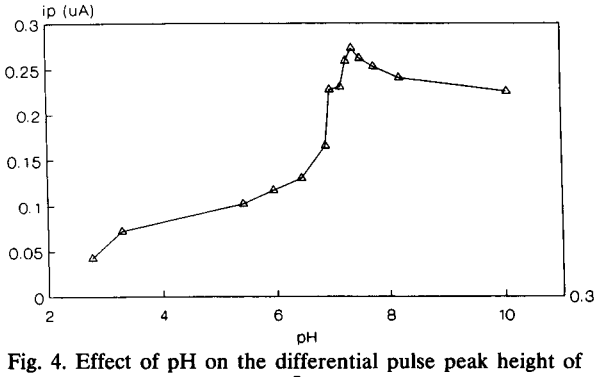

Fig. 4. Effect of pH on the differential pulse peak height of tetrathiomolybdates (4.1×10^{-7} M) in phosphate buffer. E_{in} = 0 V; pulse amplitude = −50 mV; scan rate = 10 mV s^{-1}.

TABLE 1

Replicate determinations of tetrathiomolybdates

MoS_4^{2-} added (ng ml^{-1})	MoS_4^{2-} found (Mean value) (ng ml^{-1})	R..S.D. (%) (n = 7)
16.5	16.4	3.1
276.0	273.0	2.2

TABLE 2

Recovery of tetrathiomolybdates in sheep blood plasma before and after treatment with TCA [a]

MoS_4^{2-} added (ng ml^{-1})	MoS_4^{2-} found (ng ml^{-2})		Recovery (%)	
111	115 ± 2 [b]	81 ± 2 [c]	103 [b]	73.0 [c]
252	241 ± 2 [b]	181 ± 2 [c]	95.9 [b]	71.8 [c]
323	335 ± 2 [b]	224 ± 2 [c]	105 [b]	68.7 [c]
551	530 ± 1 [b]	388 ± 1 [c]	96.3 [b]	70.4 [c]
736	764 ± 1 [b]	515 ± 1 [c]	104 [b]	70.0 [c]

[a] n = 3, confidence level 90%. [b] Standard additions were made before the sample treatment with TCA. [c] Standard additions were made after the sample treatment with TCA.

Interferences

From the common heavy metals only cadmium is reduced at about the same potential as $HgMoS_4^{2-}$ (−0.60 V) and could be a possible interference, if its concentration exceeds 1 μg ml^{-1}. However, cadmium forms a 1:1 complex with MoS_4^{2-}, as proved by amperometric titration: as the cadmium concentration increases the MoS_4^{2-} peak decreases and finally disappears,

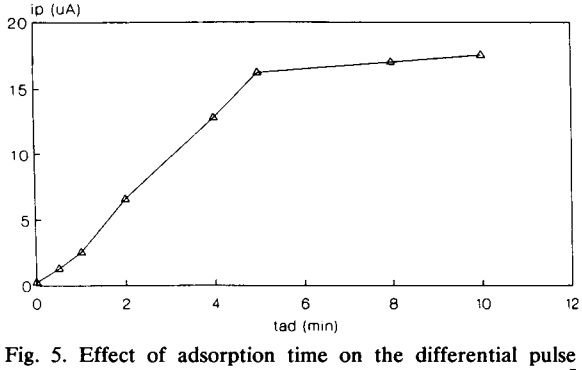

Fig. 5. Effect of adsorption time on the differential pulse adsorptive stripping height of tetrathiomolybdates (4.1×10^{-7} M), in phosphate buffer, pH 7.3. E_{ad} = −0.4 V; E_{in} = 0 V; pulse amplitude = −50 mV, scan rate = 10 mV s^{-1}.

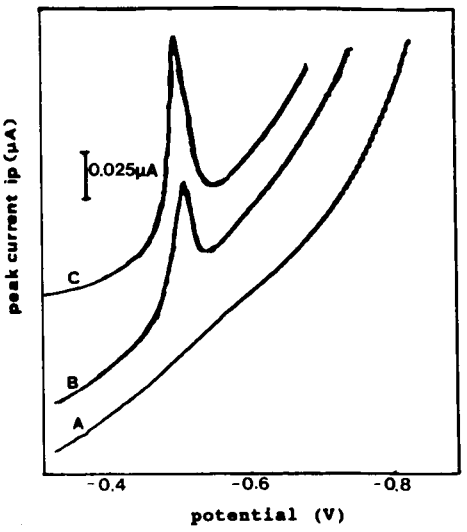

Fig. 6. Differential pulse voltammograms of sheep blood plasma treated by TCA. (A) plasma; (B) plasma + 320 ng ml^{-1} MoS_4^{2-} added before treatment with TCA; (C) plasma + 640 ng ml^{-1} MoS_4^{2-} added before treatment with TCA. $E_{in} = 0$ V; pulse amplitude = −50 mV; scan rate = 10 mV s^{-1}.

when the MoS_4^{2-}: Cd ratio reaches 1. Given that the proposed method refers to the determination of free MoS_4^{2-}, it is obvious that cadmium, if present, is complexed with MoS_4^{2-} and does not interfere.

Applications to sheep blood plasma

To validate the method, tetrathiomolybdates were determined in plasma of sheep blood after removal of proteins by TCA sample pretreatment as is shown in Fig. 6 as well as by ultrafiltration as is shown in Fig. 7. In the former procedure the

TABLE 3

Recovery of tetrathiomolybdates in sheep blood plasma by ultrafiltration sample pretreatment [a]

Sample	MoS_4^{2-} added (ppb)	MoS_4^{2-} found (ppb)	
a	632	2 ± 0.5 [b]	640 ± 1 [c]
a	781	150 ± 3 [b]	770 ± 2 [c]
b	737	10 ± 1 [b]	742 ± 2 [c]
b	948	221 ± 2 [b]	945 ± 2 [c]

[a] $n = 3$, confidence level 90%. [b] Standard additions were made before ultrafiltration. [c] Standard additions were made after ultrafiltration.

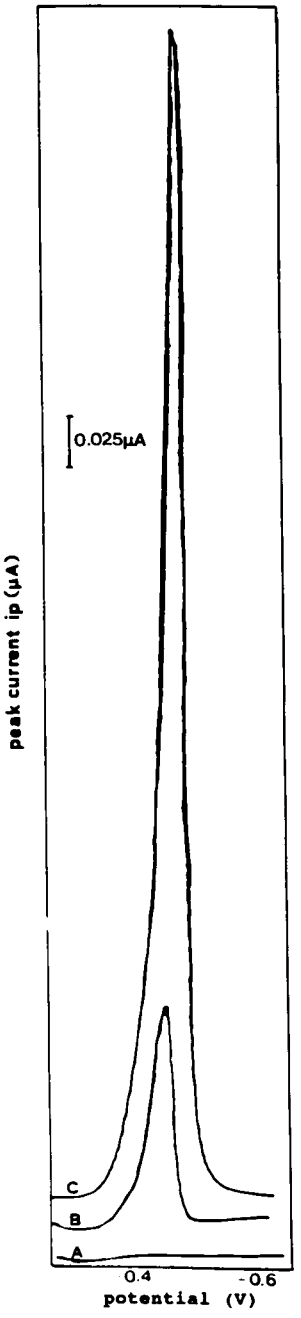

Fig. 7. Differential pulse voltammograms of sheep blood plasma after ultrafiltration. (A) plasma; (B) plasma + 320 ng ml^{-1} MoS_4^{2-} added before ultrafiltration; (C) plasma + 640 ng ml^{-1} MoS_4^{2-} added before ultrafiltration. $E_{in} = 0$ V; pulse amplitude = −50 mV; scan rate = 10 mV s^{-1}.

standard additions of MoS_4^{2-} are made before and after the sample petreatment. The results are shown in Table 2. It can be seen that if the standards are added after the TCA pretreatment the recovery is around 70% due to about 30% loss of MoS_4^{2-} by hydrolysis and coprecipitation with the plasma proteins. On the other hand, if the standards are added before the TCA pretreatment the recovery is satisfactory, because the MoS_4^{2-} contained in the sample as well as the added standards are proportionally lost. However, in the ultrafiltration sample petreatment there is a certain amount of tetrathiomolybdates bound to proteins which differs from sample to sample, as can be seen in Table 3.

Conclusions

The proposed method is very sensitive, selective, reproducible and accurate for the determination of free MoS_4^{2-}; moreover, it can be used to differentiate between MoS_4^{2-} and MoO_4^{2-}, as well as between MoS_4^{2-} bound and non-bound to proteins.

We wish to thank Dr. A. Giannakoudakis from the Physical Chemistry Laboratory and Dr. P. Arzoglou and his coworkers from the Biochemistry Laboratory of the Aristotle University of Thessaloniki for the facilities provided to take the cyclic voltammograms and to perform the ultrafiltration procedure, respectively. S.Th.G. is a post-graduate student, holding a scholarship from the Greek State Scholarship Foundation.

REFERENCES

1 S.R. Gooneratne, I. McC. Howell and J.M. Gawthor, Br. J. Nutr., 46 (1981) 457.
2 S.H. Laurie, M.A. Basinger and M.M. Jones, Inorg. Chim. Acta, 91 (1984) 121.
3 W.R. Humphries, C.F. Mills, A. Greig, L. Roberts, D. Inglis and G.J. Halliday, Vet. Rec., 119 (1986) 596.
4 W.R. Humphries, P.C. Morrice and I. Bremner, Vet. Rec., 123 (1988) 51.
5 R.L. Kincaid and C.L. White, J. Anim. Sci., 66 (1988) 3252.
6 S.H. Laurie, D.E. Pratt, J. Raynor and J. Barrie, Inorg. Chim. Acta, 123 (1986) 193.
7 J.B. Bingley, J. Agric. Food Chem., 11 (1963) 130.
8 G. Norheim and E. Waasjo, Z. Anal. Chem., 286 (1977) 229.
9 J.W. McDonald, G.D. Friesen, D.L. Rosenhein and W.E. Newton, Inorg. Chim. Acta, 72 (1983) 205.
10 E. Barrado, R. Pardo and P. Sanchez Batanero, Anal. Lett., 21 (1988) 1221.

Analytica Chimica Acta, 282 (1993) 145–152
Elsevier Science Publishers B.V., Amsterdam

Studies on electrochemical behaviour of cephalexin

Qilong Li and Shouai Chen

Department of Chemistry, Beijing Normal University, Beijing 100875 (China)

(Received 8th February 1993; revised manuscript received 28th April 1993)

Abstract

Cephalexin, which contains an unsubstituted 3-methyl group, but no reducible group, does not give a reduction peak at a dropping mercury electrode, whereas its degradation product does. The degradation of cephalexin was carried out in 0.1 M NaOH at 100°C for 20 min. A sensitive reduction peak of cephalexin was obtained by adsorptive stripping voltammetry in 0.1 M NaOH at an accumulation time of 60 s. The peak potential is −0.80 V (vs. Ag/AgCl). The peak current is directly proportional to the concentration of cephalexin, with a detection limit of 5.0×10^{-10} M. The electrochemical behaviour of cephalexin was studied. The reduction process is quasi-reversible with adsorptive characteristics. The mechanisms of degradation and electrode reaction are discussed.

Keywords: Stripping voltammetry; Cephalexin; Pharmaceuticals

Cephalexin {7-(D-2-amino-2-phenylacetamido)-3-methyl-8-oxo-5-thia-1-azabicyclo[4.2.0]oct-2-ene-2-carboxylic acid} is a cephalosporin antibiotic. It contains an unsubstituted 3-methyl group and no other reducible group, and does not give a peak at a mercury electrode, but some of its degradation products act as depolarizers. As regards the mechanism of degradation of cephalexin, Fogg et al. [1] considered that the different yields are probably associated with different degradation routes under different conditions of acidity or alkalinity. At pH 8.5 the degradation products were hydrogen sulphide, the diketopiperazine derivative and probably 2-hydroxy-3-phenyl-6-methylpyrazine at 80°C. At pH 5.7, hydrogen sulphide was obtained in relatively low yield at 80°C (about 24% of the total sulphur after 30 h). Degradation at 80°C in buffered solution at pH showed a similar pattern to that in unbuffered solution at pH 5.7, but the rate of degradation was slower. The yield of hydrogen sulphide after 4 h was only 5%. Hydrogen sulphide was more difficult to purge when the degradation was carried out at pH 10 in borate or phosphate buffer.

Determinations of cephalexin by chromatography [2–4], spectrophotometry [5–9], a fluorescence method [10] and electroanalytical methods [11–13] have been reported. The sensitivity of the fluorescence method [10] and differential-pulse polarography [12] was high, with detection limits of 0.01 and 0.1 μg ml^{-1}, respectively. The electrochemical behaviour and the mechanism have not previously been studied in detail. In this work, a sensitive adsorptive stripping voltammetric method is described for the determination of cephalexin, with a detection limit of 5.0×10^{-10} M. The sensitivity is much higher than those of the above methods. The electrochemical behaviour of cephalexin was examined further; the mechanisms of electrode and degradation reactions are discussed.

Correspondence to: Qilong Li, Department of Chemistry, Beijing Normal University, Beijing 100875 (China).

EXPERIMENTAL

Reagents

All reagents were of analytical-reagent grade. A stock standard solution of cephalexin (1.0×10^{-3} M) in water was prepared by dissolving 0.0365 g of cephalexin of 99.0% purity in doubly distilled water, transferring the solution into a 100-ml volumetric flask, diluting to volume and mixing. The solution was stored in the dark under refrigeration. Working standard solutions (1.0×10^{-5} and 1.0×10^{-7} M) were prepared by dilution with water.

Apparatus

A Model 370-8 Electrochemistry System (EG &G Princeton Applied Research) was used for linear-sweep and cyclic voltammetry and constant-potential coulometry. A Model MHM-20E pH meter (Japan) was used for pH determinations. A Model 501 thermostat (Experimental Instrument Factory, Shanghai) was used to maintain a temperature of 25 ± 0.2°C. A Model 883 polarograph (Shanghai Analytical Instrument Factory, Shanghai) was employed. A Model UV-250 ultraviolet–visible spectrophotometer (Japan) was used for recording absorption spectra. All experiments were performed at room temperature and dissolved oxygen was removed by passing pure nitrogen through the solutions.

RESULTS AND DISCUSSION

Electrochemical behaviour

The degradation of cephalexin was carried out in 0.1 M sodium hydroxide solution at 100°C for 20 min. A sensitive reduction peak of cephalexin was obtained by adsorptive stripping voltammetry in 0.1 M sodium hydroxide solution at an accumulation time of 60 s. The peak potential, E_p was -0.80 V (vs. Ag/AgCl). The peak current, I_p was directly proportional to the concentration of cephalexin, with a detection limit of 5.0×10^{-10} M.

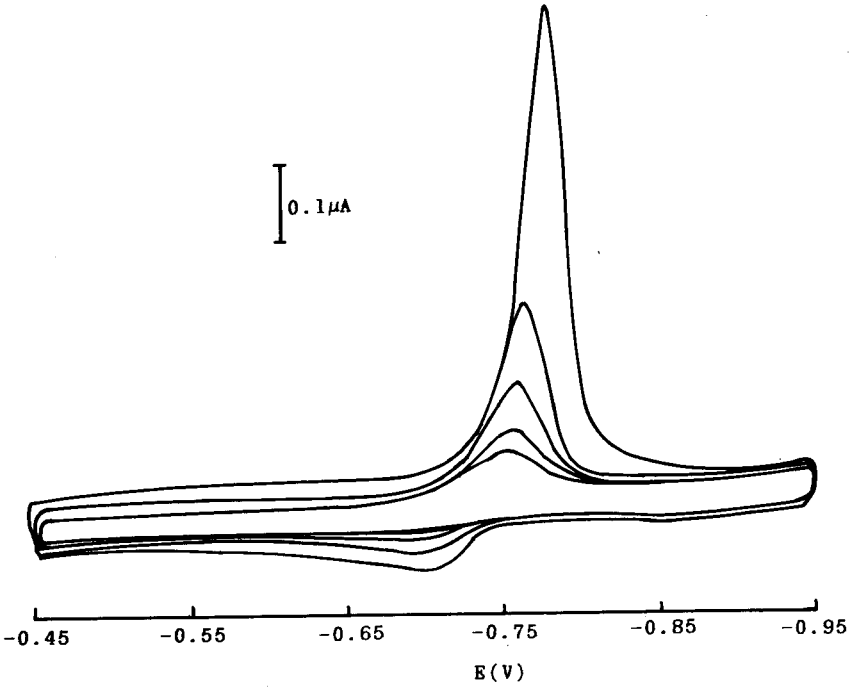

Fig. 1. Typical repetitive cyclic voltammograms. Conditions: 0.1 M NaOH, 5.0×10^{-7} M cephalexin, $E_i = -0.45$ V, $v = 100$ mV s^{-1}, $t_{acc} = 60$ s, $s = 2$ μA.

Adsorptive properties. Cyclic voltammetry of the system was investigated by using the Model 370-8 Electrochemistry System with a hanging mercury drop electrode (HMDE). Typical repetitive cyclic voltammetric curves are shown in Fig. 1. The reduction peak of cephalexin is much higher than the oxidation peak, $I_{p,c}/I_{p,a} \gg 1$. After the peak, the current decreases to the background level. After an accumulation time of 60 s, the reduction peak of the first scan is maximum, and during the scans the current decreases and the peak potential becomes more positive. The peak current of cephalexin increases with increasing accumulation time before scanning (see Fig. 2), indicating the characteristics of an adsorptive wave [14,15].

With different accumulation times, the effect of the scan rate on the peak current is different (see Fig. 3). When the accumulation time $t_{acc} = 0$, the peak current I_p is directly proportional to the square root of the scan rate, $v^{1/2}$; the relationship between I_p and v shows a downward-inclined curve, indicating that the electrode process is diffusion controlled (curve a in Fig. 3). When $t_{acc} = 60$ s, I_p is a linear function of v; the I_p vs. $v^{1/2}$ curve shows an upward inclination, indicating that the electrode process is adsorption controlled (curve b in Fig. 3) [16,17].

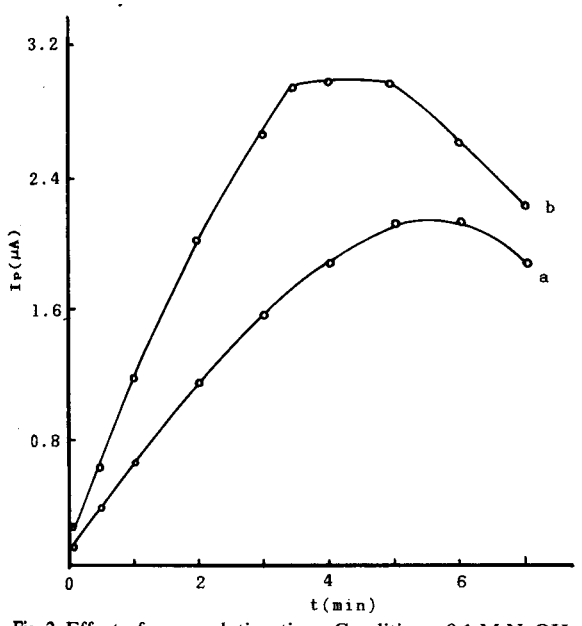

Fig. 2. Effect of accumulation time. Conditions: 0.1 M NaOH, $E_i = 0.45$ V, $v = 100$ mV s^{-1}. (a) 5.0×10^{-7} M cephalexin; (b) 1.0×10^{-6} M cephalexin.

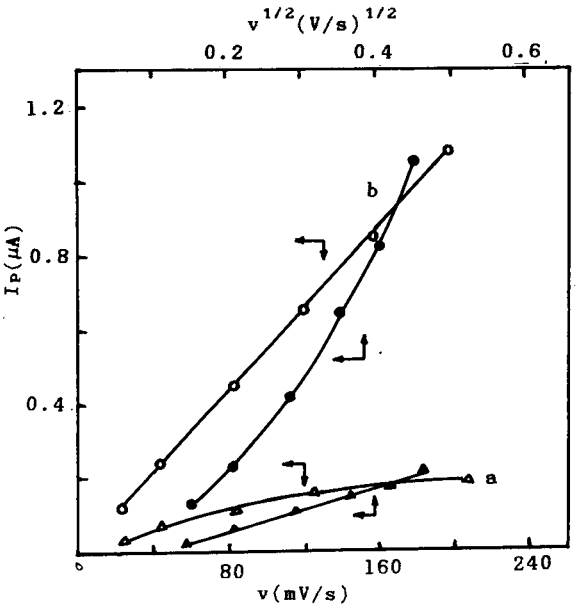

Fig. 3. Effect of scan rate. Conditions: 0.1 M NaOH, 5.0×10^{-7} M cephalexin. (a) $t_{acc} = 0$ s; (b) $t_{acc} = 60$ s.

The effect of the concentration of cephalexin on the peak current with different accumulation times is shown in Fig 4. When $t_{acc} = 0$, $I_{p,c}$ is very small and remains unchanged with increasing concentration of cephalexin, indicating that the process is diffusion controlled. When $t_{acc} = 60$ s, $I_{p,c}$ decreases sharply and tends to a stable value, indicating that the electrode process changes from being adsorption controlled to diffusion controlled [18].

Normal-pulse polarography of the system was investigated with the Model 370-8 Electrochemistry System, using a three-electrode system with a dropping mercury working electrode, a platinum counter electrode and an Ag/AgCl reference electrode. When the scan direction is negative (normal scan), a sharp peak is obtained in the normal-pulse polarogram; with a reverse scan, no peak is observed, indicating that reacting species is adsorbed at the electrode.

On adding the degradation product of cephalexin, the electrocapillary curve decreases in the

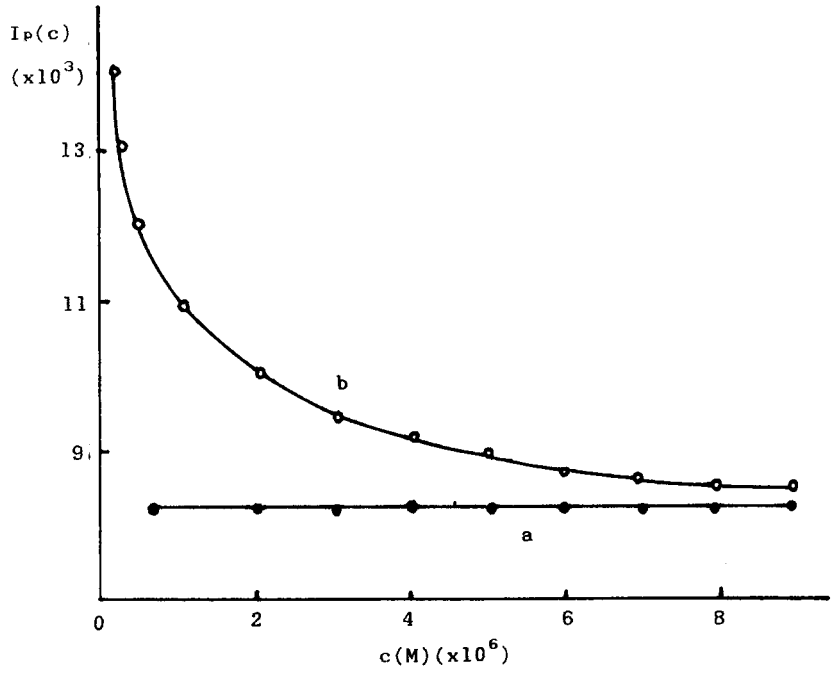

Fig. 4. Effect of concentration of cephalexin. Conditions: 0.1 M NaOH, $E_i = -0.45$ V, $v = 100$ mV s^{-1}. (a) $t_{acc} = 0$ s; (b) $t_{acc} = 60$ s.

positively charged region (see Fig. 5), and the electrocapillary maximum is shifted to a more negative potential, indicating the characteristics of anion adsorption. In the presence of a low concentration of a neutral surfactant [gelatin or poly(vinyl alcohol)], the peak current decreases; on adding a cationic surfactant the peak current remains basically unchanged, whereas an anionic surfactant strongly depresses the peak current, which also indicates anion adsorption.

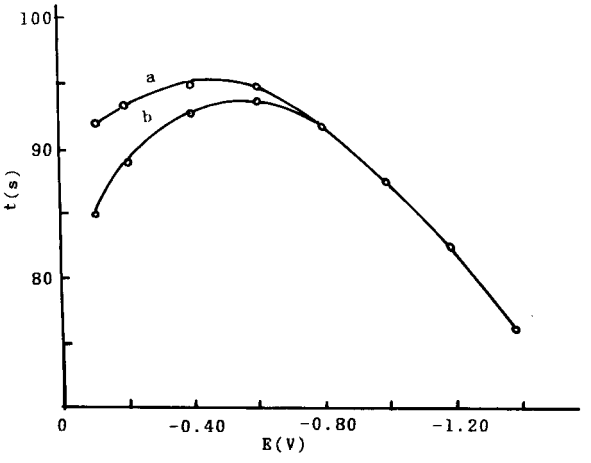

Fig. 5. Electrocapillary curves. (a) 0.1 M NaOH; (b) 0.1 M NaOH $+1.0\times10^{-4}$ M cephalexin.

Reversibility. Fig. 1 shows that the reduction peak of cephalexin is much higher than the oxidation peak. The difference between $E_{p,a}$ and $E_{p,c}$ is $\Delta E_p = 80$ mV, indicating a quasi-reversible process.

Number of electrons involved in the electroreduction. The number of electrons (n) was determined by constant-potential coulometry. Three 40.0-ml portions of 0.1 M NaOH and 1.0×10^{-4} M cephalexin were electrolysed for 2.5 h at -0.80 V (vs. Ag/AgCl), with consumption of 0.99, 0.92 and 0.96 C. The values of n thus obtained are 2.05, 1.91 and 1.99, respectively, hence $n = 2$.

Determination of αn and α. The equation for the irreversible reduction wave is

$$E = E_{1/2} + RT/(\alpha nF)\ \ln[(I_d - I_{irr})/I_{irr}]$$

A plot of $\ln[(I_d - I_{irr})/I_{irr}]$ vs. E, as shown in Fig. 6, is linear with slope $\alpha nF/RT$. The product of the electrode transfer coefficient and the number

of electrons αn can be calculated from the slope of this system to be 1.80; cephalexin undergoes a two-electron reduction, i.e., $n = 2$, hence $\alpha = 0.90$. This belongs to quasi-reversible process.

Determination of diffusion coefficient. After reaching the limiting current for an irreversible wave, the electrode reaction rate is so fast that the current is completely controlled by the diffusion. According to the Ilkovic equation:

$$I_d = 605nD^{1/2}m^{2/3}t_1^{1/6}c$$

the diffusion coefficient D can be calculated. The drop time t_1 is 3.00 s; the flow-rate of mercury m is 1.34 mg s^{-1}. The results are $D = 2.99 \times 10^{-5}$, 2.87×10^{-5} and 2.81×10^{-5} cm^2 s^{-1} for cephalexin concentrations of 1.0×10^{-4}, 1.5×10^{-4} and 2.0×10^{-4} M, respectively. The mean value $\overline{D}$ is 1.89×10^{-5} cm^2 s^{-1}.

Determination of electrode reaction rate constant. At the beginning of the irreversible wave, the electrode reaction rate constant k_1 is small and the current is controlled by the electrode reaction rate. According to the irreversible reaction current equation:

$$I_{irr}/(I_d - I_{irr}) = 0.81(t_1/D)^{1/2}k_1$$

the values of I_{irr} and I_d can be obtained from the experimental results. The plot of $I_{irr}/(I_d - I_{irr})$ vs. $t^{1/2}$ is a straight line with slope $k_1/D^{1/2}$;

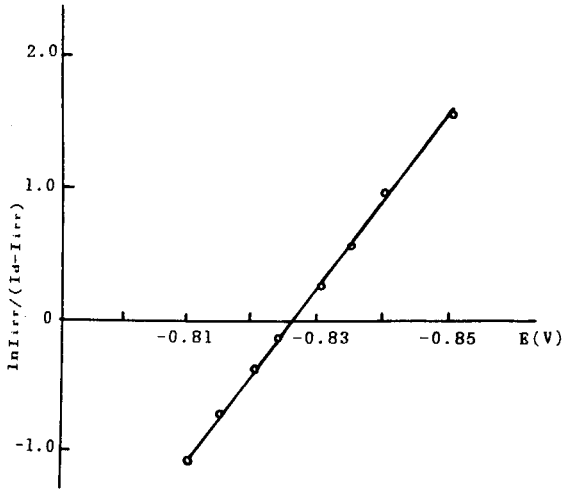

Fig. 6. Plot of $\ln[I_{irr}/(I_d - I_{irr})]$ vs. E.

$D = 2.81 \times 10^{-5}$ cm^2 s^{-1}, hence k_1 can be calculated to be 9.6×10^{-3} cm s^{-1}.

With reversible or quasi-reversible electrode reaction and the current controlled by the diffusion rate for higher concentrations of cephalexin ($> 1.0 \times 10^{-4}$ M), the following equation after by Nicholson [19] from a cyclic voltamperogram can be written:

$$\psi = r^{\alpha}k_s/(\pi aD_0)^{1/2}$$

where ψ is a kinetic parameter, $r = (D_0/D_R)^{1/2}$, α is the electron transfer coefficient, $a = (nFv/RT)$, k_s is the standard rate constant and v is the scan rate. The kinetic parameter ψ is a function of ΔE_p in the cyclic voltamperogram, and ΔE_p is obtained experimentally. The relationship between ψ and $\Delta E_p n$ is shown in Table 1. The value of k_s can be obtained from Table 1 and the Nicholson equation as 9.31×10^{-3} cm s^{-1}. The standard rate constant k_s is smaller than the rate constant k_1 in the above method. The above experiments indicate that the electrode process is quasi-reversible.

Mechanisms of degradation and electrode reactions

Mechanism of degradation. The mechanism of degradation may be represented as follows. Cephalexin, with a four-membered lactam ring, is easily degraded in sodium hydroxide solution [20]:

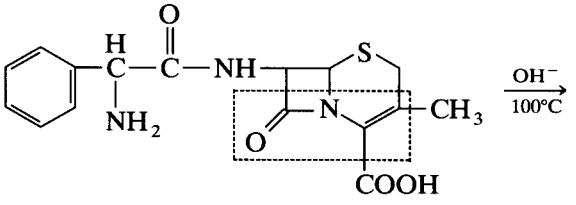

I

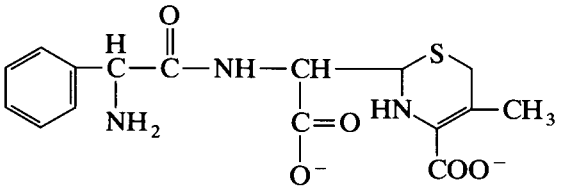

II

The product **II** is unstable, and a ring-closing reaction occurs as follows [21]:

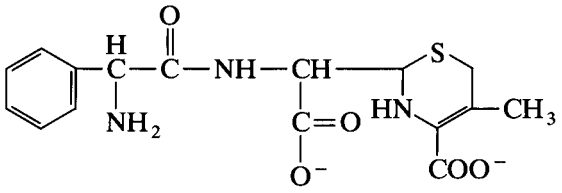

II

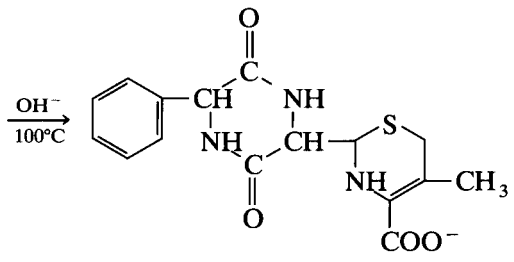

III

During the degradation, the characteristic odour of skunk secretions arises. When a small volume of the degraded solution is added to an alcohol and saturated lead(II) acetate solution is added dropwise, a yellow precipitate of $Pb(SR)_2$ is formed. This indicates that cleavage of the C–S link in **III** occurs to forming a thiol [22]:

TABLE 1

Relationship between $\Delta E_p n$ and ψ

$\Delta E_p n$	ψ	$\Delta E_p n$	ψ
61	20	84	1
63	7	92	0.75
64	6	105	0.50
65	5	121	0.35
66	4	141	0.25
68	3	212	0.10

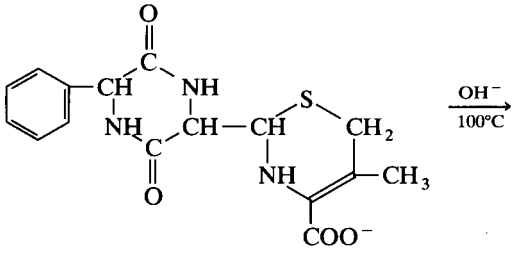

III

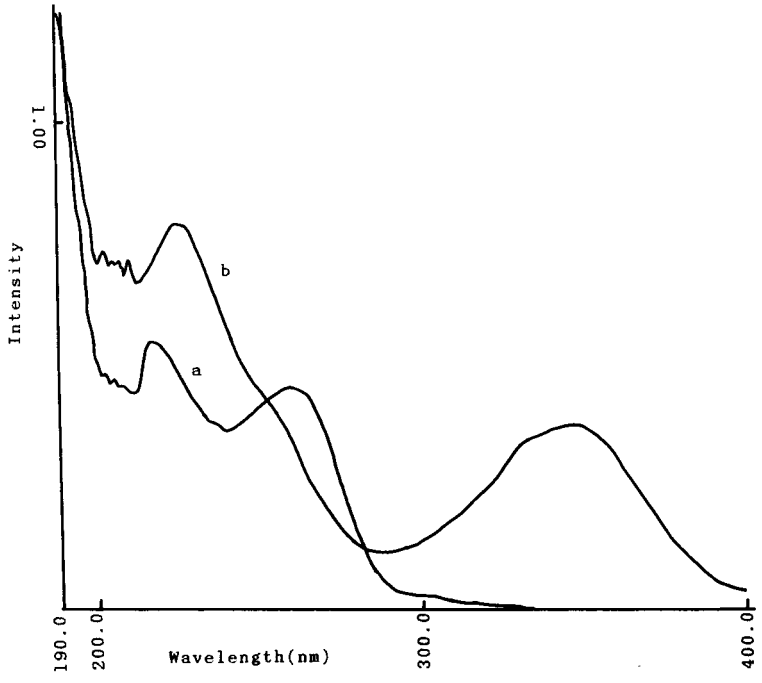

Fig. 7. UV spectra of cephalexin in 0.1 M NaOH. (a) Before degradation; (b) after degradation.

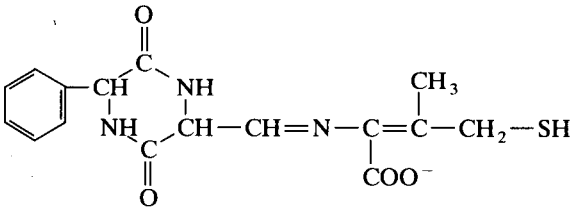

IV

UV spectra of cephalexin before and after degradation are shown in Fig. 7. Before the degradation, two absorption maxima appeared, peaks P_1 at 217 nm and P_2 at 260 nm, caused by $O{=}C{-}N{-}C{=}C-$ (see the dashed box in the formula reactant I) [23] and $-C{=}C{-}COO^-$ groups [24], respectively. After the degradation, P_2 disappeared, as result of C–N bond cleavage in the four-membered amido ring, forming the product **II**, which agrees with [20], and a new absorption peak, P_3, appeared at 345 nm, caused by the

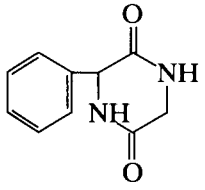

group (see the product **III**) and P_1 shifted from 217 to 225 nm, i.e., a redshift. This indicates that a conjugate group $-C{=}N{-}C{=}C-$ (COO⁻ on the second C, CH_3 on the third C) is formed, giving product **IV**.

The product **IV** has two tautomers [25]:

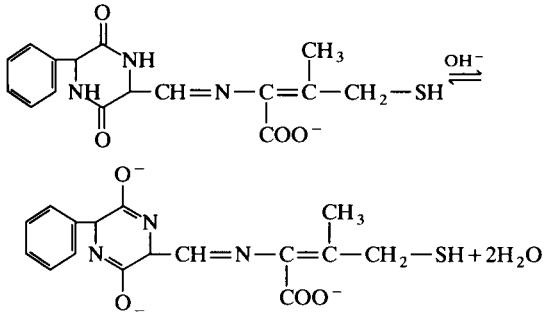

The repetitive cyclic voltamperograms are shown in Fig. 8, after degradation of cephalexin at different accumulation times. The height of

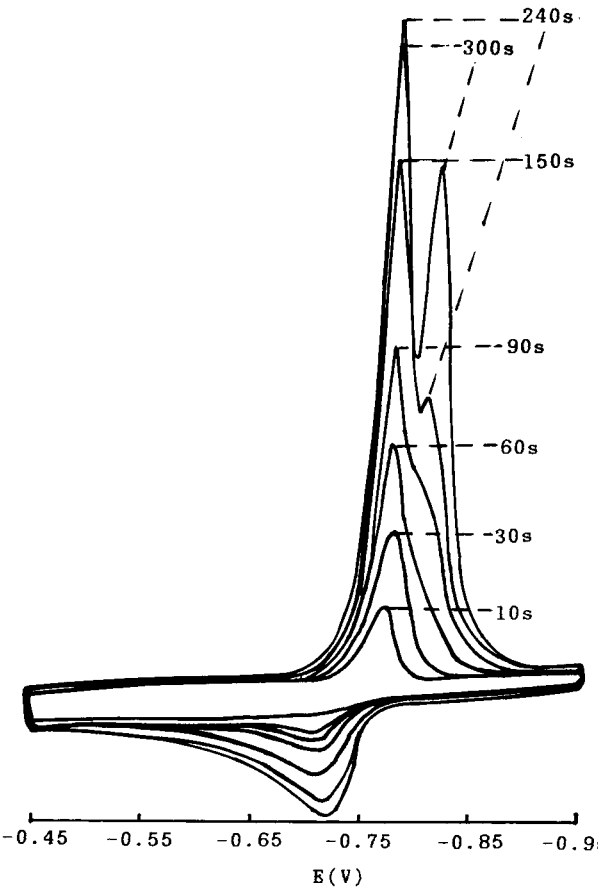

Fig. 8. Repetitive cyclic voltamperograms at different accumulation times. Conditions: 0.1 M NaOH, 1.0×10^{-6} M cephalexin, $E_i = -0.45$ V, $\upsilon = 100$ mV s^{-1}, $s = 5$ μA.

the first peak P_1 increases with increasing accumulation time. When $t_{acc} \geqslant 240$ s, a second peak P_2 appears, and the height of P_2 increases with increasing t_{acc}, whereas the height of P_1 decreases. This indicates that two tautomers exist in the system and competitive adsorption occurs at the mercury electrode [26].

Mechanism of electrode reaction. The above-mentioned degradation process suggests that the product **IV** has electroactivity. Reducible groups are $-C{=}N-$ and $-C{=}C-$ in the conjugated group $-CH{=}N{-}C{=}C-$. The $-C{=}N-$ group is more reducible than the $-C{=}C-$ group [27]. D.c. polarographic experiments indicated that two re-

duction peaks are obtained in 0.1 M sodium hydroxide solution, $P_1 = -0.84$ V (vs. SCE) for $-\underset{|}{C}=N-$ group reduction and $P_2 = -1.34$ V for $-\underset{|}{C}=\underset{|}{C}-$ group reduction.

From all the experiments and calculated results, it can be concluded that the electrode reaction mechanism of the degradation product of cephalexin is as follows:

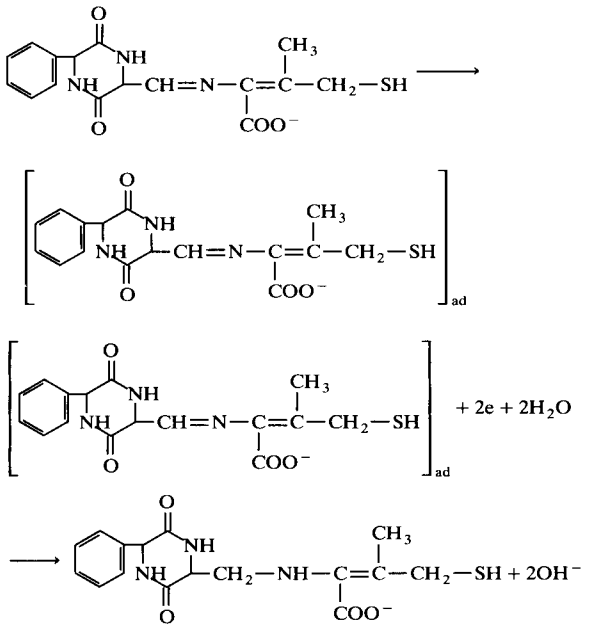

The support of the National Natural Science Foundation of China is gratefully acknowledged.

REFERENCES

1 A.G. Fogg, N.M. Fayad and C. Burgess, Anal. Chim. Acta, 110 (1979) 107.
2 J.S. Wold and S.A. Turnipseed, Clin. Chim. Acta, 78 (1977) 203.
3 R.P. Buhs, T.E. Maxim, N. Allen, T.A. Jacob and F.J. Wolf, J. Chromatogr., 99 (1974) 609.
4 T.F. Rolewicz, B.L. Mirkin, M.J. Cooper and M.W. Anders, Clin. Pharmacol. Ther., 22 (1977) 928.
5 P. Papazova, P.R. Bontchev and M. Kacarova, Pharmazie, 32 (1977) 486.
6 D.L. Mays, F.K. Bangert, W.C. Cantrell and W.G. Evans, Anal. Chem., 47 (1975) 229.
7 J. Kirschbaum, J. Pharm. Sci., 63 (1974) 923.
8 M.A. Abdalla, A.G. Fogg and C. Burgess, Analyst, 107 (1982) 213.
9 A.M. Wahbi and B. Unterhalt, Fresenius' Z. Anal. Chem., 284 (1977) 128.
10 A.B.C. Yu, C.H. Nightingale and D.R. Flanagan, J. Pharm. Sci., 66 (1977) 213.
11 D.A. Hall, D.M. Berry and C.J. Schneider, J. Electroanal. Chem., 80 (1977) 155.
12 A.G. Fogg, N.M. Fayad, C. Burgess and A. McGlynn, Anal. Chim. Acta, 108 (1979) 205.
13 A.G. Fogg, N.M. Fayad and R.N. Goyal, J. Pharm. Pharmacol., 32 (1980) 302.
14 J. Koryta, Collect. Czech. Chem. Commun., 18 (1953) 206.
15 Q.-L. Li and G. Ji, Talanta, 37 (1990) 937.
16 A. Osteryoung, G. Lauer and F.C. Anson, Anal. Chem., 34 (1962) 1833.
17 Q.-L. Li and X.-Y. Liu, Anal. Chim. Acta, 258 (1992) 171.
18 G. Ji and Q.-L. Li, Gaodeng Xuexiao Huaxue Xuebao, 11 (1991) 1642.
19 K.M. Kadish, B.B. Cocolios, C. Swistak, J.M. Barbe and R. Guilard, Inorg. Chem., 25 (1986) 121.
20 K.A. Connor, G.L. Amydon and L. Cannon, translated by W.-S. Zhou and L.-Z. Lu, Chemical Stabilities of Pharmaceuticals, Renming Weishen, Beijing, 1983, p. 70.
21 A. Heald, C. Ita and E. Schreiber, J. Pharm. Sci., 65 (1976) 768.
22 R.L. Shriner, R.C. Fuson, D.Y. Curtin and T.C. Morrill, translated by X.-T. Ding, A.-H. Zhou, G.-B. Chen, X.-L. Lu and Y.-H. Fan, The Systematic Identification of Organic Compounds, a Laboratory Manual, Fudan University Publishing House, Shanghai, 1989, p. 249.
23 R.R. Chauvette, E.H. Flynn, B.G. Jackson, E.R. Lavagnino, R.B. Morin, R.A. Müller, R.P. Pioch, R.W. Roeske, C.W. Ryan, J.L. Spencer and E. Van Heyningen, J. Am. Chem. Soc., 84 (1962) 3401.
24 L. Huang and D.-Q. Yu, Applications of Ultraviolet Spectra in Organic Chemistry, Kexue Publishing House, Beijing, 1988, p. 78.
25 R.H. Barbhaiya, R.C. Brown, D.W. Payling and P. Turner, J. Pharm. Pharmacol., 30 (1978) 224.
26 Q.-L. Li, T.-Y. Jian, Z.-H. Li and Z. Ma, Beijing Shifan Daxue Xuebao (Nat.), 4 (1992) 454.
27 Group of Analytical Chemistry, Department of Chemistry, Hangzhou University, Handbook on Analytical Chemistry, Vol. 3, Huaxue Gongye Publishing House, Beijing, 1983, p. 256.

Analytica Chimica Acta, 282 (1993) 153–168
Elsevier Science Publishers B.V., Amsterdam

Comparison of distillation with other current isolation methods for the determination of methyl mercury compounds in low level environmental samples

Part II. Water

Milena Horvat

IAEA-MEL, Marine Environmental Studies Laboratory, 19 Av. des Castellans, MC-98 000 Principality of Monaco (Monaco)

Lian Liang

Brooks Rand, Ltd., 3950 Sixth Avenue NW, Seattle, WA 98107 (USA)

Nicolas S. Bloom

Frontier Geosciences, 414 Pontius Av. N, Seattle, WA 98 103 (USA)

(Received 6th April 1993)

Abstract

In the present paper two isolation procedures for the separation of methyl mercury compounds (MeHg) from natural water samples, followed by aqueous phase ethylation, precollection on the Carbotrap, isothermal gas chromatography and cold vapour atomic fluorescence (CV-AFS) detection were compared and evaluated. The first isolation technique is based on extraction of MeHg into methylene chloride and back extraction into water by solvent evaporation. The second is based on the distillation of MeHg compounds. A comparison of these two isolation procedures was performed on 110 water samples of various origin (oxic, anoxic fresh water and sea water) and containing a wide MeHg concentration range (from 0.01 to 25 ng l^{-1}). A relatively good agreement of the results was obtained in the concentration range below 1 ng l^{-1} as Hg ($r^2 = 0.919$, $n = 61$). In anoxic, sulphide rich and organic matter rich water samples that usually contain higher MeHg values, significantly higher values (approx. 30%) were obtained by distillation. This is partly due to sulphide interference during the ethylation step, as well as incomplete release of MeHg from bound sites. Distillation was found advantageous to solvent extraction. It gives consistent and high recoveries (80–95%) for various water samples, and achieves lower detection limits (0.006 ng l^{-1} for 50 ml water sample). It is also less laborious and without the use of organic solvent. Additionally, distillation provides the specific separation of MeHg and dimethylmercury, if present.

Keywords: Gas chromatography; Atomic fluorescence spectrometry; Distillation; Methyl mercury; Solvent extraction; Waters

Correspondence to: M. Horvat, IAEA-MEL, Marine Environmental Studies Laboratory, 19 Av. des Castellans, MC-98 000 Principality of Monaco (Monaco).

It has been well known for decades that mercury is biomethylated in the environment and is then bioconcentrated up the food chain. Al-

though total and MeHg levels in surface water are extremely low ($\approx$ 1 ng l^{-1} of total Hg; 0.05 ng l^{-1} of MeHg), bioconcentration factors of up to 10^7 [1–3] often lead to MeHg levels in fish which exceed the WHO health standards (0.5 μg g^{-1} FW). During the last decade a new pattern of Hg pollution has been discerned, mostly in Scandinavia and North America [4]. Fish from low productivity lakes, even in remote areas, have been found to have high Hg content. For water bodies not directly impacted by a discharge, the dominant source of Hg is through direct or runoff precipitation [5,6]. A large number of waters are affected by widespread air pollution and the long-range transport of pollutants. It is estimated that 40–50% of the Hg° cycling through the atmosphere is initially of anthropogenic origin, largely due to the combustion of coal [4,7,8]. Additionally, acidification of surface waters further enhances the bioavailability of Hg by leading to increased in-water methylation [4,9,10].

In such studies the availability of accurate, sensitive and precise analytical methods for the determination of total Hg and its organic compounds at the picogram levels in water samples is of crucial importance. Due to carefully designed sampling, handling add analysis protocols, as well as better control of reagent and handling of blanks, a dramatic decrease in the confirmed Hg levels in sea water over the past 15 years has been found. The most wide-spread analytical technique used for the determination of total Hg in water is cold vapour atomic absorption spectrometry (CV-AAS) with preconcentration by amalgamation on gold [11,12]. Today, plasma atomic emission (plasma-AES) [13,14] and atomic fluorescence spectrometry (AFS) [15,16] are becoming increasingly important techniques.

A large number of articles for the determination of MeHg compounds in biological and sediment samples have been published. Most of them are based on solvent extraction and gas chromatographic determination. Methods are reviewed in several publications [3,17]. However, only a few analytical techniques have been developed for the determination of MeHg compounds in water samples. The methods attempted as for biological samples mentioned above were also employed for water samples. The main difference was that MeHg was isolated from relatively large volumes of water sample by resin [18], solvents [19,20], or sulfurated adsorbents [21]. The common drawbacks of these techniques are large sample volumes required, low extraction yield and unspecific separation of dimethylmercury, if present. Ultra-trace levels of organo Hg compounds in rain and river water have been isolated by ion-exchange separation and detected by CV-AAS [22]. However, it was shown that levels obtained by this method did not specifically correspond to MeHg due to unspecific isolation and determination [23]. The method has been modified by the introduction of preseparation of MeHg by distillation [23,24].

Recently, two analytical techniques for the determination of MeHg at pico- and sub-picogram levels in natural water have been published [25,26]. The first method [25] is based on the extraction of MeHg compounds into methylene chloride and then back extracted into water by solvent evaporation. MeHg was determined by aqueous phase ethylation, followed by cryogenic gas chromatography with CV-AFS detection. The detection limit was about 0.003 ng g^{-1} for a 200-ml sample. The second method [26] is based on preconcentration of MeHg on a sulphydryl cotton fiber adsorbent, elution by HCl, and extraction into organic solvent. Analysis was performed with capillary gas chromatography with electron capture detection. Methods have also been intercompared and have shown good agreement (Bloom and Lee, unpublished data). Additional intercomparison on MeHg determination in different samples including water samples has been conducted between various laboratories [27]. In both intercomparison exercises difficulties occurred, especially when comparing very humic rich or anoxic waters.

The purpose of the present paper is to compare two isolation techniques (extraction and distillation) for separation of MeHg compounds from water samples of various origin, followed by a sensitive analytical set-up based on aqueous phase ethylation, isothermal GC, and CV-AFS detection. A similar study has recently been performed on sediment samples [28]. This paper is therefore

the second of two parts concerning determination of MeHg compounds in environmental samples.

EXPERIMENTAL

Water samples of various origin were sent to the laboratory in PTFE bottles, after collection according to contamination-free trace metal sampling protocols [29,30]. Most of the water samples analyzed represent a part of various on-going research programmes in which Brooks Rand, Ltd. (Seattle, WA) was responsible for total and MeHg analyses. Depending on the requirements, samples were preacidified with HCl (for MeHg determination in unfiltered water) or unacidified if filtration had to be performed in the laboratory. It is self-explanatory that all work in connection with low level Hg determination was performed under extreme clean conditions. Two isolation techniques for separation of MeHg compounds from water samples were compared. Their principles are schematically shown in Fig. 1. The extraction isolation procedure has already been described in detail by one of the co-authors [25], while distillation has been described in our previous paper concerning separation of MeHg from sediment samples [28]. However, there are few minor differences from already published procedures, therefore a brief description is given below.

Cleaning procedure

Distillation vials and most of the other ware was made from PTFE. Extreme precautions were necessary in order to avoid contamination or losses of either total Hg or MeHg. PTFE vials and bottles were heated in concentrated nitric acid, since Hg contamination by diffusion from the inside of the material was very probable. This was particularly important for the analysis of low MeHg levels, after a sample with high Hg concentration (memory effect). On the other hand chlorine that might be trapped in the PTFE material can be released during processing and cause decomposition of MeHg. The cleaning procedure was as follows. New or used PTFE ware was placed into hot HNO_3 for 48 h. After being thoroughly rinsed with deionized water (Millipore), vials were filled with 1% HCl, tightly closed and heated at 70°C overnight and then kept in a clean place, preferably in Hg-free plastic bags. PTFE vials that had been used for oxidative destruction by BrCl for subsequent total Hg determination were never used for MeHg analyses, due to possible release of chlorine, which can cause destruction of MeHg in aqueous media.

Several blanks were run in each set of sample analysis, particularly if very low MeHg values were measured. The MeHg blank of the distillation procedure originated from poorly cleaned PTFE vials, while blanks in the extraction procedure also derived from reagents, mainly methylene chloride. High and irreproducible blanks were almost always a consequence of poorly cleaned PTFE ware.

Extraction

As described by Bloom [25] MeHg in water can be determined using aqueous phase ethylation at pH 4–7, with sodium tetraethyl borate. However, direct ethylation of natural waters results in the release of only "reactive" MeHg, which represents only 5–60% of total MeHg. Therefore the method has been modified introducing the extraction step [31]. Up to 50 ml of water sample was put into a 125-ml PTFE bottle and 5 ml of 10% HCl saturated with KCl was added. In the case of the analyses of sea water only 5 ml of 10% HCl was added (Fig. 1) 40 ml of methylene chloride was added, and the sample was shaken for one hour, while longer shaking time did not effect the result. The aqueous layer was pipetted off, leaving only the methylene chloride, containing MeHg chloride. 60 ml of ultrapure (Millipore) water was added to the bottle, and then it was placed in a water bath at about 60°C to evaporate the methylene chloride. Once the methylene chloride was visibly evaporated, the sample was purged for 5 min with Hg-free nitrogen to quantitatively remove residual methylene chloride. MeHg chloride that remained in the water phase was then buffered with 200 μl of 2 M acetate buffer [25], and brought up to 100 ml with high purity water. The yield of this single step extraction procedure varied from 80 to 90%

for relatively clean water samples. However, when humic rich and anoxic water samples were analysed the recovery was matrix dependent and was much lower (40–75%).

In the measurement step, the extracted and buffered water sample was transferred into the ethylation reaction flask [25,28,33], and 50 μl of 1% sodium tetraethyl borate (in 2% KOH) was

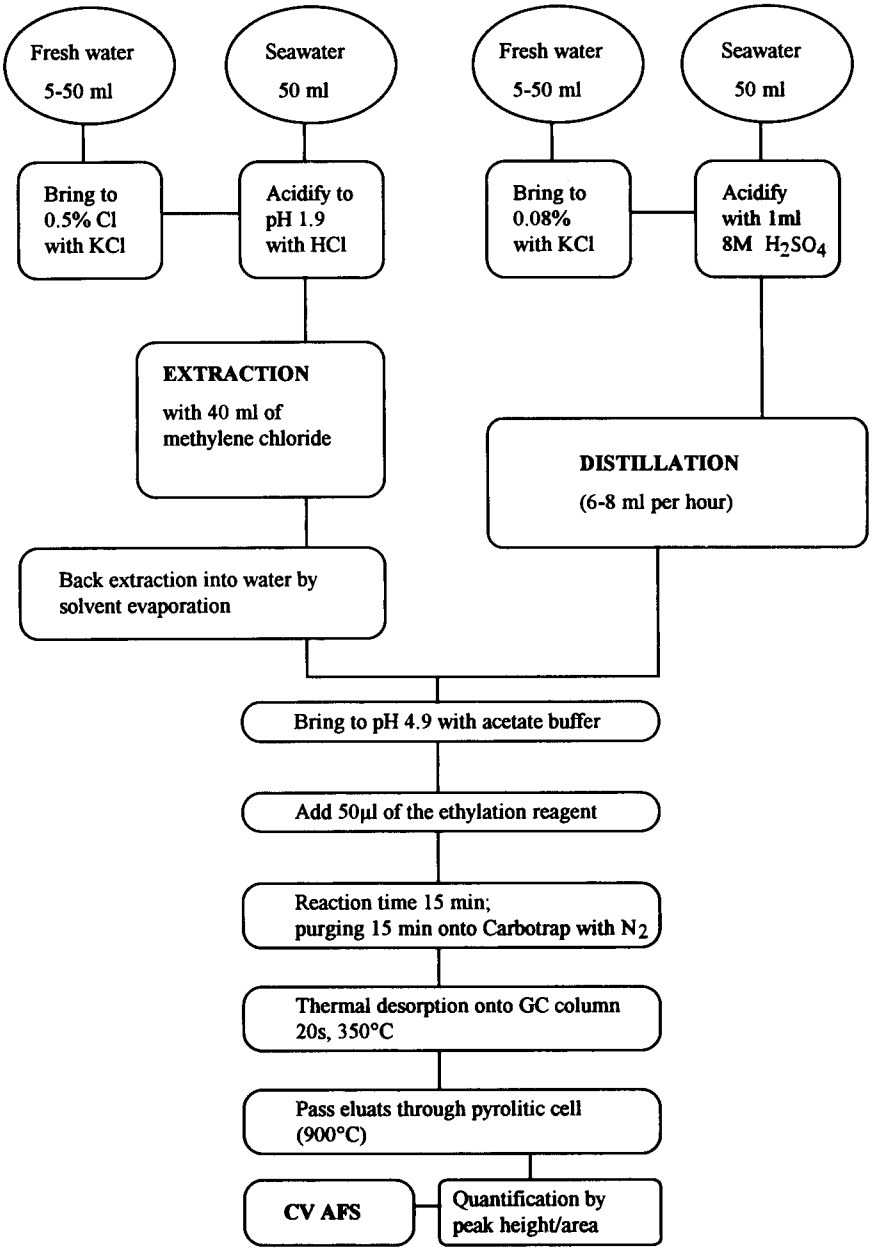

Fig. 1. Schematic flow chart of the distillation and extraction procedure for the isolation of MeHg from natural water samples followed by aqueous phase ethylation, isothermal GC, and CV-AFS detection.

added. The bubbler was tightly closed, and swirled to mix. The reaction was allowed to proceed for 15 min without bubbling, and then the volatile ethylated Hg species were purged from the sample onto Carbotrap (a 6 mm i.d. silanized silica column containing 0.15 g of Carbotrap-graphitized carbon black, Supelco 20 287) for 15 min at a nitrogen flow-rate of 300 ml min^{-1}. In the present study only Carbotrap was used. Recently some authors reported that Tenax can also be used instead of Carbotrap with good success [32,33]. After the sample was purged, dry nitrogen was allowed to pass over the trap for 7 min in order to remove water vapour, which strongly interferes with the next step, chromatographic elution and CV-AFS detection. The Hg species from the Carbotrap were released by thermal desorption onto the GC column (60 cm × 4 mm i.d.), which was filled with 15% OV-3 on Chromosorb W, AW, DMCS and kept at 90°C. Under the flow of helium the eluted Hg species were converted into Hg° by thermal decomposition at 900°C and then detected by CV-AFS. The measurement technique is more precisely described by Liang et al. [33]. The output from the detector was quantified using a standard GC plotter/integrator or a 1-mV recorder for peak height measurements. A CV-AFD-2 Mercury Analyzer produced at Brooks Rand, Ltd. was used. Its operation is described in detail by Bloom and Fitzgerald [15]. Typical chromatograms are shown in Fig. 2.

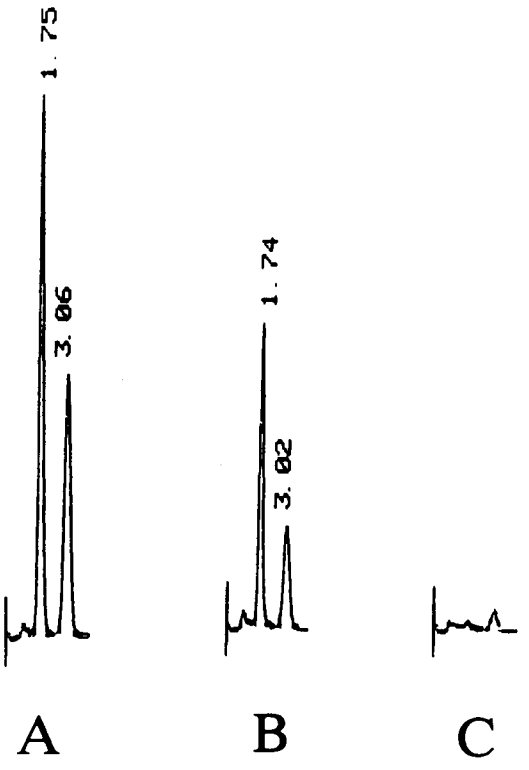

Fig. 2. Chromatograms obtained by aqueous phase ethylation, isothermal GC, and CV AFS detection. (A) Standard solution (100 pg Hg as methyl and inorganic mercury following ethylation). (B) Distilled lake water. (C) Distillation blank. Retention times: 1.75 (1.74) min, MeHgEt (corresponds to methyl mercury); 3.06 (3.02) min, EtHgEt (corresponds to inorganic Hg).

Distillation

A still made of glass or PTFE, for the distillation of MeHg is shown in other publications [23,28]. In this study only PTFE ware was used. The addition of the reagent prior to the distillation was dependent on the origin of the sample and also on whether water samples received in the laboratory were preacidified or not.

Up to 50 ml of unacidified fresh water was placed into 60-ml distillation PTFE vials, and KCl was added so that the final concentration of Cl^- was approximately 0.08% (Fig. 1). Sample was then acidified with 1 ml of 8 M H_2SO_4. The distillation was started immediately after addition of reagents at a nitrogen flow-rate of 60 ml min^{-1} and a heating block temperature of 145°C. Under the conditions in our laboratory this temperature was found to be appropriate. If too high temperature(> 150°C) was used the distillation rate was higher resulting in lower and unreproducible recoveries of MeHg. While at lower temperature the distillation rate was too slow. It should be emphasized that from the practical point of view it is more important to control the distillation rate than the temperature. Under certain laboratory conditions one should select the temperature at which the distillation rate would be 6–8 ml h^{-1}. So, in order to distill 80–85% of the 50 ml water samples, at least 5–7 h are needed. However, for water samples with the MeHg concentration higher than 0.30 ng l^{-1},

Determination of total mercury

The present study concentrated on the determination of MeHg. Total Hg was also analyzed following the procedure based on BrCl oxidation, reduction–amalgamation and CV-AFS detection. The procedure is described in detail elsewhere [34]. Results and discussion focuses only on MeHg determination, since data for total and MeHg in samples analysed were part of several on-going studies on biogeochemical cycling of Hg in its compounds in remote lakes, and will therefore be discussed elsewhere.

RESULTS AND DISCUSSION

Analytical quality control

It is well known that it is extremely difficult to control the accuracy of the results for trace elements in water samples at sub-nanogram levels. This is not only related to difficulties in the final measurement, but even more to sampling and handling protocols. Important improvements in sampling [29,30] and measurement techniques have been achieved, which have resulted in a dramatic decrease in the confirmed Hg levels in sea water over the past 15 years.

Samples were sent to the laboratory in PTFE bottles, after they were sampled according to ultraclean protocol. Apart from the sampling device (either a PTFE Go-Flo sampler or pumping the water through PTFE tubing by using a peristaltic pump) it was extremely important to use appropriate sample containers. These might be borosilicate or silica glass, or PTFE bottles. In this study only PTFE containers were used. The accuracy of Hg determination in water depends very much on the control of the *blanks*. These included blanks of the sampling device and sample handling (storage, preservation, filtration, and transportation) and blanks from the laboratory processing (filtration, digestion, extraction, and distillation). However, for this study we could only control blanks from the laboratory processing. In Table 1 information on various parameters related to the quality control data are presented. It is important to note that blank measurements represented at least 10% of all determinations. Blank values for MeHg were very stable over the period of this study. Higher blanks in a particular set of analysis were related to the poor quality of the methylene chloride or ethylation reagent. However, blanks were in most cases very reproducible. Unreproducible blanks were almost always related to contaminated PTFE ware. The detection limit (DL) was also effected by the reproducibility of blank values (DL is defined as three standard deviations of the blank). Particularly when low MeHg values were measured, several blanks were run.

Another means of confirming the accuracy of the results was to analyze a certified reference material (CRM). For total Hg, water CRM ORMS-1 (certified total Hg value 6.9 ± 1.3 ng l^{-1}) obtained from the National Research Council of Canada (NRCC) was used. Unfortunately, there are no CRMs for MeHg in water samples available. As mentioned in our previous paper concerning the determination of MeHg in sediments [28], the accuracy and performance of the measurement step (ethylation, GC separation and AFS detection) was verified by the analysis of biological RMs certified for MeHg (DORM-1, and DOLT-1). Unfortunately, this did not assure the accuracy of the preseparation technique for MeHg from water samples. So, the accuracy had to be verified by other means, including a comparison of two isolation procedures and the use of standard additions. The comparison of solvent extraction and distillation is discussed further below.

At this stage no intercomparison with other laboratories was performed. The same distillation technique has already been successfully instituted in other laboratories, which have had a lot of experience in the MeHg determination by other techniques. According to their preliminary results, they have received satisfactory agreements with other techniques [35]. A world wide intercomparison on total and particularly MeHg is definitely needed, particularly since the number of laboratories performing MeHg analysis is increasing. Such an effort has already been initiated by the co-authors of this article with the support from the Electric Power Research Institute (EPRI), Palo Alto, CA.

Reproducibility and detection limits

The detection limit is defined as three times the standard deviation of the bank. As mentioned in the previous paragraph the blank values were dependent on many factors, but during one set of analyses they were constant, which favour rather low detection limits. For the solvent extraction of 50 ml of water samples established detection limits varied from 0.015 to 0.050 ng l^{-1} depending also on the experience of the personnel performing the analyses. Lower detection limits (0.006–0.010 ng l^{-1} for distillation of a 50-ml water sample) were achieved by distillation due to lower blank values, which mainly derived from the ethylation reagent. Lower detection limits can further be achieved by distillation of larger volumes of water samples. According to data from the literature [36] the lowest concentrations of MeHg were reported for sea water (< 0.01 ng l^{-1}). The detection limits for processing 50 ml of sample were satisfactory even for such samples. Rarely do we encounter any natural water sample with MeHg value below the detection limit. The natural water samples with extremely low concentrations were sampled from Doubtful Lake, from the Northern Cascade Mountains in the USA (WA) and the sea water from Puget Sound. Results are given in Table 1. As evident from the results, a good agreement of the results between extraction and distillation isolation of MeHg values was obtained at this low level. The reproducibility of the results was also very good. For the comparison, data for two humic rich lake waters are given. Evidently, the reproducibility of the results is also very much dependent on the kind of sample analysed. The isolation of MeHg from organic rich water samples using the extraction procedure almost always resulted in lower recoveries, and less reproducible results, while distillation resulted in more consistent results and recoveries. The homogeneity of the sample also plays an important factor in its analysis. It has been often observed that frozen water samples rich in organic matter, when thawed resulted in less reproducible results, particularly if smaller sample volumes were taken for the analyses (Table 1).

Distillation

The distillation isolation procedure enables MeHgCl to be purged from the sample together with the water vapour due to increased partial pressure of the aqueous solution at the elevated temperature. Various modifications of the distillation procedures have been published [23,24,28, 37,38]. The method that is based on the isothermal volatilization of MeHg halides and cyanides in a closed convey dish at elevated temperature [39,40] gave us the idea to modify the same procedure in order to be able to isolate MeHg from large sample aliquots. This has been successfully performed for the isolation of MeHg compounds from biological and sediment samples [23,28].

In this study the final measurement was based on ethylation, GC separation and AFS detection. Before a sample was submitted for ethylation, MeHg had to be isolated into an aqueous solution with an optimum pH value of 3–5, the presence of Cl^- should be below 100 ppm and without the presence of sulphide ions, to avoid strong interferences during the ethylation. MeHgCl can only be distilled if the acidified sample also contains Cl^- ions. In the present study some experimental tests were performed to find the optimum conditions. Recently a model calculation for simulating the distillation process has provided similar conclusions to those in this paper [35]. In Fig. 3 recovery curves for MeHg from spiked lake water (clean remote mountain lake) with two different Cl^- concentrations acidified with sulphuric acid and HCl are shown. Each point in this figure represents an average value obtained by two independent distillations. Seven fractions during the distillation of 50 ml of water sample were collected sequentially. MeHg in each fraction was analyzed separately. pH was also checked in each fraction (particularly those towards the end of the distillation) in order to avoid interferences during the ethylation step.

As evident from Fig. 3, release of MeHg from sulphuric acid media with lower KCl concentration gave the highest recoveries. This has also been confirmed for the distillation of MeHg from biological samples [23]. It is interesting to note that when half of the sample was distilled recov-

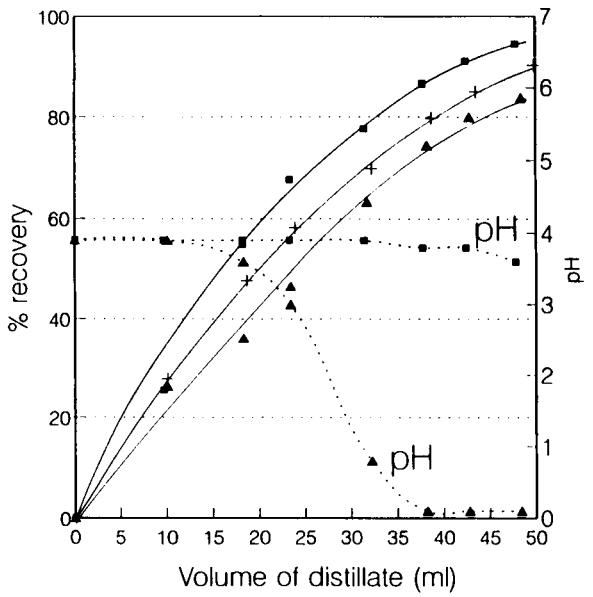

Fig. 3. Recovery curves for MeHg from 50 ml of spiked lake water. (■) Method 1: 0.08 M H_2SO_4, 0.13 M KCl. (+) Method 2: 0.08 M H_2SO_4, 0.64 M KCl (▲) Method 3: 0.1 M HCl.

ery of MeHg was about 70%. However, when more than 85% of the sample was distilled recovery was higher than 90%. With the increasing collection of the distillate recovery was only slightly increased. The pH of the last 10% of the collected distillate was only slightly lower than in the previous fractions. The distillation was stopped when 85–90% of the distillate was collected in order to prevent volatilization of substances which may undergo decomposition during the end of distillation, and can be distilled.

Increased amounts of Cl^- ions added to the sample resulted in lower recoveries throughout the distillation. When 50% of the sample was distilled the recovery was 60%, which was 10% lower than in the previous case. Lower results were also due to decomposition of MeHg in the fractions toward the end of the distillation. So, distillation should be stopped earlier, when a maximum 80% of the distillate is collected. Close examination of this curve showed that when 60–80% of the distillate was collected this corresponded to 60–80% recovery of MeHg. So, the recovery of MeHg can simply be calculated from the volume of the collected distillate. This can be used for samples that naturally contain higher Cl^- concentrations (sea water).

However, using HCl alone resulted in consistent but lower recoveries than using sulphuric acid and KCl. When about 90% of the distillate was collected the recovery was maximum 80%. The pH in the distillate fractions decreased after 20% of the sample was distilled, since HCl was also distilled and condensed in the receiving vial. In order to prevent serious interferences during the ethylation procedure, distillation was stopped when approximately 70 to a maximum of 80% of the distillate was collected. Additional experiments were performed in order to check whether lower recoveries in the last 20% of the distillate were connected to interferences during the ethylation procedure (high Cl^-concentration) or whether MeHg was decomposed in the vial containing the sample. So, the last 20% of the sample that was not yet distilled was divided in two fractions. One fraction was directly reduced by $SnCl_2$, which released only inorganic Hg which was measured by gold amalgamation and AFS detection. The other fraction was oxidized by BrCl solution, and total Hg was then measured by $SnCl_2$ reduction, amalgamation, and CV AFS detection method. MeHg was calculated from the difference between total and inorganic Hg. It was found that only 3% of MeHg was still present, while all the rest was decomposed to inorganic Hg. Therefore the maximum recovery that could be achieved by using 0.1 M HCl acid was only from 80 to 83%. In order to avoid possible interferences during the ethylation procedure the distillation was stopped when a maximum of 80% of the distillate was collected. The pH of the distillate was constantly checked and neutralized to 4.5 to 4.9 as appropriate for the ethylation step.

Sea water samples

MeHg concentrations in sea water are generally lower than in fresh water samples. In the upper layer of the world's oceans MeHg levels are lower than the detection limits of already existing methods (< 0.010 ng l^{-1}) [36]. The only sea water sample tested for this study was from Puget Sound (near shore). As mentioned previously, high Cl^- concentration in sea water de-

serves special attention, since chloride ions can also distill over and interfere with the ethylation step. A recovery curve for MeHg from 100 ml of sea wate which was spiked with 1 ng of MeHgCl as Hg and acidified with 1 ml of 8 M H_2SO_4 is shown in Fig. 4. The test was performed in two independent distillations. All individual measurements are plotted in the graph. Evidently, when approximately 60–80% of the sample was distilled this corresponded to 60–80% recovery of MeHg. Distillation of more than 80% of the sample did not significantly improve the recovery of MeHg, but rather caused the distillation of HCl and decomposed compounds formed toward the end of the distillation, which were then collected in the receiving vial and lowered the pH of the distillate and interfered with the ethylation step.

Sea water samples or any other water sample with MeHg concentrations lower than 0.010 ng l^{-1} could be analyzed by combining distillates of two or more independent distillations. For example, combining three distillates from Puget Sound sea water (from 50-ml sample aliquots) corresponded to 120 ml of water sample. The value obtained (0.021 ± 0.004 ng l^{-1}) was the same as with the analysis of only one distillate. The detection limit calculated was 0.003 ng l^{-1}. For samples with lower MeHg values a different distillation still should be designed so that larger volumes can be distilled in one distillation run.

Sulphide and humic rich aqueous samples

One of the main reasons to undertake the present study was that sulphide rich water samples seriously interfere with the solvent extraction procedure and detection of MeHg by aqueous phase ethylation, GC separation and AFS detection. However, the highest MeHg compounds concentrations were actually found in anoxic waters rich in sulphide. Therefore, it was extremely important to use the isolation technique which allowed separation of MeHg into an aqueous media without the presence of sulphide. Distillation was found to be very convenient, since sulphide, which was converted into H_2S after acidification, was purged from the sample and from the distillate receiving vial. Figure 5 shows that

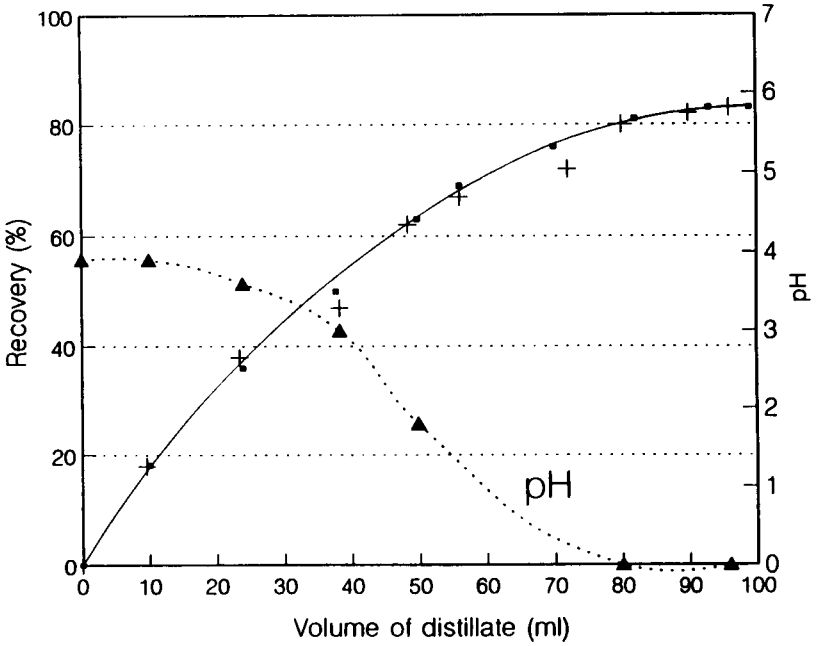

Fig. 4. Recovery curve for MeHg from 100 ml of spiked sea water acidified with 2 ml of 8 M H_2SO_4.

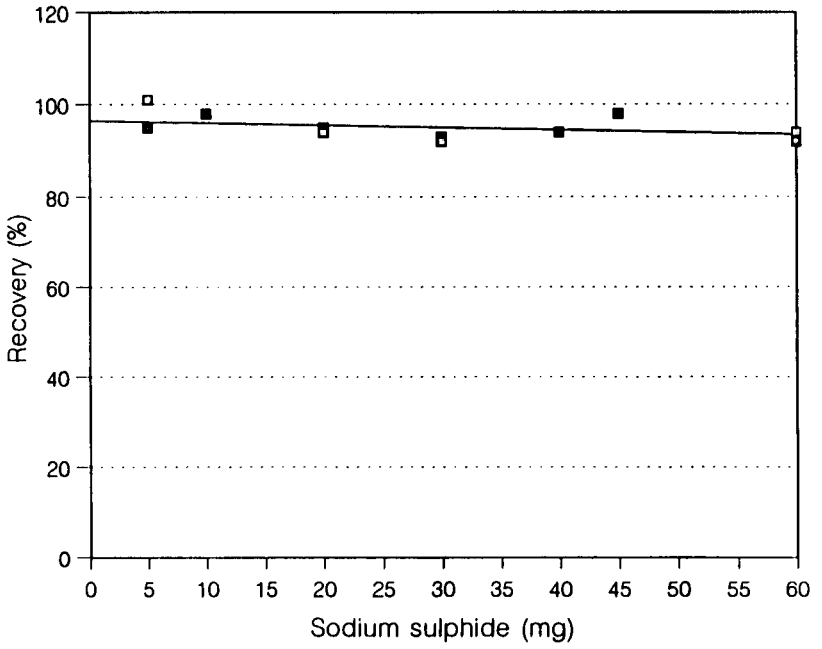

Fig. 5. Effect of the sodium sulphide on the distillation recovery of MeHg from water samples.

sulphide ions do not interfere with recovery even up to 50 mg of Na_2S present in the sample during distillation. This experiment was performed in duplicate.

Analysis of the media for sulphide reducing bacteria (concentration of sulphide was 10^{-3} M) resulted in recoveries from 78 to 93% (mean value 83%, $n = 6$). MeHg concentration was rela-

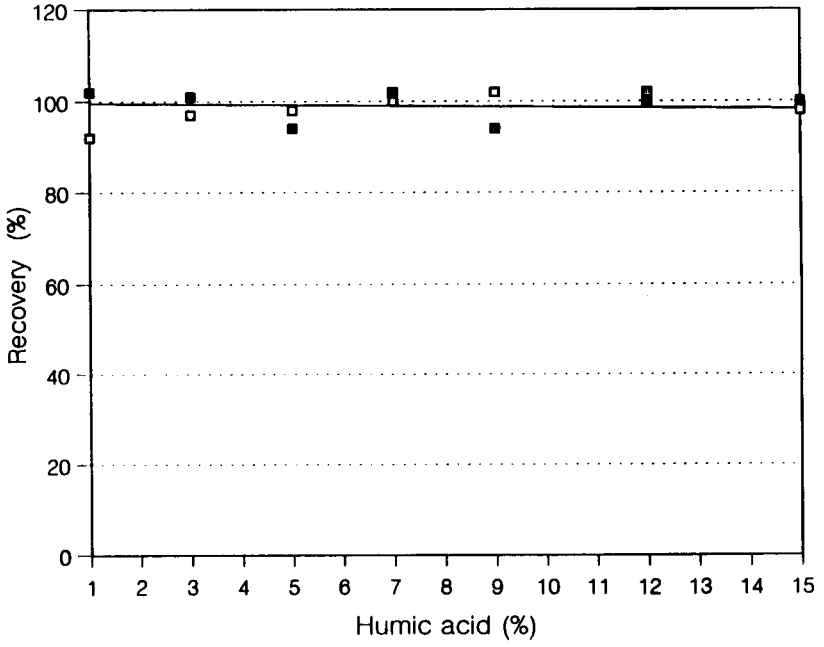

Fig. 6. Effect of the presence of humic acid on the distillation recovery of MeHg from water samples.

tively low (0.45 ng l^{-1}). Its determination by the solvent extraction procedure was not possible. In Fig. 6 the effect of humic acid (Aldrich, humic acid, sodium salt) on the recovery of MeHg obtained by distillation is shown. Evidently, there is no interference even up to 15% of humic acid.

Comparison of solvent extraction and distillation

In Fig. 7 the comparison of the extraction and distillation efficiency of MeHg from large numbers of various kinds of water samples is presented. Evidently the recovery obtained by the distillation procedure does not vary significantly over a wide range of samples. Solvent extraction procedures gave more variable recoveries, which tended to be lower with the increased concentration of MeHg. Higher MeHg concentrations in natural waters are found in anoxic, sulphide rich waters, which were, however, difficult to analyze using the solvent extraction procedure.

Comparison of the results obtained by the distillation and solvent extraction is shown in Fig.

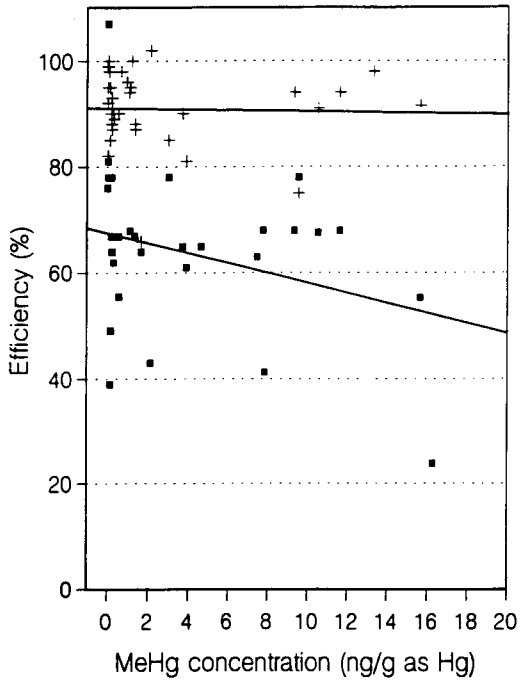

Fig. 7. Comparison of the distillation (+) and solvent extraction (■) efficiency from water samples of various origin.

8. Most of the samples were obtained from remote lakes in Wisconsin. A hundred and ten water samples were compared. On average the distillation resulted in higher results than solvent extraction. Close analysis of data has shown that a good agreement of the results for MeHg was obtained in the range below 1 ng l^{-1}. A significantly higher MeHg concentration was obtained by distillation for samples with higher MeHg concentration. This also indicates that the solvent extraction procedure is not only affected by the presence of sulphide which causes lower spiking recoveries, but is also unable to isolate MeHg compounds originally present in the sample. This can be explained by the fact that HCl used in the initial stage of the solvent extraction was not able to release MeHg compounds quantitatively from bound sites. In our study [28] on sediment samples it was also shown that HCl can not quantitatively release MeHg compounds from bound sites, particularly in sediments with higher MeHg concentrations.

Water samples with high inorganic mercury concentrations

Water samples measured in the present study were obtained from areas not under the direct influence of anthropogenic Hg. The concentration of total Hg in these samples varied from a few ng l^{-1} to 50 ng l^{-1}. However, water samples with a high concentration (influenced by a high anthropogenic input of Hg) of inorganic Hg deserve special attention. This is because the large amount of inorganic Hg present during the ethylation step may cause spurious formation of methyl ethyl mercury. The source of such a systematic positive error has already been discussed in our previous paper [28]. The same problem was also observed with water samples received from an area anthropogenically polluted with Hg. Total Hg in these water samples was very high (several thousand ng l^{-1}). High inorganic Hg was not quantitatively separated by a solvent extraction. A similar experiment as for the recovery curves for MeHg from 50 ml of water samples was performed for inorganic Hg. 50 ml of lake water (Doubtful Lake, Northern Cascade) was spiked with 200 ng of Hg(II) [corresponding to 4

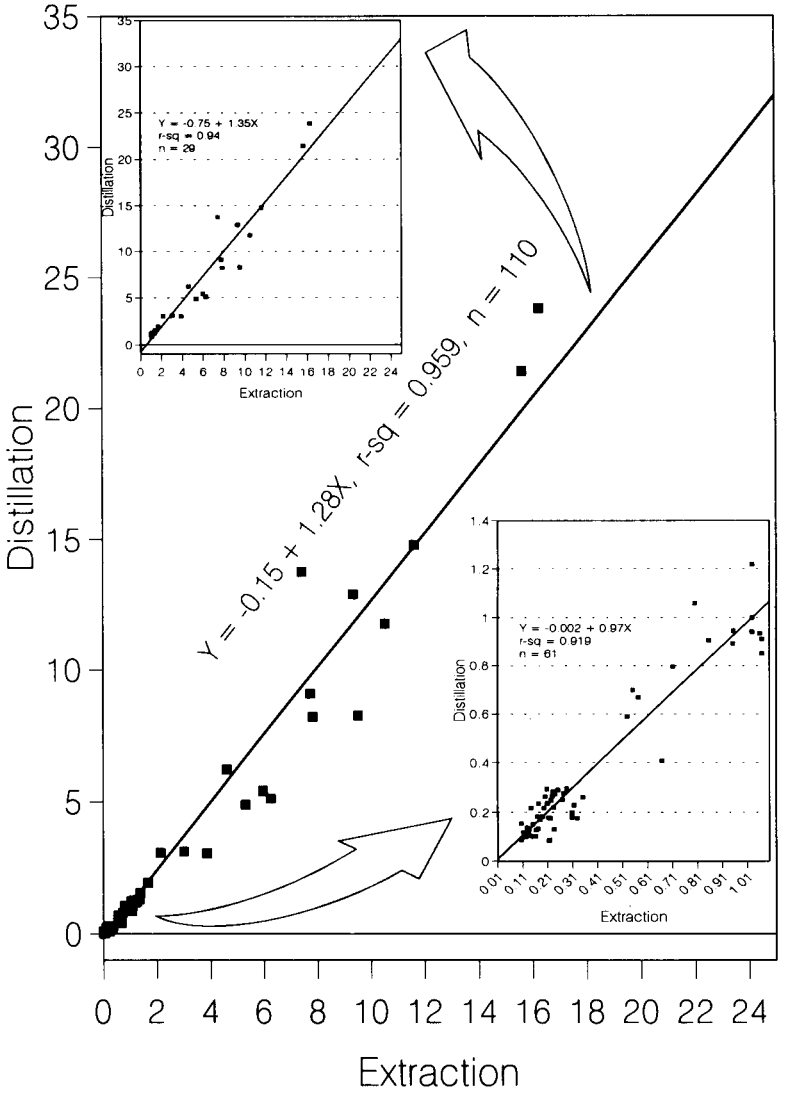

Fig. 8. Correlation of the results for MeHg obtained by distillation and solvent extraction for water samples of various origins. Results are given in ng l^{-1} as Hg.

μg Hg(II) l^{-1}]. During the distillation, seven fractions were collected and inorganic and MeHg concentrations were measured using aqueous phase ethylation, GC separation and AFS detection. The results are shown in Fig. 9. No significant difference was observed using various combinations of reagents. Evidently, in the final fraction (last 10% of the sample) inorganic Hg increased significantly. This further supported the conclusions from the previous discussion that the distillation should be stopped when approximately 80 to a maximum of 90% of the distillate was collected. The distillation of the last 10% of the sample allowed the distillation of the compounds that lowered the pH of the distillate and caused volatilization of inorganic Hg collected in the receiving vial. Both interfered with the final measurement step. Cumulative concentrations of inorganic Hg was rather high in all cases, and in combination with poor quality sodium tetraethyl

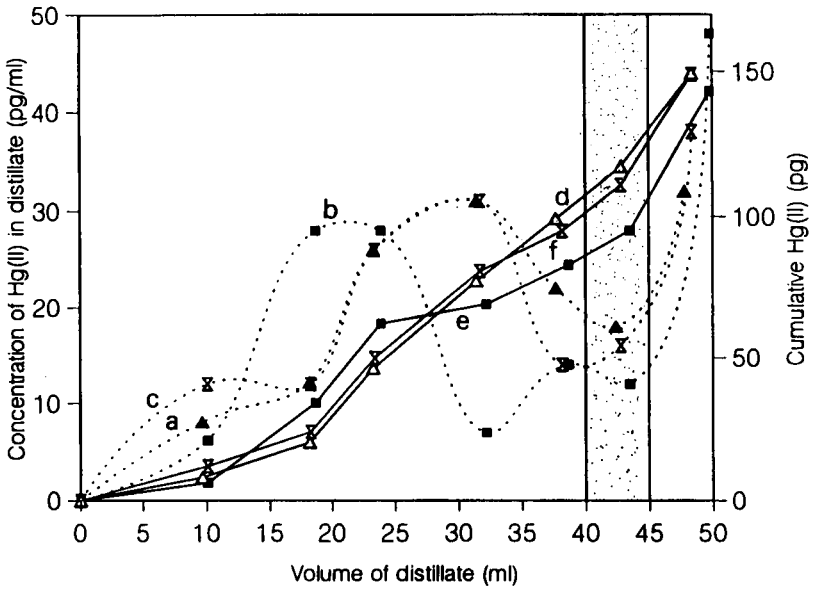

Fig. 9. Release of inorganic mercury during distillation of 50 ml of a Hg(II) spiked (4 $\mu g\ l^{-1}$) remote lake water sample. (a) Method 1: 0.08 M H_2SO_4, 0.13 M KCl, pg ml^{-1}; (b) method 2: 0.08 M H_2SO_4, 0.64 M KCl, pg ml^{-1}; (c) method 3: 0.1 M HCl, pg ml^{-1}; (d) method 1, cumul., pg; (e) method 2, cumul., pg; (f) method 3, cumul. pg.

borate a significant positive error for MeHg determination could be expected. Inorganic Hg may also be isolated by ion-exchange separation after distillation, as used by Padberg et al. [27]. However, in order to perform this separation, the sample must be acidified with HCl, which, in our case was impossible, since Cl^- strongly interferes with the ethylation reaction. It would be worth trying to use such a separation prior to distillation [41], and then diluting the sample so that the final concentration would not exceed 0.1 M HCl, and then continuing with the distillation as described for HCl preserved water samples.

Preservation of water samples

So far water samples that are to be analyzed for MeHg are preserved with HCl and stored in the dark. It has been shown that samples may be kept for days without preservation by freezing or storing them in darkness at low temperatures (0–5°C) [1]. This is very important for samples containing dimethylmercury, since this compound is rapidly converted to MeHg in the presence of HCl. In our previous study [28] concerning MeHg determination in sediments it was shown that dimethylmercury (DMM) is more slowly converted to MeHg in diluted sulphuric acid media than in HCl. This should not be neglected in further studies since low concentrations of DMM were recently detected under certain natural conditions [42,43]. The question is whether the analytical procedures used so far have been able to specify this important compound in the water environment. Some experiments have been performed using sulphuric acid instead of HCl for the preservation of water samples. Unfortunately, some odd and disturbing results have been obtained thus far. In fresh water samples, especially humic rich, acidification by any of the acids caused Hg to go to the walls. For example, in one water sample 40% of total and 25% of MeHg went to the walls upon acidification. If previously acidified and equilibrated water was poured into a new bottle, no further Hg went to the walls. This might be related to an immediate reaction, probably condensation of humic substances on the surface [44]. These phenomena will definitely be investigated further in future experiments. So far, the use of PTFE bottles, with storage unpreserved water samples at 0–4°C in the dark gave better results than adding any acids.

These preliminary experiments on preserva-

tion of water samples prior analysis showed that more systematic experiments are needed. These experiments should be done on as many various kinds of natural water samples as possible. Results obtained for the stability of different Hg forms in artificially prepared samples in the laboratory do not represent behavior in natural samples. Laboratories performing low level Hg speciation should closely collaborate in future by organizing several intercomparison exercises including sampling, preservation, isolation and measurement steps.

Conclusions

The results obtained in this study represent an important contribution toward better accuracy of results for MeHg in water samples. The study concentrated on the separation of MeHg in various kinds of water samples, into an aqueous solution for subsequent determination based on ethylation, gas chromatographic separation and CV-AFS detection. Two methods were compared: solvent extraction, and distillation. Comparisons of the results for MeHg in natural water samples have shown that distillation is preferable to solvent extraction. It gives consistent and high recoveries of MeHg in various samples and achieves better detection limits. It also specifically separates MeHg from dimethyl mercury, if present.

Solvent extraction of MeHg suffers from two disadvantages: (a) low and unreproducible recoveries from anoxic and humic rich water samples and (b) non-quantitative recovery from particulate and humic rich water samples. As with our previous study on sediment samples, it was shown that the standard addition method is certainly not sufficient to ensure the accuracy of the analytical method.

Thanks are due to the Research Community of Slovenia for partial funding of this work. Thanks are also due to IAEA for finding this work through the Research Contract No. 5747/R1/EP and EPRI (Contract No. RP-2020-10). Most of the experimental work has been accomplished at Brooks Rand, Ltd., Seattle, WA, USA. Thanks are therefore due to all co-workers at Brooks Rand. Special thanks are also due to my husband R. Rajar, who patiently collected and carried water samples from remote mountain lakes.

REFERENCES

1 N.S. Bloom and C.J. Watras, in J.P. Vernet (Ed.), Heavy Metals in the Environment, Vol. 2, CEP Consultants, Edinburgh, 1989, p. 349.
2 T. Zvonaric, M. Horvat and P. Stegnar, in J.P. Vernet (Ed.), Heavy Metals in the Environment, Vol. 2, CEP Consultant, Edinburgh, 1987, p. 461.
3 P.J. Craig, in P.J. Craig (Ed.), Organometallic Compounds in the Environment, Wiley, New York, 1986, pp. 65–110.
4 O. Lindquist (Ed.), Mercury in the Swedish Environment, Recent Research on Causes, Consequences and Corrective Methods, Kluwer, Dordrecht, 1991.
5 W.F. Fitzgerald and C.J. Watras, Sci. Total Environ., 87/88 (1989) 232.
6 J.G. Wiener, W.F. Fitzgerald, C.J. Watras and R.G. Rader, Environ. Toxicol. Chem., 9 (1990) 909.
7 C. Brosset, Water Sci. Technol, 15 (1983) 59.
8 O. Lindquist, A. Jernelov, K. Johansson and H. Rodhe, National Swedish Environmental Protection Board Publication No. 1816, 1984, Solna, Sweden.
9 I. Bjorklund, H. Borg and K. Johansson, Ambio, 13 (1984) 118.
10 C.J. Watras and N.S. Bloom, Limnol. Oceanogr, 37 (1992) 1313.
11 W.F. Fitzgerald and G.A. Gill, Anal. Chem., 51 (1979) 1714.
12 J. Olafsson, Anal. Chim. Acta, 86 (1974) 207.
13 C. Haraldson, S. Westerlund and P. Ohman, Anal. Chim. Acta, 221 (1989) 77.
14 D. Beauchemine, J.W. McLaren, A.P. Mykytiuk and S. Berman, J. Anal. Atmos. Spectrom., 3 (1988) 305.
15 N.S. Bloom and W.F. Fitzgerald, Anal. Chim. Acta, 209 (1988) 151.
16 Y. Nojiri, A. Otsuki and K. Fuwa, Anal. Chem., 58 (1986) 544.
17 J.A. Rodriquez-Vasquez, Talanta, 25 (1978) 299.
18 K. Minagawa, Y. Takisawa and I. Kifune, Anal. Chim. Acta, 115 (1979) 103.
19 K. Chiba, K. Yoshida, K. Tanabe, H. Haraguchi and K. Fuwa, Anal. Chem., 55 (1983) 453.
20 A. Paudyn and J.C. Van Loon, Fresenius' Z. Anal. Chem. 325 (1986) 369.
21 Y.H. Lee, Int. J. Environ. Anal. Chem. 29 (1987) 263.
22 K. May, M. Stoeppler and K. Reisinger, Toxicol. Environ. Chem., 13 (1987) 153.
23 M. Horvat, K. May, M. Stoeppler and A.R. Byrne, Appl. Organomet. Chem., 2 (1988) 515.
24 S. Padberg and K. May, Rossbach-Schladot-Ostapczuk (Eds.), Specimen Banking, Springer-Verlag, Berlin, Heidelberg, 1992.

25 N.S. Bloom, Can. J. Fish. Aquat. Sci., 46 (1989) 1131.
26 Y.H. Lee and J. Mowrer, Anal. Chim. Acta, 221 (1989) 259.
27 S. Padberg, A. Iverfeld, Y.-H. Lee, F. Baldi, M. Fillipelli, K. May and M. Stoeppler, presented at the International Conference on Mercury as a Global Pollutant, 1992, Monterey, CA.
28 M. Horvat, N.S. Bloom and L. Liang, Anal. Chim. Acta, 281 (1993) 135.
29 G.A. Gill and W.F. Fitzgerald, Deep Sea Res., 32 (1985) 287.
30 R.P. Mason and W.F. Fitzgerald, Water Air Soil Pollut., 56 (1991) 779.
31 Operational Manual for the CV AAS, Model-2 Mercury Analyser, Brooks Rand, Ltd., 1990.
32 S. Charbonneau, H.V. Tra and P. Pichet, presentation at the International Conference on Mercury as a Global Pollutant, Monterey CA, 1991.
33 L. Liang, M. Horvat and N.S. Bloom, Talanta, (1993) in press.
34 N.S. Bloom and E.A. Crecelius, Mar. Chem., 14 (1983) 49.
35 Y.-H. Lee, A. Iverferld and E. Lord, presentation at the International Conference on Mercury as a Global Pollutant, Monterey CA, 1991.
36 R.P. Mason and W.F. Fitzgerald, Nature, 347 (1990) 457.
37 M. Floyd and L.E. Sommers, Anal. Lett., 8 (1975) 523.
38 H. Nagase, Y. Ose, T. Sato and T. Ishikawa, Int. Environ. Anal. Chem., 13 (1987) 153.
39 V. Zelenko and L. Kosta, Talanta, 20 (1973) 115.
40 I. Gvadjancic, L. Kosta and V. Zelenko, Zh. Anal. Khim., 32 (1978) 812.
41 R. Ahmed, K. May, and M. Stoeppler, Fresenius' Z. Anal. Chem., 326 (1987) 510.
42 F. Baldi and M. Filippelli, Environ. Sci. Technol., 25 (1992) 302.
43 P. Quevauviller, O.F.X. Donard, J.C. Wassrman, F.M. Martin and J. Scneider, Appl. Organomet. Chem., 6 (1992) 221.
44 N.S. Bloom, presentation at the International Conference on Mercury as a Global Pollutant, Monterey, CA, 1991.

Analytica Chimica Acta, 282 (1993) 169–174
Elsevier Science Publishers B.V., Amsterdam

Determination of promethazine by its inhibition of the chemiluminescence of the luminol–hydrogen peroxide–chromium(III) system

Abdulrahman A. Alwarthan, Saad A. Al-Tamrah and Akel A. Akel

Chemistry Department, College of Science, King Saud University, P.O. Box 2455, Riyadh-11451 (Saudi Arabia)

(Received 1st February 1993; revised manuscript received 23rd April 1993)

Abstract

The luminol–H_2O_2–metal ion system has been widely used in chemical and biological analysis. A method is described for the determination of promethazine based on its inhibition of the intensity of chemiluminescence from the luminol system. The method is sensitive, convenient and simple with a detection limit of 3×10^{-9} M. The R.S.D. at 1×10^{-5} M promethazine is 1.3% (ten replicates). The method was applied successfully to the analysis of various commercially available dosage forms containing promethazine. The results obtained for the assay of commercial preparations compared well with those obtained by the official method and showed good accuracy and precision.

Keywords: Chemiluminescence; Flow injection; Pharmaceuticals; Promethazine

Promethazine [1,*N*,*N*-trimethyl-2-(phenothiazin-10-yl)ethylamine] is a histamine H_1-receptor antagonist. The phenothiazines are one of the most important groups of medicaments, used as antihistamines, tranquillizers, antiemetics and anti-Parkinson drugs [1].

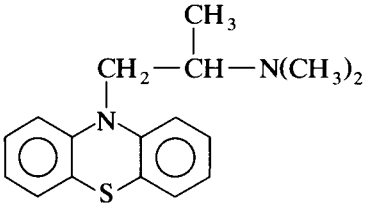

The importance of the phenothiazines and the continuing introduction of these drugs has instigated many researchers to explore methods for their determination, and numerous methods are already available in the literature. Among the methods used to assay phenothiazine derivatives both in bulk and in pharmaceutical preparations and biological fluids are titrimetric [2,3], chromatographic [4–6], spectrophotometric [7–10] and electrochemical [11,12] procedures. Some of these methods lack sensitivity and specificity [7–9], require long heating times [10,13] or involve non-aqueous media [14].

Few methods applying flow injection (FI) have been reported; one requires the use of a very high concentration (10 M) of perchloric acid [15] and another uses ammonium metavanadate as an oxidant [16].

Chemiluminescence (CL) has been exploited in a number of analytical applications owing to its great sensitivity [17] and selectivity for particular chemical forms and hence can be very useful in speciation studies [18]. The advent of FI has been one of the reasons for the increasing application of CL. The use of CL–FI as a simple means of

Correspondence to: A.A. Alwarthan, Chemistry Department, College of Science, King Saud University, P.O. Box 2455, Riyadh-11451 (Saudi Arabia).

drug detection has been applied to many drugs, including morphine [19], buprenorphine hydrochloride [20] and tetracycline [21].

In aqueous solutions, the most commonly used chemiluminescent species is luminol (5-amino-2,3-dihydrophthalazine-1,4-dione), which reacts with hydrogen peroxide in the presence of a catalyst (generally a metal or metal-containing compound) in alkaline solution to yield 3-aminophthalate in an excited electronic state which returns to ground state with the production of light [22–25]. The light intensity can easily be monitored with a photomultiplier tube (PMT), with no wavelength discrimination. Promethazine is found to inhibit this reaction. If promethazine hydrochloride is made to be the rate-limiting reagent, then the amount of emission inhibited is proportional to the concentration of promethazine, and can be used to determine the promethazine by measuring the decrease in the CL. This paper presents a CL method for the determination of promethazine, based on its inhibition of the CL emission of the luminol–H_2O_2–Cr^{3+} system, with the possibility of applying the proposed method to drug analysis.

EXPERIMENTAL

Reagents

A stock standard solution (0.01 M) of promethazine was prepared by dissolving 0.1604 g of pure promethazine hydrochloride in 50 ml of distilled water and was stored in amber-coloured bottle in a refrigerator. Working standard solutions were prepared by appropriate dilution of the stock standard solution.

Chromium nitrate (Fisher) stock standard solution (0.02 M), was prepared by dissolving 0.2000 g of chromium(III) nitrate nonahydrate in 50 ml of distilled water. A stock standard solution of luminol (general-purpose reagent, Sigma) (0.01 M) was prepared by dissolving 0.1772 g in 100 ml of 0.1 M carbonate buffer. Hydrogen peroxide solution (30% w/v) (BDH) was prepared daily by diluting a measured amount with 0.1 M carbonate buffer. The carbonate buffer (0.1 M) was prepared by dissolving 10.6 g of sodium carbonate (BDH, AnalaR) in water and diluting to 1 l. Distilled, deionized water was used throughout.

Instrumentation

The flow cell was a coil made of 1.3 mm i.d. glass tubing spiralled to a diameter of 35 mm with five turns, enabling the flowing, emitting solution to remain in view of the detector for ca. 3 s, depending on the flow-rates used.

The coiled glass flow cell was used as described previously [19], backed by a mirror for maximum light collection and a sensitive PMT (Thorn EMI, 9789QB) for measurement of the emitted light intensity. The PMT was operated at 400 V, provided by a stable high-voltage power supply (Thorn EMI, Model PM 28BN). No wavelength selection was involved.

The flow manifold used is shown in Fig. 1. A four-channel peristaltic pump (Gilson Minipuls 3MP4) was used to deliver the luminol solution through R_1, which acts as a carrier stream for the chromium(III) solution which is injected via a solenoid-activated rotary valve (Rheodyne Model 5020). This stream was merged 10 cm downstream with a stream of hydrogen peroxide (R_2) at a PTFE T-piece and merged again 15 cm downstream with a stream of promethazine solution at a second PTFE T-piece. All three carrier streams were pumped at the same flow-rate via the Gilson pump (2.1 ml min^{-1} in each channel). PTFE tubing (0.8 mm i.d.) was used throughout the remainder of the manifold. The three merged

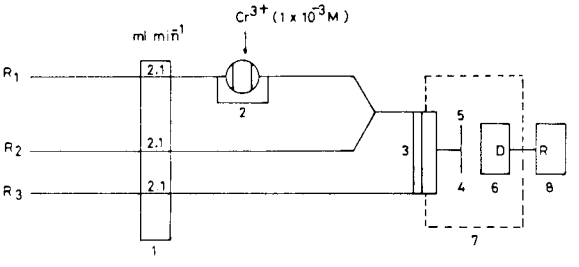

Fig. 1. Manifold used for CL determination of promethazine and some of its pharmaceutical preparations. 1 = Peristaltic pump; 2 = sample injection; 3 = Perspex T-piece; 4 = waste; 5 = coiled flow cell; 6 = PMT; 7 = housing; 8 = recorder, R_1, R_2, R_3 = flow streams.

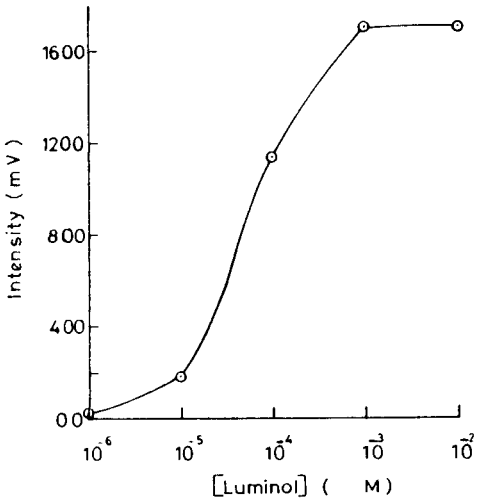

Fig. 2. Effect of luminol concentration on the net CL intensity for 1×10^{-5} M promethazine, 0.01 M H_2O_2 and 1×10^{-3} M chromium(III).

zones travelled 2.5 cm (the smallest practical distance) before passing into the flow cell.

The output from the PMT was fed to a strip-chart recorder (Yokogawa Model 3021) and the peak heights were measured manually. All results are the means of five injections of Cr(III) solution into five different promethazine solutions (promethazine solutions having the same concentrations), unless stated otherwise.

Optimization of CL flow system

A series of experiments were conducted to establish the optimum analytical variables. The parameters that affect the intensity of the CL signal were investigated, namely flow-rate, pH, reagent concentrations and the buffers used as a solvent for luminol and hydrogen peroxide.

The effect of luminol concentration on the net CL intensity was investigated. The results (Fig. 2) showed that the net CL intensity was greatest when the concentration of luminol was 1×10^{-3} M.

The CL of the luminol–H_2O_2–Cr^{3+} system was found to occur in an alkaline medium, hence 0.1 M carbonate buffer was used as a diluent for the luminol and hydrogen peroxide solutions. To study the effect of pH, the carbonate buffers

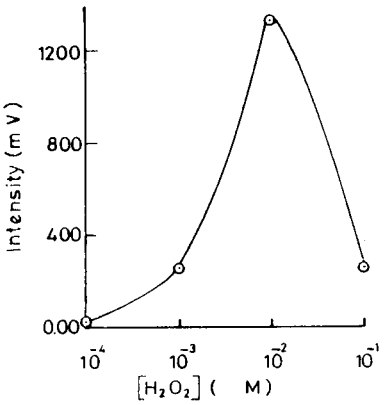

Fig. 3. Effect of H_2O_2 concentration on the net CL intensity for 1×10^{-5} M promethazine, 1×10^{-3} M luminol and 1×10^{-3} M chromium(III).

were adjusted to different pH values (9.6–10.8). The maximum net CL intensity was obtained at pH 10.5.

The effect of hydrogen peroxide concentration on the net CL intensity was also studied. The greatest intensity was obtained when 0.01 M H_2O_2 was used, as shown in Fig. 3.

As the conventional CL reaction of luminol with hydrogen peroxide is catalysed by various metal ions, several metals were tested for their effect on the luminol–H_2O_2 syhstem in presence of promethazine. The results obtained are given in Table 1. As chromium(III) gave the best signal as a catalyst for the oxidation of luminol by hydrogen peroxide in the alkaline solution, the effect of its concentration was optimized. Different concentrations of chromium(III) solution were

TABLE 1

Effect of various metal ions (each 1×10^{-4} M) as catalysts for the luminol–hydrogen peroxide reaction in the presence and absence of promethazine (1×10^{-5} M)

Metal ion	Signal height (mV) [a]	
	With promethazine	No promethazine
Ni^{2+}	–	–
Mn^{2+}	–	–
Fe^{2+}	–	0.64
Cu^{2+}	–	16.3
Cr^{3+}	29.3	59.0

[a] Dashes indicate no signal obtained.

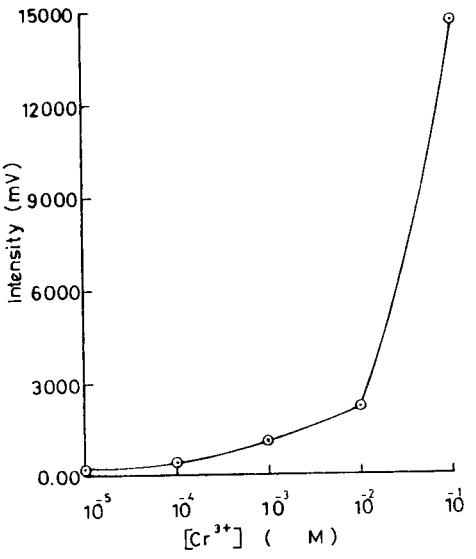

Fig. 4. Effect of chromium(III) concentration on the net CL intensity for 1×10^{-5} M promethazine, 0.01 M H_2O_2 and 1×10^{-3} M luminol.

prepared and their effects on the net CL intensity were investigated. It was found that 0.1 M chromium(III) gave the greatest intensity, as shown in Fig. 4.

Flow-rate is an essential parameter because its variation has a great influence on the emission intensity. The flow-rate is conveniently controlled by the peristaltic pump. The effect of total flow-rate was studied, keeping all other conditions constant, over the range 3.2–10.4 ml min^{-1}, with equal flows in each channel. The results obtained are summarized in Table 2, which indicates that a sufficiently high flow-rate should be used to enable the excited product to reach the detector in a minimum time and hence maximum collection of the emitted light can be achieved. In this instance, the intensity increased with increasing flow-rate. As the total flow-rate was increased from 3.2 to 10.4 ml min^{-1}, the emission intensity also increased. At flow-rates higher than 6.3 ml min^{-1} no significant increase in the emission intensity was obtained and therefore a flow-rate of 6.3 ml min^{-1} was adopted for promethazine determination.

TABLE 2

Effect of flow-rate on the emission intensity from 1×10^{-5} M promethazine, 1×10^{-3} M luminol, 0.01 M H_2O_2 and 0.1 M chromium(III) solution

Flow-rate (ml min^{-1})	Emission intensity (mV)
3.2	960
4.2	970
6.2	1140
8.3	1190
10.4	1190

It was thought that if Cr(III) solution instead of promethazine solution were pumped through R_3 a steady light intensity would be obtained, and if promethazine solution were injected into the carrier stream, then an inhibiting signal directly proportional to the concentration would be recorded. However, it was concluded that this version was less sensitive, causing a continuous shift in the baseline and had poor precision. Therefore, this version was not used for promethazine determination.

RESULTS AND DISCUSSION

The determination of promethazine is based on the inhibition of the luminol system, so that the peaks resulting from the indicator reaction will be decreased in proportion to the inhibitor concentration.

Inhibition mechanism

The chromium(III) ion is a catalyst for the luminol–H_2O_2 system. However, promethazine alone, as expected, is not a catalyst because in an alkaline solution of luminol–H_2O_2–promethazine without chromium(III) CL is not observed. The CL reaction mechanism can be briefly expressed by the following reaction [26]:

$$\text{luminol} + [\text{oxygen}] \rightarrow \text{peroxide adduct} \rightarrow \text{aminophthalate}^* \rightarrow \text{aminophthalate} + h\nu \quad (1)$$

In solution, there are two forms of oxygen which may play an important role in reacting with luminol, singlet oxygen and the superoxide anion ($O_2^{-\cdot}$). However, previous work [27] has shown

TABLE 3

Determination of promethazine in pharmaceutical preparations by the proposed method

Preparation	Amount of promethazine (mg)		Recovery (%)
	Claimed	Found [a]	
Phenergan tablet (25 mg) (Rhone-Poulenc)	25	25.6	102.4
Phenergan expectorant (5 mg in 5 ml) (Rhone-Poulenc)	5	5.23	104.6
Promantine syrup (6 mg in 5 ml) (Misr)	6	6.14	102.3

[a] Average of five injections per sample.

that singlet oxygen is not stable in alkaline solution. Therefore, it is concluded that the superoxide anion is probably the only species involved in the oxidation of luminol to aminophthalate.

The lifetime of the superoxide anion is only a few milliseconds [28], even in alkaline solution. Addition of promethazine to the luminol–H_2O_2–Cr^{3+} system shortens the duration of CL. In the concentration range studied, the inhibition is increased as the drug sample concentration is increased. This probably indicates that promethazine can combine with the superoxide anion to form a peroxide adduct which speeds up the decomposition of the superoxide. The luminescent species is aminophthalate, whether promethazine is present or not. This means that the promethazine–peroxide adduct can react with luminol to exchange superoxide anions. Clearly, a much more extensive investigation of these reactions is needed, and this is currently being undertaken.

Calibration data

Under the conditions established a log–log calibration graph was obtained covering the range 1×10^{-9}–1×10^{-3} M. The graph was linear over five orders of magnitude between 1×10^{-9} and 1×10^{-4} M. The linear range allows the determination of 1×10^{-9} M levels of promethazine. The line of regression of log (emission intensity) (I) on promethazine concentration (C) was $\log I = 2.233 - 0.085 \log C$ ($r = 0.997$, $n = 5$). The limit of detection was 3×10^{-9} M, which is slightly higher than the lowest concentration that can be measured, probably owing to the increase in σ values. The relative standard deviation is 1.3% for ten determinations of 1×10^{-5} M promethazine. A non-logarithmic graph for a narrower concentration range (1×10^{-5}–9×10^{-5} M) gave a regression line of emission intensity on promethazine concentration of $I = 985 - 9.3 \times 10^{6} C$ ($r = 0.983$, $n = 5$).

Effect of interferences

The inhibited luminescence apparent from the promethazine–luminol system is certainly of analytical value. However, two types of interferences were studied: first, quenchers of 3-aminophthalate fluorescence, which include ions derived from elements of high atomic number; and second, excipients that are normally added to pharmaceutical preparations and that may interfere and

TABLE 4

Determination of promethazine in pharmaceutical preparations by the CL and the official BP [2] methods

Preparation	Amount of promethazine (mg)			Recovery ± S.D. (%)	
	Claimed	Found [a]		CL	BP
		CL	BP		
Phenergan tablet (25 mg) (Rhone-Poulenc)	25	25.6	24.9	102.4 ± 0.25	99.6 ± 0.80
Phenergan expectorant (5 mg in 5 ml) (Rhone-Poulenc)	5	5.23	5.26	104.6 ± 1.2	100.6 ± 0.31
Promantine syrup (6 mg in 5 ml) (Misr)	6	6.14	6.18	102.3 ± 0.98	103 ± 0.26

[a] Average of five determinations per sample.

decrease the analytical sensitivity. Therefore, metal ion (and other) interferences were studied in solutions having a final concentration of 1×10^{-6} M promethazine in the presence of 1×10^{-4} M interferent. It was found that Al(III), Cd(II), Hg(II), Ni(II), Sr(II) and Zn(II) did not interfere. However, Cu(II) at concentrations $> 1 \times 10^{-4}$ M gave a negative response by quenching the CL signal, but its interference can be obviated using 3.0×10^{-3} M EDTA as a masking agent. Excipients such as fructose, glucose galactose, nicotinamide and magnesium stearate did not interfere. Riboflavin, starch and carboxypolymethylene (Carbowax) showed slight interferences.

Application

The accuracy of the proposed CL method was tested by analysing two pharmaceutical dosage forms, tablets and syrup, containing promethazine. The results are summarized in Table 3. Most of the results obtained agreed with the reported values. In order to establish the validity of the proposed CL method, the proprietary drugs containing promethazine listed in Table 4 were analysed. The same batch of samples was analysed by the BP method [2] and the recoveries and standard deviations were calculated as shown in Table 4. The results show that satisfactory accuracy was afforded by both methods.

In conclusion, the determination of promethazine by CL–FI is superior to other conventional methods in that it is very fast, simple and sensitive and manipulations by and intervention of the operator are minimal.

REFERENCES

1 J.E.F. Reynolds and A.B. Prasad, Martindale, The Extra Pharmacopoeia, Pharmaceutical Press, London, 28th edn., 1982, pp. 1294–1297.
2 British Pharmacopeia 1980, H.M. Stationery Office, London, 1980.
3 M. Gajewska, M. Ciszewska and A. Goldnik, Chem. Anal. (Warsaw), 23 (1978) 503.
4 W.T. Kok, W.H. Voogt, U.A.Th. Brinkman and R.W. Frei, J. Chromatogr., 354 (1986) 249.
5 K. Thoma and K. Albert, Arch. Pharm. (Weinheim), 317 (1984) 133.
6 J.I. Javaid, H. Dekirmenjian and J.M. Davis, J. Pharm. Sci., 71 (1982) 63.
7 P.G. Ramappa, H.S. Gowda and A.N. Nayak, Analyst, 105 (1980) 663.
8 P.G. Ramappa and K. Basavaiah, Indian J. Pharm. Sci., 47 (1985) 125.
9 F. Gurka, R.E. Kolinski, J.W. Myrick and C.E. Wells, J. Pharm. Sci., 69 (1980) 1069.
10 S.R. El-Shabouri, A.F. Youssef, F.A. Mohamed and A.I. Rageh, J. Assoc. Off. Anal. Chem., 69 (1986) 821.
11 F.W. Teare and R.N. Yadav, Can. J. Pharm. Sci., 13 (1978) 69.
12 M.M. Ellaithy, Indian J. Pharm. Sci., 42 (1980) 41.
13 P.G. Ramappa, H.S. Gowda and A.N. Nayak, Microchem. J., 28 (1983) 586.
14 M. Rizk, A.N. Zakhari, F. Ibrahim and M.I. Walash, Talanta, 33 (1986) 111.
15 M.A. Koupparis and A. Barcuchova, Analyst, 111 (1986) 313.
16 S.M. Sultan, Analyst, 116 (1991) 177.
17 A. Townshend, Analyst, 115 (1990) 495.
18 L.A. Montano and J.D. Ingle, Jr., Anal. Chem., 51 (1979) 919.
19 R.W. Abbott, A. Townshend and R. Gill, Analyst, 111 (1986) 635.
20 A.A. Alwarthan and A. Townshend, Anal. Chim. Acta, 185 (1986) 329.
21 A.A. Alwarthan and A. Townshend, Anal. Chim. Acta, 205 (1988) 261.
22 W.R. Seitz, W.W. Suydam and D.M. Hercules, Anal. Chem., 44 (1972) 957.
23 L.L. Klopf and T.A. Nieman, Anal. Chem., 55 (1983) 1080.
24 D.B. Paul, Talanta, 25 (1978) 377.
25 L.J. Kricka and G.H.G. Thorpe, Analyst, 108 (1983) 1274.
26 H.H. Selinger, Photochem. Photobiol., 73 (1975) 335.
27 R.W. Ware and M.P. Richter, J. Chem. Phys., 48 (1968) 1595.
28 F. Ross and A.B. Ross (Eds.), National Standard Reference Data Series, National Bureau of Standards, Washington, DC, 1977, p. 59.

Analytica Chimica Acta, 282 (1993) 175–180
Elsevier Science Publishers B.V., Amsterdam

Chemiluminescence detection of organotin compounds with bis(2,4,6-trichlorophenyl) oxalate by flow-injection analysis

Teruhisa Fujimaki, Takayuki Tani and Shigenobu Watanabe

Kanagawa Prefectural Public Health Laboratories, 52-2 Nakao-Cho, Asahi-ku, Yokohama 241 (Japan)

Sumiko Suzuki and Hiroyuki Nakazawa

Department of Pharmaceutical Sciences, National Institute of Public Health, 4-6-1 Shirokanedai, Minato-ku, Tokyo 108 (Japan)

(Received 15th March 1993; revised manuscript received 27th April 1993)

Abstract

The chemiluminescence (CL) reaction of bis(2,4,6-trichlorophenyl) oxalate with hydrogen peroxide was applied to the detection of fluorescent organotin–quinoline complexes using a flow-injection system. Four organotin compounds, i.e., di-*n*-butyltin dichloride (DBTC), diphenyltin dichloride (DPTC), tri-*n*-butyltin chloride (TBTC) and triphenyltin chloride (TPTC), were examined in conjunction with 2-methyl-8-hydroxyquinoline. Factors affecting the CL intensity such as solvents, reagent concentrations, pH and flow-rate were studied. The detection limits for DBTC, DPTC, TBTC and TPTC were 0.5 μM (3 ng), 1.25 μM (8.6 ng), 25 μM (162.7 ng) and 100 μM (770.9 ng), respectively, with a signal-to-noise ratio of 3.

Keywords: Chemiluminescence; Flow injection; Organotin compounds

Organotin compouds have been applied in many fields such as stabilizers for poly(vinyl chloride), fungicides and miticides in agriculture and anti-fouling agents for ships. A series of studies demonstrated that organotin compounds with short alkyl chains or phenyl substituents exhibited considerable toxicity towards both aquatic organisms and mammals. Environmental pollution and food contamination by these compounds have become a serious problem in recent years. Sensitive and accurate detection methods therefore have been investigated to elucidate the environmental fate and pollution levels of the compounds and a number of reports has been published [1].

Atomic absorption spectrometric [2], thin-layer chromatographic [3], gas chromatographic (GC) [4–6] and liquid chromatographic (LC) [7–10] methods have been reported. GC, however, is not suitable for some organotin compounds and LC lacks sensitivity.

Chemiluminescence (CL) reactions of aryl oxalates with hydrogen peroxide (H_2O_2) have recently been developed for the determination of fluorescent compounds such as dansylated amino acids [11,12], fluorescamine-labelled catecholamines [13] and derivatized amphetamine-related compounds [14] with selectivity and high sensitivity. In this work, the CL reaction with a flow-injection system was applied to the detection

Correspondence to: T. Fujimaki, Kanagawa Prefectural Public Health Laboratories, 52-2 Nakao-Cho, Asahi-ku, Yokohama 241 (Japan).

of fluorophore-derivatized organotin compounds. This paper reports basic investigations on the CL reaction of organotin compounds.

EXPERIMENTAL

Reagents

Distilled water was used after deionization and filtration with a Millipore (Bedford, MA, USA) Milli-Q water purification system. Di-*n*-butyltin dichloride (DBTC) and tri-*n*-butyltin chloride (TBTC) were purchased from Tokyo Kasei Kogyo (Tokyo, Japan) and diphenyltin dichloride (DPTC) and triphenyltin chloride (TPTC) from Aldrich (Milwaukee, WI, USA). They were of > 95% purity. Stock standard solutions of these organotin compounds in pesticide analytical grade acetonitrile from Wako (Osaka, Japan) were prepared. Quinoline compounds were purchased from Tokyo Kasei Kogyo. 2-Methyl-8-hydroxyquinoline (2-M-8-HQ), 8-hydroxyquinoline (8-HQ) and 5,7-dichloro-8-hydroxyquinoline (5,7-D-8-HQ) were recrystallized from ethanol. Analytical-reagent grade 8-mercaptoquinoline hydrochoride (8-MQ) was used without recrystallization. All quinolines were dissolved in acetonitrile. Imidazole, bis(2,4,6-trichlorophenyl) oxalate (TCPO), ethyl acetate (EtOAc) and H_2O_2 (30%) were purchased from Wako. Imidazole was dissolved in water and adjusted to pH 7.5 with HNO_3. The imidazole solution was combined with the same volume of acetonitrile. TCPO–H_2O_2 reagent solution was prepared by mixing TCPO in EtOAc with H_2O_2 in acetonitrile before use. All other chemicals were of analytical-reagent grade.

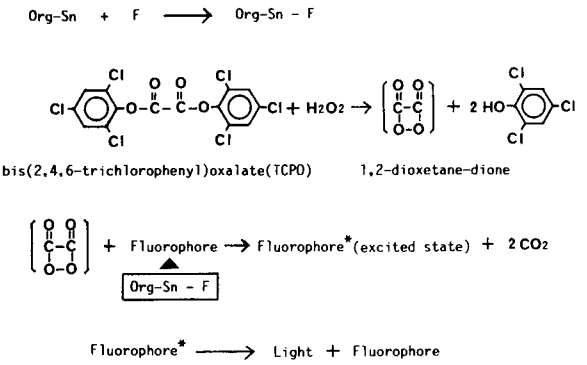

Fig. 1. Proposed mechanism for peroxyoxalate chemiluminescence. The organotin compounds and the fluorimetric reagents are indicated by Org-Sn and F, respectively.

CL measurement with flow-injection system

The CL reaction of TCPO with H_2O_2 [15] was applied to the detection of fluorescent organotin compounds (Fig. 1). The flow-injection system is shown in Fig. 2. Three pumps and three flow lines were used: the first pump (P_1) was a Model P-311 (Irica Instruments, Kyoto, Japan) for the carrier solution of quinoline, the second pump

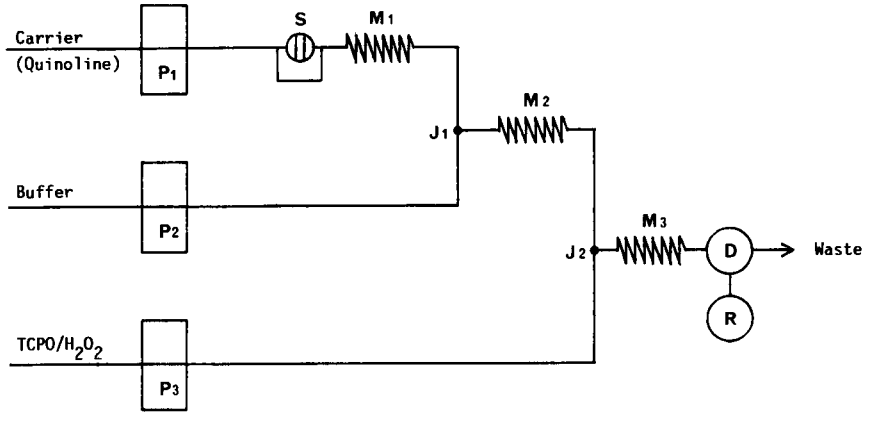

Fig. 2. Schematic diagram of flow system. P_1–P_3 = pumps; S = sample injector (20 μl); D = detector; R = integrator; J_1 and J_2 = T-joints; M_1–M_3 = mixing coils (1000 mm × 0.25 mm i.d.).

(P_2) was a Model KHD-26 (Kyowa Seimitsu, Tokyo, Japan) for the imidazole–nitrate buffer solution and the third pump (P_3) was a Model LC-200 (Oyobunko Kiki, Tokyo, Japan) for the TCPO–H_2O_2 reagent solution. Mixing coils (M_1–M_3) made of PTFE tubing (1000 mm × 0.25 mm i.d.) were wrapped with aluminium foil to prevent the photoinitiation of peroxyoxalate CL [16]. Stainless-steel and PTFE tubing of 0.25 mm i.d. were used in the whole flow line system. A Model 7125 injection valve with a 20-μl loop (Rheodyne, Cotati, CA) was used. The CL detector was a Model S-3400 with a 100-μl spiral flow cell (Soma Optics, Tokyo, Japan) and the recorder–integrator was a Chromatopac C-R6A data processor (Shimadzu, Kyoto, Japan).

Injected analyte was introduced into coil M_1 for mixing with the fluorimetric reagent. The derivatized analyte was then mixed with the buffer solution by passing through coil M_2. The reagent solution was pumped through coil M_3 to effect the organotin CL reaction and the CL intensity was measured.

Procedure for fluorescence measurement

The fluorescence intensity of organotin–quinoline complexes was determined by mixing 1.0 ml of 100 μM organotin solution with 1.0 ml of 100 μM 2-M-8-HQ solution a making measurements with an FP-777 spectrofluorimeter (JASCO, Tokyo, Japan).

RESULTS AND DISCUSSION

Selection of fluorimetric reagent

Various flavone and quinoline compounds were considered as fluorimetric reagents in the hope that the CL reaction might be applied. Morin demonstrated excellent fluorescence [17] and CL intensity, but could not be used because of the high noise. Other flavone compounds such as flavonol, fisetin and kaempferol showed a similar behaviour to morin. Therefore, quinoline compounds such as 2-M-8-HQ, 8-HQ, 5,7-D-8-HQ and 2-MQ were evaluated together with organotin compounds such as DBTC, DPTC, TBTC and TPTC. The organotin–2-M-8-HQ complexes showed excellent CL intensity (Table 1). The fluorescence excitation and emission spectra of organotin–2-M-8-HQ complexes are presented in Fig. 3. Both the TBTC– and TPTC–quinoline complexes provided weak fluorescence and CL intensity. This result might be explained in terms of the steric hindrance of the functional groups such as three *n*-butyl and phenyl groups in TBTC and TPTC, respectively.

TABLE 1

Relative chemiluminescence intensities of organotin–quinoline complexes [a]

Quinoline	Organotin compound			
	DBTC	DPTC	TBTC	TPTC
2-M-8-HQ	100.0	40.5	2.4	0.8
8-HQ	15.5	48.8	0.2	0.8
5,7-D-8-HQ	8.3	10.7	0.5	0.5
8-MQ	2.4	2.4	0.2	0.8

[a] Concentration of organotin compounds: 1×10^{-4} M. Flow conditions: P_1, 1 mM quinoline–CH_3CN, 1.0 ml min^{-1}; P_2, 0.1 M imidazole–HNO_3 (pH 7.0)–CH_3CN (1+1), 0.3 ml min^{-1}; P_3, 1 mM TCPO–EtOAc–0.1 M H_2O_2 (1+3), 1.2 ml min^{-1}. The intensity of the DBTC–2-M-8-HQ complex was arbitrarily taken as 100.

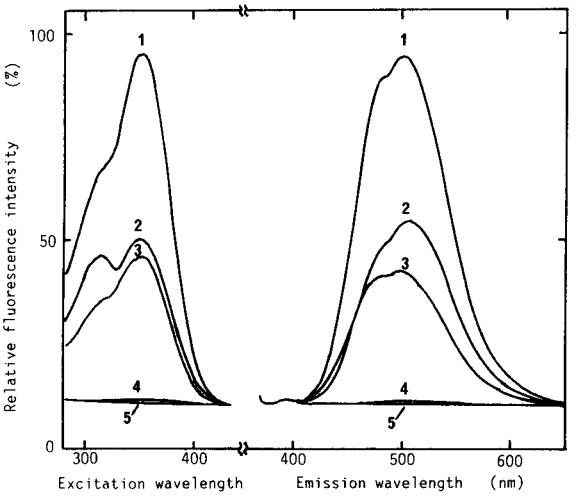

Fig. 3. Excitation and emission spectra of organotin–2-M-8-HQ complexes in acetonitrile. [DBTC], [DPTC], [TBTC], [TPTC], [2-M-8-HQ] = 1×10^{-4} M. 1 = DBTC, λ(ex) = 352 nm, λ(em) = 500 nm; 2 = DPTC, λ(ex) = 351 nm, λ(em) = 506 nm; 3 = TBTC, λ(ex) = 352 nm, λ(em) = 500 nm; 4 = TPTC, λ(ex) = 354 nm, λ(em) = 510 nm; 5 = 2-M-8-HQ alone. Slit width, 10 nm.

Effect of organic solvents

TCPO showed excellent CL intensity and stability in EtOAc [11] and acetonitrile [19]. The buffer solution greatly increased the CL intensity [18]. H_2O_2 as a solvent was studied in comparison with hydrophilic organic solvents [11,19]. The CL intensity and stability in several solvents were examined, and acetonitrile was selected (Fig. 4). Strong CL intensity was observed in both acetonitrile and acetone. Being unstable immediately after the introduction of TCPO–H_2O_2, the CL intensity became stable 30 min later in both solvents. The CL intensity in acetonitrile was higher and more stable than that in acetone. Weak CL intensity was observed in alcohols, tetrahydrofuran and 1,4-dioxane and no CL was observed in *N,N'*-dimethylformamide and dimethyl sulphoxide.

Effect of reagent concentration and pH

H_2O_2 in the concentration range 5×10^{-3}–0.5 M was examined; the maximum CL intensity was observed at 50 mM H_2O_2 (Fig. 5A).

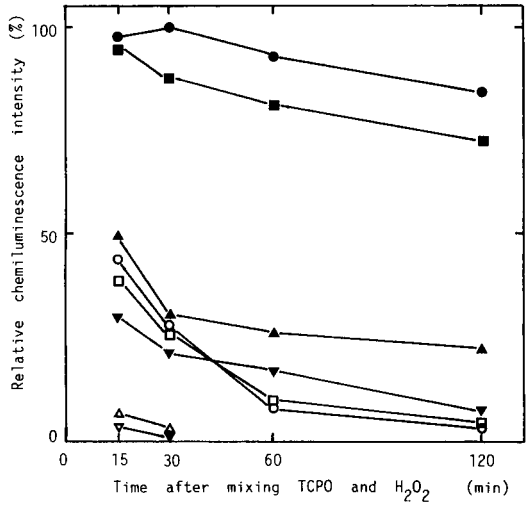

Fig. 4. Effect of solvents on chemiluminescence intensity and stability. Flow conditions: P_1 = 1 mM 2-M-8-HQ–CH_3CN, 1.0 ml min^{-1}; P_2 = 0.1 M imidazole–HNO_3 (pH 7.0)–CH_3CN (1+1), 0.3 ml min^{-1}; P_3 = 1 mM TCPO–EtOAc–0.1 M H_2O_2 (above each solvent) (1+3), 1.2 ml min^{-1}. DBTC concentration, 1×10^{-4} M. ● = Acetonitrile; ■ = acetone; ▲ = tetrahydrofuran; ▼ = 1,4-dioxane; ○ = ethanol; □ = *n*-butanol; △ = methanol; ▽ = *n*-propanol.

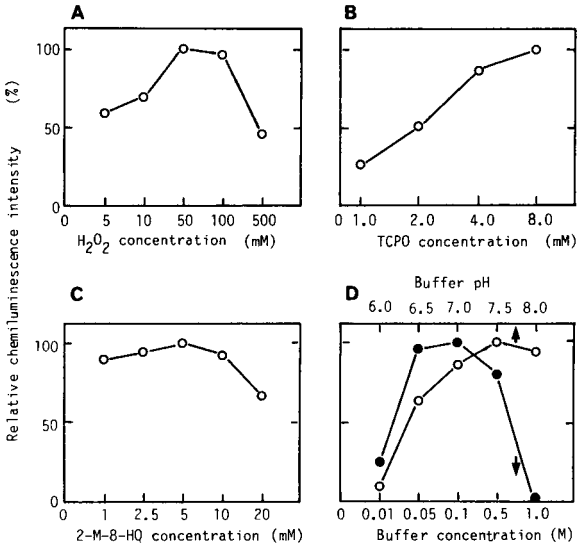

Fig. 5. Effect of reagent concentration and pH on chemiluminescence intensity. (A) P_3 = 1 mM TCPO–EtOAc–5–500 mM H_2O_2–CH_3CN (1+3); (B) P_3 = 1.0–8 mM TCPO–EtOAc–50 mM H_2O_2–CH_3CN (1+3); (C) P_1 = 1.0–20 mM 2-M-8-HQ–CH_3CN, P_3 = 4 mM TCPO–EtOAc–50 mM H_2O_2–CH_3CN (1+3); (D) ○ = buffer pH, P_2 = 0.1 M imidazole–HNO_3 (pH 6.0–8.0)–CH_3CN (1+1), P_3 = 4 mM TCPO–EtOAc–50 mM H_2O_2–CH_3CN (1+3); (D) ● = buffer concentration, P_2 = 0.01–1.0 M imidazole–HNO_3 (pH 7.5)–CH_3CN (1+1), P_3 = 4 mM TCPO–EtOAc–50 mM H_2O_2–CH_3CN (1+3). Other conditions as in Fig. 4.

Hydrolysed TCPO, i.e., 2,4,6-trichlorophenol (TCP), quenches the CL intensity [20]. The TCPO concentration is therefore critical. In mixed solvents of EtOAc and acetone, 10 mM TCPO can be dissolved [21], whereas in EtOAc 8 mM TCPO is hardly soluble (in our experiment). Increasing the TCPO concentration caused an increase in the CL intensity (Fig. 5B), but the signal-to-noise ratio was 353 and 210 at 4 and 8 mM, respectively. A TCPO concentration of 4 mM was selected for the CL reaction.

Concentration of 2-M-8-HQ from 1 to 20 mM were examined; 5 mM 2-M-8-HQ showed the maximum CL intensity (Fig. 5C).

The optimum imidazole concentration was investigated in the range 0.01–1.0 M, and 0.1 M was selected. The CL intensity initially increased with increase in imidazole concentration, but suddenly decreased at concentrations higher than 0.1 M (Fig. 5D).

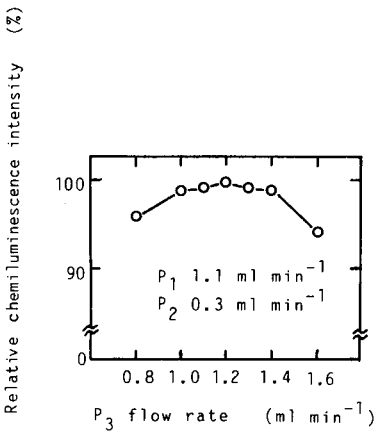

Fig. 6. Effect of flow-rate on chemiluminescence intensity. P_1 = 5 mM 2-M-8-HQ–CH_3CN; P_2 = 0.1 M imidazole–HNO_3 (pH 7.5)–CH_3CN (1+1); P_3 = 4 mM TCPO–EtOAc–50 mM H_2O_2–CH_3CN (1+3).

TCPO has been used in the pH range 6–8 [22], and a buffer solution around neutral pH has been employed [18]. The optimum buffer pH was studied and found to be 7.5 (Fig. 5D).

Effect of flow-rate

The flow-rate for each of the three pumps was examined by fixing the flow-rates of the other two pumps in turn. The optimum flow-rates for P_1, P_2 and P_3 were 1.1, 0.3 and 1.2 ml min^{-1}, respectively, as shown in Fig. 6.

Reproducibility, linearity and sensitivity

Typical recorder outputs for the DBTC–2-M-8-HQ complex with relative standard deviations obtained under the optimum analytical conditions as shown in Fig. 7. Table 2 presents linear ranges and detection limits for organotin compounds obtained with this method.

TABLE 2

Detection limits and linear range for determination of organotin compounds

Organotin compound	Detection limit [a] (10^{-6} M)	Linear range (10^{-6} M)
DBTC	0.5	0.5–50
DPTC	1.25	5–100
TBTC	25	25–1000
TPTC	100	100–1000

[a] Signal-to-noise ratio = 3.

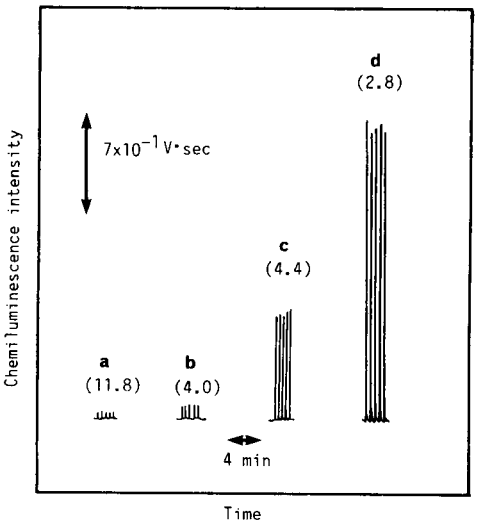

Fig. 7. Typical DBTC signals obtained for the chemiluminescence flow system. Recommended conditions: P_1 = 5 mM 2-M-8-HQ–CH_3CN, 1.1 ml min^{-1}; P_2 = 0.1 M imidazole–HNO_3 (pH 7.5)–CH_3CN (1+1), 0.3 ml min^{-1}; P_3 = 4 mM TCPO–EtOAc–50 mM H_2O_2–CH_3CN (1+3), 1.2 ml min^{-1}. DBTC concentration: (a) 5×10^{-7}; (b) 1×10^{-6}; (c) 5×10^{-6}; (d) 1×10^{-5} M. Relative standard deviations (%) are given in parentheses (n = 5).

Conclusion

The results support the usefulness of the devised CL–flow-injection system for detecting organotin compounds such as DBTC and DPTC. The detection of both TBTC and TPTC with this system, however, requires further improvements. The optimum CL reaction conditions for the detection of other organotin compounds including TBTC and TPTC are under investigation.

REFERENCES

1 M.D. Müller, L. Renberg and G. Rippen, Chemosphere, 18 (1989) 2015.
2 S. Kojima, Analyst, 104 (1979) 660.
3 P. Tomboulian, S.M. Walters and K.K. Brown, Mikrochim. Acta, II (1987) 11.
4 T. Tsuda, H. Nakanishi, T. Morita and J. Takebayashi, J. Assoc. Off. Anal. Chem., 69 (1986) 981.
5 K. Takami, T. Okumura, H. Yamasaki and M. Nakamoto, Bunseki Kagaku, 37 (1988) 449.
6 M.D. Müller, Anal. Chem., 59 (1987) 617.
7 W.A. MacCrehan and R.A. Durst, Anal. Chem., 53 (1981) 1700.

8 T.H. Yu and Y. Arakawa, J. Chromatogr., 258 (1983) 189.
9 W.G. Lakata, E.P. Lankmayr and K. Müller, Fresenius' Z. Anal. Chem., 319 (1984) 563.
10 H. Nakashima, S. Hori, S. Iwagami, H. Nakazawa and M. Fujita, Bunseki Kagaku, 36 (1987) 867.
11 S. Kobayashi and K. Imai, Anal. Chem., 52 (1980) 424.
12 K. Miyaguchi, K. Honda and K. Imai, J. Chromatogr., 303 (1984) 173.
13 S. Kobayashi, J. Sekino, K. Honda and K. Imai, Anal. Biochem., 112 (1981) 99.
14 K. Hayakawa, K. Hasegawa, N. Imaizumi, O. Wong and M. Miyazaki, J. Chromatogr., 464 (1989) 343.
15 M.M. Rauhut, Acc. Chem. Res., 2 (1969) 80.
16 R.E. Milofsky and J.W. Birks, Anal. Chem., 62 (1990) 1050.
17 Y. Arakawa, O. Wada and M. Manabe, Anal. Chem., 55 (1983) 1901.
18 K. Imai, A. Nishitani, Y. Tsukamoto, W. Wang, S. Kanda, K. Hayakawa and M. Miyazaki, Biomed. Chromatogr., 4 (1990) 100.
19 N. Imaizumi, K. Hayakawa, M. Miyazaki and K. Imai, Analyst, 114 (1989) 161.
20 K. Honda, J. Sekino and K. Imai, Anal. Chem., 55 (1983) 940.
21 K. Imai, K. Miyaguchi and K. Honda, in K. Van-Dyke (Ed.), Bioluminescence and Chemiluminescence: Instruments and Applications, Vol. 2, CRC Press, Boca Raton, FL, 1985, pp. 65–76.
22 K. Honda, K. Miyaguchi and K. Imai, Anal. Chim. Acta, 177 (1985) 103.

Analytica Chimica Acta, 282 (1993) 181–192
Elsevier Science Publishers B.V., Amsterdam

Harnessing immunochemical cross-reactivity: use of pattern recognition to classify molecular analogs

Peter Y.K. Cheung [1], Lawrence M. Kauvar, Åsa E. Engqvist-Goldstein and Stuart M. Ambler
Terrapin Technologies, Inc., 750-H Gateway Blvd., South San Francisco, CA 94080 (USA)

Alexander E. Karu
Hybridoma Facility, U.C. Berkeley College of Natural Resources, 1050 San Pablo Avenue, Albany, CA 94706 (USA)

L. Scott Ramos
Infometrix, Inc., 2200 Sixth Avenue, Suite 833, Seattle, WA 98121 (USA)

(Received 10th March 1993; revised manuscript received 21st April 1993)

Abstract

Immunoassay of molecular analogs against panels of antibodies can be used to define reproducible patterns of cross-reaction which represent distinctive "spectra" of the primary antigen and its analogs. Samples containing these compounds can thus be analyzed by applying pattern matching algorithms to the spectral signatures. Compared to conventional immunoassays, which are limited in their utility by the cross-reactivity of monoclonal antibodies against related molecular analogs, cross-reaction immuno-spectrum (CRISP) profiling improves reliability of analyte identification, with an accompanying improvement in the accuracy of analyte quantification. We demonstrate the advantages of profiling in the context of environmental monitoring, using monoclonal antibodies to the widely applied family of triazine herbicides as a test case.

Keywords: Immunoassay; Pattern recognition; CRISP; Multi-clonal immunoassay; Triazine herbicides

The utility and cost-effectiveness of immunochemical technology for detection of small organic molecules has been well established in numerous research and clinical diagnostics applications [1], and has more recently attracted attention as an approach for detection of pesticides and toxic substances in biological and environmental samples [2,3]. Interest in environmental monitoring reflects long-standing concern for the impact of industrial mutagens on human health [4]. The magnitude of the monitoring task is indicated by the annual usage of triazine herbicides, estimated at several hundred tons in California [5].

Virtually all reported immunoassays have detection limits for low molecular weight compounds in the parts-per-billion (ppb) range, roughly 10–100 nM. In many cases, however, the antibodies, both monoclonal and polyclonal, recognize (cross-react against) a variety of analogs and metabolites of the primary analyte. This

Correspondence to: L.M. Kauvar, Terrapin Technologies, Inc., 750-H Gateway Blvd., South San Francisco, CA 94080 (USA).
[1] Present address: Genelabs, 505 Penobscot Dr, Redwood City, CA 94063 (USA).

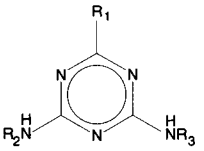

Triazine Analogs	R1	R2	R3
Atrazine	Cl	Isopropyl	Ethyl
Simazine	Cl	Ethyl	Ethyl
Propazine	Cl	Isopropyl	Isopropyl
Prometon	O-Methyl	Isopropyl	Isopropyl
Prometryne	S-Methyl	Isopropyl	Isopropyl
Ametryne	S-Methyl	Ethyl	Isopropyl
Terbutryne	S-Methyl	t-Butyl	Ethyl
Hapten-Linker Conjugates			
Atrazine-AHA	Cl	Ethyl	$(CH_2)_5COOH$
Simazine-MPA	S-$(CH_2)_2COOH$	Ethyl	Ethyl

Fig. 1. Structures of the seven triazines and conjugates used in this study.

cross-reactivity is in general a disadvantage in practical application of immunoassays because it does not allow the analyst to distinguish between samples containing one unit of an analyte reacting at the 100% level, two units of an analog that is 50% cross-reactive, or a hundred units of an analog that is 1% cross-reactive.

For most small analytes, it is impractical to overcome this problem by isolating antibodies with higher intrinsic specificity. A concrete example is provided by the family of triazine herbicides shown in Fig. 1. Some of the triazine analogs differ only in the substitution of an ethyl group by an isopropyl group. For a single antibody to be highly specific for the analog with the isopropyl motif, the bulk of the binding energy would likely need to reflect preferential recognition of that motif. That is, if a substantial part of the binding energy were due to interaction with common molecular motifs, such as the triazine ring itself, then both analogs would be expected to bind. Even if a suitably specific antibody could be easily isolated, therefore, it would have limited practical utility for analyzing real samples due to cross-reaction with unrelated components which also contain the isopropyl motif. An alternative strategy to overcoming the theoretical and practical limitations on antibody specificity is to use reproducible and characteristic patterns of cross-reactivity of two or more monoclonal antibodies to estimate the types of analytes present in a sample.

The premise of this study was that the distinct cross-reactivities could be productively analyzed by using pattern matching algorithms that have been applied to multivariate data sets from analytical chemistry [6,7], microbiology [8], astronomy [9], and other fields. To test this possibility, we performed concurrent competition enzyme linked immunosorbent assays (ELISAs) with five anti-triazine mouse monoclonal antibodies [10]. When the ELISAs were performed under optimized conditions, the relative cross-reactions of these five antibodies to seven triazine compounds across a broad range of concentrations were found to generate distinctive signatures suitable for pattern analysis. Two methods of pattern analysis were implemented and tested using simulated unknowns derived from these data. The methods were then applied to real data from a set of 24 randomized-concentration spiked samples. The combined methods resulted in correct identification of all of the analytes in this blind set with a corresponding major improvement over single antibody assays in the quantification of these unknowns.

EXPERIMENTAL

Reagents

Analytical standards of triazine analogs were purchased from Supelco (Bellefonte, PA) or AccuStandard (New Haven, CT). Immunochemicals were purchased from Zymed (South San Francisco, CA). Routine buffer components and *p*-nitrophenyl phosphate were purchased from Sigma (St. Louis, MO). Tween-20 was purchased from US Biochemicals (Cleveland, OH).

Antibodies

Production of monoclonal antibodies (MAbs) is described in [10]. Briefly, triazine analogs were

conjugated to KLH (keyhole limpet hemocyanin) using NHS (*N*-hydroxysuccinimide) and EDC [1-ethyl-3-(dimethylaminopropyl) carbodiimide hydrochloride] (Pierce, Rockford, IL) and used to immunize Swiss Webster and B10.Q mice. Spleen and P3X63AG8.653 myeloma cells were fused with 50% polyethylene glycol. Hybridomas were selected by growth in HAT medium. Wells with actively growing colonies were screened by ELISA for binding to immobilized triazine-BSA conjugate using a different linker from the immunogen (Fig. 1). Positive cultures were cloned by limiting dilution, and stable lines cultured in Iscove's Modified Dulbecco's medium with 5% fetal bovine serum. Culture supernates were collected, and aliquots were stored frozen at −20°C. Antibody IgG subtypes were determined using an isotyping kit from Zymed.

Assays

Indirect competition ELISAs were performed in 96-well microplates (Falcon 9312, PVC flat-bottom) coated overnight at 4°C with a triazine-BSA conjugate. Non-specific protein binding sites were blocked by 2 h incubation with 0.5% each of BSA and casein, followed by washing with PBS/Tween (10 mM sodium phosphate buffer, pH 7.2, 100 mM NaCl, 0.05% Tween 20). The primary antibody plus varying concentrations of the appropriate triazine analog, as appropriate for each different experiment, were prepared in assay buffer (PBS/Tween plus 0.1% each BSA and casein), added to the plate in quadruplicate wells and incubated at room temperature for 2 h. Bound primary antibody was quantified using a secondary alkaline phosphatase labeled goat anti-mouse IgG (at 1:1000) with *p*-nitrophenyl phosphate as substrate (1 mg/ml in 0.1 M diethanolamine pH 10.3, 0.5 mM $MgCl_2$). The initial rate of reaction or endpoint accumulation of reaction product was determined by measuring absorbance at 405 nm with a Vmax microplate reader (Molecular Devices, Menlo Park, CA). The endpoint method was used for preparing initial standard curves, and the more accurate kinetic analysis was used for our experimental test of CRISP. Inhibition curves were fitted using the four-parameter logistic equation in the software package Softmax (v.2.01C, Molecular Devices) or comparable two parameter equations [11,12].

CRISP profiling standard curve assays were performed as a parallel set of single dose competition ELISAs in which each of the MAbs in the panel was challenged individually with each of the relevant triazines in a single experimental run. These data comprise the reference set, from which "training" data were composed for subsequent comparisons in the pattern recognition phase. The optimal coating and MAb concentrations were previously determined for each of the antibodies in competition assays. Reduction in binding of the MAbs to the solid phase due to presence of a triazine at a particular concentration was expressed as a percentage of optical density of the zero-dose control ($R/R_0 \times 100\%$).

Pattern recognition

All computing for these studies was performed on a 386-type DOS or a 68030-type Macintosh personal computer. Computationally, profiles of binding values to five antibodies are effectively equivalent to points in a five-dimensional (5-D) space whose axes represent the extent of binding to each of the five antibodies. Classification is thus a matter of performing a multidimensional determination of the triazine reference profile that corresponds most closely to the unknown's profile. Since the competition ELISAs are not strictly independent, however, and the dose/response curves are non-linear, distance measurements between points in the 5-D space as defined by a Euclidean metric are not sufficient to characterize accurately the similarity of profiles. Two different techniques were applied to the data to overcome these obstacles. Additional multivariate tools were also applied to help visualize the results.

MEV. The first procedure, which we call minimum estimate variability (MEV), is based on the discussion of minimum variance estimates in [13]. For this procedure, an experimental sample's observed inhibition response value for antibody 1 is used to estimate from the reference dose/response curves what the corresponding concentration dose would be if the analyte were atrazine,

as well as what it would be if the analyte were simazine, etc. Antibody 2 similarly generates a family of estimates, and so forth. For the correct choice of analyte identity, the individual estimates of the 5 antibodies should agree more closely, i.e. have a smaller variability, than for an incorrect choice of analyte. Variability was computed as the variance of the estimates, and the triazine which gave the lowest variance was then assigned to the experimental sample.

To improve the performance of this algorithm, a weighting function was used to account for the different reliabilities of estimates derived from the various regions of the sigmoidal dose/response curves. More specifically, high and low dose estimates, H and L respectively, were derived for each unknown by computing the analyte concentration corresponding to responses a certain amount above or below the observed point on the reference curve. By assuming the data were normally distributed, H (or L) was calculated from the observed response plus (or minus) the sum of (1) the root mean square deviation of the fitted curve from its reference set and (2) half the length of an interpolated 95% confidence interval for the mean response. This approach takes into account the quality of the data in terms of both its observed variability and the number of measurements used to establish that variability. The weighting factor we defined was $1/(1 + [(H - L)/0.3]^2)$, the denominator being equal to $\log_{10} 2$ to adjust for the fact that the H and L values are expressed in log units.

KNN. A second procedure first classified the analyte as to the most likely triazine, and then performed quantification by comparison to the appropriate standard curve. The first step involved matching unknown profiles to those in a "training set" using an algorithm based on the method known as K-nearest neighbors (KNN) [14] in which the 5-D Euclidean distance between each unknown data point and each data point corresponding to the training set profiles was calculated. The class of each of the K nearest neighbors was determined, and the analyte was assigned to the class representing the majority of the neighbors. The optimal number for K was chosen from analysis of known samples, i.e. the training set data. The KNN classification software used in this study is incorporated in the Pirouette package (Infometrix, Seattle, WA).

Because the profiles in the reference assays had been optimized for each triazine–antibody pair independently, a variety of absolute concentrations were included in the set; that is for some antibodies, a dilution series including 100, 50, and 25 ppb was used while for others a series including 150, 75, and 37.5 ppb was used. A uniform data set for training the pattern recognition algorithm was therefore created by interpolating new data points along the assay profiles to give the same reference concentration values for each antibody.

PCA. Other standard procedures for manipulating multidimensional data sets were also applied in this study, for example scaling the responses of the antibodies to fall in a uniform 0–100% range [15], which was done for all the computations shown in this report. Principal components analysis (PCA) was used to help visualize the data. A variety of standard statistical software packages perform such calculations. This approach begins with computation of the eigenvectors of the covariance matrix of the distribution. By projecting the data from our 5-D antibody space onto the plane defined by the first two principal components (i.e. the eigenvectors with the largest associated eigenvalues) the data are displayed in a way that best preserves the scatter of the points in the 5-D space, thus permitting easier visualization of the standards and unknowns [7]. The output of any statistical package's principal components routine typically includes the factor score coefficient matrix; multiplication of the vector representing the normalized response data in the antibody space by this matrix yields the coordinates in the space defined by the principal components.

This analysis, which creates composite parameters from the antibody binding axes in order to define a new set of uncorrelated, or orthogonal, axes (the eigenvectors), also provides a rank ordering of the new axes in terms of the fraction of the variance for which they account, and again the standard packages provide a table of these values as output [16]. Furthermore, the principal

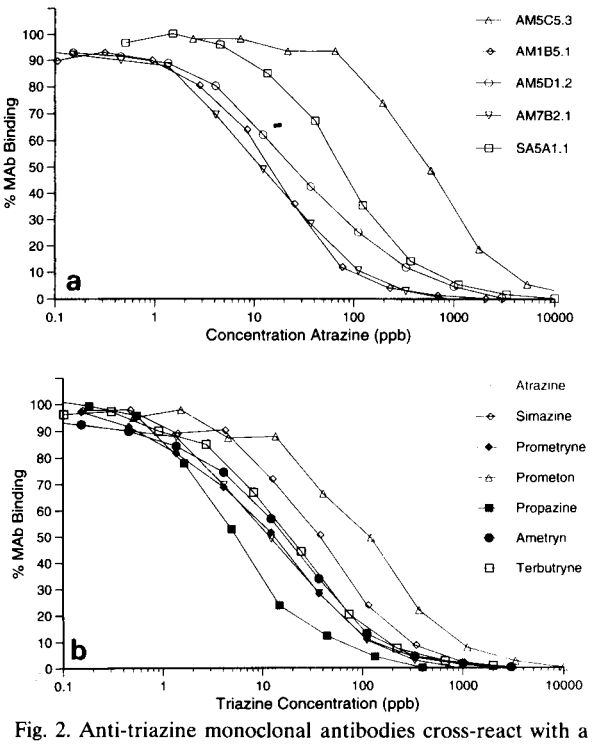

Fig. 2. Anti-triazine monoclonal antibodies cross-react with a variety of triazine analogs. Data points represent the average of quadruplicate determinations. (A) Inhibition of binding to immobilized atrazine-BSA of five anti-triazine MAbs by atrazine. (B) Inhibition of clone AM7B2.1 by seven triazine analogs.

components analysis allows determination of which antibodies are most useful for identifying unknowns since the contribution, or "loading," of each antibody to the principal components is a byproduct of the calculation, and is also delivered by the software. Thus, antibodies which contribute primarily to low information content eigenvectors are revealed as being largely redundant in the analysis.

Multiple component simulations

For computational purposes, we found it convenient to approximate the sigmoidal inhibition curves by the formula, $r = 0.5(1 - \tanh[md + b])$, where r = response (r/r_0), d = dose (in log ppb), and m and b are adjustable parameters that are used to fit the hyperbolic tangent function to the data. Other procedures, such as iterative logistic fitting, could also have been used. For estimating the response for a mixture of triazines, the formula used was $r = 0.5(1 - \tanh[M \log_{10}(\Sigma 10^k)])$, where M = the geometric mean of the m_i's for the individual fitted curves, and $k = (m_i d_i + b_i)/M$, the summation ($i = 1$ to N) being taken over the particular combination of N individual triazines in the mixture. The exponents and logarithms in this formula are needed because the sigmoid curves are based on log concentration whereas only the concentrations themselves are directly additive.

RESULTS

Determining cross-reaction profiles

Competition ELISAs, like radioimmune assays, exhibit a sigmoidal dose-response [11,17]. Typical inhibition titration curves are shown in Fig. 2. These assays were performed on standard 96-well microplates coated with a limiting amount of atrazine-BSA conjugate. An alkaline phos-

TABLE 1

Anti-triazine MAbs and their relative specificities against seven triazines

[Values are the concentration (in ppb = parts per billion, or ng/ml) of free triazine needed to half-maximally inhibit antibody binding to immobilized triazine in a competition ELISA, computed from four-parameter curve fitted equations]

Cell line	IgG subtype	IC_{50} (ppb)						
		Atrazine	Simazine	Propazine	Prometon	Prometryne	Ametryne	Terbutryne
AM5C5.3	IgG 2b K	553.4	721.3	3043.2	9791.0	613.9	1675.9	1172.1
AM1B5.1	IgG 1 K	13.2	236.1	3.0	18.5	6.0	6.5	495.2
AM5D1.2	IgG K	26.5	52.7	40.2	165.0	6.8	78.7	55.9
AM7B2.1	IgG 2b K	12.1	36.5	13.1	108.0	4.7	16.4	19.0
SA5A1.1	IgG 1 K	74.5	75.7	685.8	1833.0	57.4	1195.6	931.1

phatase labelled secondary antibody was used to quantify the amount of primary antibody bound in the presence of competing triazine. The dose-response curve is well fitted by various equations [12], and the response data may thereby be compared to the standards by non-linear fitting or by applying a linearized transformation. An easily calculated parameter from these curves is the concentration of each analog required for half-maximal inhibition of MAb binding to the coating antigen adsorbed on the EIA wells. Table 1 summarizes these "I_{50}" values for the panel of antibodies and the set of analytes used in this study. Under these reaction conditions, each of the analogs has its own pattern of cross-reactivities against the panel of antibodies used. Isotype appears to have no influence on relative specificity, nor does the immunogen used in generating the clones (in clone designations, AM = atrazine–mercaptopropionic acid and SM = simazine–hexanoic acid, referring to hapten-linker conjugates used for immunization).

To explore the utility of these apparently distinctive cross-reactions for analyte identification, we initially determined the percentage of inhibition by 50 ppb of each of the seven triazines in competition ELISAs with each of the five MAbs (Table 2). As seen in Fig. 3A, each triazine at 50 ppb gave a noticeably different pattern of relative inhibition of each MAb's binding to the immobilized conjugate. This result suggested that a library of standardized profiles for the various triazines over a range of relevant concentrations might be useful for identifying triazines both qualitatively and quantitatively. Before conducting physical assays to test the uniqueness of inhibition profiles, we used curves fitted to competition ELISA data, such as that illustrated in Fig. 2, to generate a computer simulation of the CRISP profiles expected from ELISAs over a

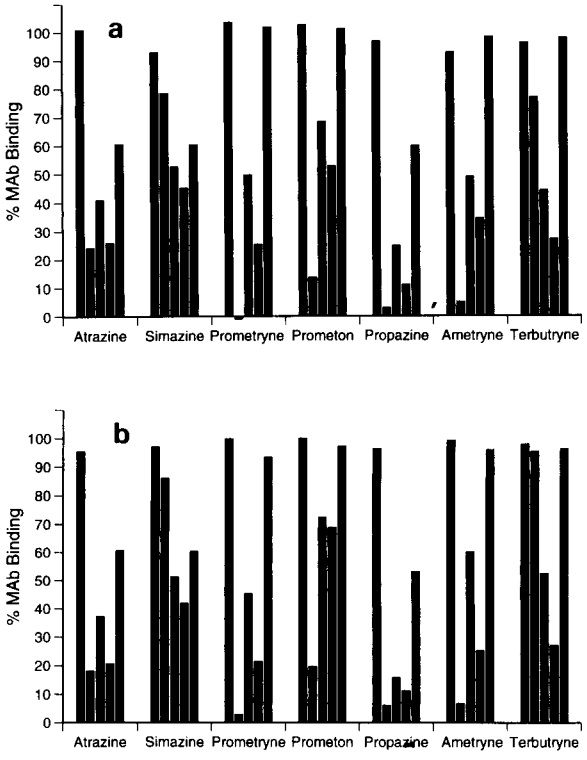

Fig. 3. Cross-reaction profiles of seven triazines at 50 ppb level. (A) Empirical profiles of the seven triazines against the panel were determined by direct assay of each compound at 50 ppb. (B) Predicted profiles were calculated from curve-fitted models of the individual inhibition curves of the triazines against the five MAbs. The order of MAbs in each profile is: AM5C5.3, AM1B5.1, AM5D1.2, AM7B2.1, SA5A1.1.

TABLE 2

CRISP profiles of triazines against anti-triazine MAbs

[Activities in the presence of 50 ppb triazine are expressed as percent of zero dose control ± standard deviation (n = 6). Average coefficient of variation is 10%]

	Atrazine	Simazine	Propazine	Prometon	Prometryne	Ametryne	Terbutryne
AM5C5.3	100.8 ± 8.1	93.0 ± 8.3	97.1 ± 12.7	103.0 ± 9.6	103.7 ± 9.1	93.2 ± 5.6	96.8 ± 4.8
AM1B5.1	24.0 ± 3.7	78.5 ± 7.9	2.8 ± 2.1	13.6 ± 3.1	−0.8 ± 2.3	4.9 ± 2.0	77.3 ± 3.6
AM5D1.2	40.9 ± 1.7	52.6 ± 2.8	24.7 ± 3.1	68.5 ± 5.6	49.7 ± 5.3	49.1 ± 4.5	44.4 ± 2.9
AM7B2.1	25.7 ± 2.1	45.1 ± 3.6	11.1 ± 2.4	52.8 ± 4.8	25.3 ± 3.0	34.4 ± 2.3	27.1 ± 2.7
SA5A1.1	60.4 ± 5.6	60.2 ± 5.2	60.1 ± 3.1	101.6 ± 5.5	102.1 ± 5.8	98.8 ± 5.6	98.6 ± 5.4

wide range of analyte concentrations. Fig. 3B shows that the computed profiles for the various triazines at 50 ppb corresponded well to the experimental data.

Computational methods applied to simulated unknowns

A set of standard profiles was computed from the inhibition curves for each of the seven triazines across the range of 10–1000 ppb, in the same manner as for the 50 ppb profiles. For this larger set of profiles, visual inspection of profiles as plotted in Fig. 3 is no longer feasible for distinguishing differences. As described in the Experimental section and illustrated schematically in Fig. 4, we were able to generate a more convenient graphical representation of the standard set through principal components analysis of the data. Initial examination of such a plot showed that ~85% of the standards were well spaced and thus readily distinguishable from each other by simple inspection. In the remaining cases, two profile points (representing different compounds at different concentrations) were too close together for reliable assignments to be easily made.

Because some of the information inherent in the five dimensional experimental profiles is inevitably lost in the reduction to two dimensions shown in Fig. 4, more sophisticated pattern matching procedures were explored than simple inspection of points mapped on a two dimensional plot. Several approaches were initially tested, including a SIMCA routine [18] and a simple back propagation neural net algorithm [19]. The two most promising methods were studied more intensively. As described in the Experimental section, one approach, designated minimum estimate variability (MEV), first made estimates of the amount of analyte present, and these results were utilized to ascertain which triazine was most likely. An alternative approach (KNN), based on matching the sample to its K nearest neighbor standards, first classified the analyte as to the most likely triazine, and then deduced quantification.

To explore the utility of the pattern matching procedures, a series of several hundred simulated "unknown" profiles were generated for individual triazines across the 10–1000 ppb range and then matched against the previously defined reference set by both procedures. For these simulations, a random number generator was used to define the unknowns, and profiles were generated from the standard curves. For both MEV and KNN, the unknown was successfully matched in about 95% of the cases, allowing quantification to within about 20% of the correct value. By contrast, the uncertainty in quantification for a

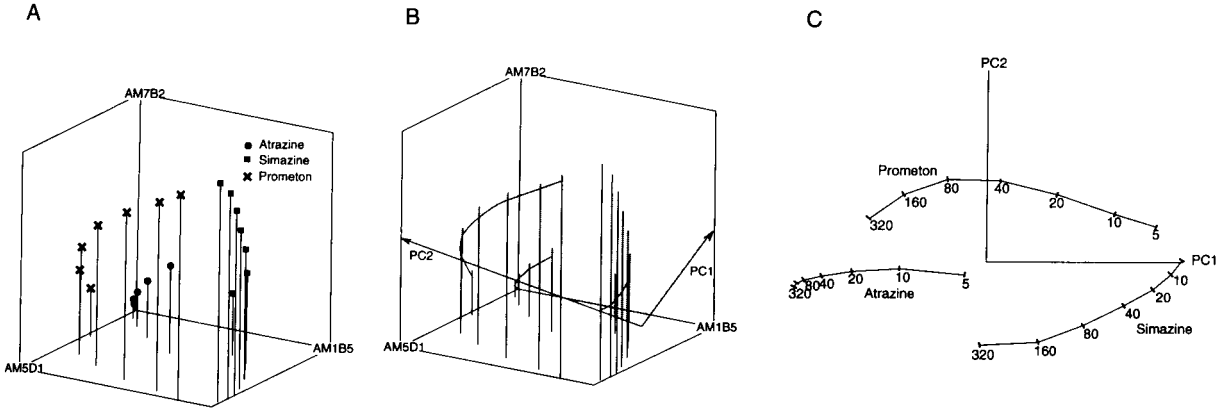

Fig. 4. (A) Multivariate analysis of cross-reaction profiles. Inhibition profiles against three antibodies for the three triazines in common use in California are plotted as points in 3-D space (panel A). Eigenvector analysis applied to the data defines the first two principal components of the distribution (shaded plane, panel B). Points in panel A were projected onto the plane illustrated in panel B to yield a two dimensional principal components representation of the reference triazine profiles (panel C). Hatch marks denote two-fold increases in ppb concentration of the indicated triazine.

single antibody assay, given the cross-reactivity of each of the compounds against each of the individual MAbs, spans several orders of magnitude.

We next extended the simulation process to explore the effect of experimental error on the pattern matching process. Gaussian random error (using the standard deviations from the reference data) was added to the individual profile components of the simulated unknowns. For this series of simulations, 100 concentrations were used that uniformly span the full logarithmic concentration range for each of the seven triazines. A criterion for a successful match was defined that required correct qualitative identification and quantification which was accurate to within 20% of the true value. Successful matches were obtained in 88% of the cases using the MEV methodology. Higher reproducibility in the assays would thus contribute to more accurate qualitative identification of profiles as well as to more accurate quantification.

One additional feature of the experimental design was also studied by simulation: the relative importance of the individual antibodies. As noted in Experimental, a benefit of the principal components analysis is that it generates a rank ordering of the antibodies with regard to the amount of the variance in the data for which they account, or effectively their predictive power. We compared this ranking to that established by repeating the MEV procedure with an incomplete set of antibodies; that is, all possible combinations of four antibodies, and three antibodies, were used and the overall quality of matching unknowns determined. The two rankings of utility for the different antibodies generally agreed, with antibody AMC5.3 judged the most dispensable and AM7B2.1 the most critical antibody for assays over the 10–1000 ppb range. With the incomplete sets of antibodies, the success rate was variable depending on which antibodies were omitted. Using four antibodies, the success rate changed from 88% for all five to 68–90% (average 80%), even using a less stringent criterion for a successful match, namely quantification accurate to within a factor of two of the true value. With only three antibodies, the success rate dropped to 55–86% (average 68%), and only about 64% on average were accurate to within the more restrictive window of ±20%.

Experimental test of computational methods

With the encouragement provided by the simulations, we performed a double-blind test of the pattern matching approach using triazine-spiked distilled water samples for which the identity and concentration of the analytes were coded throughout the assay and subsequent pattern matching analysis. To generate adequate statistics from a reasonable number of assays, only three antibodies were used (AM1B5.1, AM5D1.2, and AM7B2.1) along with the three triazines in common use in California (atrazine, simazine and prometon) across the range of 10–100 ppb. A set of 24 such samples, along with fresh sets of standards, was assayed and analyte identification was performed as in the simulations. Each sample had only one triazine, and the random number generator used to pick the concentrations was constrained to give roughly equal sampling of the whole range for each of the triazines. Samples were assayed in 4 replicates as 1 : 1 dilutions with antibody in 2 × assay buffer.

For the MEV procedure, 20 of the 24 cases yielded successful identification with root mean square (rms) quantification error across the set of 21%. In the remaining cases, the second choice would have been quantitatively correct at this level of reliability. Using the alternative KNN procedure, all 24 unknowns were correctly identified qualitatively, and thereby quantified with an rms error of 30%. A plot of the standards and unknowns on the principal components of the standards for these experiments is shown in Fig. 5A. Figure 5B provides a summary of the errors in our best estimates for the double blind test data. From the simulations, we knew that the KNN procedure was more reliable than the MEV procedure but that the quantification algorithm for the MEV was more carefully worked out. Accordingly, we used KNN to pick the triazine qualitatively and then averaged the quantitative estimates derived from the KNN and MEV procedures. Additional simulations indicated that this success rate should be typical, suggesting that our experimental errors are adequately simulated by

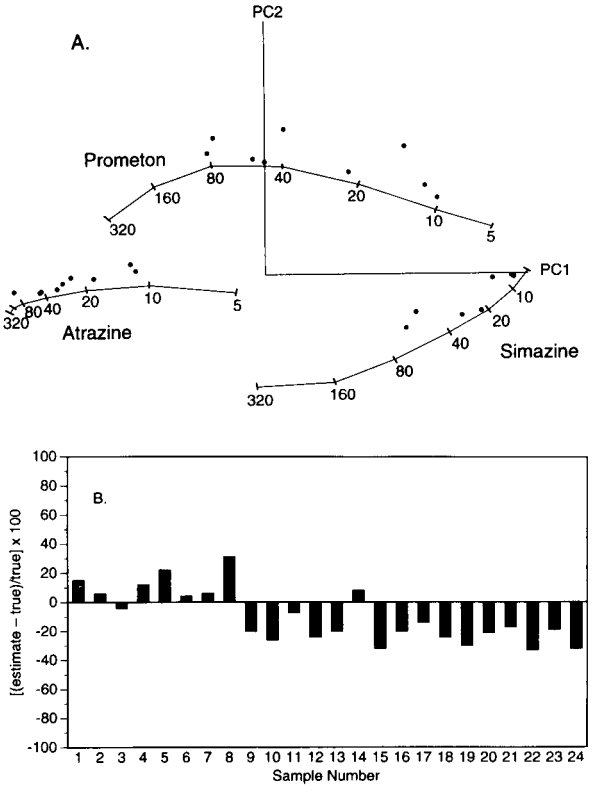

Fig. 5. Identification of 24 single component triazine spiked samples. Profiles are plotted on the standards from Fig. 4C following blind assay and analysis (panel A). The identity of each was correctly established with quantification errors shown in panel B. The errors are calculated as [(estimated value – true value)/true value]×100.

the procedures described above. Simulations using two and then one antibody confirmed that the profiling process provided a substantial improvement in accuracy over single antibody assays.

Simulated mixtures of analytes

We have also begun to explore the ability of pattern matching procedures to deal with combinations of analytes. Because atrazine is the most widely used member of the triazine family, real world samples may contain some atrazine mixed with varying amounts of another member of the family. We therefore analyzed the effect on the pattern recognition process of simulated mixtures of atrazine, simazine and prometon in the 10–1000 ppb range.

We first computed the inhibition values expected for 2600 different mixtures by linearizing the sigmoidal dose/response curves, and then combining the contributions of the individual triazines in the mixture (see Experimental section for details). For each such combination, each of the compounds was assigned one of 30 concentrations, spread evenly across the designated range, including zero. In addition, the effect of experimental error on the expected inhibition was taken into account. Each component's contribution was varied by 2 standard deviations, and the maximal inhibition value for any of these combinations was assigned to the reference point. Next, a similar set of several thousand unknown mixtures, evenly spaced across the range but generated with random error, was formed. The reference point with the most similar profile was selected, and the highest computed inhibition for that point was then assigned to the unknown.

Not surprisingly, identifying the exact composition of a mixture is more problematic than for pure components. The analysis tested so far is less refined than in the single component case, with a built in bias towards overestimating the total triazine concentration. Nevertheless, even allowing any combination of any of the three compounds, the use of pattern recognition methods allow more reliable upper limits to be placed on the total concentration of all triazines than is possible with single antibody assays, for which the uncertainties are even more extreme than in the pure component cases analyzed above. The estimates obtained in various runs of our simulations were never below the true value, but were generally high by a factor of 5 to 10. An interesting feature to emerge from the simulations is that smaller variances in the standard curves would improve the qualitative identification. More work is needed to determine the relative value of repetitions in the standards compared to the unknowns.

These preliminary results indicate that the multivariate methods we have used remain valid for mixtures. Figure 6 provides a visual rationalization of this qualitative result, by showing the reference profiles of Fig. 4 along with lines representing mixtures of constant total triazine con-

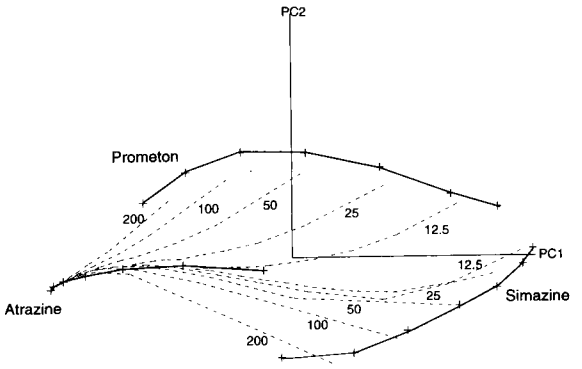

Fig. 6. Contours of constant total triazine content for mixtures of atrazine with either simazine or prometon. Mixtures (dotted lines) are shown along with the pure analyte standard curves from Fig. 4C.

centration comprising various mole fractions of either prometon or simazine with atrazine. The sort of experimental scatter seen for the 24 test specimens in Fig. 5A would clearly lead to larger uncertainties if the possibilities of mixtures were included. The identification becomes less precise gradually, however, not discontinuously.

DISCUSSION

Monoclonal antibodies are often unable to discriminate absolutely between small structural differences on molecular analogs as similar as the triazines. The obvious approach, namely design of a new hapten that will elicit antibodies with the desired selectivity, has theoretical and practical limitations which suggest that laborious attempts to derive antibodies uniquely reactive with each analog will not drastically improve selectivity over that attainable from a panel of antibodies prepared against one of the analogs.

An alternative approach to discriminating among analytes is to utilize the idiosyncratic cross-reactivities of a panel of antibodies to define analyte-specific profiles. This pattern matching technique, which we call CRISP profiling, may be put to several uses. First, as the experimental and simulated data on triazine profiles demonstrate, CRISP profiling can be used to derive information on the types and relative amounts of analogs in a mixture. This property makes it possible to use a small number of existing antibodies to improve the accuracy of immunoassays and obtain information on the identity of the analyte(s) with little increase in labor or cost. The CRISP assays work best for distinguishing individual members among a family of compounds. Actual analytical samples often include a variety of metabolites or other cross-reacting contaminants which can be thought of as distantly related analogs. CRISP profiling is thus a more stringent test for presence of the true analyte than is a single antibody assay. CRISP should therefore reduce identification error, which is a key issue in the application of immunoassays to environmental monitoring.

As a corollary, existing antibodies can be used to measure several related compounds. The seven triazines used in this study, for example, are only a sampling of the existing family of triazines, whose relative popularity among farmers has varied significantly over time [5], and new analogs are still being developed. If the profiles for the new compounds are as well scattered as those of the seven analogs studied here, then the same panel should be usable for measuring the new compounds. If not, the cross-reactivity characteristics required of a new MAb should be readily definable through simulations and used to select a suitable new panel member. Characteristics of clones needed for improving reliability in deciphering mixtures can also be explored through simulation.

A second advantage of the CRISP profiling approach is that a single type of hapten conjugate can be used to generate assays for all the compounds in a family. The preparation of conjugates between small molecules and carrier macromolecules, which is a slow and costly step in conventional immunoassay development, may thus be avoided. The principles of CRISP profiling should also apply to an immobilized-antibody competition ELISA, in which a hapten–enzyme conjugate is the competitor. Finally, the CRISP profiles will presumably change if a different hapten conjugate is used, creating the possibility of using a small number of antibodies and a diversity of hapten conjugates to generate distinctive profiles.

Under controlled assay conditions against a standardized reference panel of binding proteins, the CRISP profile of an analyte is characteristic of its molecular structure, just as is its infrared spectrum or mass spectrum. In this sense, CRISP profiling may be considered as an extension to sub-molecular scale of the sort of "immunological typing" used to define histocompatibility antigens [20] or to map subunits in macromolecular assemblies such as ribosomes [21].

The sensitivity of CRISP profiling immunoassays is determined by the affinity of the individual antibodies, the label used, and the reproducibility of the assay conditions. The ability to distinguish profiles of different compounds, however, is determined by the independence of the antibodies, not simply by their number. Thus, in theory CRISP profiling should be applicable to immunoassays using sets of independent polyclonal sera [22], as well as monoclonal antibodies. Furthermore, the same principles apply equally well to recognition assays in which the probe is not a natural antibody but is instead some other binding protein, such as immunoglobulins created by recombinant DNA technology [23], including single-chain antibodies [24]. We speculate that as methods for "antibody engineering" evolve [25,26] and are applied more widely, it may prove increasingly easy to derive antibodies suitable for CRISP profiling compared to antibodies with unique specificity for a small analyte such as a triazine.

For their input throughout this project and review of the manuscript, we thank Ted Puck, John Sedat, Mike Buchmeier, Gerry Rubin, and John Tainer. We also thank Ron Konopka for technical assistance. Carol Topp provided much appreciated editorial and graphics assistance. We gratefully acknowledge receipt of triazine conjugates and analogs from the laboratory of Bruce Hammock of the Univeristy of California at Davis.

The anti-triazine antibodies were prepared at the UC Berkeley Hybridoma Facility under Contract 3586 to Alex Karu from the California Dept. of Food and Agriculture.

REFERENCES

1 A. McMichael and J. Fabre, Monoclonal Antibodies in Clinical Medicine, Academic Press, London, 1982.
2 J. Van Emon and R. Mumma (Eds.), Immunochemical Methods for Environmental Analysis, American Chemical Society, Washington, DC, 1990.
3 M. Vanderlaan, L. Stanker, B. Watkins and R. Roberts (Eds.), Immunoassays for Monitoring Human Exposure to Toxic Chemicals in Food and the Environment, American Chemical Society, Washington, DC, 1990.
4 Technologies and Management Strategies for Hazardous Waste Control, Office of Technology Assessment report, Washington, DC, 1983.
5 California Dept. of Pesticide Regulation: Pesticide Use Report, Calendar Year 1990, California Dept. of Food and Agriculture, Sacramento, CA.
6 J. Stetter, P. Jurs and S. Rose, Anal. Chem., 58 (1986) 860.
7 D. Massart, B. Vandeginste, S. Deming, M. Michotte and L. Kaufman, Chemometrics: a Textbook, Elsevier, Amsterdam, 1988.
8 B. Bochner, Am. Soc. Microbiol. News, 55 (1989) 536.
9 F. Murtagh and A. Heck, Multivariate Data Analysis, Reidel, Boston, 1987.
10 A.E. Karu, R.O. Harrison, D.J. Schmidt, C.E. Clarkson, J. Grassman, M.H. Goodrow, A. Lucas, B.D. Hammock, J.M. Van Emon and R.J. White, in M. Vanderlaan, L. Stanker, B. Watkins and R. Roberts (Eds.), Immunoassays for Monitoring Human Exposure to Toxic Chemicals in food and the Environment, American Chemical Society, Washington, DC, 1990, pp. 59–77.
11 P. Canellas and A. Karu, J. Immunol. Methods, 47 (1981) 375.
12 D. Rodbard and D. Hutt, Radioimmunoassay and Related Procedures in Biology and Medicine, International Atomic Energy Agency, Vienna, 1974.
13 J. Mandel, The Statistical Analysis of Experimental Data, Dover, New York, 1964, pp. 132–135.
14 B.R. Kowalski and C.F. Bender, J. Am. Chem. Soc., 94 (1972) 5632.
15 Pirouette software documentation: Multivariate Data Analysis for IBM PC Systems, Infometrix, Inc., Seattle, WA, 1991.
16 E.R. Malinowski and D.G. Howery, Factor Analysis in Chemistry, Wiley Interscience, New York, 1980.
17 D. Rodbard, in W. Odell (Ed.), Principles of Competitive Protein-Binding Assays, J.B. Lippincott, Philadelphia, PA, 1971, pp. 204–259.
18 S. Wold, C. Albano, W.J. Dunn, K. Esbensen, S. Hellberg, E. Johansson and M. Sjoestroem, Anal. Chem. Symp. Ser., 18 (Mod. Trends Anal. Chem., Pt. B) (1984) 157.
19 J.L. McClelland and D.E. Rumelhart, Explorations in Parallel Distributed Processing, MIT Press, Cambridge, 1988.
20 W. Payne, D. Marshall, R. Shockley and W. Martin, Clin. Microbiol. Reviews, 1 (1988) 313.

21 G. Stoffler and M. Stoffler-Meilicke, Ann. Rev. Biophys. Bioeng., 13 (1984) 303.
22 M. Goodrow, R. Harrison and B. Hammock, J. Agric. Food Chem., 38 (1990) 990.
23 J.S. Huston, D. Levinson, M. Mudgett-Hunter, M.S. Tai, J. Novotny, M.N. Margolies, R.J. Ridge, R.E. Bruccoleri, E. Haber, R. Crea and H. Oppermann, Proc. Nat. Acad. Sci. USA, 85 (1988) 5879.
24 R.E. Bird, K.D. Hardman, J.W. Jacobson, S. Johnson, B.M. Kaufman, S.M. Lee, T. Lee, S.H. Pope, G.S. Riordan and M. Whitlow, Science, 242 (1988) 423.
25 W. Huse, L. Sastry, S.A. Iverson, A.S. Kang, M. Alting-Mees, D.R. Burton, S.J. Benkovic and R.A. Lerner, Science, 246 (1989) 1275.
26 J. McCafferty, A.D. Griffiths, G. Winter and D.J. Chiswell, Nature, 348 (1990) 552.

Analytica Chimica Acta, 282 (1993) 193–198
Elsevier Science Publishers B.V., Amsterdam

Alternating current field enhanced latex immunoassay for human myoglobin as measured by image analysis

Min Ik Song, Keisuke Iwata, Michihisa Yamada [1], Eiichi Tamiya and Isao Karube

Research Center for Advanced Science and Technology, University of Tokyo, Komaba, 4–6–1, Meguroku, Tokyo 153 (Japan)

(Received 8th February 1993; revised manuscript received 16th April 1993)

Abstract

Square-wave alternating current (ac) was used to accelerate the immunoreaction of latex beads with human myoglobin. The antibody to human myoglobin was adsorbed on the surface of latex beads which had been labeled with a fluorescent dye. The antibody bound latex beads were reacted with its antigen, and the agglutinated beads were counted using a fluorescence image analysis system consisting of a fluorescent microscope, charge-coupled device (CCD) camera, monitor and personal computer. The lowest detection limit for myoglobin was 1 ng/ml with this method. The immunoreaction was accomplished by applying an ac field for 1 min at different potentials and frequencies. This conjugation effect from a square-wave ac is probably due to pearl-chain formation which increases the collision frequency between latex beads.

Keywords: Immunoassay; Square-wave alternating current; Fluorescence latex; Image analysis; Latex agglutination; Pearl-chain formation

Immunoreactions are characterized by their specificity for an antigen. In addition to using immunoassay for many clinical diagnoses, it is also useful for analysis of other compounds.

There are several kinds of labels used in immunoassay including radioisotopes, enzymes and fluorescent dyes. Usually these immunoassays involve a bound/free (B/F) separation. This separation is needed to separate the label bound to the antigen from that with which the immnoreaction did not occur. Thus this B/F separation step makes these assays cumbersome and time consuming. The latex immunoassay using antibody bound latex beads is simple and rapid because this method does not need the B/F separation. Turbidimetry, nephelometry or the automatic particle counter is used to measure the reaction rate [1–5]. Recently, fluorescent microspheres were used with a flow cytometer to obtain a more sensitive immunoassay than with simple fluorescent labels and yet still retain the advantage of not using B/F separation [6].

An alternating current (ac) field-induced force on microscopically sized particles causes alignment of the particles in pearl-chain formation [7]. The use of direct current (DC) field will also cause pearl-chain formation [8]. Pearl-chain formation is the result of attractive forces between induced dipoles on neighboring particles. There are several factors to be considered in forming the pearl chain effectively [7]. These are: (1) the radius of the microparticle; (2) the dielectric constant of both the particle and the solution medium; (3) the electrical conductivity; (4) the strength and frequency of the electric field. This pearl-chain formation is used in cell fusion tech-

Correspondence to: I. Karube, Research Center for Advanced Science and Technology, University of Tokyo, Komaba, 4–6–1, Meguroku, Tokyo 153 (Japan).
[1] Organon Teknika K.K., Kabukicho, 2–31–11, Shinjukuku, Tokyu 160 (Japan).

nology especially with monoclonal antibody production [9–11].

In latex immunoassay, the reaction can be used to form a cluster, a product of the agglutination reaction. However, the surface of the latex is usually negatively charged in order to make a stable suspension. This makes the immunoreaction slow down. Thus, formation of the pearl chain can act to increase the reaction rate. Our previous papers showed that the use of a dc pulse accelerated the immunoreaction for *Candida albicans* and antibody-bound latex [12,13]. An ac field may have the advantage that it makes it easier to form a pearl chain. With an ac field of lower potential, it is less invasive to the protein. Therefore, in this study we look at the effect of an ac field on the agglutination of latex beads and its acceleration of a latex immunoreaction.

Human myoglobin was used as a model antigen. The protein is a single polypeptide chain of 153 residues (17.8 Kdalton) which binds oxygen reversibly as hemoglobin. Its content in urine or serum can have a relation to acute necrosis of the myocyte [14,15].

MATERIALS AND METHODS

Materials

Human myoglobin and its antibody (the IgG fraction of rabbit serum) were purchased from Cappel, Durham, NC. Fluorescence microspheres (2 μm FITC labeled) were purchased from Polysciences Inc., Warrington, PA. All other reagents were commercially available and of analytical grade.

Apparatus

An arbitrary waveform synthesizer (Toa Electronics Ltd. FS-2121), wide-band oscillator (Toa Electronics Ltd. VK-301A) and power amplifier (Mifuji Denki) were used to apply the ac field. A fluorescence microscope (Nikon Optiphot) and charge-coupled device (CCD) camera (NEC) were used to obtain an image. The computing hardware for calculating area distribution data for agglutinated latex beads is composed of the FDM 98–1 from Photron Ltd. and a NEC PC-9801 computer with the software developed using the FDM operating system (Fig. 1).

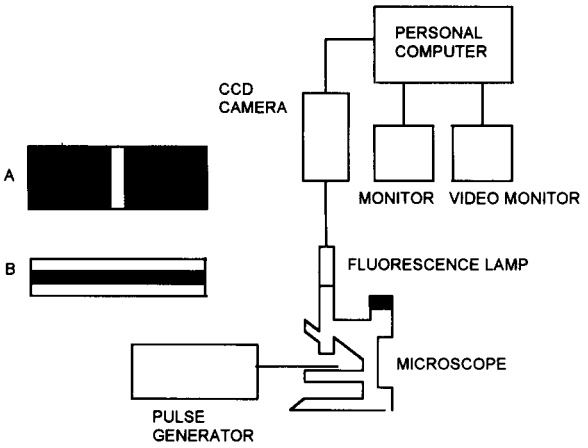

Fig. 1. Pulse immunoassay–image sensor system. (A) Top-side view of the electrode; (B) front-side view of the electrode. White = glass-slide; grey = silver electrode; black = room for reaction buffer ($10 \times 500 \times 5000$ μm).

The image analysis system was the same as described previously [16]; however, a small modification was made in the data process. After getting a background-subtracted image, the area of each latex cluster was measured and divided by the area of a single latex. This information was used to obtain a frequency distribution of each bead cluster (Fig. 2).

Preparation of antibody-bound latex

One volume of 1% fluorescent microsphere in glycine-buffered saline (GBS) buffer (100 mM glycine, 50 mM NaCl, 0.1% NaN_3, pH 8.6) was added to one volume (75 μg/ml) of the IgG fraction of anti-myoglobin antiserum. The suspension was gently stirred at room temperature for two hours. The latex–IgG suspension was washed with GBS–bovine serum albumin (BSA) buffer (containing 0.2% BSA), three times by centrifuging. The latex–IgG reagent was diluted to 0.5% and preserved in the refrigerator until use.

Use of the glass-slide reactor for the immuno-reaction

A glass-slide type reactor was used for the immunoreaction. The latex–IgG solution was

mixed with its antigen and immediately transferred to the glass-slide reactor and an ac field was applied for 1 min. After standing for another 1–2 min to allow dispersion of the latex that does not immunoreact with antigen, the number of agglutinated beads were counted by fluorescence image analysis. This immunoreaction was compared against the use of 37°C incubation as the control condition. As a control, one volume of latex–IgG (0.1%) and one volume of human myoglobin (100 ng/ml) were incubated at 37°C for 20 min with gentle stirring. The mixture was transferred to the same slide type reactor, and the agglutination ratio (AR) was measured. The AR was defined as the percentage of the number of agglutinated beads over the number of total beads. It was measured for five different fluorescent images and the average value was determined.

RESULTS AND DISCUSSION

Agglutination ratio change according to applying ac wave

One volume of latex–IgG (0.1%) and one volume human myoglobin (100 ng/ml) were placed under 100 KHz, 20 V/mm ac field for 1 min to form the pearl chain and were then left for another 1 or 2 min without ac field to allow dispersion of the latex which did not immunoreact. Figure 3 shows that the AR increased for 1 min with ac field, and decreased slightly in the presence of substantial antigen (100 ng/ml) without ac wave. However, in the absence of antigen, the AR decreased rapidly. The AR at 1 min in the presence of antigen is about the same as that in the absence of antigen at 1 min.

Condition of ac wave in pearl-chain formation

Different potentials of 100 KHz ac field were applied for 1 min to form the pearl chain and then left standing for another 1 min to disperse the latex with which the immunoreaction did not occur. Figure 4 shows that with an ac field of 20 V/mm, about 90% of the latex beads were agglutinated in 1 min which is similiar to that reported by Schwan [7]. The AR curves at 1 min and 2 min in the presence of antigen are parallel, which means that the AR at 2 min is dependent on the rate of pearl-chain formation.

Different frequencies of 20 V/mm ac field were applied for 1 min and then left standing for

AREA OF EACH LATEX AGGLUTINATED(ARBITARARY UNIT)

7 35 13 6 28 8 10 27 6 40 20 30 50
46 106 33 6 37 35 17 8 18 16 15 19 20
22 6 7 8 9 36 5 78 18 5 11 80 7
73 65 67 56 54

AREA OF SINGLE LATEX: 8

FREQUENCY DISTRIBUTION

(NUMBER OF AGGLUTINATION——FREQUENCY)

1 — 12, 2 — 6, 3 —7, 4 —3, 5 — 6,
6 — 1, 7 — 2, 8 — 0, 9 —2, 10 — 2,
14 — 1,

NUMBER OF TOTAL LATICES; 153

A. R. = (141/153) x 100 = 92.2 %

Fig. 2. An example of a measured image and its data processing for area distribution. Fluorescent latices were agglutinated with ac field. The area for each latex cluster was measured and the frequency distribution of each bead cluster was used to determine AR.

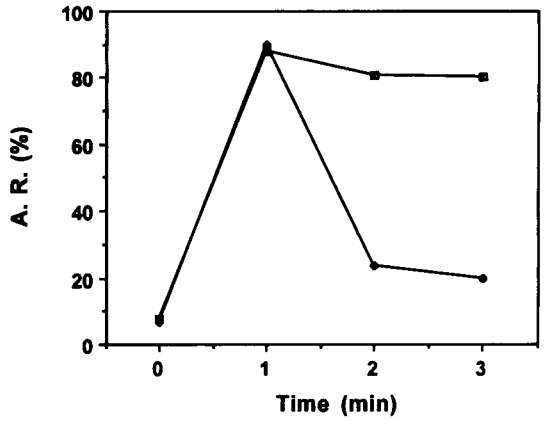

Fig. 3. Effect of the ac wave on the AR value. 100 KHz, 20 V/mm ac was applied for 1 min and left standing for another 1 or 2 min without ac wave. The reaction solution was one volume of latex–IgG (0.1%) and one volume of myoglobin (100 ng/ml). (□) AR with Ag; (♦) AR without Ag.

another 1 min. In Fig. 5 there is some variation of the AR in the absence of antigen at 2 min. The reason for the level of AR observed in the absence of antigen is partially nonspecific agglutination and partially just apparent agglutination which is the result of standing for 1 min to allow dispersion of latex by the repulsive surface charge of latices. The dielectric constant of latex, buffer and a protein varies with the ac frequency [17,18].

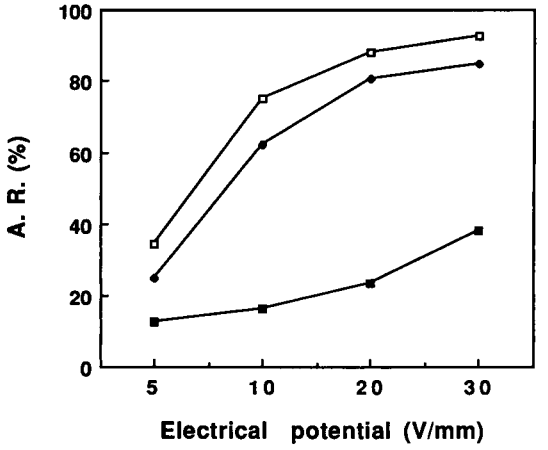

Fig. 4. Effect of the strength of the ac field. Various potentials of 100 KHz ac were applied for 1 min and left standing for another 1 min. The reaction solution was one volume of latex–IgG (0.1%) and one volume of myoglobin (100 ng/ml). (□) AR at 1 min with Ag; (♦) AR at 2 min with Ag; (■) AR at 2 min without Ag.

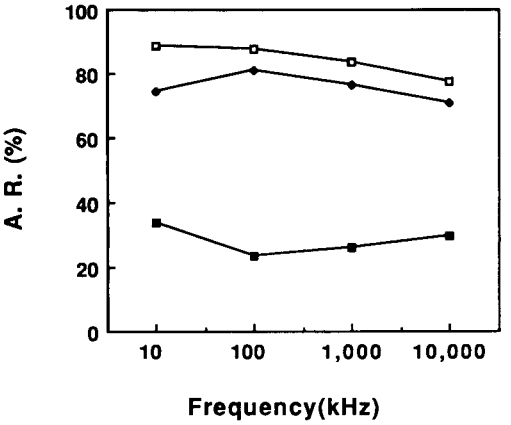

Fig. 5. Effect of the frequency of the ac field. Various frequencies of 20 V/mm ac were applied for 1 min and left standing for another 1 min. The reaction solution was one volume of latex–IgG (1%) and one volume of myoglobin (100 ng/ml). (□) AR at 1 min with Ag; (♦) AR at 2 min with Ag; (■) AR at 2 min without Ag.

Thus the frequency affects the attractive force between particles. It may be considered that if the attractive force is so strong that particles cannot be easily dispersed, then the AR may increase without any specific immunoreaction.

Effect of latex concentration on forming the pearl chain

Different concentrations of latex–IgG and 100 ng/ml of human myoglobin were reacted under 100 KHz, 20 V/mm ac field. The ac field was applied for 1 min and then left standing for another 1 min. In Fig. 6, the concentrations of latex particles also affect the rate of pearl-chain formation. The greater the number of latex particles, the shorter the distance between latex particles. This means that it is easier to form the pearl chain with the same attractive force. Practically it is good to use a latex solution of more than 0.075 percent. The AR in the absence of antigen increased steeply with a latex concentration increasing from 0.1% to 0.125%. Because the concentration of latices is so high that the distance between latices is small, many latices only look like they have aggregated. In this experiment, the AR at 2 min with antigen was also dependent on the AR at 1 min.

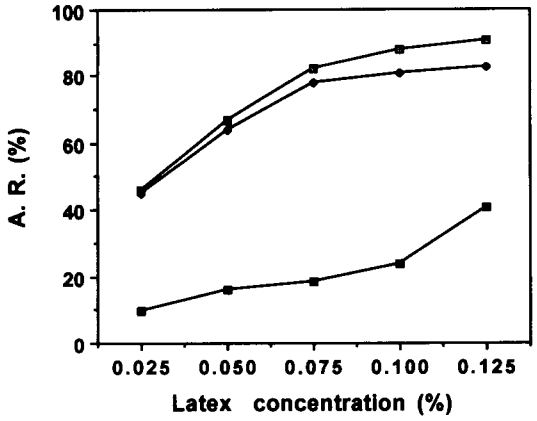

Fig. 6. Effect of the concentration of latices. Various concentrations of latices were used to apply 100 KHz, 20 V/mm ac for 1 min and left standing for another 1 min. The Ag was 100 ng/ml of myoglobin. (□) AR at 1 min with Ag; (♦) AR at 2 min with Ag; (■) AR at 2 min without Ag.

Time course for immunoreaction

Figure 7 shows the time course curve for agglutination. Different concentrations of human myoglobin and 0.1% latex–IgG were reacted under 100 KHz, 20 V/mm ac field. The AC field was applied for 30 s, 1 min and 1.5 min and left standing for another 1 min. The AR increased tp 1 min and reached a plateau. Figure 8 shows the

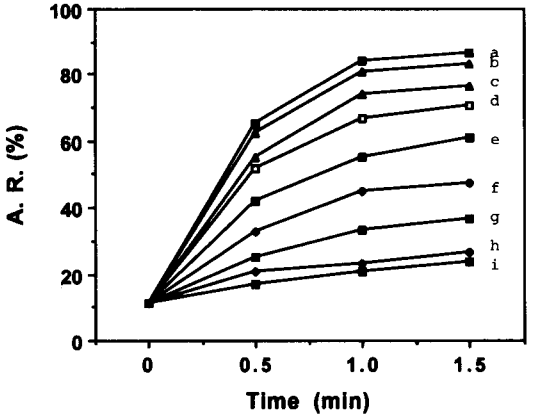

Fig. 7. Reaction rate in time course. Various concentrations of Ag were used to apply a 100 KHz, 20 V/mm ac field for 0.5, 1, 1.5 min and left standing for another 1 min. The latex–IgG was 0.1%. (a) AR with Ag 250 ng/ml; (b) 100 ng/ml; (c) 50 ng/ml; (d) 25 ng/ml; (e) 10 ng/ml; (f) 5 ng/ml; (g) 2.5 ng/ml; (h) 1 ng/ml; (i) 0 ng/ml.

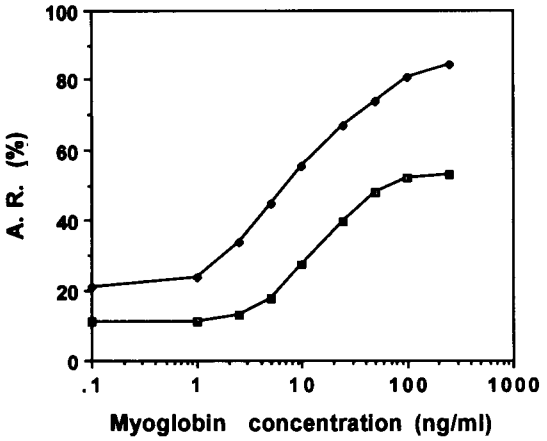

Fig. 8. Standard calibration curve of ac field-enhanced reaction and usual incubation immunoreaction. The conditions of the reaction enhanced by AC were the same as those in Fig. 5, except ac was applied for 1 min. Control reaction was done at 37°C for 20 min. (♦) AR with ac field; (□) AR without ac field.

standard calibration curve from the result of AR at 1 min in Fig. 7. The least detectable amount of myoglobin is 1 ng/ml, much more sensitive than that of turbidimetric measuring [19]. It seems that the sensitivity of fluorescence image analysis is nearly the same as that of the automatic particle counter [4].

Reaction rate with ac field compared with reaction rate without ac field

In Fig. 8, the rate of reaction enhanced by an ac field was compared with that of the reaction without an ac field as a control. The conditions of the reaction enhanced by the ac field were the same as in Fig. 6 with 0.1% latex concentration. In the standard calibration curve, linearity was seen from 1 ng/ml to 100 ng/ml in the reaction with the ac field whereas there was a linearity from 5 ng/ml to 50 ng/ml in the control reaction. Latex immunoassay usually uses sub-μm sized latex. Larger particles were used in this experiment because it is easier to form the pearl chain for larger latex particles than sub-μm sized ones [7], and another merit of larger particles is the better resolution of images from the light microscope.

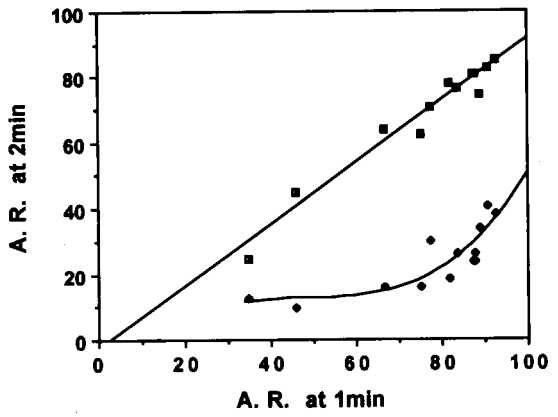

Fig. 9. Correlation diagram of the rate of pearl-chain formation and the rate of immunoreaction. The data were from Figs. 2, 3 and 4. The ac field was applied for 1 min and left standing for another 1 min, thus the AR at 1 min represents the rate of pearl-chain formation and the AR at 2 min represents the rate of immunoreaction. (□) AR with Ag; (♦) AR without Ag.

Correlation between the rate of pearl-chain formation and the rate of immunoreaction

In Fig. 9, it is shown that there is a correlation between the rate of pearl-chain formation and the rate of immunoreaction. From the result of Figs. 4, 5 and 6, every point of AR at 1 min and 2 min in the presence or in the absence of antigen was taken and plotted on the x and y axis. The correlation coefficient was 0.98 which means the rate of immunoreaction was substantially dependent on the rate of pearl-chain formation if the antigen is sufficient. In the absence of antigen, the AR curve increased from 70% the in x axis, partly because of non-specific agglutination and partly because of too much latices.

In the latex immunoassay, there is a two-reaction step. The first step is the binding of latex–IgG to free antigen, the second step is binding of latex–IgG–Ag to another latex–IgG which looks like the rate-determining step. Thus in the correlation between the rate of pearl-chain formation and the rate of immunoreaction, it may be considered that the heat generated by the ac field does not have a significant effect on acceleration of the second step in the latex immunoassay.

Conclusions

A more rapid and sensitive latex immunoassay was developed. Because this assay uses larger particles while still maintaining a high reactivity, the sensitivity of this assay is good. The phenomenon of pearl-chain formation enhanced by an ac field has the effect of increasing the collision frequency making this assay rapid. The rate of this immunoassay is dependent on the rate of pearl-chain formation. The rate of pearl-chain formation varies with the strength and frequency of an electric field and the concentration of latex particles. The agglutination of beads formed by this electric field is in the form of a pearl chain, which is different from the cluster form seen in the current incubation method for latex immunoassay.

REFERENCES

1 P. Blume and L. Grunbergn, J. Clin. Chem., 21 (1975) 1234.
2 C.L. Cambiaso, A.E. Leek, F. De Steenwinkel, J. Billen and P.L. Masson, J. Immunol. Methods, 18 (1977) 33.
3 J. Grange, A.M. Roche and G.A. Quash, J. Immunol. Methods, 18 (1977) 364–375.
4 P.L. Masson, C.L. Cambiaso, D. Collet-Cassart, C.G.M. Magnusson, C.B. Richards and C.J. Sindic, Methods Enzymol., 74 (1981) 106.
5 A.M. Bernard and R.R. Lauwerys, Clin. Chim. Acta, 119 (1982) 335.
6 T.M. McHugh, J.Y. Wang, H.O. Chong, L.L. Blackwood and D.P. Stites, J. Immunol. Methods, 116 (1989) 213.
7 H.P. Schwan and L.D. Sher, J. Electrochem. Soc., 116 (1969) 22C.
8 A.A. Furedi and R.C. Valentine, Biochim. Biophys. Acta, 56 (1962) 33.
9 M.M.S. Lo, T.Y. Tsong, M.K. Conrad, S.M. Strittmatter, L.D. Hester and S.H. Snyder, Nature, 310 (1984) 792.
10 U. Zimmermann, Biochim. Biophys. Acta, 694 (1982) 227.
11 Y. Takahashi, K. Suzuki, T. Niimura, T. Kano and S. Takashima, Biotechn. Bioeng., 37 (1991) 790.
12 H. Matsuoka, H. Tamiya and I. Karube, Anal. Chem., 57 (1985) 1998.
13 E. Tamiya, N. Watanabe, H. Matsuoka and I. Karube, Biosensors, 3 (1988) 139.
14 M.J. Stone, J.T. Willerson, C.E. Gomez-Sanchez and M.R. Waterman, J. Clin. Invest., 56 (1975) 1334.
15 N.P. Kubasik, W. Gulney, K. Warren, J.P. d'Souza, H.E. Sine and B.B. Brody, Clin. Chem., 24(11) (1978) 2047.
16 H. Matsuoka, S. Tanioka and I. Karube, Anal. Lett., 20 (1987) 63.
17 E.H. Grant and G.P. South, Adv. Mol. Relaxation Processes, 3 (1972) 355.
18 R. Pethig, IEEE Trans. Electr. Insul., EI-19 (1984) 453.
19 E. Toft, J. Stetoft and P.T. Anderson, Clin. Chem., 34 (1) (1988) 177.

Analytica Chimica Acta, 282 (1993) 199–207
Elsevier Science Publishers B.V., Amsterdam

Multi-element analysis of aluminium-based ceramic powders by instrumental and radiochemical neutron activation analysis

M. Franek and V. Krivan

Sektion Analytik und Höchstreinigung, Universität Ulm, D-89069 Ulm (Germany)

(Received 29th March 1993)

Abstract

Instrumental and radiochemical neutron activation analysis have been applied to a comprehensive trace characterization of aluminium oxide and aluminium nitride powders using conventional irradiation conditions as well as a special facility providing an extremely low ratio of fast to thermal neutrons enabling to reduce essentially the production of ^{24}Na via the reaction $^{27}Al(n, \alpha)$. Irradiation modes and experimental parameters are given for the determination of 56 elements leading to limits of detection below 100 ng g^{-1} for 39 elements. For the analysis of sample materials of good and high purity using usual neutron flux profiles, the selective removal of ^{24}Na was achieved by its adsorption on a hydrated antimony pentoxide (HAP) column from 12 M HCl. For a number of elements, the results obtained on materials of different purity grades are compared with those obtained by inductively coupled plasma atomic emission spectrometry within an interlaboratory intercomparison.

Keywords: Inductively coupled plasma spectrometry; Neutron activation methods; Radiochemical methods; Aluminium nitride; Aluminium oxide; Ceramics; Multi-element analysis

Aluminium oxide belongs to the most important advanced ceramics for various fields of technology. In some of its applications, for instance in microelectronics as substrate and package material in integrated circuits and in medicine for the production of bioceramic endoprotheses, materials of highest purity are required [1–3]. Owing to high thermal conductivity and a low thermal expansion coefficient, ultra-pure aluminium nitride has advanced to be a promising substitution material for beryllium oxide ceramics in high-efficiency electronic devices [1,4].

The starting powders used for the production of dense aluminium oxide and aluminium nitride ceramics must fulfill certain requirements regarding purity and physical characteristics. Oxides of Cr, Fe, Mg, Na and Ti affect the electrical resistivity of ultra-pure aluminium oxide whereas the oxides of Ca, Fe, Mg, Na, Si and Zr reduce the thermal stability and shock resistance [5–7]. It was observed that the elements Ca, Cr, Fe, Mg, Mn, Si and Ti influence the crystal growth of aluminum nitride, and the elements Fe, Mg and Si cause also a strong decrease in the thermal conductivity [5,8]. In microelectronic applications of these two ceramics, the contents of the natural radioactive elements Th and U are of special interest due to the so-called "soft error effect" caused by the particles emitted in their decay [9,10]. As a consequence of the influence on the material properties of trace impurities even at their very low contents, a comprehensive trace

Correspondence to: V. Krivan, Sektion Analytik und Höchstreinigung, Universität Ulm, D-89069 Ulm (Germany).

characterization of the starting ceramic powder is necessary.

For the bulk analysis of aluminium oxide powders, a number of methods based on wet-chemical decomposition with alkali salts or mineral acids and different determination principles were published [11–17]. However, the efficiency of the analysis of the resulting sample solutions by graphite furnace atomic absorption spectrometry (GFAAS) [15], inductively coupled plasma atomic emission spectrometry (ICP-AES) [15–17] and especially by ICP mass spectrometry (ICP-MS) and total reflection x-ray fluorescence spectrometry (TRXRFS) is considerably limited by blank introduced in the stages prior to the measurement. So far, the analysis of aluminium nitride powders has been reported only by ICP-AES [15,18,19] and flame AAS [20] techniques involving sample decomposition.

Because of the refractory character of these two materials, direct determination methods using solid sample are of great interest. Aluminium oxide has been analysed by ICP-AES using direct solid sample insertion by electrothermal vaporization [21] and spark ablation [22]. Sample introduction by nebulization of powder suspensions was used for the determination of B, Ca, Co, Cu, Fe, Mg, Mn, Si and Ti in fine aluminium oxide powders by ICP-AES [15] and Ga and Pb were determined by slurry sampling GFAAS [23,24]. Solid state mass spectrometric methods such as spark source MS [25] and secondary-ion MS [26] provide excellent limits of detection, but they need matrix-containing standards and have to face problems arising from the non-conductivity of ceramic matrices. Concentrations of impurities at the concentration level of 10 $\mu g\ g^{-1}$ and higher can be determined also by x-ray fluorescence spectroscopy (XRFS) [27].

In spite of the fact that aluminium-based ceramics are suitable matrices for neutron activation analysis (NAA), only a few applications to analysis of these materials have been reported, dealing mostly with the determination of a small group of elements in samples of lower purity [15,28–32]. However, NAA has been applied to multi-element analysis of high-purity aluminium [33–35].

In this work, a separation procedure was developed as a basis for radiochemical NAA (RNAA), which in addition to instrumental NAA (INAA) was applied to a comprehensive characterization of both aluminium oxide and aluminium nitride powders.

EXPERIMENTAL

Reagents and radiotracers

All reagents used were of analytical-reagent grade obtained from Merck (Darmstadt). The hydrated antimony pentoxide (HAP) was supplied by Carlo Erba (Milan) and dried at 105°C for 48 h before use. Radiotracers were produced by irradiation of evaporated standard stock solutions in the nuclear reactor described below and monitored for radiochemical purity by γ-ray spectrometry.

Samples and standards

The samples Al_2O_3-1 and Al_2O_3-2 were obtained from the Gesellschaft Deutscher Metallhütten und Bergleute (Clausthal–Zellerfeld, Germany). The samples Al_2O_3-3 and AlN-1 were commercially available materials supplied by Sumitomo (Osaka) and by H.C. Starck (Berlin), respectively. For checking the accuracy, the quartz material BCS-CRM 313/1 (Bureau of Analysed Samples, Middlesbrough, UK) was used which has been well characterized by an interlaboratory comparison [36].

Standards were prepared from the standard stock solutions supplied by Merck or by Johnson Matthey/Alfa (Karlsruhe, Germany). For the elements Br, Ca, Cs, Rb, Ta, Th, U, W and Zr, the stock standards were prepared either from high-purity salts or metals. For the long irradition, samples and standards were sealed in ampoules made of Suprasil quartz tubes (Heraeus Quarzschmelze, Hanau, Germany), cleaned by surface etching with dilute hydrofluoric acid. For short irradiations, high-purity polyethylene capsules (Stichting Hart Wool Research Foundation, Amsterdam) were used. Depending on the irradiation mode, different sets of multi-element standards were used with a combination of indicator ra-

dionuclides (IRNs) suitable with respect to half-lives and spectral interferences.

Irradiation

For the production of long-lived indicator radionuclides (mode A), sample portions of 100–150 mg were irradiated simultaneously with standards in the FRG-2 reactor of the GKSS Research Centre (Geesthacht, Germany). The activation analysis via medium-lived indicator radionuclides was carried out in quartz ampoules (mode B) and in polyethylene capsules (mode C), respectively, by irradiation in the FRJ-2 reactor of the Nuclear Research Centre of Jülich and in the FRM-1 reactor of Garching, TU Munich. The respective flux of thermal, epithermal and fast neutrons of each irradiation facility used for the different irradiation modes is given in Table 1. After irradiaton, the quartz ampoules were etched outside again, and the polyethylene capsules were cleaned with dilute hydrochloric acid.

γ-Ray spectrometer system

The high resolution γ-ray spectrometer system used consisted of an intrinsic Ge detector with an efficiency of 44% [3 × 3 in. NaI(Tl)], an energy resolution of 1.72 keV (^{60}Co, 1.332 MeV), and a peak-to-Compton ratio of 78 : 1. The detector was connected with an ADCAM (analog-to-digital converter and multi-channel analyser) of 919 type (16 K) and an AT-286 computer for monitoring, processing and storaging of the spectra using the MS-DOS-based Omnigam software package (Vs. 3.5), all obtained from EG&G Ortec (Munich).

Radiochemical procedures

After addition of 10 μg carrier for each element, the irradiated powder samples were decomposed under pressure in 25-ml PTFE liners with 6 ml 12 M HCl by heating for 10 h at 240°C using the digestion system II supplied by Berghof (Eningen, Germany). The resulting solution was used for the separation of ^{24}Na on HAP. For this purposes, columns of 16 mm × 9 mm i.d. with an active bed of 1 ml made of polyethylene syringes were filled with HAP and pretreated with 10 ml of 12 M HCl. The sample solution was passed through the column using a peristaltic pump with a flow rate of 0.5 ml min^{-1} and the column was then eluted with 12 M HCl till a volume of 40 ml was obtained.

For the removal of ^{46}Sc and radioisotopes of other lanthanide elements, a recently published separation procedure based on cation exchange was adapted [37]. The resulting solution after decomposition was evaporated in polymethylpentene (TPX) beakers under an IR lamp to nearly dryness and the residue was taken up with 6 ml of 2 M HCl. Columns of 100 mm × 8 mm i.d. with an active bed of 4 ml made of polystyrene pipettes were filled with the resin Dowex 50W × 8 and pretreated with 10 ml of 2 M HCl. The sample solution was passed through the column under the same conditions as described above for ^{24}Na. The column was then eluted with 2 M HCl till a

TABLE 1

Irradiation facilities used and their neutron flux profiles

Reactor	Experimental mode	Neutron flux Φ (cm^{-2} s^{-1}) thermal/epithermal/fast	Ratio Φ_f/Φ_{th}
Geesthacht (FRG-2)	Mode A	$10^{14} : 2 \times 10^{12} : 10^{13}$	~ 1 : 10
Garching (FRM-1)	Mode B 1	$2 \times 10^{13} : 4 \times 10^{11} : 2 \times 10^{12}$	~ 1 : 10
	Mode C	$1.3 \times 10^{13} : 4 \times 10^{11} : 2 \times 10^{12}$	~ 1 : 7
Jülich (FRJ-2, BE 4)	Mode B 2	$9 \times 10^{12} : 2.3 \times 10^{9} : 1.6 \times 10^{9}$	~ 1 : 5600

TABLE 2

Nuclear reactions induced on aluminium oxide and aluminium nitride with reactor neutrons [38]

Target nuclide	Nuclear reaction	Half-life	Cross section (mb) [a]	Main γ-lines (keV) and their intensities (%)
^{27}Al (100%)	^{27}Al(n, γ)^{28}Al	2.31 min	232 ± 3	1779 (100)
	^{27}Al(n, p)^{27}Mg	9.46 min	4.0 ± 0.45	844 (71.4); 1014 (28.6)
	^{27}Al(n, α)^{24}Na	15.02 h	0.725 ± 0.045	1369 (100); 2754 (100)
^{14}N (99.64%)	^{14}N(n, γ)^{15}N	Stable	75 ± 5	–
	^{14}N(n, p)^{14}C	5736 a	1810 ± 50	No γ-lines
	^{14}N(n, 2n)^{13}N	9.96 min	3×10^{-2}	511 (200)
^{16}O (99.756%)	^{16}O(n, γ)^{17}O	Stable	0.178 ± 0.025	–
^{17}O (0.039%)	^{17}O(n, α)^{14}O	5736 a	235 ± 10	No γ-lines

[a] mb = millibarns = 10^{-27} cm^2.

TABLE 3

Limits of detection (3σ) obtained by INAA and by RNAA via medium-lived indicator radionuclides ($t_{1/2}$ = 2–66 h) for high-purity aluminium oxide Al_2O_3-3 irradiated with neutrons of a conventional Φ_f/Φ_{th} ratio (I) and by INAA using a low Φ_f/Φ_{th} ratio (II)

Element/IRN	Half-life $t_{1/2}$ (h)	Main γ-lines (keV) and their intensity (%)	Limits of detection (μg g^{-1}) [a]		
			INAA (I)	INAA (II)	RNAA
As/^{76}As	26.3	559.10 (45.0)	0.05	0.001	0.00035
Au/^{198}Au	64.8	411.80 (95.5)	0.0001	5×10^{-5}	2×10^{-5}
Br/^{82}Br	35.3	776.49 (83.4)	0.05	0.01	
Cu/^{64}Cu	12.7	1345.76 (0.5)	10	0.2	0.1
Dy/^{165}Dy	2.33	545.70 (1.8)	2		
Er/^{171}Er	7.52	308.30 (63.0)	0.5		
Ga/^{72}Ga	14.1	834.03 (95.6)	0.1	0.002	0.0005
Gd/^{159}Gd	18.6	363.56 (10.8)	1	0.05	0.015
Ho/^{166}Ho	26.8	1379.43 (0.9)	0.4	0.01	0.005
K/^{42}K	12.2	1524.70 (17.9)	10	0.1	0.03
La/^{140}La	40.3	1596.49 (95.5) [b]	0.004	0.0005	0.0001
Mn/^{56}Mn	2.58	846.75 (98.9)	0.2		
Mo/^{99}Mo	66.0	739.50 (13.0)	5	2	0.2
Pd/^{109}Pd	13.5	88.10 (3.7)	1	0.1	0.01
Pr/^{142}Pr	19.1	1575.60 (3.7)	0.5	0.01	0.005
Re/^{188}Re	17.0	155.00 (15.0)	0.1	0.005	
Sb/^{122}Sb	64.8	564.10 (71.0)	0.005	0.005	0.001
Sm/^{153}Sm	46.8	103.18 (28.3)	0.001	0.001	0.0005
Sr/^{87m}Sr	2.81	388.40 (83.0)	25		
U/^{239}Np	56.6	277.60 (14.2)	0.03	0.03	0.002
W/^{187}W	23.9	685.74 (26.4)	0.02	0.001	0.0005
Y/^{90m}Y	3.19	202.52 (97.0)	2		
Zn/^{69m}Zn	13.8	438.60 (94.8)	5	0.1	0.05
Zr/^{97}Zr	16.8	743.40 (98.0)	500	20	

[a] Experimental conditions (see also Table 1): INAA (I): t_{ir} = 8 h, t_d = 24 h, t_c = 5000–10000 s (mode B 1); for IRNs with $t_{1/2}$ < 8 h: t_{ir} = 1/2 h, t_d = 8 h, t_c = 5000 s (mode C). INAA (II): t_{ir} = 12 h, t_d = 36 h, t_c = 10000–25000 s (mode B 2). RNAA: t_{ir} = 13.3 h, t_d = 32 h, t_c = 60000 s (mode B 1). [b] In presence of high gallium contents, the 487.03-keV γ-ray was counted because of the interference from the 1596.8-keV γ-ray of ^{72}Ga (limit of detection: 0.0005 μg g^{-1}).

volume of 40 ml was obtained, which was then counted by γ-ray spectrometry.

RESULTS AND DISCUSSION

Method

In order to explore the potential provided by NAA, it was performed in three experimental modes essentially directed to the optimum assay of medium- and long-lived IRNs. As can be seen from Table 2 surveying the nuclear reactions which can be induced by reactor neutrons on aluminium oxide and aluminium nitride, these matrices are suitable for INAA. In irradiation of aluminium-based ceramics with reactor neutrons, high matrix activity originating from the short-lived nuclides ^{28}Al and ^{27}Mg is produced via the (n, γ)- and (n, p)-reaction, respectively. For this reason, INAA using short-lived IRNs cannot be performed effectively. ^{24}Na is formed by (n, α)-reaction induced by the fast neutrons of the reactor neutron spectrum. The high Compton background resulting from its 1368.6-keV and 2754.1-keV lines strongly decreases the detection limit of medium-lived IRNs whereas the measurement of long-lived nuclides is not affected if appropriate decay times are applied.

By the choice of an irradiation facility providing a fission spectrum with a low flux of fast neutrons, the extent of the interfering ^{27}Al(n, α)^{24}Na reaction (energetic threshold 6 MeV [39]) can be reduced up to several orders of magnitude compared with conventional irradiation. As can be seen from Table 1, the position used at the Jülich reactor FRJ-2 provides a ratio Φ_f/Φ_{th} of about 1:5600 whereas the Garching reactor FRM-1 provides a ratio of about 1:10. Limits of detection (3σ) achievable by INAA of a high-purity aluminium oxide powder via 24 medium-lived IRNs with half-lives from 2.33 h (Dy) to 66 h (Mo) by using these two different neutron spectra are compared in Table 3. The achievable improvement of limits of detection in irradiation with neutrons of a low fast to thermal ratio depends, however, also on the content of some impurities which are strongly activated with thermal neutrons. For instance, higher concentrations of Ga, W and various lanthanide elements cause a considerable increase in the limits of detection of many other elements. The strongest effect of ^{24}Na on the limits of detection occurs when the half-lives of the IRNs are at about the same level as the half-life of ^{24}Na (15 h), i.e., in counting the medium-lived IRNs for As, Br, Cu, Dy, Er, Ga, Gd, Ho, K, La, Mn, Pd, Pr, Sr, W, Y, Zn and Zr.

For the 19 elements determined via IRNs with half-lives ≤ 40 h, the limits of detection were improved by factors between 5 for Br ($t_{1/2} = 35.3$ h) and 100 for K ($t_{1/2} = 12.2$ h) when the high-purity aluminium oxide powder samples were irradiated in the FRJ-2 reactor. On the whole, by INAA via medium-lived IRNs, the limits of detection were < 1 ng g^{-1} for 5 elements, between 1 and 100 ng g^{-1} for 11 elements and > 100 ng g^{-1} for the remaining 8 elements.

Another possibility to reduce or almost completely eliminate the interfering effect of the ^{27}Al(n, α)^{24}Na reaction is the removal of ^{24}Na on a HAP column from 12 M HCl. With the developed separation procedure, more than 99.9% of ^{24}Na is removed, and due to the small size of the HAP column, significant co-retention of the indicator radionuclides is avoided. All medium-lived IRNs excluding that for Sb, could be quantitatively obtained in the eluate (see Table 4). The advantage of this approach is that no special

TABLE 4

Recoveries of elements obtained by the radiotracer technique in the separation procedure for the removal of ^{24}Na on HAP from 12 M HCl with 40 ml eluate

Element/IRN	Recovery (%)	Element/IRN	Recovery (%)
As/^{76}As	99 ± 1	Na/^{24}Na	$\ll 0.1$
Au/^{198}Au	> 99	Pd/^{109}Pd	96 ± 4
Ba/^{131}Ba	> 99	Pr/^{142}Pr	99 ± 1
Ca/^{47}Ca	97.5 ± 2	Rb/^{86}Rb	96 ± 2
Cd/^{115}Cd	> 99	Re/^{188}Re	> 99
Cu/^{64}Cu	99 ± 1	Sb/^{122}Sb	84 ± 2
Ga/^{72}Ga	> 99	Sm/^{153}Sm	98.5 ± 1
Gd/^{159}Gd	98 ± 1	Sr/^{89m}Sr	98 ± 1
Ho/^{166}Ho	> 99	U/^{239}Np	> 99
K/^{42}K	98 ± 2	W/^{187}W	98.5 ± 1
La/^{140}La	> 99	Zn/^{69m}Zn	> 99
Mo/^{99}Mo	99 ± 1	Zr/^{97}Zr	99 ± 1
/^{99m}Tc	> 99		

irradiation facilities fulfilling the requirements regarding reactor neutron spectra are necessary. The separation procedure is simple, as the sample solution resulting from the decomposition with 12 M HCl can directly be used for separation. Applying this separation procedure, the limits of detection for the medium-lived IRNs assayed could be improved by factors between 2 (for Sm) and 200 (for Ga and K) compared to the INAA using conventional ratios of Φ_f/Φ_{th}, and they were decreased by factors between 2 and 15 (see Table 3) relatively to INAA using the extremely low Φ_f/Φ_{th} ratio at the Jülich reactor. For illustration, in Fig. 1, γ-ray spectra of an irradiated high-purity aluminium oxide powder without and with radiochemical separation are shown.

The INAA of aluminium-based ceramics via long-lived IRNs can be performed without any interference from the matrix (for analytical parameters and experimental mode, see Table 5). However, in some instances, depending on the raw materials and the production process, aluminium oxide and aluminium nitride powders can contain higher concentrations of certain elements which are strongly activated with thermal neutrons. Typical impurities producing long-lived radionuclides with dominating activities are the elements Ce, Eu, Sc and Tb. They can cause a considerable increase in detection limits of other trace elements determined via long-lived radionuclides.

By using INAA via long-lived IRNs, up to 37 elements were assayed in several aluminium oxide and aluminium nitride materials. The limits of detection (3σ) for a high-purity aluminium oxide powder were below 1 ng g^{-1} for 14 elements, between 1 and 100 ng g^{-1} for 12 elements and > 100 ng g^{-1} for the remaining 11 elements.

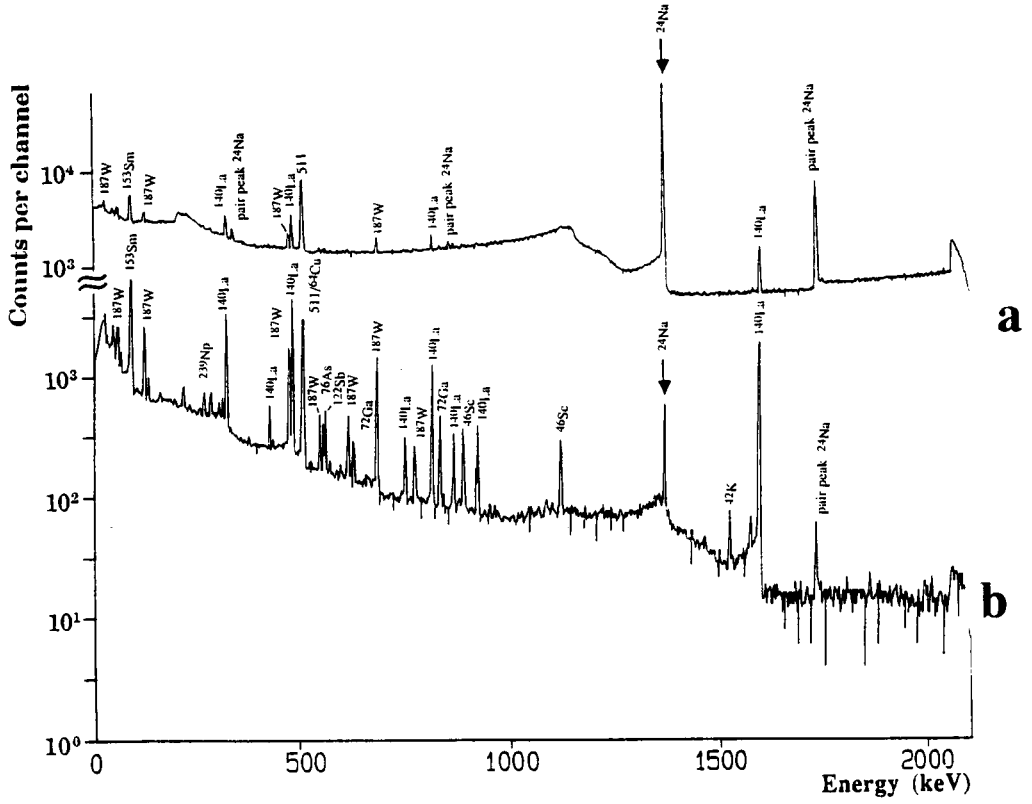

Fig. 1. High-resolution γ-ray spectra of high-purity aluminium oxide Al_2O_3-3 irradiated with reactor neutrons of a conventional ratio of fast to thermal neutron flux ($\sim 1:10$). (a) Instrumental NAA ($t_{ir} = 8$ h, $t_d = 44$ h, $t_c = 4600$ s); (b) radiochemical NAA, after separation of ^{24}Na ($t_{ir} = 8$ h, $t_d = 50.5$ h, $t_c = 5000$ s).

TABLE 5

Limits of detection (3σ) obtained by INAA via long-lived IRNs for high-purity aluminium oxide Al_2O_3-3 in a long irradiation at a high thermal neutron flux ($\Phi_{th} = 10^{14}$ cm^{-2} s^{-1})

Element/ IRN	Half-life $t_{1/2}$ (days)	Main γ-lines (keV) and intensities (%)	Limits of detection [a] (μg g^{-1})
Ag/^{110m}Ag	249.8	657.76 (94.6)	0.0005
Ba/^{131}Ba	11.8	216.09 (19.9)	0.3
Ca/^{47}Ca	4.54	1297.09 (74.9)	50
Cd/^{115}Cd	2.23	527.90 (27.5)	0.05
Ce/^{141}Ce	32.5	145.44 (48.4)	0.004
Co/^{60}Co	1925.2	1332.50 (100)	0.0004
Cr/^{51}Cr	27.7	320.08 (9.8)	0.008
Cs/^{134}Cs	753.1	795.85 (85.4)	0.0001
Eu/^{152}Eu	4868.6	1408.01 (20.9)	0.0002
Fe/^{59}Fe	44.5	1099.25 (56.5)	1
Ge/^{77}As	1.62	239.0 (1.7)	300 [b]
Hf/^{181}Hf	42.4	482.16 (83.0)	0.0002
Hg/^{203}Hg	46.6	279.19 (81.6)	0.002
In/^{114m}In	49.5	190.27 (15.4)	0.003
Ir/^{192}Ir	73.8	316.51 (83.0)	$5\cdot10^{-6}$
I/^{126}I	13.0	388.47 (32.4)	40 [b]
Lu/^{177}Lu	6.71	208.36 (11.0)	0.001
Nd/^{147}Nd	11.0	531.02 (13.1)	0.04
Ni/^{58}Co	70.8	810.77 (99.5)	0.05
Pt/^{191}Pt	2.8	538.87 (13.7)	6 [b]
Rb/^{86}Rb	18.7	1076.70 (8.8)	0.025
Ru/^{103}Ru	39.4	610.33 (5.6)	0.01
Sb/^{124}Sb	60.2	1690.98 (47.3)	0.0003
Sc/^{46}Sc	83.9	889.26 (100)	$3\cdot10^{-5}$
Se/^{75}Se	119.8	264.66 (59.1)	0.002
Sn/^{113}Sn	115.1	391.69 (64.2)	0.25 [b]
Sr/^{85}Sr	64.7	513.99 (98.3)	0.5 [b]
Ta/^{182}Ta	114.7	1221.42 (27.1)	0.0002
Tb/^{160}Tb	72.3	879.36 (29.5)	$4\cdot10^{-5}$
Te/^{131}I	8.0	364.48 (81.2)	1 [b]
Th/^{233}Pa	27.0	311.98 (36.0)	0.0005
Ti/^{48}Sc	1.82	983.4 (100)	100 [b]
Tm/^{170}Tm	128.6	84.26 (10.0)	0.0003
U/^{239}Np	2.36	277.60 (14.2)	0.01 [b]
/^{140}Ba	12.8	537.38 (20.0)	0.05 [b]
Yb/^{175}Yb	4.19	396.32 (6.5)	0.001
Zn/^{65}Zn	244.1	1115.52 (50.7)	0.02
Zr/^{95}Zr	64.0	756.73 (54.5)	1

[a] Experimental conditions (see also Table 1): $t_{ir} = 5$ days, $t_d = 7$–47 days $t_c = 60000$ s (mode A). [b] Limits of detection determined for a material of lower purity grade (Al_2O_3-1).

However, the lower the purity grade of the sample material and/or the higher the content of an impurity giving rise to a dominating activity (as it was the case with ^{46}Sc in the sample AlN-1), the higher the achievable detection limits. Therefore, in analysis of sample materials like AlN-1, a selective separation of ^{46}Sc and other lanthanide elements becomes necessary. The described procedure developed for this purpose provides limits of detection for many elements determined via long-lived indicator radionuclides (Ag, Co, Cr, Cs, Fe, Ir, Ni via ^{58}Co, Rb, Ru, Sb, Sn and Zn) at the same level as obtained by INAA for high-purity materials (see Table 5).

Analysis of aluminium-based ceramic powders

The optimized INAA procedure and the developed RNAA procedure were applied to analysis of different aluminium-based ceramic powders for more than 50 elements.

The relevance of possible primary interference reactions induced by fast neutrons and by the uranium fission was examined. For all elements investigated, the extent of the interference by (n, p)-, (n, α)- and (n, 2n)-reactions was found negligible ($< 1\%$). Due to different scandium contents in the samples, the contribution from titanium via the reaction ^{46}Ti(n, p)^{46}Sc to the indicator radionuclide of scandium, ^{46}Sc, was estimated to be $< 1\%$ for titanium contents < 70 μg g^{-1} in both aluminium oxide samples and < 140 μg g^{-1} in the aluminium nitride sample. As estimated by ICP-AES, the titanium contents were clearly below these limits.

In the sample materials Al_2O_3-1 and AlN-1, serious interferences occurred in the determination of Nd, Ru, Sm, Te and Zr from fission products of ^{235}U being identical with the indicator radionuclides for these elements (^{147}Nd, ^{103}Ru, ^{153}Sm, ^{131}I and ^{95}Zr). The contributions of the fission products amounted to 50% or more, and, therefore, no reliable corrections were possible. In the case of cerium and molybdenum, the contribution to their indicator radionuclides was about 50% (Al_2O_3-1) and 20% (AlN-1) for ^{141}Ce and about 30% (AlN-1) for ^{99}Mo, respectively. The interference in the determination of lanthanum via ^{140}La, which can also be produced directly by uranium fission and via the decay of ^{140}Ba, could be handled well for both the materials when short cooling times (< 70 h) were applied. The corrections were made on the basis of

fission yields obtained by simultaneous irradiation of uranium standards. However, according to former investigations, the commercial uranium salt $UO_2(NO_3)_2 \cdot 6H_2O$ used for standardization is known to be altered with respect to the natural abundance of ^{235}U (0.72%). The degree of this alteration was estimated experimentally by determining uranium in a reference material via the indicator radionuclides ^{140}Ba and ^{131}I and comparing the results with those obtained on the basis of the $^{238}U(n, \gamma)^{239}U$ reaction leading to the indicator radionuclide ^{239}Np. In this way, a depletion factor of 2 was determined.

A typical spectral interference occurred for the normally used analytical γ-ray of ^{140}La at 1596.5 keV from the 1596.8-keV line of ^{72}Ga at higher contents of gallium. However, in such a case, another suitable γ-ray of ^{140}La could be used. For the determination of lower contents of zinc via ^{65}Zn emitting the only γ-ray at 1115.5 keV, radiochemical separation, as performed in the analysis of the sample AlN-1, is unavoidable if higher contents of scandium (main γ-line of ^{46}Sc at 1120.5 keV) are present in the sample too.

The contribution of the blank from the quartz ampoules and polyethylene capsules used as irradiation vessels was found to be negligible for all elements detected.

In Table 6, the contents of 19 common trace impurities determined by NAA in two aluminium oxide powders of different purity grades and, in addition, in an aluminium nitride powder are compared with results obtained from other laboratories by ICP-AES within a round robin study. As can be seen from this comparison, the element contents obtained by NAA for the material

TABLE 6

Comparison of results for some common elements obtained by INAA and RNAA in this work with those of other laboratories obtained by ICP-AES

Element	Element content in $\mu g\ g^{-1}$				
	Al_2O_3-1, good purity		Al_2O_3-2, high purity		AlN-1
	NAA [a]	Other laboratories [b]	NAA [a]	Other laboratories [b]	NAA [a]
As	0.16 ± 0.04 (R)	–	0.002 ± 0.0005 (R)	–	0.013 ± 0.006 (R)
Ba	47.5 ± 2.5	–	< 1	–	4.2 ± 0.6
Ce	(~ 0.2) [c]	< 10/< 15/< 5/< 10; 0.3*	0.37 ± 0.06	< 30/< 10/< 5/< 10; 0.8*	(0.5 ± 0.1) [c]
Co	0.39 ± 0.04	4/< 5/< 2/< 1; 0.4*	0.007 ± 0.001	4/< 5/< 1/< 1; 0.06*	0.38 ± 0.01
Cr	1.04 ± 0.06	< 5/< 2/< 1; 1.0*	0.90 ± 0.07	< 5/< 5/< 2/< 1; 1.2*	5.6 ± 0.15
Cu	< 5 (R)	1.6/< 5/1.5/1/2/< 2	< 0.2 (R)	< 0.5/< 5/< 5/< 0.5/< 5/< 2	22.8 ± 3.2 (R)
Fe	244 ± 8	238/254/254/237/241/259; 245*	< 5	4/< 5/5.1/5/6/2.8; < 12*	69 ± 2
Ga	89 ± 3	93/124/87/86/88/89; 87*	10.5 ± 0.25	11/< 10/11/10/13; 11*	13.3 ± 1.3 (R)
K	< 10 (R)	< 50/36/9/10; < 6*	61 ± 3 (R)	70/< 100/61/36/48; 68*	3 ± 1 (R)
La	(0.06 ± 0.02) [c] (R)	< 5/< 1/< 1; 0.056*	0.002 ± 0.0002 (R)	< 2/< 5/< 1/< 1; < 0.02*	(0.37 ± 004) [c] (R)
Mn	1.6 ± 0.15	6/< 5/1.7/3/1.6/2	< 0.2	4/< 5/< 5/< 0.5/< 1/7	–
Ni	9.9 ± 0.5	10/10/12/9	< 0.2	< 5/< 5/< 4/< 1	1.75 ± 0.15
Sb	0.042 ± 0.002	–	0.004 ± 0.001	–	0.057 ± 0.001
Sc	0.020 ± 0.002	–	0.020 ± 0.002	–	0.043 ± 0.001
Th	0.031 ± 0.001	–	< 0.001	–	0.082 ± 0.003
U	0.83 ± 0.03	–	< 0.01	–	0.63 ± 0.08 (R); 0.5 ± 0.1 (via ^{140}Ba)
W	0.19 ± 0.02 (R)	–	0.008 ± 0.002 (R)	–	3.3 ± 0.2 (R)
Zn	3.0 ± 0.2	5/< 5/< 5/6/6/10; 4*	1.5 ± 0.2	1/< 5/< 5/< 3/< 5/6.5; 2.1*	1.06 ± 0.07 (R)
Zr	(~ 12) [c]	9/9/9/10/4.3; < 18*	< 4	< 5/< 0.5/< 1/< 1; < 3.5*	(< 10) [c]

[a] R = Element contents determined by RNAA based on separation of ^{24}Na (As, Cu, Ga, K, La, U, and W) in all materials and RNAA based on separation of ^{46}Sc (Zn) in AlN-1. [b] Results obtained by ICP-AES after various wet-chemical decomposition procedures and by NAA (*). Contents by ICP-AES of Na in Al_2O_3-1: 715/718/694/667/762 $\mu g\ g^{-1}$; in Al_2O_3-2: 26/28/16/36 $\mu g\ g^{-1}$. [c] Contents given in brackets: concentration corrected for the contribution from ^{235}U-fission products.

Al_2O_3-1 are in good agreement with results of ICP-AES which, however, could not detect a number of elements because the contents were below the limits of detection. A number of low-concentration elements, occurring especially in the high-purity material Al_2O_3-2, could be determined only by NAA with sufficient accuracy and precision or even principally.

From the results obtained, it can be concluded that NAA, mainly because of the freedom of blank, is an excellently suitable method for a comprehensive trace characterization of aluminium-based ceramic powders of good- and high-purity grade. For the most elements to be determined, extremely low limits of detection can be achieved even by the instrumental performance, however, only when neutrons with a low fast to thermal ratio are available and when no trace component in the sample material gives rise to the production of a high-activity radionuclide. For some materials, owing to their unsuitable trace composition for INAA, sufficiently low limits of detection can be achieved only by radiochemical separations. However, some relevant impurities such as B, Mg and V are not detectable by the modes of NAA used.

The authors gratefully acknowledge the financial support of this work by Deutsche Forschungsgemeinschaft (Bonn) and providing the irradiation facilities free of charge by GKSS (Geesthacht, Germany), by KFA (Jülich, Germany) and by Reaktorstation Garching (TU Munich).

REFERENCES

1 L.M. Sheppard, Am. Ceram. Soc. Bull., 70 (1991) 1467.
2 Ph. Logan, Sprechsaal, 122 (1989) 833.
3 G. Heimke, Adv. Mater., 2 (1990) 45.
4 Th. Quiel, Sprechsaal, 121 (1988) 1176.
5 F. Aldinger and H.-J. Kalz, Angew. Chem., 99 (1987) 381.
6 G. DeWith and N. Hattu, J. Mater. Sci., 16 (1981) 841.
7 H. Endl and H. Hausner, Ber. Dtsch. Keram. Ges., 57 (1980) 128.
8 T. Sakai and M. Iwata, J. Mater. Sci., 12 (1977) 1659.
9 T.C. May and H.M. Woods, IEEE Trans. Electron Devices, 26 (1979) 2.
10 P.M. Carter and B.R. Wilkins, IEE J., Solid-State Electron Devices, 134 (1987) 32.
11 J. Huang, Lihua Jianyan, Huaxe Fence, 23 (1987) 50.
12 British Standard, BS 4140: Part 5: (Si), Part 7 (Fe), Part 11 (Na), Part 12 (V), Part 17 (F), Part 18 (P), Part 19 (B), British Standard Institution, 1986, p. 6.
13 Y. Fan, J. Lu and S. Jiang, Guangpuxue Yu Guangpu Fenxi, 7 (1987) 59.
14 B. Nikolova and N. Jordanov, Talanta, 29 (1982) 861.
15 T. Graule, A. von Bohlen, J.A.C. Broekaert, E. Grallath, R. Glockenkämper, P. Tschöpel and G. Tölg, Fresenius' Z. Anal. Chem., 335 (1989) 637.
16 H. Morikawa, Y. Iida, T. Ishizuka and F. Yokota, Bunseki Kagaku, 35 (1986) 636.
17 Y. Harada and N. Kurata, Bunseki Kagaku, 35 (1986) 641.
18 C. Martinez-Lebrusant and F. Barba, Analyst, 115 (1990) 1335.
19 M. Hayashi and H. Endo, Bunseki Kagaku, 37 (1988) T 202.
20 T.P. Mikhailova, V.P. Klimashova and L.V. Babueva, Izv. Sib. Otd. Akad. Nauk, SSSR, Ser. Khim. Nauk, (1973) 135.
21 H. Nickel, M. Reisch and M. Mazurkiewicz, Fresenius' Z. Anal. Chem., 335 (1989) 631.
22 A. Aziz, J.A.C. Broekaert, K. Laqua and F. Leis, Spektrochim. Acta, Part B, 39 (1984) 1091.
23 J. Marecek and V. Sydek, J. Anal. At. Spectrosc., 5 (1990) 385.
24 R. Karwowska and K.W. Jackson, J. Anal. At. Spectrosc., 2 (1987) 125.
25 M. Sasaki, Y. Umada, H. Watanabe and H. Umezaki, Bunseki Kagaku, 35 (1986) 753.
26 H. Morikawa, Y. Uwamino and T. Ishizuka, Analyst, 114 (1989) 679.
27 R.M. Agrawal and S.K. Kapoor, X-Ray Spectrom., 18 (1989) 151.
28 C. Friedli, M.E. Colin and M. Rousseau, J. Trace Microprobe Technol., 8 (1990) 197.
29 H. Rausch, S. Torok and A. Simonitis, Isotopenpraxis, 21 (1985) 223.
30 J. Vucina, V. Scepanovic and R. Draskovic, J. Radioanal. Chem., 44 (1978) 371.
31 T. Bereznai, G. Keömley, M. Miskei and M. Vigvari, Radiochem. Radioanal. Lett., 23 (1975) 369.
32 B.A. Thompson and E.C. Miller, J. Res. Natl. Bur. Stand. Sect. A, 75 (1971) 429.
33 K.-P. Egger and V. Krivan, Fresenius' Z. Anal. Chem., 331 (1988) 394.
34 K.-P. Egger and V. Krivan, Fresenius' Z. Anal. Chem., 323 (1986) 827.
35 I.P. Alimarin, Yu.V. Kovlev and V.P. Kolotov, Zh. Anal. Khim., 38 (1983) 158.
36 H. Baumann and J. Pavel, Microchim. Acta, III (1989) 413.
37 M. Franek and V. Krivan, Anal. Chim. Acta, 264 (1992) 345.
38 G. Erdtmann, Neutron Activation Tables, Verlag Chemie, Weinheim, 1976.
39 D. Brune and J.J. Schmidt (Eds.), Handbook on Nuclear Activation Cross-Sections, IAEA, Wien, 1974.

Analytica Chimica Acta, 282 (1993) 209–213
Elsevier Science Publishers B.V., Amsterdam

Subattomole detection of amino acids by capillary electrophoresis based on semiconductor laser fluorescence detection

Tetsuhiro Fuchigami and Totaro Imasaka

Faculty of Engineering, Kyushu University, Hakozaki, Fukuoka 812 (Japan)

Masanobu Shiga

Dojindo Laboratories, Tabaru 2025–5, Mashiki-machi, Kamimashiki-gun, Kumamoto 861–22 (Japan)

(Received 15th February 1993; revised manuscript received 13th April 1993)

Abstract

A pyronin succinimidyl ester fluorescent in the deep-red region is synthesized, whose absorption maximum and molar absorptivity are 663 nm and 8.2×10^4, respectively. This compound is used for fluorescence labeling of amino acids such as alanine, arginine, glycine, glutamic acid, and aspartic acid. The sample containing the labeled amino acids is separated by capillary electrophoresis and is detected by semiconductor laser fluorometry. A sheath flow cell is used for reduction of the light scatter from the cell wall. This compact and inexpensive analytical system allows detection of 0.8–4.5 attomole of amino acids.

Keywords: Fluorimetry; Amino acids; Capillary electrophoresis

Laser spectrometry provides an ultrasensitive means, and detection of even a single atom, ion, and molecule has already been demonstrated. However, a real sample, e.g. a biological fluid, contains many impurities, and therefore a separation procedure is essential before detection of the chemical species of interest. Liquid chromatography (LC) is currently used for separation of proteins, metabolites, and amino acids, and more recently capillary electrophoresis has attracted much attention because of its better separation resolution [1]. However, the amount of sample injected into a capillary is very small, typically one nanoliter, and the detection volume should be minimized to picoliter levels. A laser fluorescence detector may be successfully used for this purpose, because of its high sensitivity and high spatial resolution [2]. However, such an analytical instrument has up to now seldom been commercialized [3]. This is due to high capital and running costs of the laser and difficulties in maintenance and operation.

Recently, a semiconductor laser was commercialized and used in a compact disk and a bar-code reader. The semiconductor laser is already used for determination of biological substances such as proteins, enzymes, and metabolites [4]. Semiconductor laser fluorometry may be combined with HPLC [5] and since recently to capillary electrophoresis [6]. However, only 10-picomole amino acids have been determined so far, due to poor fluorescence labeling and detection efficiencies.

Correspondence to: T. Imasaka, Faculty of Engineering, Kyushu University, Hakozaki, Fukuoka 812 (Japan).

In this study, we labeled amino acids with a new reagent, i.e. 9-cyano-*N*,*N*,*N*′-triethyl-*N*′-(5′-succinimidyloxycarbonylpentyl) pyronin, chloride (pyronin succinimidyl ester) synthesized for the present purpose. This compound has a chromophore similar to Rhodamine 800, which is known to be an efficient laser dye fluorescent in the near-infrared region. Simultaneously, the compound has a succinimidyl ester for combination with an amino group. The sample containing labeled amino acids was separated by capillary electrophoresis and detected by semiconductor laser fluorometry. A sheath flow cell was used to reduce the light scatter from the cell wall for ultrasensitive determination at zeptomole levels.

EXPERIMENTAL

Apparatus

The sample containing amino acids was injected into a capillary (50 μm i.d., 375 μm o.d., 50 cm long) by a siphon method, the injection volume being 1 nl. A high voltage (30 kV, 40 μA) was applied to the solution for a sample inlet side. The fluorescence detection system, based on the method using a sheath flow [2], is schematically shown in Fig. 1. Instead of a large argon ion laser a semiconductor laser (660 nm, 2 mW) is used as a light source. The laser beam is passed through an interference filter (short pass; 90% transmittance at 660 nm; < 0.5% transmittance at 700 nm) to block non-lasing broadband emission and is focused into a ~ 10-μm liquid column formed in a sheath flow cell (square bore, 700 μm; flow rate, 30 μl/min). The semiconductor laser and an objective lens for a microscope (magnification, 20; numerical aperture, 0.4; working distance, 11 mm) and the flow cell are mounted on optical stages with 0.3-μm precision. Fluorescence is collected by an objective lens (magnification, 50; numerical aperture, 0.6; working distance, 4 mm) and is passed through interference (long pass; 2% transmittance at 660 nm; 60% transmittance at 700 nm) and spatial (~ 400 μm i.d.) filters, and subsequently detected by a photomultiplier. The overall dimension of the detector is 36 cm × 18 cm × 40 cm, including the exciting laser. The size of the detector is not minimized, and the dimension is mainly determined by the box containing the filters. If necessary, the dimension will be substantially reduced in future studies.

Reagents and procedure

The labeling reagent was synthesized from *m*-aminoanisol through eight steps. The scheme is shown in Fig. 2. Five amino acids, i.e. alanine,

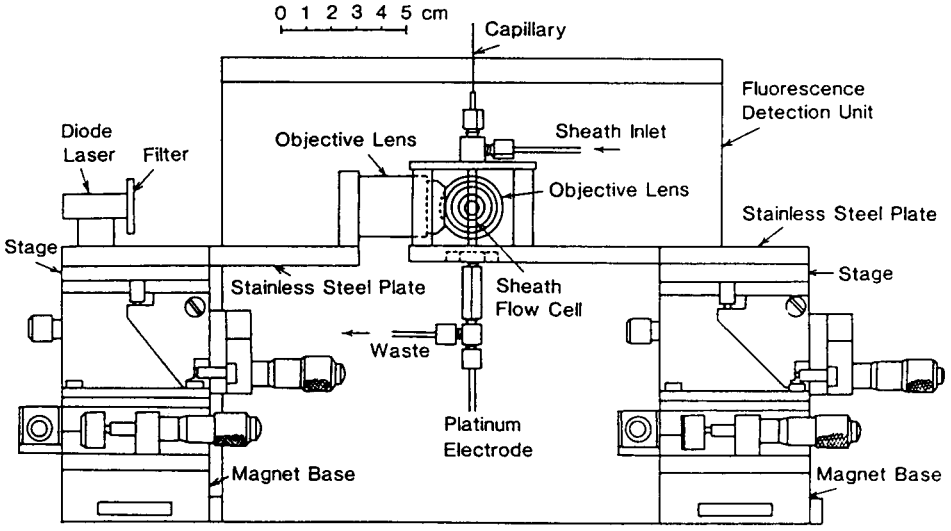

Fig. 1. Detector for capillary electrophoresis. A semiconductor laser (660 nm, 2 mW) is used as an exciting source.

arginine, glycine, glutamic acid, and aspartic acid, were reacted with the labeling reagent as follows: 10 μl of 1 mM amino acids dissolved using NaOH were mixed with 50 μl of 10 mM pyronin succinimidyl ester and with 100 μl of 100 mM *N*-2-hydroxyethylpiperazine-*N'*-2-ethanesulfonic acid

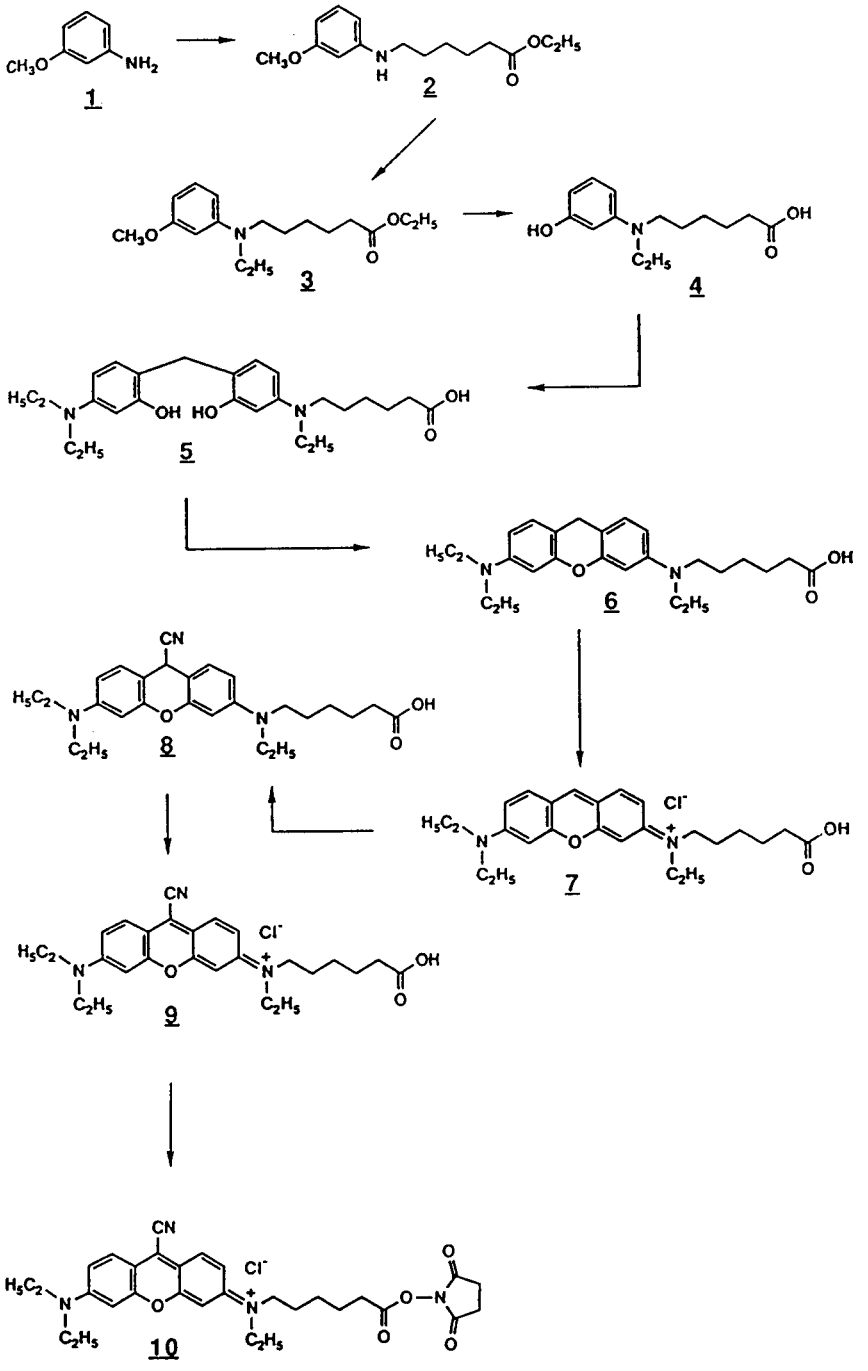

Fig. 2. Scheme for the organic synthesis of the labeling reagent.

(HEPES) buffer (pH 7.0). The solution was incubated for 1 h at 37°C. The excess amounts of labeling reagent and decomposed products were removed by extracting twice with chloroform.

RESULTS AND DISCUSSION

The labeling reagent synthesized is soluble at least to 10 mM in an aqueous solution at pH 7.0. It is less stable at higher pH. The molar absorptivity is 8.2×10^4 at 663 nm. The excitation and fluorescence spectra are shown in Fig. 3. The fluorescence quantum yield was not measured accurately, but it was 1/40 time smaller than that of carboxyfluorescein though the spectral response of the fluorescence spectrometer was not corrected. The electropherogram for the sample containing the five amino acids is shown in Fig. 4.

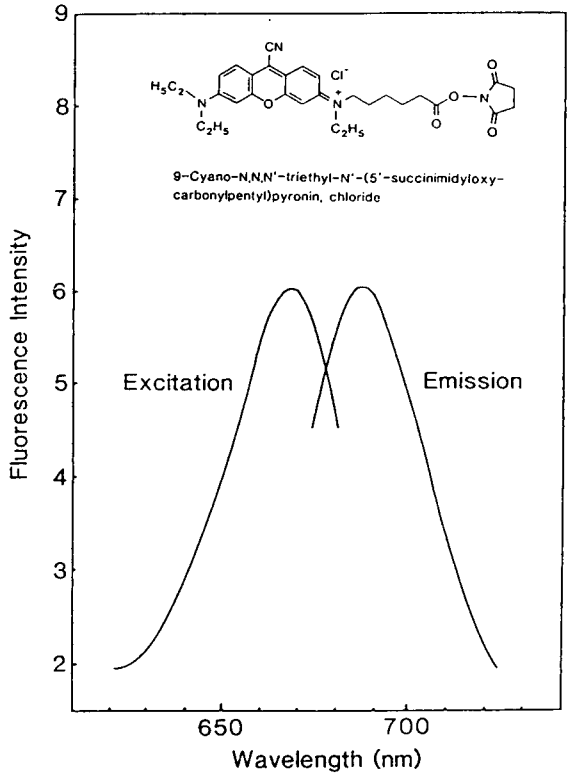

Fig. 3. Excitation and fluorescence spectra for pyronin succinimidyl ester. The structure and the formal name are indicated in the figure.

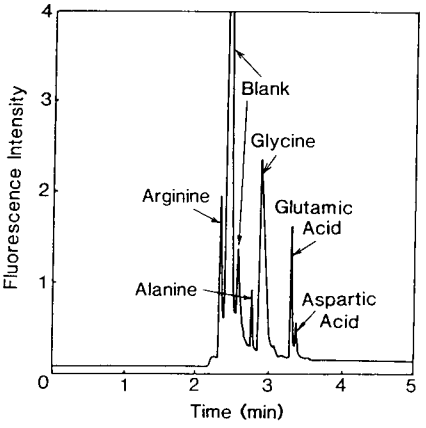

Fig. 4. Electropherogram for the sample containing the five amino acids (50 fmol each). Phosphate buffer, 16 mM, pH 5.0; Sheath flow rate, 28 μl min^{-1}. Assignments are indicated in the figure. The peaks 'Blank' originate from the reagent blank.

All the components are separated within 4 min. The theoretical plate number achieved is 270000, which is similar to the value reported elsewhere [2]. The peak for glycine is slightly tailed; this could be observed at different pH values. The reason is unknown; however, glycine labeled with pyronin succinimidyl ester might be neutral or positively charged and might be adsorbed on the capillary wall which is negatively charged by dissociation of silanol groups. A negatively charged labeling reagent such as fluorescein isothiocyanate (FITC) seems to be preferred to avoid this interaction.

The analytical sensitivity was investigated by injecting the sample stepwise diluted. The detection limits, defined as the concentrations providing a signal-to-noise ratio of 2, were 0.8–4.5 attomole for the amino acids studied (800 zeptomole for glycine, 300 zeptomole for labeling reagent). This is an improvement of seven orders of magnitude in comparison with the result obtained in the preliminary study [6]. It is due to a higher labeling efficiency of the synthesized dye and to higher efficiencies in fluorescence detection and background reduction. Only one labeling reagent is tested and experimental conditions are not optimized in this study. Moreover, a semiconductor laser with a higher output power is already commercialized (e.g. 10 mW), and the back-

ground signal may be further reduced by cooling the photomultiplier. Therefore, the detection limit will be improved to low zeptomole levels, as already demonstrated by using FITC or fluorescein thiohydantoin and argon ion laser excitation [2,7].

In trace analysis, the detection limit is practically determined by background fluorescence occurring from impurities. Such unwanted fluorescence is much weaker in the deep-red or near-infrared regions, since most organic compounds have absorption bands in the ultraviolet or visible region. Furthermore, a semiconductor laser can be operated continuously for several years without maintenance. Then, semiconductor laser fluorometry is preferred for practical applications, e.g. for real samples such as biological fluids.

In the human genome project, slab gel electrophoresis is widely used for the determination of deoxyribonucleic acid (DNA) sequence; DNA is a double helix consisting of four different bases, i.e. adenine, guanine, cytosine, and thymine. Since the amount of DNA is limited and a human genome consists of 3×10^9 base pairs, it is necessary to develop a new analytical instrument with a higher sensitivity, a higher separation resolution, and lower capital and maintenance costs; the price for determination of a base pair must be reduced to one cent. Up to now, the optimum method to accomplish this international project has not yet been established. The method developed in this study already fulfils most of the above requirements. Furthermore, semiconductor lasers emitting at several wavelengths, e.g. 635, 680, 750, 820 nm, are commercially available and are directly controlled by integrated circuits, which may greatly simplify the signal detection and data processing systems for DNA sequencing.

This work is supported by Grants-in-Aid for Scientific Research from the Ministry of Education, Science and Culture of Japan, from the Steel Industry Foundation for the Advancement of Environmental Protection Technology (SEPT), and from the Nakatani Electronic Measuring Technology Association of Japan.

REFERENCES

1 W.G. Kuhr, Anal. Chem., 62 (1990) 403R.
2 Y.F. Cheng and N.J. Dovichi, Science, 242 (1988) 562.
3 To our best knowledge, only Beckman Instruments Inc. supplies a capillary electrophoresis system combined with an argon laser excitation source, Chem. Eng. News, 18 (1991) 58.
4 T. Imasaka and N. Ishibashi, Anal. Chem., 62 (1990) 363A.
5 K. Sauda, T. Imasaka and N. Ishibashi, Anal. Chem., 58 (1986) 2649.
6 T. Higashijima, T. Fuchigami, T. Imasaka and N. Ishibashi, Anal. Chem., 64 (1992) 711.
7 S. Wu and N.J. Dovichi, Talanta, 39 (1992) 173.

Analytica Chimica Acta, 282 (1993) 215–220
Elsevier Science Publishers B.V., Amsterdam

Synergic extraction of rare earths with 2-thenoyltrifluoroacetone and phosphoryl-type bidentate ligands such as tetraphenyldiphosphine dioxide or bis(diphenylphosphinyl)methane

Saeko Satake, Satoshi Tsukahara and Nobuo Suzuki

Department of Chemistry, Faculty of Science, Tohoku University, Aoba-ku, Sendai 980 (Japan)

(Received 8th March 1993; revised manuscript received 20th April 1993)

Abstract

The synergic extraction of rare earth(III) ions (RE; La, Sm, Tb and Lu) using 2-thenoyltrifluoroacetone (Htta) and phosphoryl-type uncharged bidentate ligands, such as tetraphenyldiphosphine dioxide (tpdpo) or bis(diphenylphosphinyl)methane (bdppm), was investigated in benzene. The synergic enhancement was attributed to the formation of the adduct $RE(tta)_3S_n$ ($n = 1$ or 2 for tpdpo and $n = 1$ for bdppm) in benzene, where S denotes the uncharged ligand. The adduct formation constants (β_S) and the synergic extraction constants were determined. For each RE(III), the $\beta_{S,1}$ value for bdppm is larger than the $\beta_{S,1}$ and $\beta_{S,2}$ values for tpdpo and the β_S values for both ligands decrease with increasing atomic number of RE(III).

Keywords: Extraction; Rare earth elements

Systematic studies of the synergic extraction of rare earth(III) [RE(III)] ions using an acidic chelating agent and a bidentate neutral ligand have recently been conducted by the use of various nitrogen-containing bidentate ligands, such as bipyridine and 1,10-phenanthroline. These synergic extraction systems gave interesting results, e.g., the extraction efficiency can be greatly enhanced compared with systems using common unidentate ligands such as tributyl phosphate (tbp) [1–5]. However, systematic studies on the synergic extraction of RE(III) by use of these bidentate uncharged ligands have rarely been conducted except for cases using nitrogen-containing ligands. To understand the characteristic synergism observed with nitrogen-containing bidentate ligands it is necessary to examine other bidentate uncharged ligands involving oxygen as donor atom.

This study involved the use of tetraphenyldiphosphine dioxide (tpdpo) and bis(diphenylphosphinyl)methane (bdppm), as a phosphoryl-type uncharged bidentate ligand. Bdppm has only been used together with a chelating agent such as 1-phenyl-3-methyl-4-benzoyl-5-pyrazolone in the synergic extraction of several doubly charged first transition series and alkaline earth metal ions [6,7]. As an acidic chelating agent, 2-thenoyltrifluoroacetone (Htta), which is a β-diketone and widely used in synergic extraction was chosen in this study. From the equilibrium data for the synergic extraction of the rare

Correspondence to: S. Tsukahara, Department of Chemistry, Faculty of Science, Tohoku University, Aoba-ku, Sendai 980 (Japan).

earths La(III), Sm(III), Tb(III) and Lu(III), the equilibrium constants were determined.

EXPERIMENTAL

Materials and apparatus

The radioisotopes ^{140}La, ^{153}Sm, ^{160}Tb and ^{177}Lu, used as tracers, were produced by neutron irradiation of 0.03–2 mg of metal nitrate in the JRR-4 nuclear reactor of the Japan Atomic Research Institute at a thermal neutron flux 5.5×10^{13} n cm^{-2} s^{-1} for 12 h. A radioactive solution of RE(III) was prepared by dissolving a known amount of the irradiated sample in 0.1 M nitric acid, evaporating to dryness and dissolving the residue in 1×10^{-3} M hydrochloric acid or perchloric acid before use.

2-Thenoyltrifluoroacetone (Htta) [4,4,4-trifluoro-1-(2-thienyl)butane-1,3-dione] (Dojindo Laboratories, Kumamoto) (98% purity) was purified by vacuum sublimation at 40°C. Tetraphenyldiphosphine dioxide (tpdpo) was prepared by oxidation of tetraphenyldiphosphine (Kanto Chemical) (98.0% purity) with dry air in toluene [8]. The product was recrystallized from toluene. Tpdpo: m.p. 169.5–171.0°C; elemental analysis, calculated for $C_{24}H_{20}P_2O_2$, C 71.26, H 4.88; found, C 71.63, H 5.02%. Bis(diphenylphosphinyl)methane (bdppm) [methylenebis(tetraphenyldiphosphine oxide)] was prepared by oxidation of bis(diphenylphosphino)methane (Kanto Chemical) (96.0% purity) with hydrogen peroxide solution in acetone. Bdppm: m.p. 186–187°C; elemental analysis, calculated for $C_{25}H_{22}P_2O_2$, C 71.70, H 5.45; found, C 72.11, H 5.33%. (These found values in the elemental analysis agreed with the calculated value with a relative error of less than 3%.)

Benzene was stirred with concentrated sulphuric acid, washed with water and distilled after drying. Other reagents used were of guaranteed reagent grade.

The γ-activity of each radioisotope was measured with an NaI(Tl) well-type scintillation detector (BICRON) connected with a single-channel analyser (NAIG). The pH of the equilibrated aqueous phase was measured with an HM26S glass electrode (Toa Denpa).

Extraction procedure

An aqueous solution (5 cm^3) containing 1×10^{-7}–1×10^{-5} M RE(III) labelled with its radioisotope was placed in a 20-cm^3 centrifuge tube with a stopper. The pH of the aqueous phase was adjusted to 3.2–5.4 with 1×10^{-3}–1×10^{-2} M sulphanilic acid and sodium hydroxide solution. In this pH range the formation of RE hydroxides can be ignored [9]. The ionic strength was adjusted to 0.1 with sodium perchlorate for tpdpo and sodium chloride for bdppm; in the latter instance perchlorate is replaced with chloride in order to avoid deposition of an ion associate such as ClO_4^-–bdppm or RE(III)–ClO_4^-–bdppm [10]. A benzene solution (5 cm^3) containing 1×10^{-4}–1×10^{-2} M Htta and 1×10^{-5}–1×10^{-2} M uncharged ligand was added to the aqueous solution, shaken for 1 h at 25°C and centrifuged. An aliquot was taken from each phase, the γ-activity was measured and the distribution ratio of RE(III) was calculated as the radioactivity ratio. The equilibrium pH was measured immediately after phase separation.

THEORY

The distribution ratio (D_0) of a cation M^{3+} with a chelating extractant (HA) can be expressed as

$$D_0 = \frac{[\overline{MA_3}]}{[M^{3+}] + \Sigma[MA_m^{3-m}]} = \frac{K_{ex} P_{HA}^3 [A^-]^3}{K_{HA}^3 (1 + \Sigma \beta_{A,m} [A^-]^m)} \quad (1)$$

where the bar denotes the organic phase, K_{HA} and P_{HA} are the acid dissociation constant and the partition coefficient of HA, respectively, $\beta_{A,m}$ is the formation constant of MA_m^{3-m} and A^- is the chelating anion in the aqueous phase. K_{ex} denotes the extraction constant for the following equilibrium:

$$M^{3+} + 3\overline{HA} \rightleftharpoons \overline{MA_3} + 3H^+ \quad (2)$$

In the region where the concentration of A^- is very low, $\Sigma\beta_{A,m}[A^-]^m$ is negligibly small in Eqn. 1, hence D_0 is proportional to the third power of $[A^-]$.

In the synergic extraction of M^{3+} with HA and an uncharged ligand (S), the distribution ratio (D) can be expressed as

$$D = \frac{[\overline{MA_3}] + \Sigma[\overline{MA_3S_n}]}{[M^{3+}] + \Sigma[MA_m^{3-m}]}$$

$$= \frac{K_{ex}P_{HA}^3[A^-]^3(1 + \Sigma\beta_{S,n}[\bar{S}]^n)}{K_{HA}^3(1 + \Sigma\beta_{A,m}[A^-]^m)} \quad (3)$$

where $\beta_{S,n}$ is the adduct formation constant in the organic phase corresponding to the formation constant of the following equilibrium:

$$\overline{MA_3} + n\bar{S} \rightleftharpoons \overline{MA_3S_n} \quad (4)$$

From Eqns. 1 and 3, the following equation is obtained:

$$D/D_0 = 1 + \Sigma\beta_{S,n}[\bar{S}]^n \quad (5)$$

If MA_3S_n is the dominant species in the organic phase, D/D_0 will be proportional to the nth power of $[\bar{S}]$. The synergic extraction constant ($K_{ex,S,n}$) for the following equilibrium:

$$M^{3+} + 3\overline{HA} + n\bar{S} \rightleftharpoons \overline{MA_3S_n} + 3H^+ \quad (6)$$

can be calculated from the simple relationship

$$K_{ex,S,n} = K_{ex}\beta_{S,n} \quad (7)$$

RESULTS AND DISCUSSION

Synergic extraction with Htta and bdppm

The extraction of La(III), Tb(III) and Lu(III) with 3×10^{-4}–1×10^{-2} M Htta and 5×10^{-4} M bdppm in benzene was carried out, and the logarithm of the distribution ratio of RE(III) was plotted against the logarithm of the equilibrium concentration of tta^- in the aqueous phase as shown in Fig. 1. The equilibrium concentration of tta^- in the aqueous phase was calculated by considering its partition and dissociation as follows:

$$[tta^-] = \frac{C_{HA}}{1 + (P_{HA} + 1)[H^+]/K_{HA}} \quad (8)$$

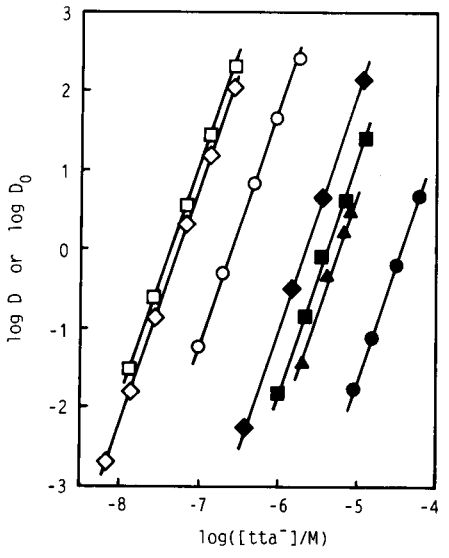

Fig. 1. Distribution ratio of RE(III) as a function of tta^- concentration in the presence or absence of bdppm in benzene. ○ = La, □ = Tb and ◇ = Lu in the presence of bdppm; ● = La, ▲ = Sm, ■ = Tb and ◆ = Lu in the absence of bdppm.

where C_{HA} denotes the initial concentration of Htta. The literature values of K_{HA} and P_{HA} were adopted, i.e., $pK_{HA} = 6.23$ [11] and $\log P_{HA} = 1.62$ [12].

A large synergic effect is observed as compared with the plots of $\log D_0$ in the absence of bdppm in Fig. 1. The slopes of these plots were calculated to be 2.87, 2.92 and 2.97 for La(III), Tb(III) and Lu(III), respectively, by the least-squares method. Therefore, it is proved that three tta^- anions participate in the synergic extraction of RE(III) with Htta and bdppm.

The adduct formation constant can be obtained by Eqn. 5 using the equilibrium concentration of the uncharged ligand, $[\bar{S}]$. The partition coefficient of bdppm has not been reported. A benzene solution containing 3×10^{-3} M bdppm was shaken with an aqueous solution of pH 3 for 30 min. The absorbance of bdppm in the benzene phase at 280 nm was constant within the measurement error (5%) before and after shaking. Therefore, it was assumed that the equilibrium concentration of bdppm is equal to its initial concentration. The plots of $\log(D/D_0)$ against

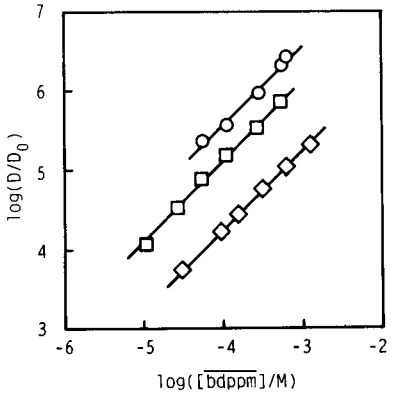

Fig. 2. Effect of bdppm concentration in benzene on the synergic extraction of RE(III) with Htta and bdppm. ○ = La; □ = Tb; ◇ = Lu.

log[bdppm] in the synergic extraction of RE(III) with 1×10^{-3} M Htta and 1×10^{-5}–1×10^{-2} M bdppm in benzene are shown in Fig. 2. The value of D_0 under comparable conditions can be calculated from Eqn. 1 using K_{ex} as given in Table 1. The slopes of the plots were found to be 1.01, 0.99 and 0.98 for La, Tb and Lu, respectively, by the least-squares method, which show that $RE(tta)_3(bdppm)$ is the extracted species corresponding to Eqn. 4 and no evidence for the formation of a higher adduct, such as $RE(tta)_3(bdppm)_2$, was observed. The adduct formation constant, $\beta_{S,1}$, calculated from Eqn. 5 and the synergic extraction constant, $K_{ex,S,1}$, calculated from Eqn. 7, are listed in Table 1.

Bdppm contains two phosphoryl groups and is considered to behave as a bidentate ligand. This

TABLE 1

Extraction constants (K_{ex}) in RE(III)–Htta–benzene systems and adduct formation constants ($\beta_{S,n}$) and synergic extraction constants ($K_{ex,S,1}$) in RE(III)–Htta–S–benzene systems

S	RE(III)	Log K_{ex}	Log $\beta_{S,1}$	Log $\beta_{S,2}$	Log $K_{ex,S,1}$
bdppm	La	−10.19 [a]	9.60	– [b]	−0.59 [a]
	Tb	−7.35 [a]	9.10	– [b]	1.75 [a]
	Lu	−6.75 [a]	8.23	– [b]	1.48 [a]
tpdpo	La	−10.19	5.22	7.74	−4.97
	Sm	−7.80	4.79	7.32	−3.01
	Tb	−7.35	4.72	6.62	−2.63
	Lu	−6.56	4.64	6.18	−1.92

[a] Ionic strength 0.1 M (H^+, Na^+)Cl^-. [b] Not observed.

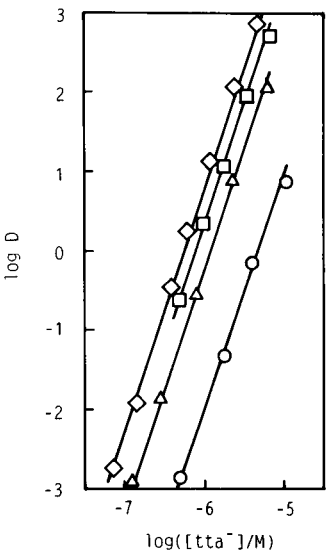

Fig. 3. Distribution ratio of RE(III) as a function of tta^- concentration in the presence of tpdpo in benzene. ○ = La, 1.10×10^{-3} M tpdpo; △ = Sm, 1.15×10^{-3} M tpdpo; □ = Tb, 1.82×10^{-3} M tpdpo; ◇ = Lu, 1.83×10^{-3} M tpdpo.

is supported by the fact that only one adduct with a large $\beta_{S,1}$ value is observed. The adduct formation constant for bdppm must be compared with those for anologous unidentate ligands tbp and trioctylphosphine oxide (topo), e.g., log $\beta_{S,1}$ and log $\beta_{S,2}$ in La(III)–Htta–tbp–carbon tetrachloride are 4.83 and 9.33, respectively [13], and log $\beta_{S,1}$ and log $\beta_{S,2}$ in Tb(III)–Htta–topo–benzene are 6.32 and 11.57, respectively [14], i.e., $\beta_{S,1}$ for bdppm is substantially higher than $\beta_{S,1}$ for tbp and topo.

Synergic extraction with Htta and tpdpo

The same experiments were done for another bidentate ligand of the same type, tpdpo. The extraction of La(III), Sm(III), Tb(III) and Lu(III) was carried out with 4×10^{-4}–8×10^{-2} M Htta and 1×10^{-3} M tpdpo in benzene. The plots of the logarithm of the distribution ratio of RE(III) against the logarithm of the equilibrium concentration of tta^- in the aqueous phase are shown in Fig. 3. The synergic effect can be observed by comparison with the plots of log D_0 in the absence of tpdpo in Fig. 1. The plots for these synergic extraction systems are straight lines with slopes of 3.01, 2.90, 2.88 and 3.12 for La, Sm, Tb

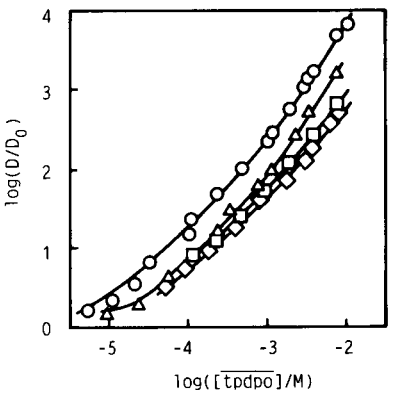

Fig. 4. Effect of tpdpo concentration in benzene on the synergic extraction of RE(III) with Htta and tpdpo. ○ = La; □ = Tb; △ = Sm; ◇ = Lu.

and Lu, respectively. Therefore, similarly to the bpdpm system, it is proved that three molecules of tta^- participate in the synergic extraction of RE(III) with Htta in the presence of tpdpo.

The plots of $\log(D/D_0)$ against $\log[\overline{\text{tpdpo}}]$ in the synergic extraction of RE(III) with 1×10^{-2} M Htta and 1×10^{-5}–1×10^{-2} M tpdpo in benzene are shown in Fig. 4. The partition coefficient of tpdpo has not been reported, but its high partitioning was confirmed by carrying out the same experiment as for bdppm, hence $[\overline{\text{tpdpo}}]$ is assumed to be equal to its initial concentration. The plots of RE(III) in the high concentration range of tpdpo deviate positively from the straight line with a slope of 1.0. This suggests that at high concentrations of tpdpo, the 1:1 and the 1:2 adducts are present. The adduct formation constants, $\beta_{S,1}$ and $\beta_{S,2}$, calculated from Eqn. 5 by the non-linear least-squares method, and the synergic extraction constants, $K_{ex,S,1}$ and $K_{ex,S,2}$, calculated from Eqn. 7 are summarized in Table 1.

The $\beta_{S,1}$ and $\beta_{S,2}$ values for tpdpo are smaller than those for topo. Tpdpo contains also two phosphoryl groups and is expected to be a bidentate ligand like bdppm, but two adduct formation constants, $\beta_{S,1}$ and $\beta_{S,2}$, are observed. No crystal data for a RE–tta–tpdpo and RE–tta–bdppm ternary complexes are available. According to an x-ray structure analysis of the tpdpo crystal, its two oxygen atoms are *trans* to each other [15]. On the other hand, it was observed that in the $Sn(C_6H_5)_2(NO_3)_2$(bdppm) crystal, two oxygen atoms of bdppm coordinate to the Sn atom [16]. Therefore, tpdpo in the adduct formation may behave as a unidentate ligand via coordination of one phosphoryl group to the central RE(III) and thus $\beta_{S,1}$ for every RE(III) is smaller than that of bdppm.

As summarized in Table 1, the adduct formation constants decrease slightly in order of increasing atomic number of RE(III), but the synergic extraction constant $K_{ex,S}$ increases slightly in order of increasing atomic number of RE(III). This result must be compared with that for another type of bidentate ligand involving nitrogen such as bipyridine and 1,10-phenanthroline, where $K_{ex,S}$ clearly increases in order of increasing atomic number of RE(III). The noticeably different trends among different types of bidentate uncharged ligands are very interesting.

The synergic extraction constant, $K_{ex,S}$, especially for the bdppm system, is large, which makes it possible to extract RE(III) ions quantitatively at relatively low pH. The small difference among the $K_{ex,S}$ values for these RE(III) ions is not sufficient to improve the mutual separation efficiency using the present synergic system. An improvement of the separation efficiency with the synergic extraction system may be possible by a combination of a chelating agent and a polydentate ligand.

This work was supported in part by the Inter-University Joint Research Programme using the Japan Atomic Energy Research Institute Facilities and a Grant-in-Aid for Scientific Research from the Ministry of Education, Science and Culture of Japan.

REFERENCES

1 S. Nakamura and N. Suzuki, Polyhedron, 5 (1986) 1805.
2 S. Nakamura and N. Suzuki, Inorg. Chim. Acta, 114 (1986) 101.
3 S. Nakamura and N. Suzuki, Polyhedron, 7 (1988) 155.
4 S. Nakamura and N. Suzuki, Anal. Chim. Acta, 270 (1992) 95.
5 S. Nakamura and N. Suzuki, Bull. Chem. Soc. Jpn., 66 (1993) 98.

6 S. Umetani, S. Kihara and M. Matsui, Chem. Lett., (1986) 1545.
7 S. Umetani, S. Kihara and M. Matsui, Anal. Chim. Acta, 232 (1990) 293.
8 W. Kuchen and H. Buchwald, Chem. Ber., 91 (1958) 2871.
9 C.F. Baes, Jr., and R.E. Mesmer, The Hydrolysis of Cations, J. Wiley, New York, 1976, pp. 129–138.
10 S. Umetani, N. Shigemura, S. Kihara and M. Matsui, Talanta, 38 (1991) 653.
11 J.C. Reid and M. Calvin, J. Am. Chem. Soc., 72 (1950) 2948.
12 T. Wakahayashi, S. Oki, T. Omori and N. Suzuki, J. Inorg. Nucl. Chem., 26 (1964) 2255.
13 L. Farbu, J. Alstad and J.H. Augustson, J. Inorg. Nucl. Chem., 36 (1974) 2091.
14 A.T. Kandil and K. Farah, J. Inorg. Nucl. Chem., 42 (1980) 1491.
15 A.J. Blake, G.P. McQuillan and I.A. Oxton, J. Mol. Struct., 78 (1982) 265.
16 S. Dondi, M. Nardelli, C. Pelizzi, G. Pelizzi and G. Predieri, J. Organomet. Chem., 308 (1986) 195.

Analytica Chimica Acta, 282 (1993) 221–225
Elsevier Science Publishers B.V., Amsterdam

Alkylene bisdithiocarbamates as complexing agents for the preconcentration of trace metals in aquatic samples

Tsing-Pai Hsieh and Lilian Kao Liu

Department of Chemistry, National Taiwan Normal University, Taipei 117 (Taiwan)

(Received 3rd December 1992; revised manuscript received 15th April 1993)

Abstract

A series of alkylene bisdithiocarbamates (BDTCs) were synthesized and shown to be excellent chelating agents for heavy metal ions such as Cu(II), Fe(III), Zn(II), Ni(II), Cd(II), Pb(II), Co(II), Mn(II) and Cr(VI) in aqueous solution. The pH dependence of extraction with these chelating agents was extensively studied from pH 2.5 to 10.0. Except for Cr(VI) and Mn(II), most of the cations were recovered with near 100% efficiency within the working pH range of 4–8. If the pH was fixed at 5.0–5.5, even Cr(VI) could be successfully extracted with hexamethylene BDTC (HMBDTC) (95%). The efficiency of HMBDTC for the extraction of most ions was comparable to that of ammonium tetramethylenedithiocarbamate and sodium diethyldithiocarbamate and was better for extracting Cr(VI). Stock solutions of these bisdithiocarbamates were stable for at least 3 weeks after preparation. The detection limits were found to be in the range 3–90 ng l^{-1}. Therefore, these alkylene BDTCs, particularly HMBDTC, can be applied to the preconcentration of trace heavy metals in environmental aquatic samples.

Keywords: Sample preparation; Alkylene bisdithiocarbamates; Preconcentration; Sea water; Trace metals; Waters

Heavy metal ions play important roles in the aquatic environment, so the determination of their contents in various water samples is very important. Because they are present at trace levels and usually in complicated matrices, preconcentration and/or matrix separation techniques have to be employed prior to their determination by instrumental methods. One widely used technique is chelation and liquid–liquid extraction, such as the use of dithiocarbamates in certain organic solvents for simultaneous multi-element extractions [1–12]. Among the dithiocarbamates, ammonium tetramethylenedithiocarbamate [ammonium pyrolidinedithiocarbamate (APDC)] and sodium diethyldithiocarbamate (NaDDC) are the two most commonly used. Sometimes, these two reagents are used together for better results [3].

Correspondence to: L.K. Liu, Department of Chemistry, National Taiwan Normal University, Taipei 117 (Taiwan).

Bisdithiocarbamates have hardly been used. Some diammonium bisdithiocarbamates have been synthesized and characterized [13,14]. Spectrophotometric methods for the determination of metals by using bisdithiocarbamates have been developed [13–15].

Preliminary investigations indicated that dithiocarbamates usually formed 2:1 metal complexes, while alkylene bisdithiocarbamates formed 1:1 one metal complexes. The complexing ability depended on the alkylene chain length. In this work, a detailed study was carried out. A series of alkylene bisdithiocarbamates, namely ethylene bisdithiocarbamate (EBDTC), propylene bisdithiocarbamate (PBDTC), butylene bisdithiocarbamate (BBDTC), pentamethylene bisdithiocarbamate (PMBDTC) and hexamethylene bisdithocarbamate (HMBDTC), were prepared and the extraction effect of these reagents as complexing agents was studied.

EXPERIMENTAL

Apparatus

An Instrumentation Laboratory VIDEO-12 atomic absorption spectrometer equipped with a deuterium arc background corrector was used to determine spiked samples by flame atomic absorption spectrometry (AAS). For the determination of detection limits, a Perkin-Elmer 5100 PC atomic absorption spectrometer equipped with a Perkin-Elmer HGA 600 graphite furnace, an AS-60 autosampler and a Zeeman-effect background corrector was used. The pH of the aqueous solution was measured with a Corning Model 130 pH meter. All glassware was soaked in 10% nitric acid for at least 24 h, then rinsed thoroughly with deionized water before use.

Reagents

APDC, NaDDC and starting materials such as diamines, carbon disulphide and sodium hydroxide were purchased from Merck or Aldrich. Deionized water was obtained by passing distilled water through a mixed-bed ion-exchange column, then a Milli-Q water-purification system (Millipore). Nitric acid and ammonia solution (Ultragrade) were purchased from Seastar Chemicals. All metal stock standard solutions (1000 μg ml^{-1}), except chromium(VI), were purchased from Merck. The Chromium(VI) stock standard solution (1000 μg ml^{-1}) was prepared by dissolving potassium dichromate in deionized water. Multi-element standard working solutions were prepared from the single-element stock standard solutions by appropriate mixing and dilution.

Buffer solutions were prepared from 0.1 M potassium hydrogenphthalate with 0.1 M HCl or NaOH (pH 3–6) and potassium dihydrogenphosphate with disodium hydrogenphosphate (pH 6–8).

Isobutyl methyl ketone (IBMK) was shaken twice with 3 M nitric acid in a separating funnel and then washed four times with deionized water. Aqueous solutions of various alkylene bisdithiocarbamates were shaken with IBMK (25 ml) to remove contaminated metals.

Chelating reagent solutions (1%, w/v) were prepared by dissolving 1 g of each compound in 100 ml of deionized water and purified by shaking with 25 ml of IBMK for 20 min.

Alkylene bisdithiocarbamates were synthesized as follows. The individual diamine (0.05 mol) in tetrahydrofuran (THF) (100 ml) was placed in a 250-ml three-necked flask, equipped with a condenser, a separating funnel and a magnetic stirrer. Carbon disulphide (3.80 g, 3.02 ml, 0.05 mol) in 20 ml of THF was added dropwisely through the separating funnel and the mixture was stirred for 2 h at room temperature (about 30°C). Sodium hydroxide (2.0 g, 0.05 mol) in 20 ml of water was then added and the mixture was stirred for 30 min. The last two steps were repeated twice. After removing the THF using a rotary evaporator at 30°C the viscous oil obtained was dissolved in water–ethanol (1 + 1) (100 ml). The product usually appeared as a white powder after storage of the solution in a freezer overnight.

Extraction procedure

Normally, 400 ml of water sample, 5 ml of buffer solution, 5 ml of alkylene bisdithiocarbamate (1%) and 25 ml of IBMK were pipetted into a 500-ml separating funnel for extraction. The solution was shaken vigorously for 20 min, then kept quiescent to allow the phases to separate completely. A 15 ml volume of the extract was removed by pipette and combined with 5 ml of nitric acid (3M) for the next extraction.

The mixture was shaken vigorously for 5 min and the aqueous phase was then transferred into a 20-ml vial for AAS analysis.

Stability test

The stabilities of these bisdithiocarbamates were tested by both extraction and precipitation. In the former process, the recovery of spiked metal ions with bisdithiocarbamates was measured every other day. In the latter, the process was as follows: 1 ml of a bisdithiocarbamate solution was added to 50 ml of standard solution [200 mg l^{-1} of Cu(II) at pH 4], stirred for 20 min and then allowed to stand overnight. The solution was filtered through a 0.45-μm Millipore filter and the Cu(II) content in the filtrate was measured by flame AAS.

RESULTS AND DISCUSSION

Effect of pH on the extraction of trace elements

The effect of pH on the extraction of Cu(II), Fe(III), Zn(II), Ni(II), Cd(II), Pb(II), Mn(II), Co(II) and Cr(VI) ions with different bisdithiocarbamates was studied. These results were obtained by using deionized water spiked with 10 $\mu g\ l^{-1}$ of each of the nine metal ions and adjusting to the desired pH value. All these complexing agents gave over 95% recoveries for Cu(II), Fe(III), Zn(II), Ni(II), Cd(II), Pb(II) and Co(II) over pH range 4–8. For Mn(II), a nearly quantitative recovery was obtained at pH 10. Figure 1 indicated that a good recovery of Cr(VI) could be obtained if HMBDTC was used as the complexing agent at pH 5.0–5.5. Under the same conditions, the recovery for Cr(III) was only 35–45% and was not improved at other pH values. Therefore, the extraction of Cr(VI) will be significantly affected by both the pH and the chain length of the alkylene bisdithiocarbamates.

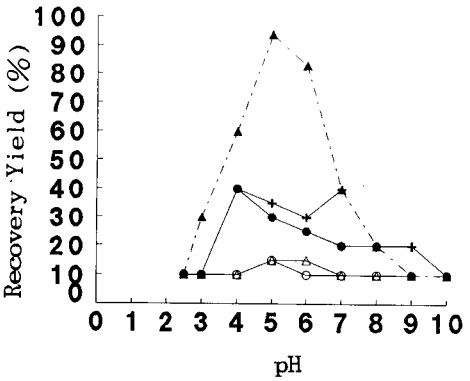

Fig. 1. Effect of pH on extraction of Cr(VI) in deionized water by various bisdithiocarbamates. △ = EBDTC; ○ = PBDTC; + = BBDTC; ● = PMBDTC; ▲ = HMBDTC.

Choice of organic solvent

To study the effects of various organic solvents such as chloroform, dichloromethane and IBMK on the extraction of metal complexes, extractions were done at pH 5.0–5.5 from water samples by the extraction procedure mentioned above. The results showed that the extraction was quantitative only with IBMK as extraction solvent.

Shaking time for extraction and back-extraction

To determine the optimum extraction times, nine metal ions were added to and extracted from the water samples (pH 5.0–5.5) with 5 ml of 1% HMBDTC, 5 ml of buffer solution and 25 ml of IBMK, the shaking time being varied from 5 to 20 min. The results are given in Table 1. It is obvious that a shaking time of 15 min is sufficient to extract quantitatively all nine metals. In further experiments, a shaking time of 20 min was used.

After extraction for 20 min, 15 ml of the IBMK phase were pipetted into a 60-ml separating funnel and 5 ml of 3 M nitric acid were added. The funnel was shaken for different times from 2 to 10 min. From the results it appeared that shaking for 4 min is sufficient for the complete back-extraction of all nine metals. In subsequent work, a shaking time of 5 min was used for back-extraction.

Choice of acid concentration for back-extraction

After extraction for 20 min, the organic phase was re-extracted with 1, 2, 3 and 4 M nitric acid for 5 min, then the concentration of each metal in the aqueous phase was measured by AAS. It was found that 3 M nitric acid is sufficient for back-extraction.

TABLE 1

Recoveries as a function of the shaking time for the extraction of metal complexes with HMBDTC at pH 5.0–5.5 into IBMK

Time (min)	Recovery (%)							
	Cu(II)	Fe(III)	Zn(II)	Ni(II)	Cd(II)	Pb(II)	Co(II)	Cr(VI)
5	80	98	98	85	90	100	100	65
10	100	100	100	100	95	100	100	75
15	100	100	100	100	100	100	100	95
20	100	100	100	100	100	100	100	95

TABLE 2

Absorbance of trace elements in sea water by standard additions method with HMBDTC at pH 5.0–5.5

Metal ion added ($\mu g\ l^{-1}$)	Found (absorbance)							
	Cu(II)	Fe(III)	Zn(II)	Ni(II)	Cd(II)	Pb(II)	Co(II)	Cr(VI)
0	0.006	0.043	0.072	0.004	0.000	0.001	0.005	0.000
5	0.028	0.059	0.125	0.015	0.045	0.005	0.017	0.005
10	0.050	0.078	0.183	0.028	0.089	0.010	0.029	0.009
15	0.070	0.094	0.227	0.041	0.137	0.015	0.041	0.014

Preconcentration of metal ions from sea water

It is well known that sea water is a complex matrix with low concentrations of heavy metals. In order to determine the concentrations of metals in sea water, many preconcentration and matrix elimination techniques such as coprecipitation [16], chelation and liquid–liquid extraction [2,6,8–10] and the use of chelating ion-exchange resins [17] have been developed. We were interested in applying these alkylene bisdithiocarbamates to sea water analysis. Sea water from Chin-Shan, Taiwan (pH 8.1), was filtered with a 0.45 μm Millipore filter and analysed using the standard additions method. The sea-water sample was spiked with different concentrations (5, 10 and 15 $\mu g\ l^{-1}$) of various metal ions and extracted according to the described extraction procedure with different alkylene bisdithiocarbamates. A linear relationship was obtained for the extraction of Cu(II), Fe(III), Zn(II), Cd(II), Pb(II), Co(II) and Ni(II) with all the bisdithiocarbamates. These results clearly indicate that these alkylene bisdithiocabamates could be used for the determination of trace metals in sea water. Further, as HMBDTC could extract Cr(VI) successfully at pH 5.0–5.5, nine metal ions were added to sea water and the pH was adjusted to 5.0–5.0. The results obtained with HMBDTC are given in Table 2. Except for Mn(II), the recovery was quantitative for all the elements.

TABLE 3

Comparison of recoveries for Cr(VI) and Mn(II) from spiked sea water with different chelating agents

Metal ion added [a]	Found ($\mu g\ l^{-1}$) [b]			
	HMBDTC	NaDDC	APDC	NaDDC+APDC
Cr(VI)	18.9±3.8	5.4±0.2	15.1±0.7	14.9±2.4
Mn(II)	~0	21.3±0.9	~0	21.1±1.0

[a] Concentration added: 20 $\mu g\ l^{-1}$. [b] Mean±S.D. of five determinations.

Comparison of recovery yields with differert chelating agents

To compare the present reagents and reagents used previously, hexamethylene bisdithiocarbamate (HMBDTC) was chosen as an example. Extraction efficiencies for different metals in sea water with APDC and a mixture of NaDDC and APDC were determined for comparison. Sea wa-

TABLE 4

Stabilities of different metal–bisdithiocarbamate complexes in IBMK

Reagent	Time (h)							
	Cu(II)	Fe(III)	Zn(II)	Ni(II)	Cd(II)	Pb(II)	Co(II)	Cr(VI)
EBDTC	3	3	3	9	3	9	35	–
PBDTC	9	9	3	9	3	9	35	–
BBDTC	9	3	3	9	3	9	35	–
PMBDTC	3	3	3	9	3	9	9	–
HMBDTC	3	3	3	9	3	3	9	3

ter from Chin-Shan was filtered with 0.45-μm Millipore filter and 20 μg l^{-1} each of the nine metal ions were added. The described extraction procedure was used for HMBDTC, whereas for NaDDC, APDC and the mixture of NaDDC and APDC the method reported by Jane and Young [5] was followed. The extraction results for Cu(II), Fe(III), Zn(II), NI(II), Cd(II), Pb(II) and Co(II) obtained by these four chelating reagents agreed to within 10%. Only the NaDDC-containing reagents gave a good recovery for Mn(II). For Cr(VI), HMBDTC was more efficient than either APDC or NaDDC. The results for Mn(II) and Cr(VI) are given in Table 3.

Stability of bisdithiocarbamates and metal complexes

All five aqueous bisdithiocarbamates were found to be stable for at least 3 weeks after preparation.

The stability of the metal complexes in the organic phase (IBMK) was measured by examining the concentration at different time intervals. The results are given in Table 4. It is clear that the results of the analyses should be correct if they were obtained within 3 h after extraction.

Detection limits

Using HMBDTC as chelating reagent, the detection limits for the elements based on three times the standard deviation of the blank signals and a 48-fold concentration factor were as follows: 17 ng l^{-1} for Pb(II), 22 ng l^{-1} for Cu(II), 18 ng l^{-1} for Co(II) and Ni(II), 3 ng l^{-1} for Cd(II), 80 ng l^{-1} for Fe(III), 90 ng l^{-1} for Zn(II) and 7 ng l^{-1} for Cr(VI). The relatively high detection limits for Zn(II) and Fe(III) might be due to contamination from the nitric acid and/or the buffer solution used in sample preparation. The detection limits of the proposed extraction method and chelating reagent are sufficiently low for the determination of metal ions in environmental aquatic samples.

Conclusions

This study has shown that alkylene bisdithiocarbamates can quantitatively extract Cu(II), Fe(III), Zn(II), NI(II), Cd(II), Pb(II) and Co(II) with IBMK in a single extraction step in a broad working pH range (4–8). A broader working pH range is always convenient for the simultaneous extraction of heavy metal ions in various aqueous samples. One of the bisdithiocarbamates, HMBDTC, can extract eight metal ions quantitatively in different aquatic samples at pH 5.0–5.5.

In extracting Cr(VI), the efficiency of HMBDTC is better than that of all the other reagents studied. Because of the reasonable stability and the sufficiently low detection limits, these alkylene bisdithiocarbamates can be widely used for the determination of metal ions in environmental aquatic samples.

The authors thank the National Science Council of the Republic of China for financial support (Grant No. NSC 81-0208-M-003-10). T.-P. Hsieh also thanks the Taiwan Electric Power Company for providing a research fellowship for this study.

REFERENCES

1 A. Hulanicki, Talanta, 14 (1967) 1371.
2 R.R. Brooks, B.J. Preasley and I.R. Kaplan, Talanta, 14 (1967) 809.
3 J.D. Kinrade and J.C. Van Loon, Anal. Chem., 46 (1974) 1894.
4 L.G. Danielsson, B. Magnusson and S. Westerlund, Anal. Chim. Acta, 98 (1978) 47.
5 T.K. Jane and D.R. Young, Anal. Chem., 50 (1978) 1250.
6 R.G. Smith, Jr., and H.L. Windom, Anal. Chim. Acta, 113 (1980) 39.
7 A. Suquimae, Anal. Chim. Acta, 121 (1980) 331.
8 C.W. McLeod, A. Otsuki, K. Okamoto, H. Haraguchi and K. Fuwa, Analyst, 106 (1981) 419.
9 J.M. Lo, J.C. Yu, F.I. Hutchlson and C.M. Wai, Anal. Chem., 54 (1982) 2536.
10 H. Tao, A. Miyazaki, K. Bansho and Y. Umezaki, Anal. Chim. Acta, 156 (1984) 159.
11 M. Sugiyama, O. Fujino, S. Kihara and M. Matsui, Anal. Chim. Acta, 181 (1986) 159.
12 D. Ramesh Babu and P.R. Naidu, Talanta, 38 (1991) 175.
13 D. Yamamoto and M. Aoyama, Meiji Daigaku Nagakubu Kenkyo Hokoku, 68 (1985) 69; C.A., 104 (1986) 198955x.
14 D. Yamamoto, M. Tsukada and S. Hiraoko, Meiji Daigaka Nogakubu Kenkyo Hokoku, 67 (1984) 31; C.A., 104 (1986) 161092n.
15 A.L.J. Rao, N. Verma, J. Indian Chem. Soc., 65 (1988) 746.
16 A.S. Buchanan and P. Hannaker, Anal. Chem., 56 (1984) 1379.
17 J.N. King and J.S. Fritz, Anal. Chem., 57 (1985) 1016.

PUBLICATION SCHEDULE FOR 1994

	S'93	O'93	N'93	D'93	J	F						
Analytica Chimica Acta	281/1 281/2 281/3	282/1 282/2 282/3	283/1 283/2	283/3 284/1 284/2	284/3 285/1 285/2	285/3 286/1 286/2						
Vibrational Spectroscopy		6/1			6/2							

INFORMATION FOR AUTHORS

Detailed "Instructions to Authors" for *Analytica Chimica Acta* was published in Volume 256, No. 2, pp. 373–376. Free reprints of the "Instructions to Authors" of *Analytica Chimica Acta* and *Vibrational Spectroscopy* are available from the Editors or from: Elsevier Science Publishers B.V., P.O. Box 330, 1000 AH Amsterdam, The Netherlands. Telefax: (+31-20) 5862845.

Manuscripts. The language of the journal is English. English linguistic improvement is provided as part of the normal editorial processing. Authors should submit three copies of the manuscript in clear double-spaced typing on one side of the paper only. *Vibrational Spectroscopy* also accepts papers in English only.

Abstract. All papers and reviews begin with an Abstract (50–250 words) which should comprise a factual account of the contents of the paper, with emphasis on new information.

Figures. Figures should be prepared in black waterproof drawing ink on drawing or tracing paper of the same size as that on which the manuscript is typed. One original (or sharp glossy print) and two photostat (or other) copies are required. Attention should be given to line thickness, lettering (which should be kept to a minimum) and spacing on axes of graphs, to ensure suitability for reduction in size on printing. Axes of a graph should be clearly labelled, along the axes, outside the graph itself. All figures should be numbered with Arabic numerals, and require descriptive legends which should be typed on a separate sheet of paper. Simple straight-line graphs are not acceptable, because they can readily be described in the text by means of an equation or a sentence. Claims of linearity should be supported by regression data that include slope, intercept, standard deviations of the slope and intercept, standard error and the number of data points; correlation coefficients are optional.

Photographs should be glossy prints and be as rich in contrast as possible; colour photographs cannot be accepted. Line diagrams are generally preferred to photographs of equipment.

Computer outputs for reproduction as figures must be good quality on blank paper, and should preferably be submitted as glossy prints.

Nomenclature, abbreviations and symbols. In general, the recommendations of the International Union of Pure and Applied Chemistry (IUPAC) should be followed, and attention should be given to the recommendations of the Analytical Chemistry Division in the journal *Pure and Applied Chemistry* (see also *IUPAC Compendium of Analytical Nomenclature, Definitive Rules*, 1987).

References. The references should be collected at the end of the paper, numbered in the order of their appearance in the text (*not* alphabetically) and typed on a separate sheet.

Reprints. Fifty reprints will be supplied free of charge. Additional reprints (minimum 100) can be ordered. An order form containing price quotations will be sent to the authors together with the proofs of their article.

Papers dealing with vibrational spectroscopy should be sent to: Dr J.G. Grasselli, 150 Greentree Road, Chagrin Falls, OH 44022, U.S.A. Telefax: (+1-216) 2473360 (Americas, Canada, Australia and New Zealand) or Dr J.H. van der Maas, Department of Analytical Molecule Spectrometry, Faculty of Chemistry, University of Utrecht, P.O. Box 80083, 3508 TB Utrecht, The Netherlands. Telefax: (+31-30) 518219 (all other countries).

0003-2670/93/$06.00

This issue is printed on acid-free paper.

PRINTED IN THE NETHERLANDS

Sampling of Heterogeneous and Dynamic Material Systems

Theories of Heterogeneity, Sampling and Homogenizing

by **P.M. Gy**, Sampling Consultant, Cannes, France

Data Handling in Science and Technology Volume 10

Although sampling errors inevitably lead to analytical errors, the importance of sampling is often overlooked. The main purpose of this book is to enable the reader to identify every possible source of sampling error in order to derive practical rules to (a) completely suppress avoidable errors, and (b) minimise and estimate the effect of unavoidable errors. In short, the degree of representativeness of the sample can be known by applying these rules.

The scope covers the derivation of theories of probabilistic sampling and of bed-blending from a complete theory of heterogeneity which is based on an original, very thorough, qualitative and quantitative analysis of the concepts of homogeneity and heterogeneity. All sampling errors result from the existence of one form or another of heterogeneity. Sampling theory is derived from the theory of heterogeneity by application of a probabilistic operator to a material whose heterogeneity has been characterized either by a simple scalar (a variance: zero-dimensional batches) or by a function (a variogram: one-dimensional batches). A theory of bed-blending (one-dimensional homogenizing) is then easily derived from the sampling theory.

The book should be of interest to all analysts and to those dealing with quality, process control and monitoring, either for technical or for commercial purposes, and mineral processing.

Although this book is primarily aimed at graduates, large portions of it are suitable for teaching sampling theory to undergraduates as it contains many practical examples provided by the author's 30-year experience as an international consultant. The book also contains useful source material for short courses in Industry.

ELSEVIER
SCIENCE PUBLISHERS

Contents:

1992 xxx + 654 pages
Price: Dfl. 425.00 / US$ 243.00
ISBN 0-444-89601-5

ORDER INFORMATION

For USA and Canada
ELSEVIER SCIENCE PUBLISHERS
Judy Weislogel
P.O. Box 945
Madison Square Station,
New York, NY 10160-0757
Tel: (212) 989 5800
Fax: (212) 633 3880

In all other countries
ELSEVIER SCIENCE PUBLISHERS
P.O. Box 211
1000 AE Amsterdam
The Netherlands
Tel: (+31-20) 5803 753
Fax: (+31-20) 5803 705

US$ prices are valid only for the USA & Canada and are subject to exchange fluctuations; in all other countries the Dutch guilder price (Dfl.) is definitive. Books are sent postfree if prepaid.

711/414\143\0001-00

0003-2670(19931005)282:1;1-H